# SYNTHESIS AND CHARACTERIZATION OF RED EMITTING PHOSPHORS FOR WHITE LIGHT EMITTING DIODE APPLICATIONS

**Thesis submitted to**

**THE UNIVERSITY OF KERALA**

**For the award of**

**DOCTOR OF PHILOSOPHY**

**in**

**PHYSICS**

**under**

**THE FACULTY OF SCIENCE**

**by**

**ASWATHY B A**

**Under the Supervision of**

**Dr. P. PRABHAKAR RAO**

**Materials Science and Technology Division**
**CSIR - National Institute for Interdisciplinary Science and Technology (NIIST)**
**Research Centre, Kerala University**
**Thiruvananthapuram - 695019**
**Kerala, India**

**DECEMBER 2020**

# DECLARATION

I hereby declare that the PhD thesis entitled "**Synthesis and characterization of red emitting phosphors for white light emitting diode applications"** is an independent work carried out by me and it has not been submitted anywhere else for any other degree, diploma, or title.

Aswathy B A

THIRUVANANTHAPURAM

Date: December 21, 2020

सीएसआईआर- राष्ट्रीय अंतर्विषयी विज्ञान तथा प्रौद्योगिकी संस्थान
CSIR- National Institute for Interdisciplinary Science and Technology
(वैज्ञानिक तथा औद्योगिक अनुसंधान परिषद)
(Council of Scientific & Industrial Research)

विज्ञान और प्रौद्योगिकी मंत्रालय, भारत सरकार / Ministry of Science & Technology Govt. of India
औद्योगिक एस्टेट पोस्ट Industrial Estate PO, तिरुवनंतपुरम, केरल Thiruvananthapuram, Kerala -695019
भारत India

**Dr. P. Prabhakar Rao** **Tel Ph: +914712515311**
**CSIR Emeritus Scientist** **Email:padala_rao@yahoo.com**
**Material Science and Technology Division**

**21.12.2020**

# CERTIFICATE

This is to certify that the work embodied in the thesis entitled "**Synthesis and characterization of red emitting phosphors for white light emitting diode applications"** has been carried out by **Mrs. Aswathy B A** under my supervision and guidance in the Materials Science and Technology Division of National Institute for Interdisciplinary Science and Technology (NIIST), CSIR, Thiruvananthapuram, for the degree of Doctor of Philosophy in Physics under the faculty of Science, University of Kerala and has not been included in any other thesis submitted for the award of any degree.

THIRUVANANTHAPURAM
Date: December 21, 2020

**Dr. P. Prabhakar Rao**
(Supervising Guide)

## *ACKNOWLEDGEMENTS*

*It took many years of effort for the completion of this dissertation. I am greatly indebted to many persons who supported me in many different ways for the completion of this thesis. First I will start with my research supervisor, Dr.P.Prabhakar Rao, his constant support, guidance and encouragement was there throughout the journey. I express my sincere gratitude towards him for choosing me as his student and helping me to complete the thesis on time. My sincere gratitude towards Dr. A. Ajayaghosh, directror CSIR NIIST for providing all the research facilities. I am thankful to Dr.S.Savitri, Dr. K. Harikrishna Bhat and Dr. P. Prabhakar Rao present and former Head of Materials Science and Technology Division for maintaining discipline and academic facilities. I wish to thank scientists and technical staff of NIIST for their help during the course of this research work.*

*I extend my gratitude to staff in Administrative, Finance, Accounts, Stores, Purchase, Library and IT sections for their help and services.I acknowledge CSIR for the financial assistance during my research. I would like to thank Mr. M. R Chandran, Mr. Shanoj P. S, Mrs Soumya V, Mr. Pruthiviraj N, Mr. M. P Varkey and Mr. Harish Raj for SEM imaging and technical support. I also thank Department of Physics, University of Kerala for the quantum yield measurement analysis.*

*My research life at NIIST started from the time of my Msc project work, which was a truly inspirational experience to enter into the field of research. I am extremely thankful to my friend Nitha for her best companionship and support during those days. Special thanks to all my lab seniors Dr. Mahesh S.K, Dr. Linda Francis, Dr. Sumi.S, Dr. Vaisakhan Thampi, Dr.Divya S, Dr. Athira K.V.Raj, Dr. Sreena S, Dr. Bradha Madhavan, Dr Renju.U.A and Dr. Parvathi S.Babu for their help and support. I express my love and gratitude for my fellow lab mate Ajuthara for her best companionship and advices. I am greatly indebted to Suchithra V.G for her best friendship, moral support and help during the past five years. I would like to express my gratitude towards my room-mates Ramya, Surabhy and Asa for their support, care and friendship during my pregnancy time.*

*I am greatly thankful to all my teachers who have encouraged me. Special thanks to my teachers of Department of Physics, University of Kerala kariavattom Dr.Biju V, Dr.Subodh G, Dr.Sibi.K.S, Dr. Udayachandran Thampi, Dr. C .I. Muneera, Dr.Jawahar I.N for their academic lessons and moral support.*

*Finally I want to acknowledge the special persons in my life. Words are inadequate to express my gratitude towards my parents (Babu.M and Anithakumary S.), who were always there for me with prayers. They supported me in every decisions that I have taken and had faith in me. My heartful thanks to both of you for the unconditional love, care, advices and sacrifices. I express my sincere gratitude towards my Grandpa (Viswanathan), Brother (Anoop B.A) and Sisters in law (Lajimol L.L and Keerthi. A) for their love, care and support in every manner. Special thanks to my Mother in law (Lalitha Lakshman) for her love, care and patience. She look after my child in a better way than I can do. Without her support I was not able to complete my research work. I am also thankful to brother like person Mr. Gopinath.M for his help and support all over the time. Thanks to MeghaNanda and Athmika for their innocent love. I am extremely thankful to my son Lakshith Prem Lalaj (Lachuttan), my antidepressant and the ray of hope. He brought a new dimension to my life. During the hard phases of life his heavenly smile with sparkling eyes forced me to move forward. Words fail in expressing my thanks to a very special person, my life partner, Lalaj.L.L. I am extremely happy and proud to have such a man in my life. He supported me in every possible manner for the completion of this work with timely advices. Thank you for the understanding, support, patience, love, care and sacrifices throughout the journey.*

*At the end, I would like to thank all those people who were there with me to make this thesis possible*

*Aswathy B.A*

# CONTENTS

## LIST OF TABLES

# LIST OF FIGURES

# ABBREVATIONS

| | |
|---|---|
| ASTM | : American Society for Testing and Materials |
| CCT | : Correlated Color Temperature |
| CIE | : Commission Internationale de I' Eclairage |
| CN | : Coordination Number |
| CRI | : Color Rendering Index |
| CT | : Charge Transfer |
| DIN | : Deutsches Institute fur Normung (German Standards Organisation |
| ED | : Electric Dipole |
| EDS | : Energy Dispersive Spectroscopy |
| FWHM | : Full Width Half Maximum |
| ISO | : International Organization for Standardisation |
| JCPDS | : Joint Committee on Powder Diffraction Standards |
| LED | : Light Emitting Diode |
| LMCT | : Ligand to Metal Charge Transfer |
| Ln | : Lanthanide |
| MD | : Magnetic Dipole |
| NIR | : Near Infrared |
| NTSC | : National Television Standards Committee |
| pc-WLED | : Phosphor Converted White Light Emitting Diode |
| PL | : Photoluminescence |
| PMMA | : Poly(Methyl Methacrylate) |
| PTFE | : Poly–tetrafluoroethylene |
| QE | : Quantum Efficiency |
| RE | : Rare Earth |
| SEM | : Scanning Electron Microscopy |
| SSL | : Solid State Lighting |
| TEM | : Transmission Electron Microscopy |
| UV-vis | : Ultraviolet Visible |
| XPS | : X-ray Photoelectron Spectroscopy |
| XRD | : X-ray Diffraction |

# PREFACE

Low energy consuming lighting devices are the need of the hour to meet the energy crisis, which takes share of one fifth of the total energy consumption. In this direction, white light-emitting diodes (WLEDs) have become the best choice of solid-state lighting sources due to their superior properties, such as small size, high luminous efficiency, energy savings, long operation lifetime, and environment friendliness. At present, the commercially available way to fabricate WLEDs is to combine blue InGaN LED chip with $Y_3Al_5O_{12}:Ce^{3+}$ yellow phosphors, which has some advantages such as the process is simple and the production cost is low. Unfortunately, in this combination lack of red emission of the spectrum, results in white light with high correlated color temperature (CCT) and low color rendering index (CRI). An alternative method is to excite red-, green- and blue-emitting phosphors by a near-ultraviolet (UV) LED chip to achieve white light. Obviously, red-emitting phosphors play an important role in both of these methods. Currently available red phosphors are mainly based on sulfide based systems ($CaS:Eu^{2+}$, $Y_2O_2S:Eu^{3+}$) which lacks thermal and chemical stability. Therefore, it is highly demanded to find a red-emitting phosphor with good luminescence properties.

Trivalent Europium is well known for its orange red luminescence due to the intraconfigurational f-f transitions. $Eu^{3+}$ ion exhibits mainly two emission lines and the emission profile is determined by their local environment in host crystals. Incorporating $Eu^{3+}$ with various host lattices such as pyrochlore, powellite, fluorite, etc., lot of red phosphors have been developed. But they exhibit low absorption in blue or near UV region because they have high activator concentration, poor energy transfer from the host lattice to the activator ions, low concentration quenching, lack of thermal stability of luminescence around 150-200°C, etc. Recently there has been a growing interest on the optical properties of perovskite type red phosphors because of their very high physical and chemical stability, broad charge transfer (CT) band in the near UV region and the ability to capture radiation from a GaN based LED over a range of wavelengths etc., In this context the present thesis is

aimed to develop some new perovskite based red phosphors with good photoluminescence properties.

The present research work is organized into seven chapters. Introduction chapter discusses about solid state lighting technology and different methods for white light generation with their advantages and practical challenges. The details of luminescence in $Eu^{3+}$ activated phosphors is also emphasized. Major objectives of the present work are highlighted and the motivation and importance of choosing perovskite based host lattice is also emphasized.

The second chapter discusses the effect of variation of B' cation on the structural and optical characteristics of the series $SrGd_{0.5}B'_{0.425}O_3 : 0.075Eu^{3+}$ (B' = Nb, Ta, Sb). Better results were obtained for Nb system with broad and intense charge transfer band and the sharp peaks corresponding to $O^{2-}$-$Eu^{3+}$ charge transfer and intraconfigurational 4f-4f transitions of $Eu^{3+}$ ions in the host. By fixing Nb at the B' site and varying $Eu^{3+}$ concentration, optical, structural and morphological characterization of the series, $SrGd_{(0.5-x)}Nb_{0.5}O_3:xEu^{3+}$ is done and included in this chapter. The phosphors have strong excitation energy levels in both near UV and blue regions and they exhibit intense orange red emissions with good quantum efficiency values better than some of the reported perovskites.

In the third chapter, the influence of various B site cations (Y, Gd and In) keeping Nb on the B' site on the structural and photoluminescence properties have been investigated in detail. The compositions, $SrB_{(0.425)}Nb_{0.5}O_3:\mathit{0.075}Eu^{3+}$ (B =Y, Gd, In) were developed by the conventional solid state route. Yitrium system was found to be better with its high asymmetric ratio, intense red emission and high efficiency values. By fixing Yitrium at the B site and varying $Eu^{3+}$ concentration, a series of red phosphors $SrY_{(0.5-x)}Nb_{0.5}O_3:xEu^{3+}$ were synthesized and the optical, structural and morphological characterizations are discussed in this chapter.

The fourth chapter discusses about two new series of perovskite type red phosphors . $Ba_3Ca_{(1-x)}Nb_2O_9:xEu^{3+}$ and $Ba_2Y_{(1-x)}NbO_6:xEu^{3+}$. The structural, optical and morphological characterizations were done. $Ba_3Ca_{(1-x)}Nb_2O_9:xEu^{3+}$ is found to be a 1:2 ordered triple

perovskite phosphor exhibiting narrow orange emission. Broad nature of excitation and narrow emission spectra in these phosphors is found to be very suitable for WLED applications.

Fifth and sixth chapters details about self charge compensating double perovskite phosphors prepared via ball milling method. Structural, optical and morphological characteristics of $Na_{(1+x)}Ca_{(1-2x)}xEuSnNbO_6$ ( $x$ = 0.05, 0.10, 0.15, 0.20, 0.25) phosphors are discussed in chapter 5. Powder X-ray diffraction patterns of the sample indicates minor $SnO_2$ peaks beyond 10 mol% $Eu^{3+}$ concentration. So the $Eu^{3+}$ concentration is fixed at 10 mol% and studied the effect of substitution of Ti on Sn site. The prepared series of phosphors are $Na_{(1.1)}Ca_{(0.8)}Eu_{0.1}Sn_{(1-x)}Ti_xNbO_6$ ($x$ = 0, 0.2, 0.4, 0.6, 0.8, 1). Ti substitution has positive effects on the structural and photoluminescent characteristics. Further a series of samples $Na_{(1+x)}Ca_{(1-2x)}xEuTiNbO_6$ ($x$ = 0.05, 0.10, 0.15, 0.20, 0.25) was synthesized and their structural, optical and photoluminescent characteristics are discussed in chapter 6. The optimization of the photoluminescent properties by varying calcination temperature from 1000-1200˚C is also discussed here. The optimized phosphor samples exhibit intense red emission as that of commercial $Y_2O_3$: $Eu^{3+}$ phosphor, very good chromaticity values and excellent color purity value of 94%.

Chapter seven summarizes the major findings and conclusions drawn from the work and gives the scope for further studies

# Chapter 1

## Introduction and Literature Review

*This chapter gives an introduction about the importance of solid state lighting technologies and the basic concepts of phosphors. It includes the need for developing novel and efficient red phosphors. Characteristics of $Eu^{3+}$ ion as an activator ion and the properties of perovskite type structure is also discussed here.*

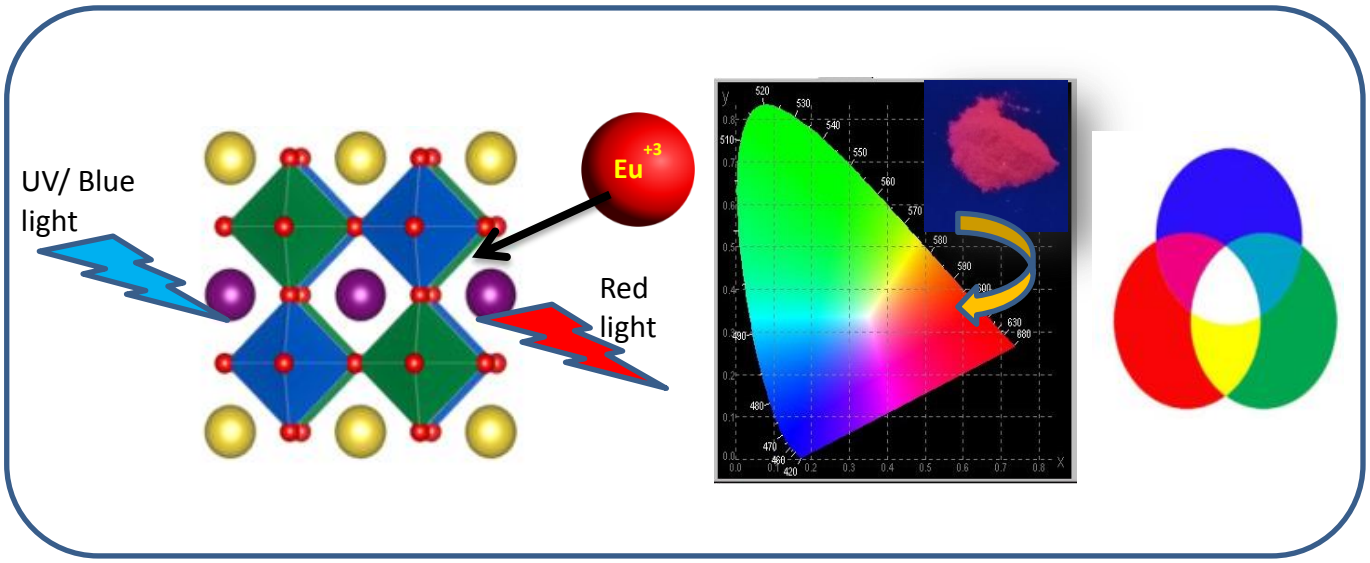

## 1.1 Introduction

Light is the physical stimulus that allows us to see the world around us. Sun is our natural light source. The non availability of natural light always prompted our ancestors to seek for different methods for creating light. The history of artificial lighting starts from 50,000 years ago. It starts first from fire and oil lamps then to electrical light sources such as incandescent lamps, gas discharge tubes, halogen lamps etc. The lighting techonologies such as incandescent and fluorescent lamps have many disadvantages. In incandescent lamps, tungsten filament is heated using electricity upto it emits white light. In these devices, ~ 98% of electrical energy is ends up as heat. They act as source of heat energy rather than light. Their control over the radiation spectrum is limited. Discharge lamps works on the principle of excitation of atoms or ions through acceleration of electrons. In low pressure mercury vapour about 63% of energy can be converted into UV radiation. After converting UV to visible overall efficiency of resulting lamp is 28%. In the case of fluorescent lamps about 10-15 % of electrical input can be converted as light energy but it has a serious disadvantage that each lamp contains a small amount of mercury which is hazardous to the environment (Steigerwald *et al.* 2002). Alternate lighting devices are based on the semiconductor LEDs which works on the principle of injection electroluminescence. Under forward bias, when electric current flows, electrons and holes crosses the PN junction and they acquire the potential energy to overcome the bandgap energy and their recombination causes light emission (Shur *et al.* 2005). LED can be considered as an ultimate form of lamp because its efficiencies are limited by the quality and performance of materials used and device structure etc (Phillips *et al.* 2007). Artificial lighting plays an important role in the quality and productivity of human life. Nowadays large amount of energy have been using for lighting purposes. About 20% of world's electrical energy is used for lighting. So energy efficient lighting sources are the need of the hour. In this scenario, solid state lighting technologies (SSL) with the promising properties such as rapidly improving efficiency, durability and reliability, usability in products of various sizes, environmentally friendly constituents are extensively replacing the incandescent and fluorescent lamps (Morgan *et al.* 2009, Nikol *et al.* 1998).

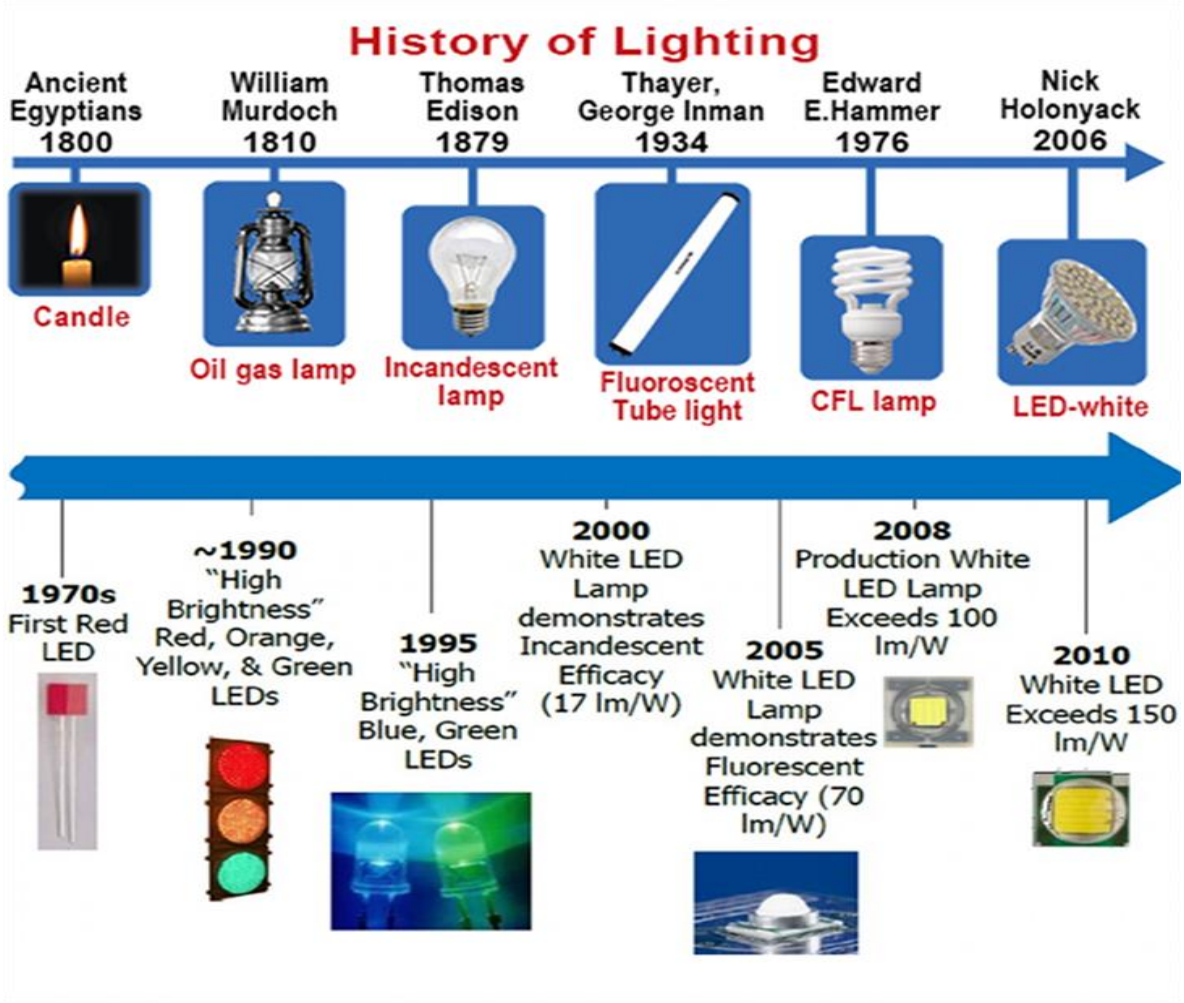


**Fig. 1.1 :** Evolution of artificial lightsources.

(https://decodeals.wixsite.com/bahamasledsolutions/history-of-light)

## 1.2 Solid state lighting

Lighting technologies that uses semiconductor devices such as Light Emitting Diodes (LED), Organic LEDs, or light emitting polymers as source of illumination is referred to as solid state lighting (SSL) (Crawford *et al.* 2009). First light emitting diode was invented by H. J. Round in 1907. He published on the light emission from a Silicon Carbide junction diode. Decades later in 1962, the first practical visible spectrum LED was developed by Nick Holonyak at General Electric. The potentiality of the invention remained unknown at that time and LEDs were extensively used for signaling and numerical applications. Later the situation was changed with the Shuji Nakamura's

invention of double hetero structure InGaN/GaN blue LED in 1993 (Nakamura *et al.* 1993). Later they invented high power InGaN/GaN blue LED for general lighting applications in 1994. Nichia corporation developed first commercially available white light emitting diode (WLED) in 1996 (Steigerwald *et al.* 2002). After the invention rapid development had taken place in the field of solid state based lighting technology. The promising advantages such as high brightness, long lifetime, environmental friendliness, high luminous efficiency, energy savings, new luminaire design possibilities etc. makes WLEDs as a best choice of light source (Ferreira *et al.* 2019).

### 1.3 Different approaches for white light generation

There are various approaches to get efficient solid state sources for white light generation. One can directly mix light from three or more monochromatic sources, red, green and blue to produce a white source. Another method is to use a blue LED to pump one or more visible light emitting phosphors that has been integrated into the

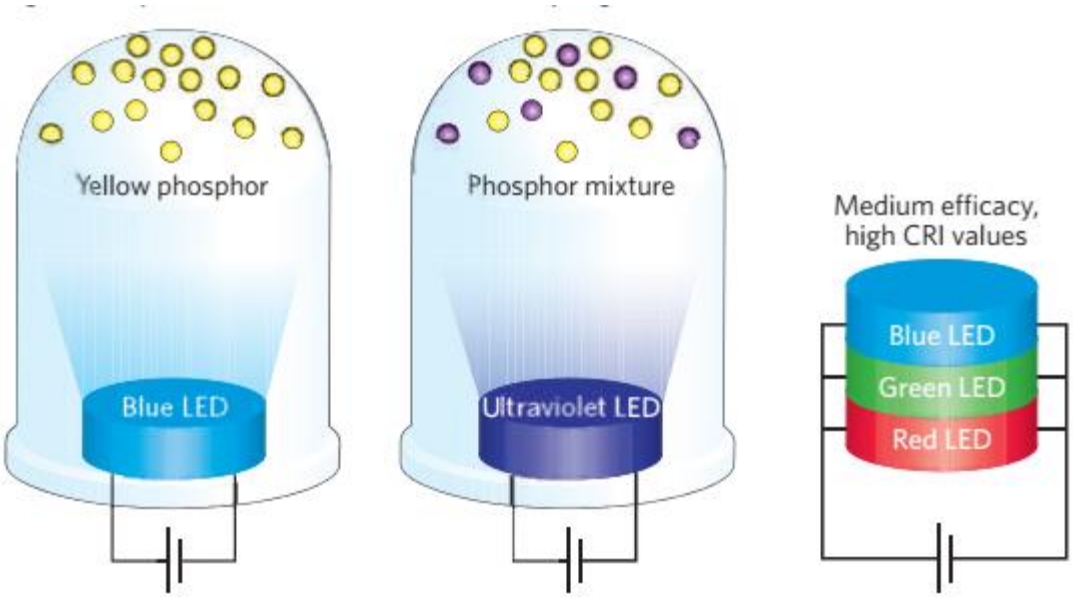


**Fig. 1.2** : Different methods for white light generation

(https://www.electrical4u.com/white-led/)

phosphor-converted LED (pc-LED) package. The pc-LED is designed to leak some of the blue light beyond the phosphor to generate blue portion of the spectrum, while the phosphor converts the remainder of the blue light into red and green portions of the spectrum. Third method is to use an UV LED to pump a combination of red, green and blue phosphors in such a way that none of the pump LED is allowed to escape (Steigerwald *et al.* 2002). Each of the approaches has potential advantages and technical challenges. Mixing the emission from red, blue and green coloured LEDs is the most straight forward technique since there is no quantum deficit arising from Stokes shift and hence offers infinitely graduated colour and white point colour. However, this form requires independent output power control on each LEDs and there is a gap in the operating voltages between them making the operation quite cumbersome. Phosphor converted LEDs are the most common LEDs based white light source where a blue LED is used with a yellow emitting phosphor. The yellow light stimulates the red and green receptors of th eye, the resulting mix of the blue and yellow light give the appearance of white. The pc-WLED represent an innovation in solid state lighting, because they are small, light weighted, have long life time and are easy to operate (Smet *et al.* 2011). However, they were inherently less effficient than RGB source because of the unavoidable energy loss. The third approach is to have UV LEDs. In this case, the UV light is completely absorbed by the phophors and the mixed RGB output appears white. The quantum deficit between the UV pump and the phosphors, especially the low energy red phosphor,dissipates significant energy and makes the approach inherently less efficient than either the RGB or pc LED schemes for generating white light. But the UV LED approach has the advantage that colour can be controlled by the phosphor mix atleast at one point in time and at one temperature and hence the colour rendering should be excellent (George *et al.* 2013).

### 1.4 Phenomenon of Photoluminescence

Lminescence is a process in which matter emits non-thermal radiation which is characteristic of the material at normal or lower temperature. In luminescence process, when some sort of external energy hit the substance, electrons get excited to the higher energy states and when they return to the ground state the excess energy is given off as

light. Depending upon the type of excitation, luminescence can be classified into different types such as photoluminescence, chemiluminescence, mechano luminescence, electroluminescence etc. Photoluminescence is the phenomenon in which substance emit visible radiation under the excitation of photons. Photoluminescence can be classified into fluorescence and phosphorescence depending on its lifetime and process of radiation. Flourescence occurs between electronic states having same multiplicity ie singlet- singlet or triplet to triplet transitions. Fluorescence has a very short decay time (~1ns to 1ms) and stops as soon as the excitation source is removed. Since the fluorescent emission is spin allowed its probability is higher than phosphorescence (Blasse and Grabmeir 1994).

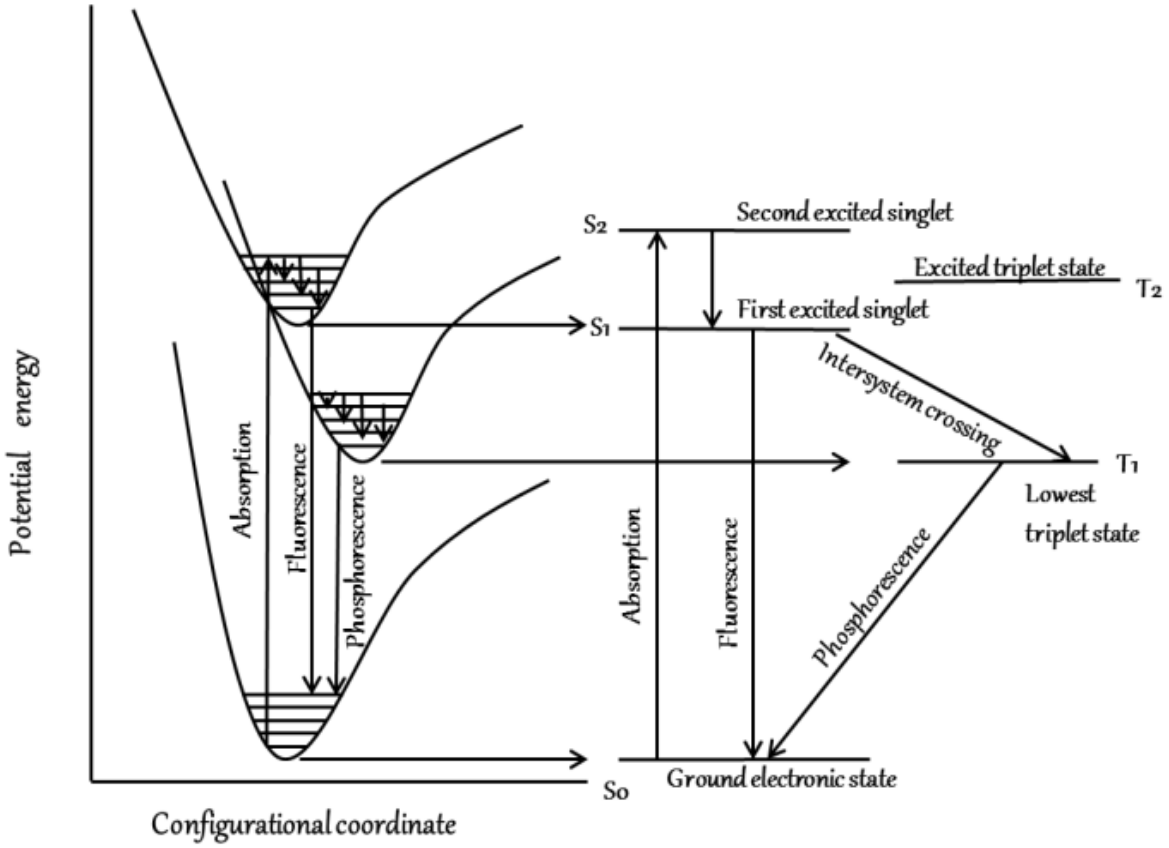


**Fig. 1.3** : Phenomenon of flurescence and phosphorescence (Feldman *et al*. 2003)

In phosphorescence transition occurs between states with different multiplicity. A molecule in the excited triplet state may not always use intersystem crossing to

return to the ground state. It could lose energy by emission of a photon. A triplet-singlet transition is much less probable than a singlet-singlet transition. The lifetime of the excited triplet state can be up to 10 seconds, in comparison with $10^{-5}$ s to $10^{-8}$ s average lifetime of an excited singlet state. Emission from triplet/singlet transitions can continue after initial irradiation (Feldman *et al*. 2003)

### 1.5 Basic Aspects of Phosphors

Phosphors the word means light bearer. They are the luminescent materials capable of emitting visible radiation when subjected to suitable excitations such as UV radiation, X-rays , electron bombardment etc. Phosphors are usually composed of a suitable host material to which an activator ion is added. Host material can be oxides, oxynitrides, nitrides, silicates, sulfides, selenides, halides etc of various transition elements and rare earth metals. Activator ions can be $Eu^{3+}$, $Eu^{2+}$, $Dy^{3+}$, $Pr^{3+}$, $Ce^{3+}$, $Dy^{3+}$, $Er^{3+}$ etc. Activators are the luminescent centres where absorption and radiative re-emission takes place. Different energy processes taking place in a phosphor material includes absorption of energy from various sources, excitation of activator ion to form an excited state ($10^{-11}$ s), non radiative relaxation within the various vibration levels to reach the lowest vibrational level of the excited state ($10^{-8}$ s) and relaxation to the ground state by the emission of a lower energy photon ($10^{-9}$ to 10 s) (Blasse and Grabmeir 1994). In a phosphor material, activator ion can be directly get excited or by the transfer of energy from the host. There are different excited energy levels are available in the activator ion. The energy of the exciting photon determines to which excited level the activator is get excited. Photoluminescence mechanism of the activator can be described using configurational co-ordinate diagram. Total energy E of the activator can be plotted as a function of r, the distance between metal cations and anions in the lattice. Horizontal lines in the ground state and excited states denote the vibrational levels (Nalwa *et al.* 2003). When the activator absorbs some radiation, lattice expansion occurs near the activator ion and activator is raised to the excited state. The excitation and emission processes can be represented as vertical arrows in the configurational co-ordinate diagram. Since the atomic nucleus is $10^3$ to $10^5$ times

heavier than the electron, nucleus remains at the same position during these processes. The energy difference between excitation and emission is termed as Stoke's shift. In

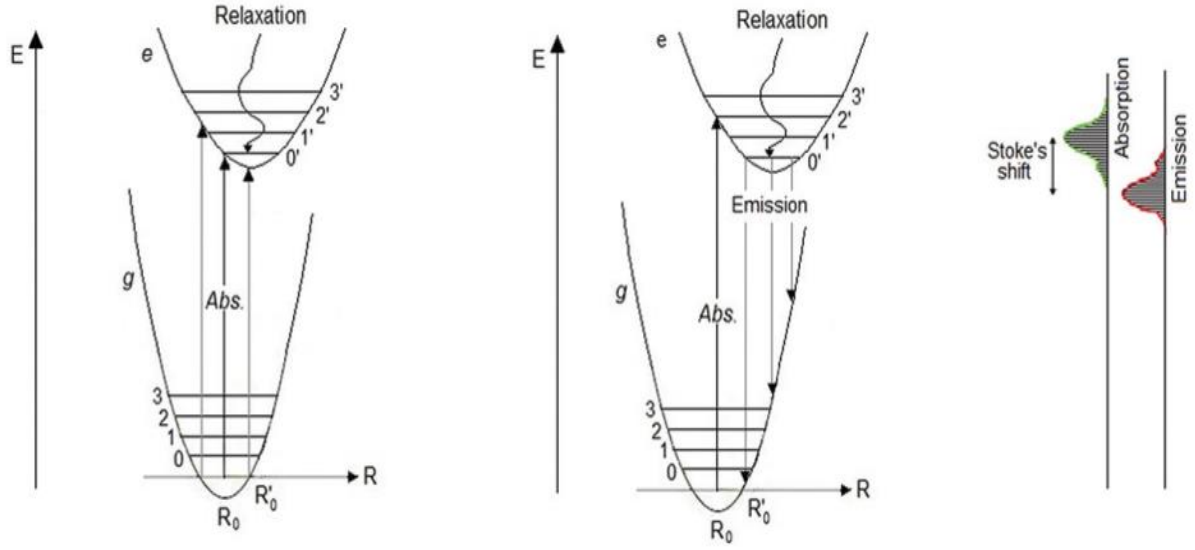


**Fig. 1.4** :Configurational co-ordinate diagram showing absorption transition emission transition and stokes shift (Nalwa *et al.* 2003).

some cases activators are not able to efficiently absorb the radiant energy. In such cases some ions or ionic groups can be added to the system in order to absorb the excitation energy and efficiently transfer it to the activator. These ions which are responsible for the absorption of energy is known as sensitizer and the activator which luminesces is the emission center. This process is termed as sensitized luminescence. In some cases, host itself absorbs the excitation energy and transfer to luminescent centre and such type of luminescence is termed as lattice sensitized luminescence. Depending on the electronic transitions, principal luminescent centres can be classified as follows (Shionoya *et al*. 2006)

i. $1s \leftrightarrow 2p$ ; F
ii. $ns^2 \leftrightarrow nsnp$; $Ga^+$, $In^+$, $Ge^{2+}$, $Sn^{2+}$, $Pb^{2+}$etc
iii. $nd^{10} \leftrightarrow nd^9 (n+1)s$; $Cu^+$, $Ag^+$ and $Au^+$
iv. $3d^n \leftrightarrow 3d^n$ , $4d^n \leftrightarrow 4d^n$ first and second transition metal ion.
v. $4f^n \leftrightarrow 4f^n$ , $5f^n \leftrightarrow 5f^n$ ; rare earth and actinide ions.

vi. $4f^n \leftrightarrow 4f^{n-1}5d$, $Ce^{3+}$, $Sm^{2+}$, $Eu^{2+}$, $Tm^{2+}$,$Yb^{2+}$

vii. A charge transfer transition or a transition between an anion p electron and an empty cation p orbital. E.g: Intra molecular transitions in complexes such as $VO_4^{3-}$, $MoO_4^{2-}$ and $WO_4^{2-}$ etc.

In general, Lanthanide ions exhibit three types of excitation transitions (Blasse 1979).

i. 4f-4f transitions

Groups of narrow lines are visible in the absorption spectra of Lanthanide doped single crystals and lanthanide salts. These sharp lines correspond to the electronic transitions taking place in the 4f shell. Since the 4f electrons are well shielded by the 5s and 5p electrons, 4f-4f transitions are very sharp but the intensity of these transitions are weak. The lifetimes of these transitions are of milliseconds range because of their forbidden character.

ii. 4f-5d transitions

Here one of the electron from 4f orbital is raised to higher 5d orbital and is denoted as $4f^{n-1}$-5d. Since these transitions are parity allowed ones, they have strong and broad absorption cross section.

iii. Charge transfer state transitions

In charge transfer state transition, 2p electron from surrounding anion is promoted to 4f shell. They are parity allowed transitions, resulting in broad and intense absorption transitions.

## 1.6 Basic Terminology

An excellent light source for indoor lighting applications should have promising properties such as excellent color rendering index, high luminous efficacy and good output color purity. Basic terms associated with PC-WLEDs are given below.

### 1.6.1 CIE Chromaticity co-ordinates

CIE color co-ordinate diagram was introduced by Commission Internationale de l'Eclarirage in 1931 which represents all the chromaticities visible to an average person on a scale of x and y. A color space can be defined as a three dimensional space specified

by a set of tristimulus values (X, Y and Z). Any color can be expressed as a combination of three primary colors red, green and blue. In CIE color system each color can be expressed as the combination of X, Y and Z. The chromaticity co-ordinates x, y and z can be defined as the ratio of X,Y and Z to their sum. Since sum of the primary colors must always be 100%, sum of x, y and z is always 1. So it is necessary only to quote two of the co-ordinates (x, y). The National Television Standards Committee (NTSC) standard color co-ordinate defined for red are (0.67, 0.33) (Stevens *et al*. 1969)

### 1.6.2 Color Rendering Index (CRI)

Color Rendering Index (CRI) is the ability of a light source to render or reproduce the color of an object in comparison to a natural light source. Value of CRI ranges from 0

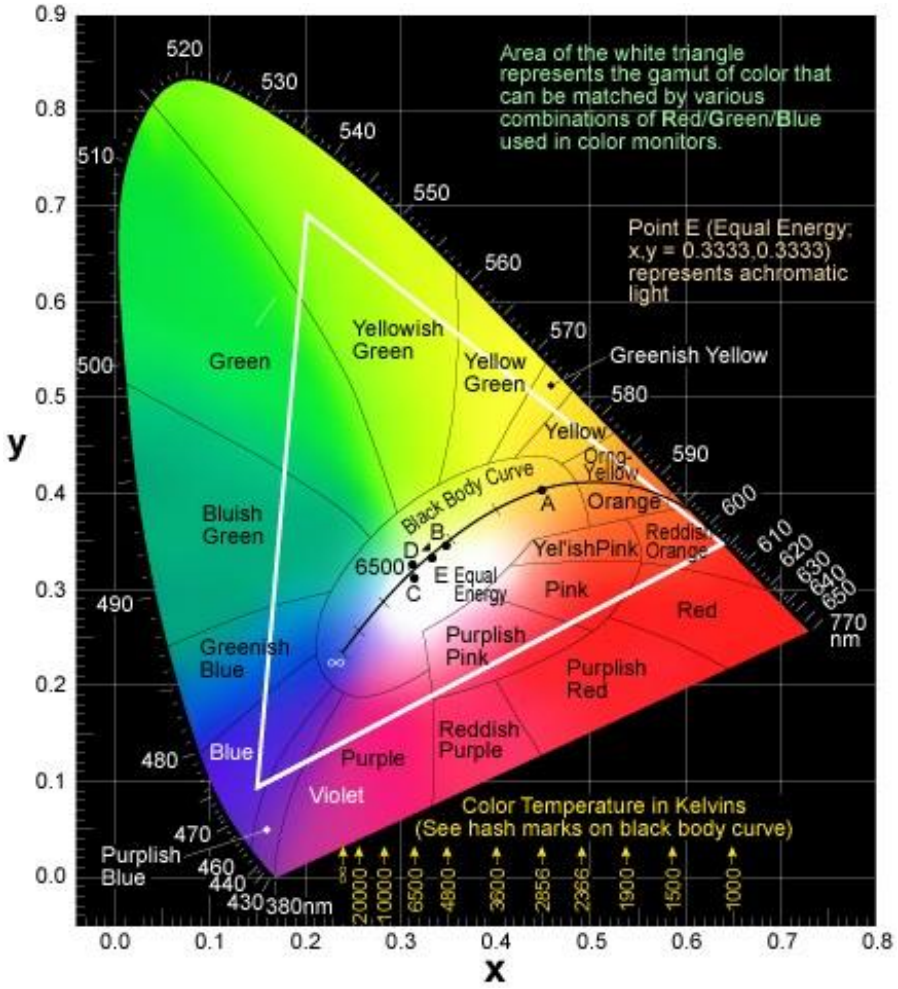


**Fig. 1.5** : CIE Chromaticity diagram (http://www.color-theory-phenomena.nl/10.02.htm)

to 100, lower the CRI less accurately the colors will be reproduced. Sunlight has the maximum CRI value of 100 (Jones *et al.* 2001).

### 1.6.3 Luminous Efficacy

It is a metric used for the performance comparison of various light sources. It is a measure of how well a light source produces visible light. It is the ratio of luminous flux to power, measured in lumens per watt. The lumen is defined as 1/683W of monochromatic green light (555 nm). So the theoretically attainable maximum value of efficacy is assuming complete conversion of energy at 555nm giving 683lumen/W. For a light source it is impossible to improve both CRI and luminous efficacy at the same time. Better CRI value requires proper spectral dispersion over all the visible range, but it may lead to the decrease in luminous efficacy below 683 lm/W. So there should be some compromise between these two. The maximum theoretical efficiency for a solid state lamp source with correlated color temperature (CCT) of 3800K and CRI of 85 is 400lm/W (Morgan *et al.* 2009).

### 1.6.4 Correlated Color Temperature (CCT)

White light can be classified as warm, cool or neutral with respect to white light emitted by an ideal white light source. CCT can be defined as the temperature of a black body radiator that has the same color as that of the light source (Kaufman *et al*. 1972). Temperarure of an ideal black body ranges from 2000K to 10000K. When the temperature increases emitted white light goes from reddish to bluish. Luminous efficacy and color rendering index of radiation increases as CCT decreases. Warm white light is suitable for residential applications.

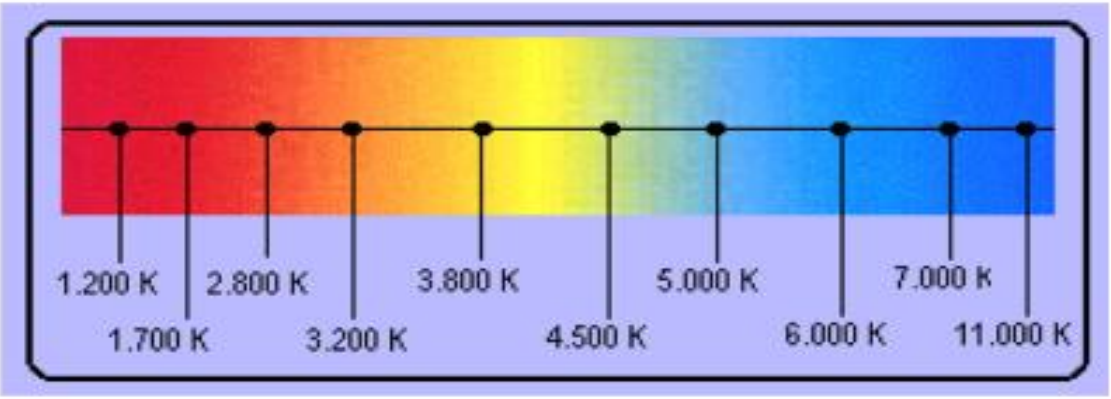


**Fig. 1.6** : Correlated color temperature for different colors (de Souza *et al.* 2019)

## 1.7 Basic requirements of phosphor materials

The basic requirements a phosphor material should possess in order to apply for WLED applications to meet some of the above parameters are listed below (Smet *et al.* 2011)

- Phosphor should have high absorption in the emission range of LED and excitation maximum should fall in the range of pumping LED.
- Emission of phosphor material developed in combination with emission of pumping LED or another phosphor materials should lead to pure white emission with good CCT and CRI.
- They should possess high internal quantum efficiency such that overall electric to optical conversion efficiency of phosphor should be high.
- They should have reduced thermal quenching in order to operate at elevated temperatures.
- They should be thermally and chemically stable and should be free from photobleaching
- Synthesis route should be easy so as to produce phosphors at a large scale
- They should be nontoxic and fabrication use and disposal of phosphors should be environmentally benign as possible.

## 1.8 Need for red phosphors

There are various approaches for white light generation in solid state lighting technology. The combination of blue LED and yellow phosphor and UV LED and tri color phosphors are commonly used. Commercial PC WLEDs are using 450-470 nm blue GaN LED chip covered by yellowish phosphor coating ($Y_3Al_5O_{12}$: $Ce^{3+}$). However, the white light obtained from this configuration possess low Color Rendering Index (CRI <80) due to lack of red component. Addition of suitable red phosphors easily pumped by NUV or blue LED combination can improve CRI (Huang *et al.* 2014).Yet another technique is to incorporate blue, green and red emitting phosphors with near UV (380-420 nm) LED chip. Currently used red phosphors are sulphide or nitride based ones such as $Y_2O_2S$: $Eu^{3+}$, CaZnS: $Eu^{2+}$, $Sr_2Si_5N_8$: $Eu^{2+}$ and $Sr[LiAl_3N_4]$: $Eu^{2+}$. But for practical applications,

they are chemically unstable and also the nitride and oxynitride phosphors are difficult to synthesize because of its tedious synthesis conditions such as nitrogen pressure and high temperature calcinations. So there is a great demand for energy efficient and stable oxide red phosphors that can be excited by near UV/ blue LEDs (Antic *et al.* 2009, Chien *et al.* 2016)

### 1.9 Rare earth activators

Rare earth elements are the series of elements with atomic numbers 57 to 71. They are Lanthanum, Cerium, Praseodymium, Promethium, Samarium, Europium, Gadolinium, Terbium, Dysprosium, Yittrium and Scandium. Rare earth ions possess characteristic properties due to the presence of partially filled deep lying 4f shells. These 4f shells are screened by the outer electron shell and give rise to discrete energy levels. The presence of crystal lattice hardly affect the position of these discrete energy levels, so there is a close resemblance between energy level diagram of free ion and an incorporated ion. All the rare earth ions possess +3 oxidation state. +4 and +2 valance states are stable for rare earth ions half fill, completely empty or completely filled f shells. $RE^{3+}$ has maximum possible number of unpaired f electrons (Ropp 2014).

Lanthanides starting from $Ce^{3+}$ to $Lu^{3+}$ possess one to fourteen 4f electrons in their inner shell configuration and are equivalent to Xenon. Ions having no 4f electrons $Sc^{3+}$, $Y^{3+}$, $La^{3+}$ and $Lu^{3+}$ have no electronic energy levels which gives absorption and emission in the visible region. Ions from $Ce^{3+}$ to $Yb^{3+}$ have partially filled 4f orbitals have luminescent properties in the visible region. Many of the RE ions can be used as activators in phosphor materials, by replacing $Gd^{3+}$, $La^{3+}$, $Lu^{3+}$ and $Y^{3+}$ in various compounds. Electronic states of the ions can be represented by term symbols. A term symbol has the general form $^{2S+1}L_{J,}$ where 2S+1 is the multiplicity of the term, S is the total spin angular momentum quantum number and J is the total orbital angular momentum quantum number. Figure 1.6 depicts the energy level diagram of RE ions (Ronda *et al.* 1998). A crystal field perturbation of aspherical nature causes the removal of degeneracies of $^{2S+1}L_J$ levels of rare earth ions embedded in a compound when they are excited by optical excitations (Belsky *et al*. 1999).

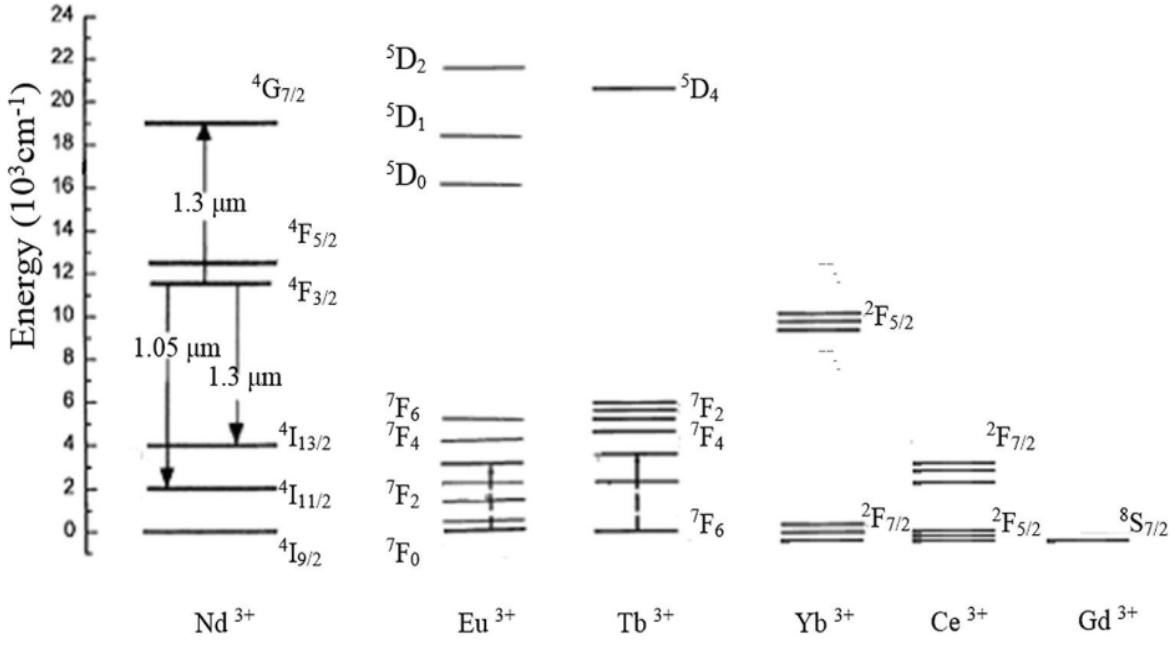


**Fig. 1.7** : Energy level diagram of rare earth ions $Nd^{3+}$, $Eu^{3+}$, $Tb^{3+}$, $Yb^{3+}$, $Ce^{3+}$, $Gd^{3+}$ (Belsky *et al*. 1999).

### 1.10 Luminescence properties of $Eu^{3+}$

Trivalent europium is well known for its strong orange- red luminescence. They possess even number of electrons in the 4f shell ($4f^6$). Crystal field perturbation of host material causes partial or complete lifting of degeneracies of $^{2s+1}L_J$ levels. $Eu^{3+}$ emits red upon irradiation with UV. The fine structure and relative intensities of transitions in the absorption and luminescence spectra of $Eu^{3+}$ can be used to probe the local environment around $Eu^{3+}$ ion. $Eu^{3+}$ ions show broad bands in the UV regions of electromagnetic spectra. These bands arise due to the electronic transfer taking place from one or more neighbouring atoms to $Eu^{3+}$ ion. These absorption bands are termed as charge transfer bands or precisely ligand to metal charge transfer band. Energy position of charge transfer band strongly depends on nature of the ligands. These transitions are very intense compared to f-f transitions they are allowed by the Laporte selection rule (Binnemans *et al.* 2015). $Eu^{3+}$ ions are well known for its narrow emission. They exhibit narrow emission line due to internal f-f transitons. When $Eu^{3+}$ ions are embedded in a site with inversion symmetry, $^5D_0$-$^7F_1$ magnetic dipole transition is dominating and we get orange emission (~592 nm). If they are embedded

in a site without inversion symmetry, $^5D_0$-$^7F_2$ electric dipole transition is dominating and we will get red emission (610-620 nm) (Chien *et al.* 2016). In practical inorganic phosphors, both electric dipole and magnetic dipole transitions occurs simultaneously, but their intensities will be different. The fluorescence intensity ratio of $^5D_0$-$^7F_2$ to $^5D_0$-$^7F_1$ is known as asymmetry ratio. It gives a measure of degree of distortion of local environment around $Eu^{3+}$ ion. The split in $^5D_0$-$^7F_0$ transition gives information about the site occupancy of $Eu^{3+}$ ion. The appearance of $^5D_0$-$^7F_0$ transition is an indication of lowering of site symmetry and it shows a red shift with increase in covalancy of $Eu^{3+}$ ion (Linda *et al.* 2016). $Eu^{3+}$ doped red phosphors are of great importance due to their high lumen equivalent, high stability, photostabiity at the same time. Moreover a fluorescent light emitter with red line emitter (610-615 nm) is a best compromise between color rendering and efficacy (Binnemans *et al.* 2015).

Important properties of $Eu^{3+}$ in brief

- Emission wavelength of $Eu^{3+}$ strongly depends on its local environment, co-ordination number and degree of distortion
- Magnetic dipole f-f transitions are parity allowed
- Electric dipole f-f transitions are parity forbidden
- When $Eu^{3+}$ occupies a site with inversion symmetry, $^5D_0$-$^7F_1$ magnetic dipole transition dominates, orange emission dominates.
- When $Eu^{3+}$ occupies a site without inversion symmetry, $^5D_0$-$^7F_2$ electric dipole transition dominates, red emission dominates
- The split in $^5D_0$-$^7F_0$ determines the site occupancy of $Eu^{3+}$.

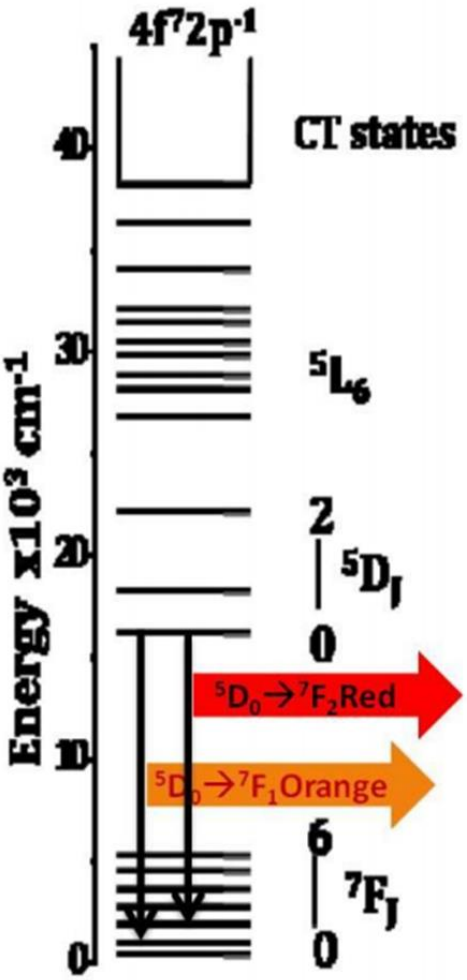


**Fig. 1.8** : Energy level diagram of $Eu^{3+}$(Feldman *et al*. 2003)

### 1.11 Perovskite structure

Perovskites are the class of inorganic crystalline materials having a general formula $ABX_3$. Where A and B are cations and X is anion. Perovskites are of great interest because most structures are close to ideal cubic structure, but frequently they are highly distorted resulting in structures having lower symmetry such as orthorhombic, tetragonal, trigonal etc. The lattice distortions can be governed by temperature, pressure, chemical composition etc. They have potential applications in various fields due to their interesting electronic, electromechanical and conductive properties. This structure is named after the mineral perovskite $CaTiO_3$, which was the first known material having this structure. Perovskites can be widely found at

anywhere and almost every elements in the periodic table can be incorporated to this structure (Davies *et al*. 2008). The ideal perovskite has a stoichiometry $ABX_3$, where A and B are cations and X is anion. A cations are usually larger and more electropositive cations. B site cations are relatively smaller and electronegative metals. A site can be occupied with alkali metals, alkaline earth metals, lanthanides, or $6^{th}$ period p block elements such as $Pb^{2+}$, $Bi^{3+}$. B site can be occupied with transition metals, also p block elements such as $Al^{3+}$, $Ga^{3+}$, $Ge^{4+}$, $As^{5+}$, $Sb^{5+}$, $Te^{6+}$ etc. Most common anions are oxide ions. The most common way to visualize the perovskite structure is the three dimensional array of corner sharing $BX_6$ octahedra with A site cation occupying the 12 co-ordinate cuboctahedral cavity that is formed between 8 octahedra. Ideal cubic perovskite belongs to space group Pm-3m. Perovskite is a highly versatile structure in which vide variety of structural variations are possible (Saparov *et al.* 2016). The distortions can arise due to octahedral tilting or first or second order JahnTeller distortions. One important factor determines the structure of perovskite is the relative size of A and B cations. If the A cation perfectly fit the cavity formed by 8 $BX_6$ octahedra. The ideal perovskite structure will be obtained. The degree of distortion from ideal symmetry can be expressed in terms of tolerance factor ($\tau$).

$$\tau = \frac{(RA + RB)}{\sqrt{2}RB+RX}$$

$R_A$, $R_B$, $R_X$ are the ionic radii of A cation, B cation and X anion. $\tau = 1$means size match between ions are perfect and leads to formation of cubic perovskite. When $\tau$ is larger than 1 it means size of A cation is too large to fit the cavity and if $\tau$ is smaller than 1 it means A cation is too small compared to the cavity formed by 8 $BX_6$. The $BX_6$ octahedra can expand, contract or tilt in order to compensate for the mismatch in ionic radii of A and B site cations (Davies *et al*. 2008).

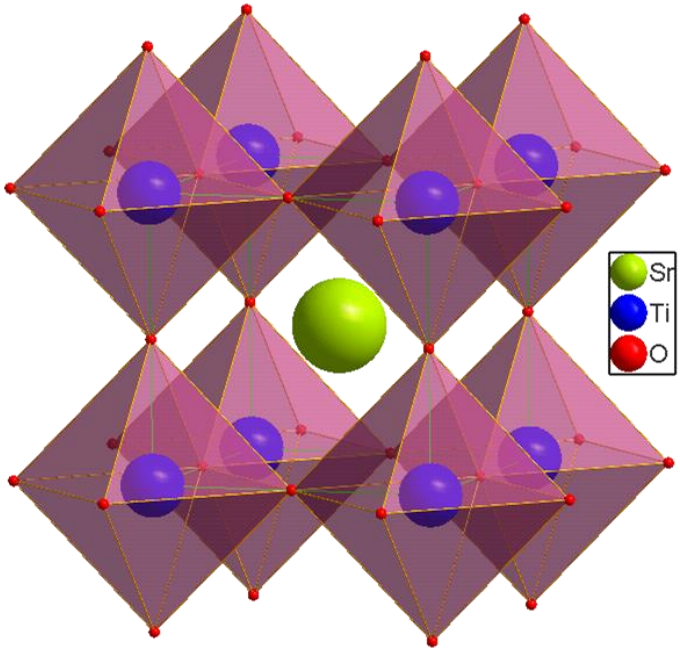


**Fig. 1.9** : Simple Perovskite structure(Davies *et al*. 2008)

### 1.12 Double Perovskites

Double perovskites are named so because their unit cell is double as that of simple perovskite. They are an important class of material because of its flexibility in structure and its vastness and configurationally space spanning. We can tailor the properties of perovskite type compounds by the partial substitution of ions on A or B sites. Recently double perovskites with general formula $AA'BB'O_6$, $A_2BB'O_6$ and $AB_{1/3}B'_{2/3}O_3$ have been received much attraction due to their interesting properties in various fields such as ferroelectrics, super conductors, photonics, photocatalysts and host etc. They offer a lot of scope for aliovalent cation substitutions at A and B sites. (Howard *et al.* 2003) Because of this a lot of compositional modifications can be achieved in this system. Among the double perovskites, $A_2BB'O_6$, obtained by the partial substitution of half of B site cation with another cation B', shows great interest as the host material of photoluminecent applications (Valsala *et al.* 2014).

Most of $A_2BB'O_6$ perovskites possess a divalent cation at the A site. B site cations have a large range of oxidation state combinations with divalent A cation. The average B site cation oxidation state is four. This can be obtained by the suitable combinations B

$^{2+}$/B'$^{6+}$, B$^{1+}$/B'$^{7+}$, B$^{3+}$/B'$^{5+}$ and B$^{4+}$/B'$^{4+}$. Thus with varying oxidation states from 1+ to 7+ almost every element in the periodic table can be included. For an A$^{3+}$cation, average B

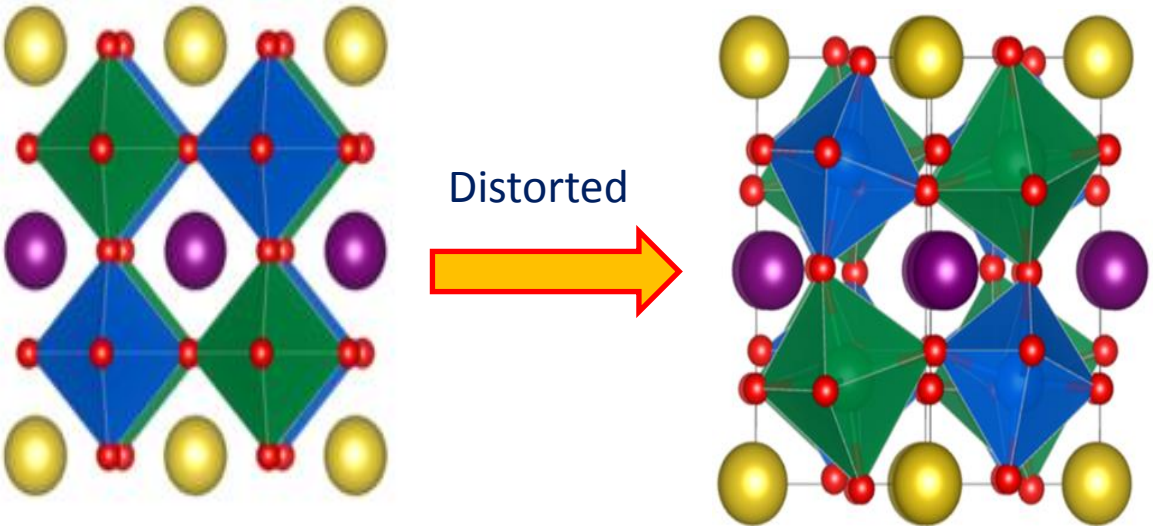


**Fig. 1.10** : Ideal double perovskite structure and distorted perovskite structure (Anderson *et al.* 1994).

site cation oxidation state is three, which can be obtained by the combinations of B$^{4+}$/B'$^{2+}$, B$^{3+}$/B'$^{3+}$ and B$^{1+}$/B'$^{5+}$. Here the B site cations can remain disordered or they can order in different ways to obtain B site ordered double perovskites (Anderson *et al.* 1994).

There are three types of ordering that are exhibited by A and B cations in double perovskites. Most commonly found ordering is rock salt type ordering. It is the most symmetric type of ordering. Here B and B' (or A and A') cations order analogous to cation and anion positions in the rock salt type structure. Rock salt arrangement is also known as 0D ordering, because here every B'$X_6$ octahedra isolated from all the other B'$X_6$ octahedra. Another type of ordering is the columnar ordering where B cations alternate in two different directions. It is also termed as 1D ordering. But this type of ordering occurs only for compounds with two different A cations. When B' cation is occupied with a d$^0$ transition metal in high oxidation state ( Mo$^{6+}$, W$^{6+}$, Nb$^{5+}$, Ta$^{5+}$, Ti$^{4+}$).

B and B' cations can order in a layered manner, where they alternate in only one direction. Dual cation ordering occurs in double perovskites AA'BB'$O_6$, $A_2BB'O_6$ such as Table 1.1 : Table of Different ordering types, aristo type space group and corresponding examples of double perovskites.

| Ordering Type | Aristo type Space group | Examples |
|---|---|---|
| **B site rock salt type** | $Fm\bar{3}m$ | $Ba_2MgWO_6$ |
| **Columnar** | P4/mmm | $NdSrMn^{3+}Mn^{4+}O_6$ |
| **Layered** | P4/mmm | $La_2CuSnO_6$ |
| **A site rock salt** | $Fm\bar{3}m$ | $NaBaLiNiF_6$ |
| **Columnar** | $P4_2/mmc$ | $CaFeTi_2O_6$ |
| **Layered** | P4/mmm | $YBaMn_2O_5$ |
| **Body centered** | $Im\bar{3}$ | $CaCuTi_4O_{12}$ |

layered ordering of A cations and rock salt type ordering of B site cations. B and B' cations having large difference in size and ionic radii is the driving force for cation ordering (King *et al.* 2010, Anderson *et al.* 1994). Rock salt type ordering is highly favourable because it maximizes the distance between B cation which are highly charged. Here each B' cation has 6 B cation as nearest neighbours. In columnar ordering each B'cation has 4 B and two B' cation as nearest neighbours. Layered ordering is least preferable ordering with respect to electro statically, because each B' cation has two B cation and four B' cation as nearest neighbours (Davies *et al*. 2008)

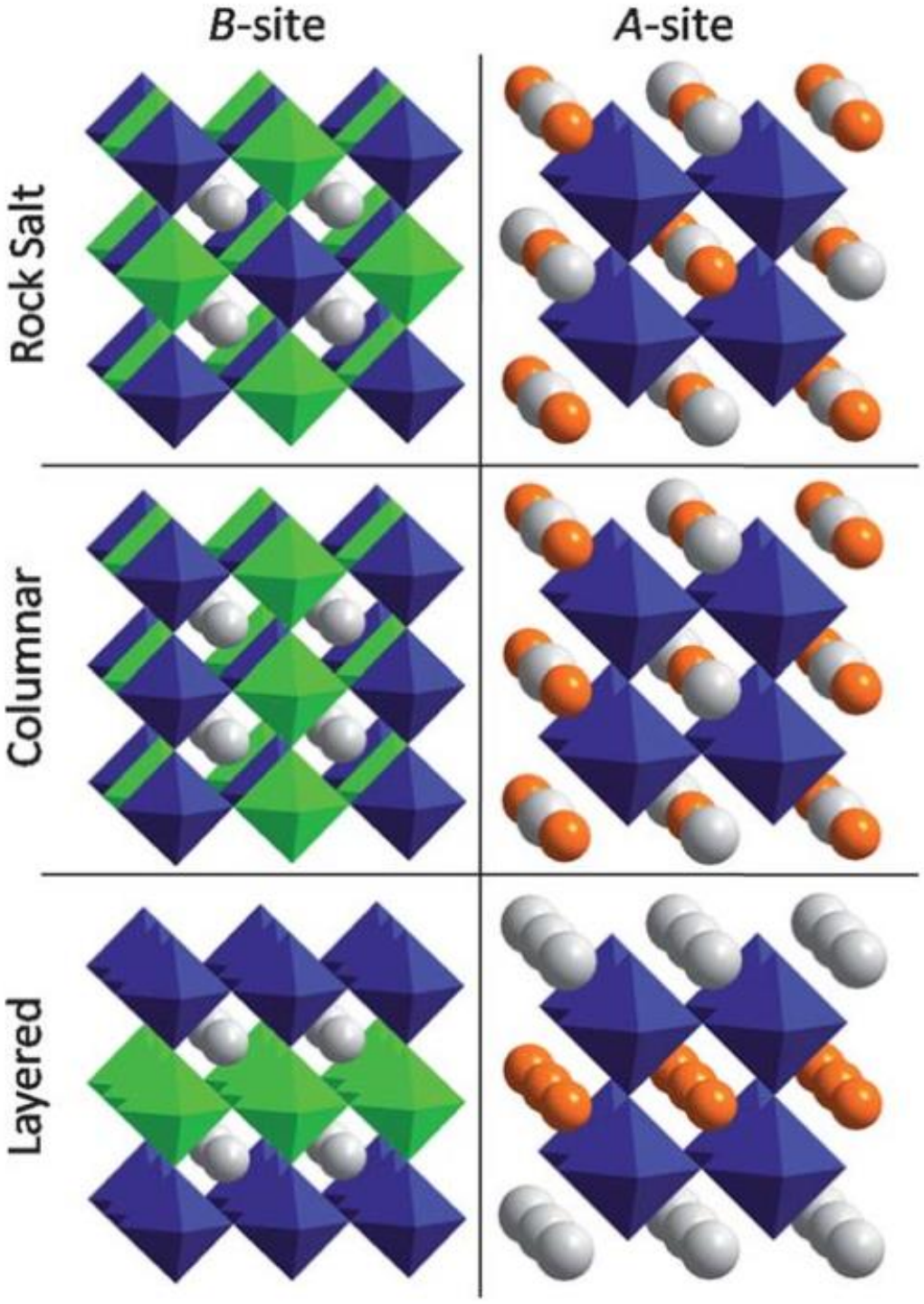


**Fig. 1.11** : Different cation ordering mechanisms in double perovskites (Davies *et al*. 2008)

## 1.13 Literature Review of Perovskite type red phosphors

Ha *et al.* have investigated the photo physical properties of europium-doped calcium titanate for near ultra-violet excitation. $CaTiO_3:Eu^{3+}$(*x*=0.1, 0.5, 1, 3, 7, 8.5 mol %) phosphors were synthesized by using the solid-state reaction method. The structures and basic properties of the phosphors were characterized by using X-ray diffractometer, scanning electron microscope, UV-visible spectrophotometer, and X-ray photoelectron spectrometer. UV Visible absorption spectra showed that a strong absorption band in NUV was observed around 397 nm, corresponding to $^7F_0$-$^5L_6$ arising from doped $Eu^{3+}$ ions. Strong red luminescence corresponding to $^5D_0$-$^7F_2$ transition of $Eu^{3+}$ under near ultra-violet excitation was observed at 614 nm. The intensities of the CTB were 0.2% of f-f transitions of $Eu^{3+}$ at 397 nm ($^7F_0$-$^5L_6$), which were quite insignificant. Therefore the contribution of this CTB to the emission process in these phosphors was almost negligible. It was found that $CaTiO_3:Eu^{3+}$ was a red-emitting phosphor and had higher efficiency for operation under near ultra-violet excitation (Ha *et al.* 2011).

Hou *et al.* have developed a novel perovskite type red phosphor $CaLa_{1-x}MgM'O_6:xEu^{3+}$(M'=Nb,Ta,0<x<1) by high temperature solid-state reaction in air and their structural and optical properties were investigated. The peaks in the excitation spectrum mainly exist at about 466 and 396nm, which are attributed to the $^7F_0$-$^5D_2$ and $^7F_0$-$^5L_6$ transitions of $Eu^{3+}$ ions. In the emission spectrum dominant red emission peak at 617nm is observed and is due to the electric dipole transition $^5D_0$-$^7F_2$. The optimal concentration of $CaLaMgM'O_6:Eu^{3+}$ to obtain the strongest PL intensity were 40% and 30% respectively.$Ca(La_{0.6}Eu_{0.4})MgNbO_6$ achieved high quantum efficiency of 31.2% of $Y_2O_3:Eu^{3+}$ and 98.4% of commercial red emitting compound $Sr_2Si_5N_8:Eu^{3+}$ excited by blue(466) light.: The CIE chromaticity coordinates of red emission of the $Ca(La_{0.6}Eu_{0.4})MgTaO_6$ and $Ca(La_{0.6}Eu_{0.4})MgNbO_6$ phosphors (x=0.662, y=0.338) are found to be very close to the standard of NTSC(x=0.670, y=0.330).The obtained results have demonstrated the potentiality of $CaLa_{1-x}MgM'O_6 : xEu^{3+}$(M'=Nb, Ta) phosphors for the fabrication of near UV/blue GaN – based WLEDs ( Hou *et al.* 2012).

Zhao *et al.* have successfully synthesized novel red phosphor $Eu^{3+}$ doped $Ca_2AlNbO_6$ by high temperature solid state reaction technique and its photo

luminescent properties were investigated. XRD analysis indicate that these phosphors possess a monoclinic structure. Upon excitation with 398nm and 466nm the phosphor showed strong red emission at 617nm, corresponding to the $^5D_0$-$^7F_2$ transition of $Eu^{3+}$ ion. The PL properties of $Ca_2AlNbO_6$:0.05$Eu^{3+}$ phosphors are found to be not significantly influenced by the calcinations time and charge compensation. The emission intensity is found to be two times more than that of commercial $(Y_{.95}Eu_{0.05})_2O_3$ phosphors under blue light irradiation. The CIE chromaticity coordinates of red emission of this new phosphor are found to be (0.654, 0.346) which are close to that of standard NTSC. The obtained results have demonstrated the potentiality of this phosphor for the fabrication of near UV/blue GaN – based WLEDs ( Zhao *et al*. 2011)

Yin *et al.* have successfully synthesized a novel red phosphor $La_{2(1-x)}MgTiO_6$:2$x$$Eu^{3+}$ by conventional solid-state reaction method. From their systematic investigations, the optimum doping concentration was identified to be 15%.When excited by UV (395nm) or blue light (465nm) $La_{1.7}MgTiO_6$:0.3$Eu^{3+}$ shows intense red emission, about three times more than that for common red phosphor $Y_2O_3$:$Eu^{3+}$, and two times more intense than that of $Sr_5Si_5N_8$: $Eu^{2+}$.The calculated CIE chromaticity coordinate(x=0.657, y=0.343) showed high color purity and potential for application in lighting field (Yin *et al.* 2012)

Sivakumar *et al*. have synthesized and characterized a series of novel orange red emitting phosphor compositions $Sr_{1.9-x}Ba_xEu_{0.05}Li_{0.05}CaWO_6$ ($x$ = 0-1.9 ). XRD results revealed the phase transition from monoclinic to pseudo-cubic structure for $x \leq 0.2$. All the compositions showed broad charge transfer band and orange red (MD and ED emission). Here the PL studies have been carried out for $Eu^{3+}$ substituted (both A and B sites)$A_2CaWO_6$(A=Sr,Ba) phosphor and the results revealed that A- substituted compositions show both ED and MD transitions for Sr analogue composition whereas only intense MD transitions are found for Ba analogue compositions. The ED and MD transitions are found for all compositions (under CT band/394nm); however it is found that relative emission intensity depend on Ba content present in the host lattice. All the compositions showed dominant ED transitions under blue ray excitation(465nm). The red emission of $Sr_{1.9-x}Ba_xEu_{0.05}Li_{0.05}CaWO_6$ ($x$=0-1.9) is found to be 4.5 times greater than that of commercial red phosphor under 465 excitation and hence this phosphor

could be a potential candidate for WLED based on blue GaN LED (Sivakumar *et al*. 2008) .

Sun *et al.* have developed thermally stable $La_2Ti_2O_7:Eu^{3+}$ phosphors for blue chip white LEDs with high color rendering index via solid state reaction method. This phosphor showed intense red emission around 612 nm corresponding to $^5D_0$-$^7F_2$ transition of $Eu^{3+}$ ion. The luminous intensity of this phosphor material excited at 465 nm showed comparable intensity as that excited at 396nm.The concentration quenching was occurred at 30 mole %. The emission intensity increased steadily with increasing calcinations temperature till $1500^0$C. The WLED fabricated by coating a mixture of $Y_3Al_5O_{12}:Ce^{3+}$ and $La_2Ti_2O_7:Eu^{3+}$ onto blue InGaN chip showed higher color rendering index than $Y_3Al_5O_{12}:Ce^{3+}$ WLED. The phosphor obtained by their experiments could find high power commercial $Y_3Al_5O_{12}$: $Ce^{3+}$ WLEDs (Sun *et al.* 2010).

Zhu *et al.* had studied the crystal structure of double perovskite systems $Ca_{2-x}Ba_xLaNbO_6:Eu^{3+}$ phosphors by means of powder XRD and Rietveld refinements. Depending upon value of Ba/Ca ratio the structure of the compound changes from monoclinic phase P21/n($Ca_2LaNbO_6$) to monoclinic phase C2/m ($Ba_2LaNbO_6$). $Eu^{3+}$ ions act as a structural probe to investigate the phase transitions and evolution of photoluminescent properties. $Ca_2LaNbO_6$ : $Eu^{3+}$ exhibit intense red emission due to the high distortion of $LaO_8$ polyhedra in the system. In $Ca_2LaNbO_6$, $Eu^{3+}$ is occupying in a centrosymmetric site resulting in weak magnetic dipole transitions. This study is guide to explore new luminescent materials with controllable optical properties via variation in the local co-ordination environment (Zhu *et al.* 2015)

Yu *et al.* have studied the photoluminescent properties of $Eu^{3+}$ doped triple tellurium double perovskite type phosphors $LiBaLaTeO_6$, $NaBaLaTeO_6$, $NaCaBiTeO_6$ and $LiBaBiTeO_6$. $NaCaBiTeO_6$ exhibit emission in orange red region corresponding to the $^5D_0$-$^7F_1$ magnetic dipole transition. All the other three compositions showed dominant red emission with short decay time corresponding to the forced electric dipole transition. Difference in photoluminescent properties can be linked with the difference in the co-ordination environment of $Eu^{3+}$ ion. In $NaCaBiTeO_6$ system $Eu^{3+}$ ion is occupying in the B site (Na,Bi). In the other three compositions $Eu^{3+}$ ion is occupying in the A site. $NaCaBiTeO_6$ system is preferred with high quantum efficiency value of 38.

6% and orange red emission with UV excitation. Also $NaBaLaTeO_6$ : $0.1Eu^{3+}$ phosphor exhibited bright red emission having high quantum efficiency value of 32.8% and 16.5% by UV and blue excitations. The quantum efficiency values are found to be higher than commercially available phosphors and $Eu^{3+}$ doped perovskite type red phosphors, indicating that this phosphor can be a potential candidate for WLED applications (Yu *et al.* 2014).

Lal *et al.* have studied the structural photoluminescent and judd-offelt analysis of red emitting $Eu^{3+}$ doped $SrLaLiTeO_6$ red emitting phosphor. XRD analysis confirms that no phase change occurs with $Eu^{3+}$doping. Raman analysis shows the complete A site substitution of $Eu^{3+}$ions in the lattice. As $Eu^{3+}$ion concentration increases the band gap is found to be decreased it can be linked with the reduction in lattice volume. Photoluminescence spectra shows dominant red emission and concentration quenching occurs at 10 mol% $Eu^{3+}$doping. Thermal stability the phosphor was confirmed by using temperature dependant photoluminescence analysis. With a maximum quantum efficiency value of 55% and color purity value close to 100, the prepared phosphors can be a suitable candidate for WLED application (Lal *et al.* 2019).

Li *et al.* have developed $Eu^{3+}$doped double perovskite type red phosphors $LiLaMgWO_6$ for WLED applications. The prepared phosphors can be indexed by the monoclinic perovskite type structure having space group C2/m. They can be excited by CT band, near U V (393 nm) and blue (463 nm) excitations. Due to the decreased symmetry of A site in these systems strong red emission occurs at 615 nm. Concentration quenching occurs at 30 mol%. The mechanism of concentration quenching can be ascribed to dipole - quadrupole type interaction taking place between $Eu^{3+}$ ions. Temperature dependent photoluminescence shows some decrease in the PL intensity with temperature, activation energy is found to be 0.225 eV. They exhibit high quantum yield value of 87% and good chromaticity co-ordinates in the red region (Li *et al.* 2016).

Liu *et al.* have developed $Eu^{3+}$doped $NaLaMgWO_6$ double perovskite type red emitting phosphors and their structural evolution and delayed quenching mechanism had studied. Phosphors were fitted with monoclinic space group of C2/m. Layered ordering of A site cation and alternate ordering of $MgO_6$ and $WO_6$ octahedra is found in

this system. The Raman mode T2g (1) shows a blue shift which indicates A site uniformly substituted double ordered perovskites. Delayed quenching concentration upto 50 mol% was obtained for the system. The concentration quenching occurs mainly due to quadrupole-quadrupole interaction. These phosphors also exhibit good thermal stability. The results `suggest that the host material is excellent candidate for solid state lighting applications (Liu *et al.* 2016).

Sun *et al.* had developed $Ca_2LuTaO_6$ red emitting phosphors for WLED applications. These phosphors exhibit dominant red emission peaking at 616 nm, optimum doping concentration was found to be 40%. Mechanism of energy transfer between the $Eu^{3+}$ions is found to be dipole-dipole interaction among the activator ions. CIE chromaticity co-ordinates are found to be (0.66, 0.33) with a color purity of 95.8%. The integrated emission intensity of the sample is about 3.79 times great as commercial $Y_2O_3$ : $Eu^{3+}$ red phosphor. $Ca_2LuTaO_6$: $0.4Eu^{3+}$ exhibit high internal quantum efficiency of 74% and good thermal stability (Sun *et al.* 2019).

**1.14 Importance of present work**

White Light emitting diodes have brought a lighting revolution over the existing lighting technologies with its spectacular properties such as high brightness, long operation time and environment friendliness. They are supposed to be the light source for future. Most of the WLED approaches are based on wavelength conversion by one or more phosphor materials. Common approach for white light generation is the combination of blue InGaN LED and $Y_3Al_5O_{12}$: $Ce^{3+}$ yellow phosphor (Ye *et al.* 2013). However, the white light obtained from this configuration possess low Color Rendering Index (CRI <80) due to lack of red component. Addition of suitable red phosphors easily pumped by NUV or blue LED combination can improve CRI .Yet another technique is to incorporate blue, green and red emitting phosphors with near UV (380-420 nm) LED chip. Currently used red phosphors are sulphide or nitride based ones such as $Y_2O_2S$: $Eu^{3+}$, CaZnS: $Eu^{2+}$, $Sr_2Si_5N_8$: $Eu^{2+}$ and Sr[$LiAl_3N_4$]: $Eu^{2+}$. But for practical applications, they are chemically unstable and also the nitride and oxynitride phosphors are difficult to synthesize because of its tedious synthesis conditions such as nitrogen pressure and high temperature calcinations. So there is a great demand for energy efficient and stable

oxide red phosphors that can be excited by near UV/ blue LEDs (Zhang *et al.* 2017, Yu *et al*. 2014).

Perovskite type red phosphors are found to possess promising luminescent characteristics. Perovskite systems possess high chemical and physical stability. Perovskite systems offer a lot of scope for wide variety of aliovalent cation substitutions at the A and B sites Because of this, lot of compositional modifications can be achieved in this system to tune the properties induced by the structural distortions. From the Literature review of the perovskite red phosphors, it is found that most of them were prepared via conventional solid state route. The high energy ball milling process can enhance the reactivity of the system and reduce the reaction temperature. Also ball milling produces finely grinded particles with uniform size distribution and better morphology that will reduce scattering loses and assist luminescence (Kong *et al.* 2002, Yang *et al.* 2010 ) We have tried ball milling method for phosphor synthesis also in addition to solid state reaction method. Also photoluminescent characteristics can be improved with appropriate charge compensation methods. Most commonly charge compensation method is done by the suitable addition of alkali metals such as Li, Na, K, etc. However, such charge compensation methods are carried out intentionally by addition of some monovalent ions which may lead sometimes to some secondary phases. In the present study, the charge compensation is built in systems wherever it is needed.

# Chapter 2 A

## Influence of B site cation on the photoluminescence properties of perovskite type $SrGd_{0.425}M_{0.5}O_3$ : $0.075Eu^{3+}$ (M = Nb, Sb, Ta) red phosphors.

*In the perovskite system, role of B site cation in the photoluminescent characteristics of $SrGd_{0.425}M_{0.5}O_3$ : $0.075Eu^{3+}$ (M = Nb, Sb, Ta) red phosphors is discussed in this chapter. Optical studies reveals that niobate sample possess better luminescence properties compared to the other two, that means efficient energy transfer to $Eu^{3+}$ ions takes place in the niobate system. Higher luminescent intensity, high quantum efficiency of 30.8%, color purity value of 82% and CIE color co-ordinates values of (0.61, 0.36) suggests the niobate sample as a good phosphor candidate.*

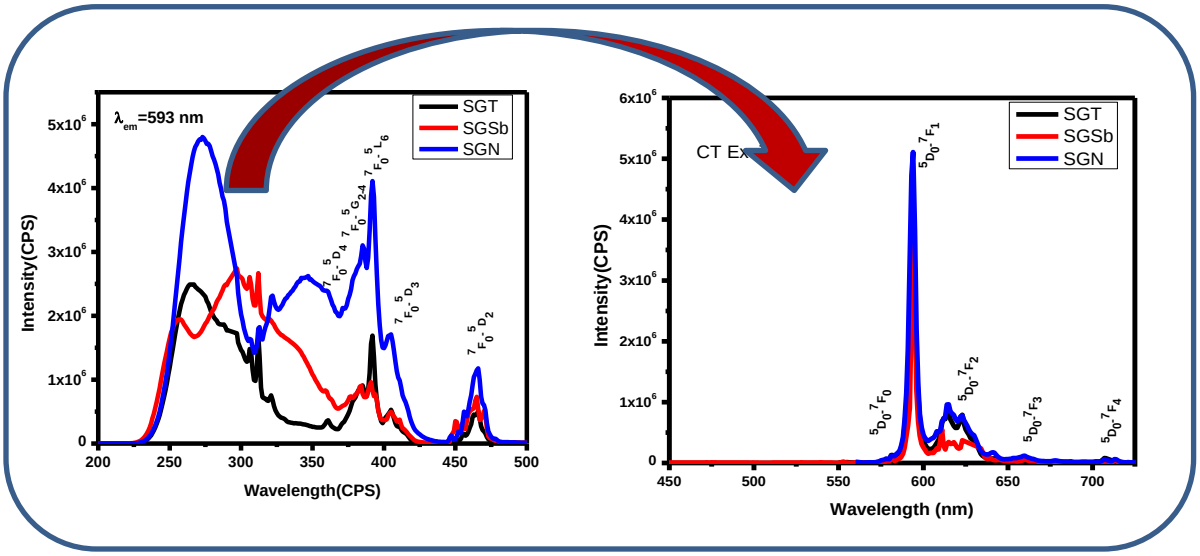

## 2A.1 Introduction

White light emitting diodes have been seeking great attention for general lighting applications. They offer many promising characteristics such as environmental friendliness, high luminous efficiency and long life time etc. Commercial pc-WLEDs normally use a 450–470 nm blue GaN LED chip covered by a yellowish phosphor coating, which is usually made of YAG:$Ce^{3+}$. White light emitted by this combination lacks red component and thus the color rendering index is low. Warm white light with improved CRI can be obtained by two different ways: One is to combine an UV chip with tricolor (red, green and blue) phosphors and the other is to compensate the red light deficiency of YAG:$Ce^{3+}$ based LED with a separate red-emitting phosphor (Crawford, *et al*.2009*)*. Sulfide based phosphors are currently used in that approach which is highly harmful to the environment. Also, the current red phosphor cannot absorb light efficiently in UV region and its brightness is about 8 times less than that of the available green and blue phosphors. In addition there are some draw backs such as, lack of chemical stability, environmental pollution etc. A novel phosphor material that can be effectively excited in the near UV and visible region with good absorption and emission properties, good thermal and chemical stability, minimal thermal quenching, high quantum yield and preferably inexpensive phosphors should be developed to meet the above requirements (George *et al*. 2013).

Perovskites with a general formula $ABO_3$ are the most studied class of compounds due to their high symmetry and versatile application potential. Multiple ion substitution in the structure can be used to alter their physical properties and results in complex perovskites. They possess immense application potential in various fields such as super conductors, ferro- electrics, magneto dielectrics etc. The structure is so feasible that we can substitute about 80% of elements in the lattice (King *et al.* 2007). Perovskite systems are known to be excellent host for photoluminescent materials. They possess good chemical stability, high levels of absorption in near UV region etc. $Eu^{3+}$ ion possess strong emission in red spectral region. Doping with suitable host materials, we can develop potential red phosphors for white light emitting diode (WLED) applications (Lei *et al.* 2008).

There is a great influence of host structure in the photoluminescent properties of phophors. B site cation plays an important role in the photoluminescent properties of the perovskite systems. Thus by varying the B site cation we can tailor the photoluminescent properties of $AB_{0.5}B'_{0.5}O_3$, perovskite system. Double perovskites of the type $A_2LnMO_6$ (A- alkaline earth metal, Ln- Lanthanide, M- transition metal, d block metal) are of interest as good phosphor hosts (Lei *et al.* 2013). With these considerations, we have prepared perovskite type red phosphors with formula $SrGd_{0.425}M_{0.5}O_3$:$0.075Eu^{3+}$ (M = Nb, Sb, Ta) by the conventional solid state reaction route. The variation in their photoluminescent characteristics with variation in B site cation is studied.

## 2A.2 Experimental

Perovskite type red phosphors, $SrGd_{0.425}M_{0.5}O_3 : 0.075Eu^{3+}$ (M = Nb, Sb, Ta) were synthesized by the conventional solid state reaction method using $SrCO_3$ , $Gd_2O_3$ , $Nb_2O_5$ , $Sb_2O_5$, $Ta_2O_5$ and $Eu_2O_3$ as the starting materials. The stoichiometric amount of the reagents were mixed and grinded well in an agate mortar with acetone as the wetting medium. Mixing is followed by drying in a hot air oven at 100˚C. Mixing and drying processes were carried out thrice to obtain a homogeneous mixture. The obtained mixture was calcined at 1400 ˚C for 6h. The crystalline structure of the samples was examined with an X-ray powder diffractometer (X'Pert Pro PANalytical, operated at 40 kV and 30 mA, Cu-Kα = 0.15406nm, 2θ range = 10–90). Absorbance study of the samples were carried out using a Shimadzu, UV-2450 UV–Vis spectrophotometer in the 200–800 nm wavelength range using barium sulfate as a reference. The excitation and emission spectra were recorded on a Fluorolog HORIBA fluorescence spectrophotometer with a Xe lamp (450 W) as the excitation source. Luminescence lifetime of the phosphors was recorded by the phosphorimeter attached to Fluorolog3 spectrofluorimeter. All measurements were taken at room temperature.

## 2A.3 Results and Discussion

### 2A.3.1 XRD Analysis

Figure 2A.1 shows the powder XRD analysis of the samples, $SrGd_{0.425}M_{0.5}O_3$ : $0.075Eu^{3+}$ (M = Nb, Sb, Ta). All the peaks can be indexed to orthorhombic perovskite type structure with a space group Pbam(55)(JCPDS file no 01-087-0568). Having $AB_{0.5}B'_{0.5}O_3$ perovskite structure, Sr is expected to occupy in XII Co-ordinated site and Gd and Nb in VI co-ordinated site. Also 1:1 ordering of the cations is possible with $Gd^{3+}$ and $M^{5+}$ occupying alternate B site in a NaCl type arrangement, maximizing the distance between similar cations (Jing *et al*. 2015, Davies *et al.* 2008). Lattice parameters of the phosphors were calculated using the equation, $1/d^2_{hkl} = (h^2/a^2) + (k^2/b^2) + (l^2/c^2)$.

An ideal perovskite structure ($ABX_3$) can be viewed as a combination of $BX_6$ octahedra and $AX_{12}$ cuboctahedra. For ideal case, $(R_X+R_A) = \sqrt{2}\ (R_X+R_B)$. But in reality, because of the mismatch of ionic radii of A and B cations distortions from ideal structure occurs. The degree of distortion is termed as tolerance factor and can be calculated as $\tau = (R_X+R_A)\ /\sqrt{2}\ (R_X+R_B)$ *(Valsala et al.* 2014). The ionic radii of the cations

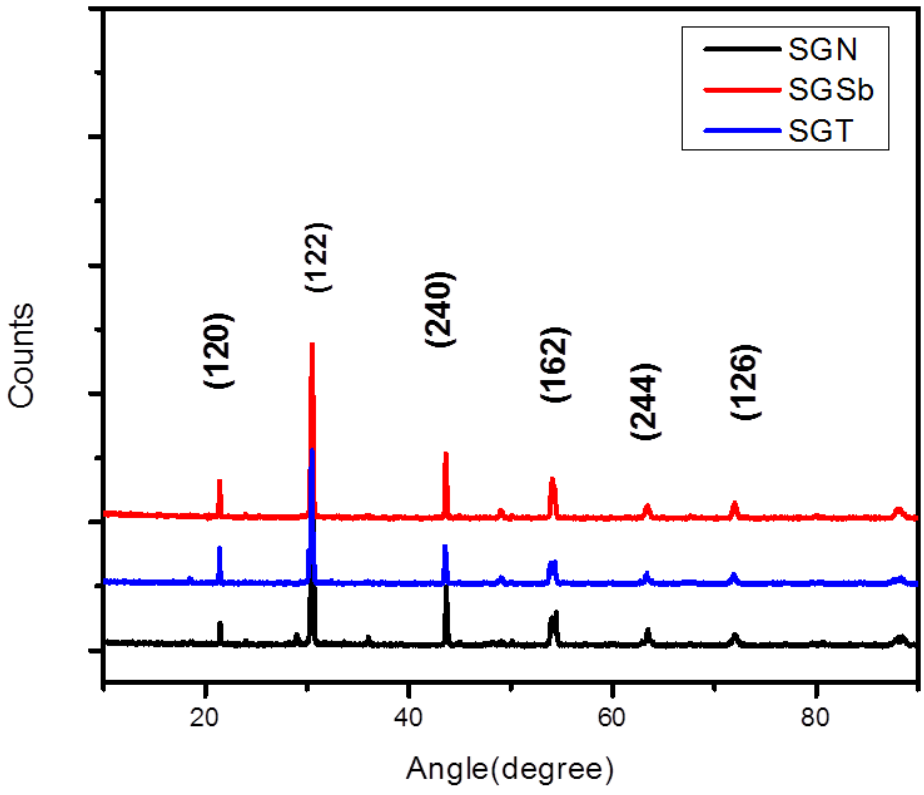


**Fig. 2A.1** : Powder XRD analysis of $SrGd_{0.425}M_{0.5}O_3$ : $0.075Eu^{3+}$ (M = Nb, Sb, Ta) samples.

Table 2A.1 : Lattice parameters, cell volume and tolerance factor of the $SrGd_{0.425}M_{0.5}O_3$ : $0.075Eu^{3+}$ (M = Nb, Sb, Ta) samples.

| Samples | a (Å) | b (Å) | c (Å) | Cell Volume ($Å^3$) | τ |
|---|---|---|---|---|---|
| **SGN** | 5.8723 | 11.7408 | 8.2878 | 571.40 | 0.92 |
| **SGSb** | 5.8868 | 11.7033 | 8.2812 | 570.53 | 0.89 |
| **SGT** | 5.8683 | 11.7318 | 8.2915 | 570.83 | 0.92 |

are Sr (1.44 Å ), Gd (0.938Å), Sb (0.76 Å ), Nb (0.64 Å), Ta (0.64 Å ), $Eu^{3+}$ (0.947 Å) respectively. Tolerance factor, lattice parameters and cell volume of the sample are listed in Table 2A.1. Values of τ are close to unity, indicating the formation of orthorhombic perovskite structure.

### 2A.3.2 UV-Visible Analysis

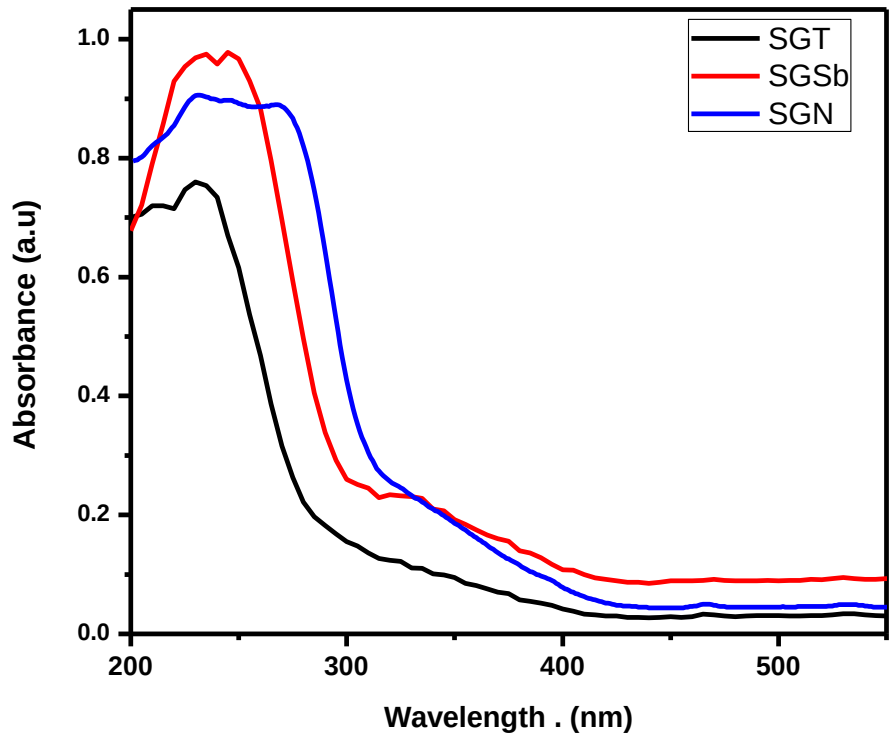


**Fig. 2A.2** : UV visible absorption spectra of $SrGd_{(0.425)}M_{0.5}O_3$:*0.075*$Eu^{3+}$ (M = Nb, Sb, Ta).

Figure 2A.2 represents the UV visible absorption spectra of $SrGd_{(0.425)}M_{0.5}O_3$:*0.075*$Eu^{3+}$ (M = Nb, Sb, Ta). All the samples exhibit strong absorption in the 200-400 nm range. These broad absorption can be linked to the metal to ligand

charge transfer transition (Ropp, 2004). Band gap values are calculated from the absorption spectra using Shapiro's method, by extrapolating the onset of absorption to the wavelength axis and estimated bandgap values are listed in Table 2A.2. Band gap values are found to be increasing in the order SGN< SGSb< SGT. Low band gap value of 3.8eV makes the niobate sample suitable for application in pc-WLEDs.

### 2A.3.3 Photoluminescence Properties

Photoluminescence excitation spectra of the three samples were recorded for an emission at 593 nm. Niobate phosphor exhibit broad and intense charge transfer band (CT band) compared to the other two. A red shift of C T band is observed for niobate and tantalate samples. It can be linked with the lower ionisation potential of Nb (6.88 eV) in comparison with Ta (7.89 eV) and Sb (8.64 eV) (Linda *et al.* 2014). Characteristic f-f transition peaks of $Eu^{3+}$ is found to be less intense compared to CT band. This indicates that these phosphors have efficient excitation under near UV light. The sharp excitation peaks at 360 nm, 384 nm, 392 nm, 404 nm and 465 nm can be attributed to

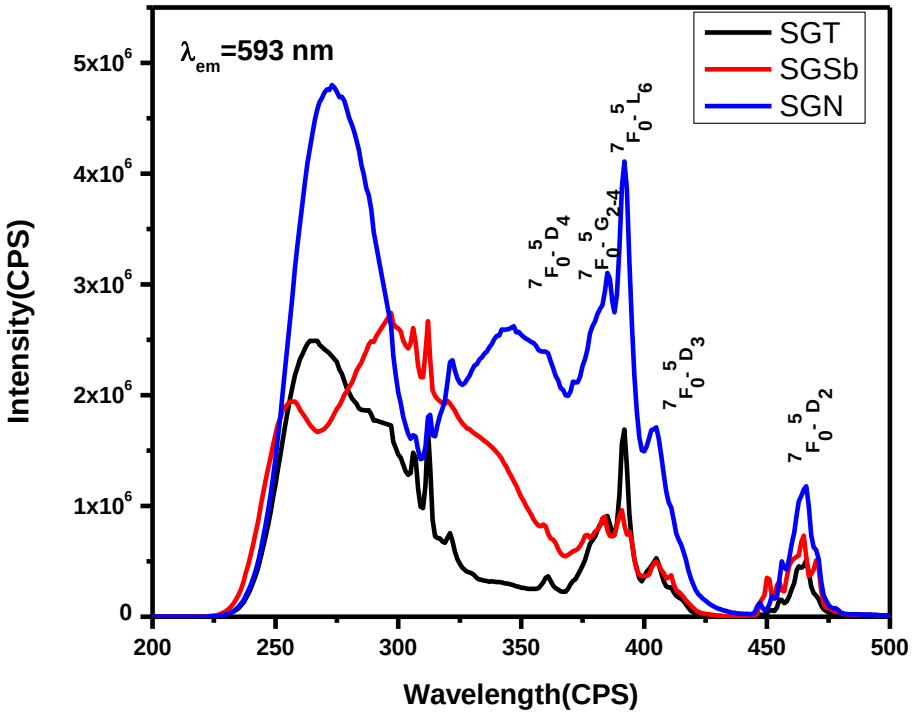


**Fig. 2A.3** : Photoluminescence excitation spectra of $SrGd_{(0.425)}M_{0.5}O_3$:*0.075*$Eu^{3+}$

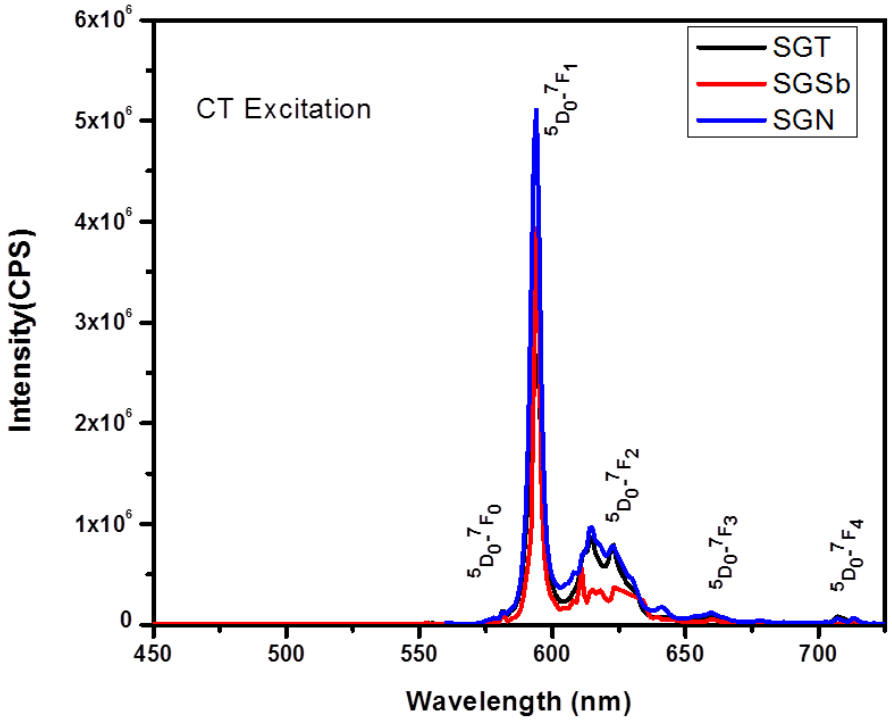


**Fig 2A.4**: Photoluminescence emission spectra of $SrGd_{(0.425)}M_{0.5}O_3$:*0.075*$Eu^{3+}$ (M = Nb, Sb, Ta) for CT band excitation

$^7F_0$-$^5D_4$, $^7F_0$-$^5G_{2\text{-}4}$,$^7F_0$-$^5L_6$, $^7F_0$-$^5D_3$, $^7F_0$-$^5D_2$ transitions of $Eu^{3+}$ ions in the host (Hou *et al.* 2012, Liu *et al.* 2017). The f-f transition peak at 392 nm ($^7F_0$-$^5L_6$) is very intense in the niobate phosphor compared to tantalate and antimonite sample, which indicates that efficient energy transfer to $Eu^{3+}$ ions takes place in niobate sample. So the niobate sample is found to be suitable for WLED applications compared to the other two.

Photoluminescence emission spectra of the samples for CT band excitation is given in Fig 2A.4. All the samples exhibit sharp and dominant orange emission at 593 nm due to $^5D_0 \rightarrow {}^7F_1$ magnetic dipole transition. In accordance with the photoluminescent excitation spectra, the emission intensity is also greater for the niobate phosphor sample. Also the emission peaks are found to be very narrow (fwhm~4nm). The narrow emitting phosphors are of great interest for WLED applications.

Photoluminescence emission spectra of the samples for an excitation of 392 nm is recorded. The emission intensities are in accordance with the intensities of $^7F_0$-$^5L_6$ transition peaks in the excitation spectrum. Niobate sample exhibit intense red emission compared to the other two. The emission profiles of niobates and tantalates looks similar. The phosphor samples exhibit two peaks at 593 nm and 614 nm. The orange emission at 593 nm due to $^5D_0 \rightarrow {}^7F_1$ magnetic dipole transition is dominating

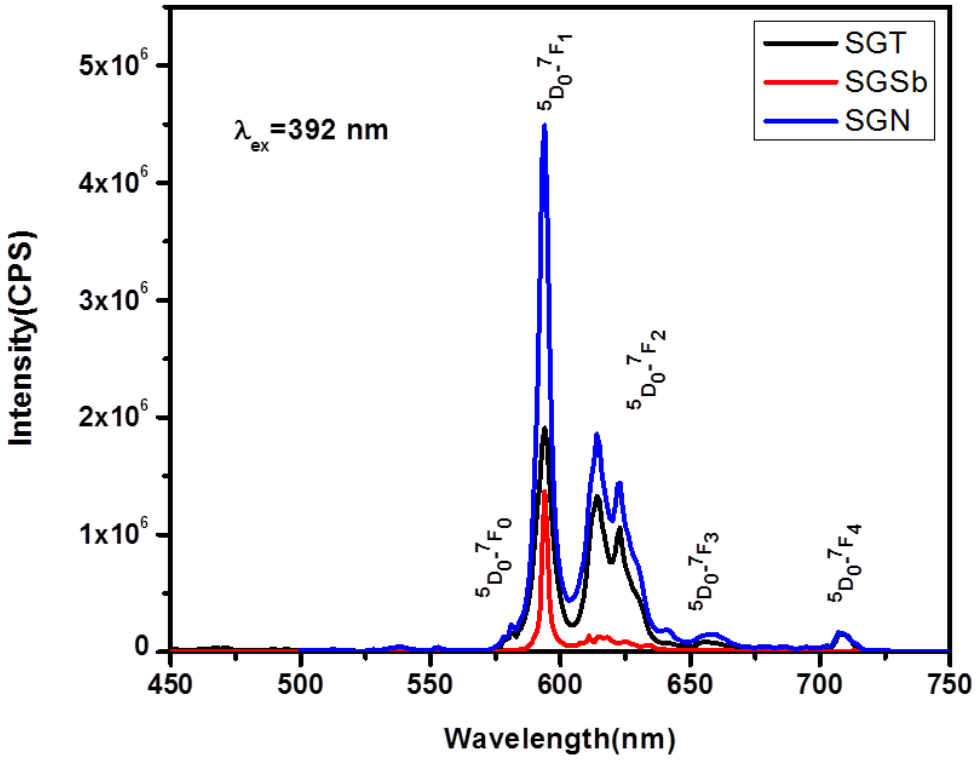


**Fig. 2A.5**: Photoluminescence emission spectra of $SrGd_{(0.425)}M_{0.5}O_3$:*0.075*$Eu^{3+}$ (M = Nb, Sb, Ta).

than the red emission at 614 nm due to $^5D_0 \rightarrow {}^7F_2$ forced electric dipole transition. This indicates that $Eu^{3+}$ is mainly situating in a centro symmetric site in the lattice. The luminescence intensity ratio of $^5D_0 \rightarrow {}^7F_2$ to $^5D_0 \rightarrow {}^7F_1$ is termed as the asymmetric ratio. It can be considered as a probe to detect inversion symmetry around $Eu^{3+}$ ions in the lattice. Asymmetric ratio of the samples are listed in Table 2A.2. Low values of asymmetric ratio indicates highly symmetric environment of $Eu^{3+}$ in the lattice. There

was no evident split was observed for $^5D_0 \rightarrow {}^7F_0$ transition, which indicates the single site occupancy of $Eu^{3+}$ in the lattice (Liu *et al.* 2019).

### 2A.3.4 Lifetime analysis

Lifetime analysis of the samples was carried out. The decay curves of the samples under UVexcitation is shown in Figure 2A.6. The decay curves exhibit a single exponential behavior and the decay curves can be fitted to a single exponential function, $I = A \exp(-x/\tau)$ .where I, A and τ are intensity, fitting parameter, and decay time respectively. This confirms the single site occupancy of $Eu^{3+}$ in the lattice. Lifetime values of the samples are given in Table 2A.2.

Table 2A.2: Lifetime, asymmetric ratio and efficiency of $SrGd_{(0.425)}M_{0.5}O_3$:*0.075*$Eu^{3+}$ (M = Nb, Sb, Ta) phosphors

| Sample | Lifetime (ms) | Bandgap (eV) | Asymmetric ratio | Efficiency (%) | CIE color co-ordinates | Color purity (%) |
|---|---|---|---|---|---|---|
| **SGN** | 1.91 | 3.8 | 0.42 | 30.8 | (0.61, 0.36) | 82 |
| **SGT** | 2.54 | 4.2 | 0.68 | 30.7 | (0.60, 0.35) | 79 |
| **SGSb** | 2.46 | 4.0 | 0.10 | 14 | (0.60, 0.37) | 80 |

Assuming that only radiative and non radiative processes are essentially involved in the depopulation of $^5D_0$ states of $Eu^{3+}$ ion, the quantum efficiency ( η) can be expressed as;

$$\eta = A_{rad}/(A_{rad} + A_{nrad}) \rightarrow (2A.1)$$

where $A_{rad}$ and $A_{nrad}$ are radiative and non radiative transition probabilities respectively. The emission intensity (I) can be taken as the integrated (S) of $^5D_0 - {}^7F_{0\text{-}4}$ emission curves as;

$$I_{i\text{-}j} = \hbar\, \omega_{i\text{-}j}\, A_{i\text{-}j}\, N_i \sim S_{i\text{-}j} \rightarrow (2A.2)$$

Where i and j are initial ($^5D_0$) and final ($^7F_{0\text{-}4}$) levels respectively; $\hbar\omega_{i\text{-}j}$ is the transition energy, $A_{ij}$ is the Einstein's coefficients of spontaneous emission and $N_i$ the population

of $^5D_0$ emitting level. The experimental coefficient of spontaneous emission ($A_{0j}$) can be calculated based on the relation

$$A_{oj} = A_{o1} (I_{oj}/ I_{o1}) (\upsilon_{01}/ \upsilon_{0j}) \quad \rightarrow (2A.3)$$

$\upsilon_{01}$ and $\upsilon_{0j}$ are the energy baricenters of the $^5D_0$ - $^7F_1$ and $^5D_0$ -$^7F_j$ energy levels determined from the emission peaks of $Eu^{3+}$ ion. $A_{01}$ is the Einstein's coefficients of spontaneous emission between $^5D_0$ and $^7F_1$ energy levels given as.

$$A_{0\text{-}1} = n^3(A_{0\text{-}1})vac \sim 50S^{-1} \quad \rightarrow (2A.4)$$

where n, average refractive index 1.506 and $(A_{0\text{-}1})$ vac = 14.65 $S^{-1}$. The lifetime ($\tau$) of the $^5D_0$ states, $A_{rad}$, $A_{nrad}$ are related as ;

$$A_{tot} = 1/\tau = A_{rad} + A_{nrad} \quad \rightarrow (2A.5)$$

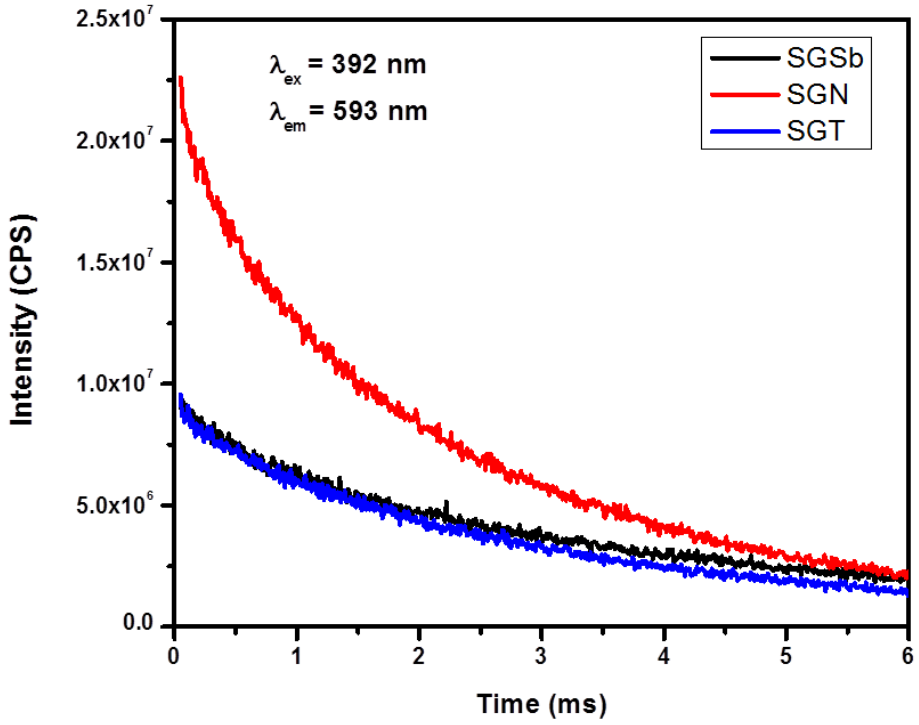


**Fig 2A.6**: Lifetime analysis of $SrGd_{(0.425)}M_{0.5}O_3$:*0.075*$Eu^{3+}$ (M = Nb, Sb, Ta).

Using equations (2A.1-2A.5) quantum efficiency values are calculated and tabulated (Su *et al.* 2008, Linda *et al.* 2014). Niobate and tantalate samples exhibit high efficiency than that of antimonate phosphor sample. CIE color co-ordinates was calculated using chromaticity color co-ordinate calculator. Color co-ordinates are tabulated in Table 2A.2. Color purity of the sample was checked using the equation, $color\ purity =$

$\frac{\sqrt{\{(x-xi)2+(y-yi)2\}}}{\sqrt{\{(xd-xi)2+(yd-yi)2\}}} \times 100$, where (x,y) are the color co-ordinates of the sample, ($x_i$,$y_i$) are color co-ordinates of white illuminant, and ($x_d$,$y_d$) are chromaticity co-ordinates of the dominant wavelength. Here (x,y) = (0.65,0.33), ($x_i$,$y_i$) = (0.33,0.33) and ($x_d$,$y_d$) = (0.67,0.33) ( Wu *et al.* 2012).

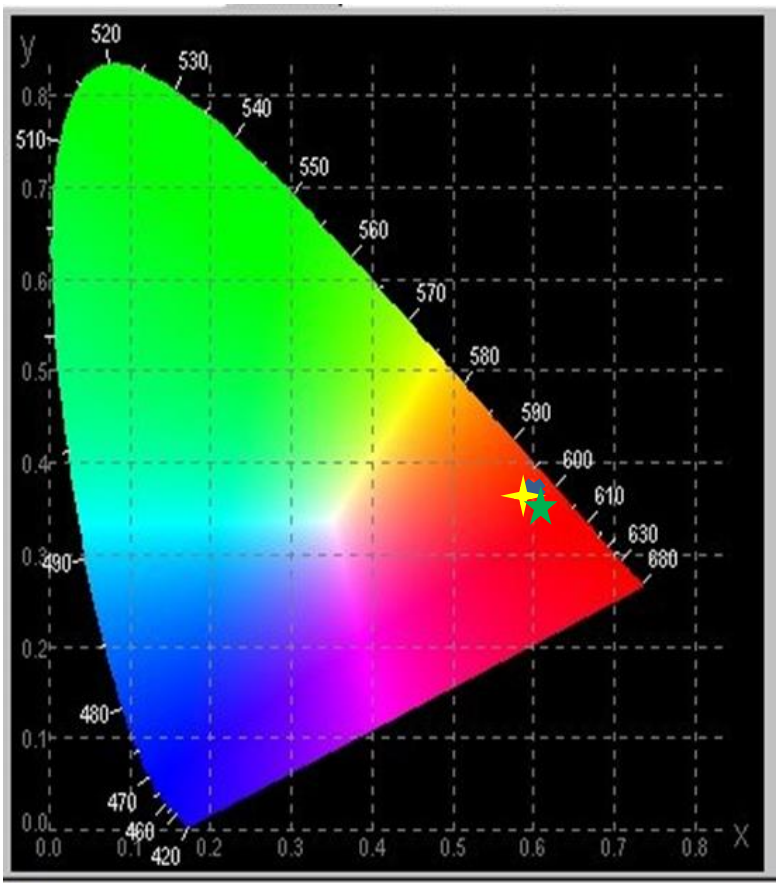


**Fig. 2A.7** : CIE chromaticity diagram $d_{(0.425)}M_{0.5}O_3$:*0.075*$Eu^{3+}$ (M = Nb, Sb, Ta,).

## 2A.4 Conclusions

In summary the structural and optical properties of the systems $SrGd_{(0.425)}M_{0.5}O_3$:*0.075*$Eu^{3+}$ (M = Nb, Sb, Ta) was studied. Studies reveals that niobate sample showed better luminescence properties in terms of luminescence intensity, quantum efficiency and color purity. It is due to the efficient energy transfer to $Eu^{3+}$ taking place in the niobate sample. Higher luminescent intensity, high quantum efficiency of 30.8%, color purity value of 82% and CIE color co-ordinates values of (0.61,0.36) suggests the niobate sample as a good phosphor candidate.

# Chapter 2B

## New Perovskite type Orange Red Emitting Phosphors, $SrGd_{0.5}Nb_{0.5}O_3$ : *x* $Eu^{3+}$ for WLED Applications

*New perovskite type orange red emitting phosphors, $SrGd_{(0.5-x)}Nb_{0.5}O_3:xEu^{3+}$ were synthesized using a high temperature solid state reaction method. $Eu^{3+}$ doped $SrGd_{0.5}Nb_{0.5}O_3$ phosphors has a strong absorption in the UV region. Intense orange red emission is observed for both near UV (392 nm) and blue (465 nm) excitations matching with the output wavelengths of UV and blue LED chips, which can be attributed to the magnetic and electric dipole transitions($^5D_0$-$^7F_{1,2}$) of $Eu^{3+}$. The prepared intense orange red emitting phosphor with higher quantum efficiency could be a promising candidate for white light emitting diode applications.*

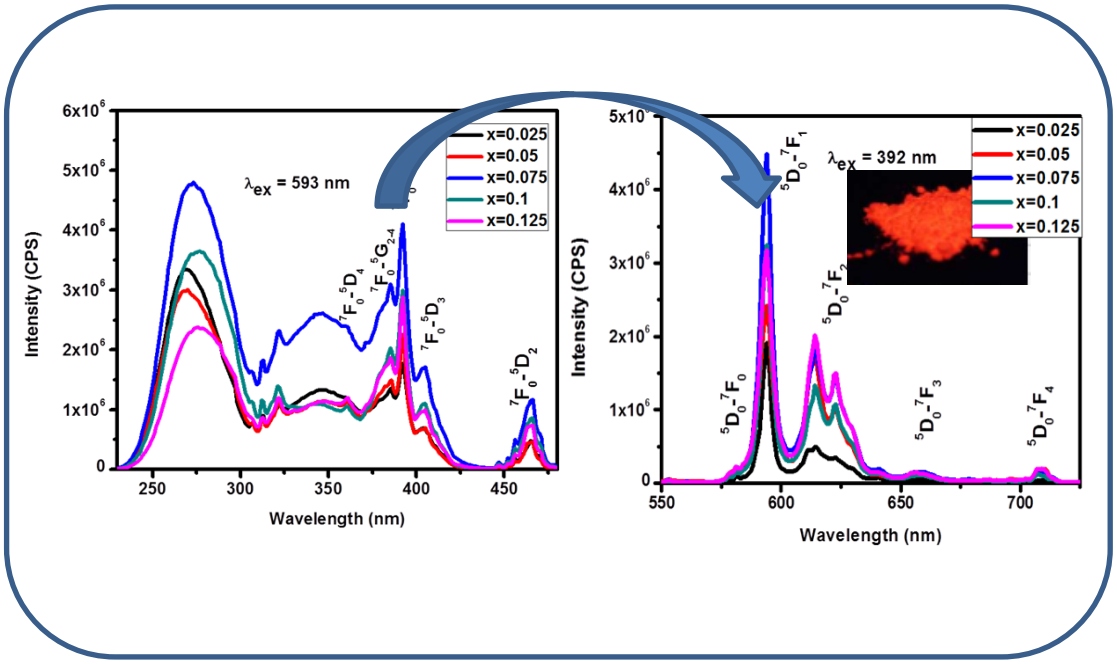


**Aswathy *et al. Mater Lett. 2018, 229, 182-184***

## 2B.1 Introduction

Trivalent Europium is well known for its orange red luminescence due to the intraconfigurational f-f transitions. $Eu^{3+}$ ion exhibits mainly two emission lines and the emission determined by their local environment in host crystals. The fine structure and relative intensities of transitions in the absorption and luminescence spectra of $Eu^{3+}$ can be used to probe the local environment of $Eu^{3+}$ ion (Li et al. 2016, Binnemans et al. 2015). The properties such as good chemical stability, broad charge transfer (CT) band in the near UV region and the ability to capture radiation from a GaN based LED over a range of wavelengths etc., make perovskites as good host lattices for phosphor materials. $Eu^{3+}$ doped perovskite oxides have been given great attention due to their possible applications as phosphor materials (Nguyen *et al.* 2012, Li *et al.* 2013).

In chapter 2 A, the variation in the photoluminescent characteristics with variation in B site cation is studied. On Comparing, we got good results for $SrGd_{0.425}Nb_{0.5}O_3$: $0.075Eu^{3+}$ system. So the host system is fixed and a series of red emitting phosphors, $SrGd_{(0.5-x)}Nb_{0.5}O_3 : x\ Eu^{3+}$ ($x$ = 0.025, 0.05, 0.075, 0.1, 0.125) were prepared by conventional solid state reaction route and structural, optical and morphological characterizations were done .

## 2B.2 Experimental procedure

A series of $SrGd_{(0.5-x)}Nb_{0.5}O_3 : xEu^{3+}$ ($x$= 0.025, 0.05, 0.075, 0.1, 0.125) phosphors were prepared by a conventional solid state reaction route by using $SrCO_3$, $Gd_2O_3$, $Nb_2O_5$ and $Eu_2O_3$ as the starting materials. The required stoichiometric amounts of these materials were weighed and mixed thuroughly in an agate mortar in acetone medium. The homogeneous mixture was then calcined at 1400˚C for 6h. The crystalline structure of the samples was examined with an X-ray powder diffractometer (X'Pert Pro PANalytical, operated at 40 kV and 30 mA, Cu-Kα = 0.15406nm, 2θ range = 10–90°). The morphological studies of the samples were done by a scanning electron microscope (JEOL, JSM-5600LV) operated at 15kV. Absorbance study of the samples were carried out using a Shimadzu, UV-2450 UV–Vis spectrophotometer in the 200 –800 nm wavelength range using barium sulfate as a reference. The excitation and emission

spectra were recorded on a Fluorolog HORIBA fluorescence spectrophotometer with a Xe lamp (450 W) as the excitation source. Luminescence lifetime of the phosphors was recorded by the phosphorimeter attached to Fluorolog3 spectrofluorimeter.

### 2B.3. Results and Discussion

### 2B 3.1 Structural Studies

Powder X-ray diffraction patterns of $SrGd_{(0.5-x)}Nb_{0.5}O_3$ : *x* $Eu^{3+}$ are given in Figure 2B.1. All the peaks are in good agreement with the reported diffraction pattern of $PbZrO_3$ (JCPDS file no 01-087-0568; orthorhombic perovskite with a space group Pbam (55). With $AB_{0.5}B'_{0.5}O_3$ perovskite structure one expects the Sr to occupy in XII co-ordinated site and Gd and Nb in VI co-ordinated site. Also 1:1 ordering of the cations is possible with $Gd^{3+}$ and $Nb^{5+}$ occupying alternate B site in a NaCl type arrangement, maximizing the distance between similar cations (Jing *et al*. 2015, Davies *et al.* 2008).

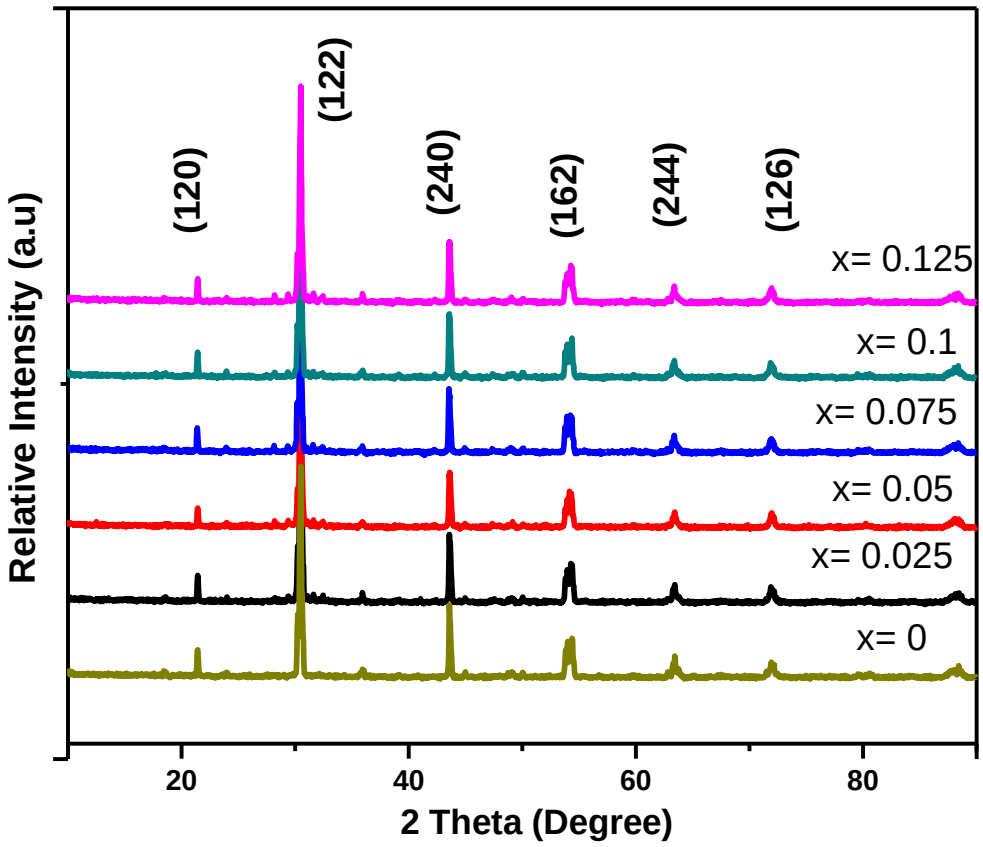


**Fig. 2B.1** : Powder X-ray diffraction patterns of $SrGd_{(0.5-x)}Nb_{0.5}O_3$:*x*$Eu^{3+}$(*x*= 0-0.125)

Due to matching ionic radii and valency $Eu^{3+}$ (0.947 nm) is expected to replace $Gd^{3+}$ (0.938 nm) ions.

### 2B.3.2 Morphological Studies

Figure 2B.2 shows the scanning electron micrographs of the samples. The particles are slightly agglomerated and have a size distribution of 1-5µm.

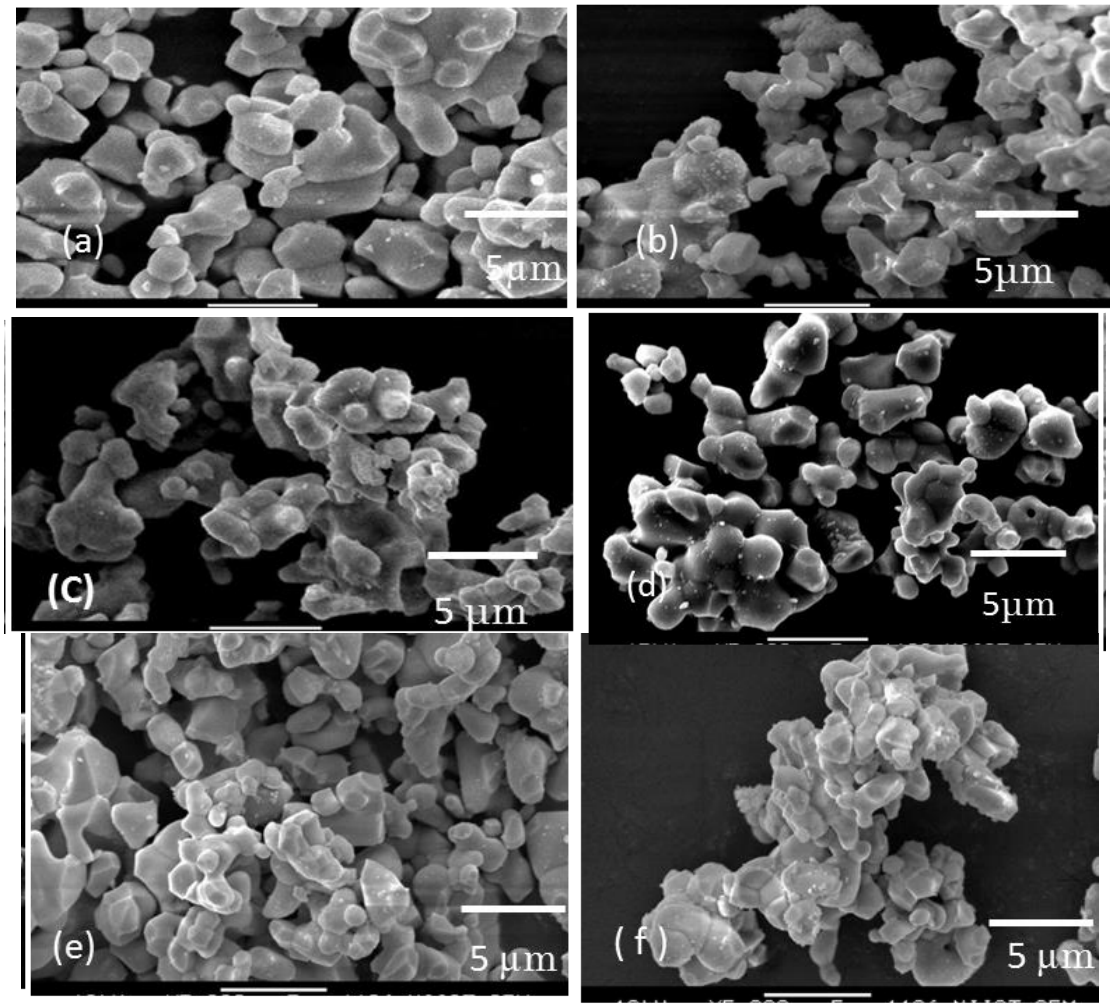


**Fig. 2B.2**: Scanning electron micrographs of $SrGd_{(0.5-x)}Nb_{0.5}O_3$:$xEu^{3+}$ (a) $x$ = 0, (b) $x$ = 0.025, (c) $x$ = 0.05, (d) $x$ = 0.075, (e) $x$ = 0.1 and (f) $x$ = 0.125.

## 2B 3.3 Edax Analysis and Elemental Mapping Analysis

Figure 2B.3 shows the edax analysis of $SrGd_{0.425}Nb_{0.5}O_3$: *0.075*$Eu^{3+}$. Inset table shows the elemental and atomic weight percentage distribution. All the elements are present in the Stoichiometric amount.

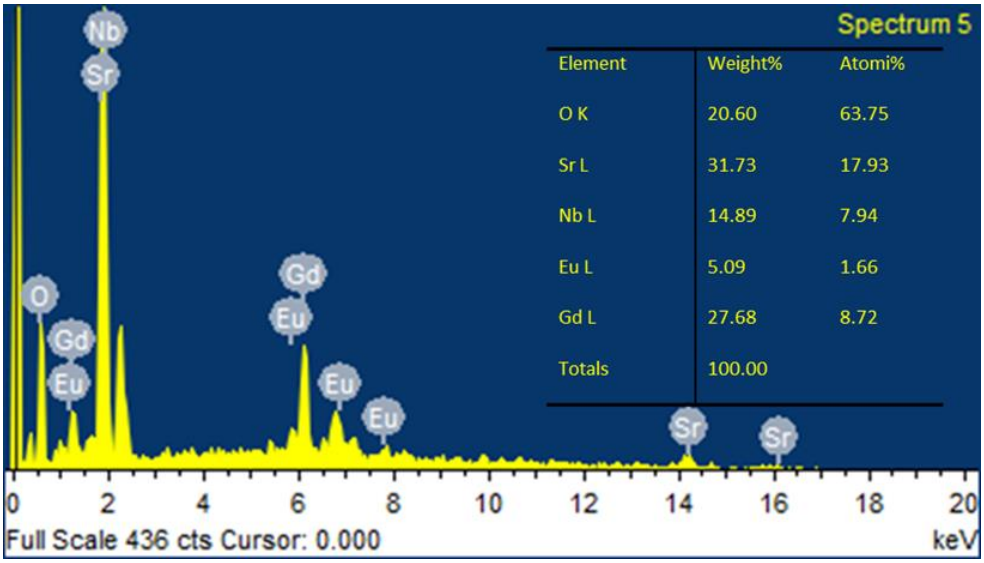


**Fig. 2B.3**: EDAX pattern of $SrGd_{(0.425}Nb_{0.5}O_3$:*0.075*$Eu^{3+}$ (Inset shows the elemental weight and atom. % distribution)

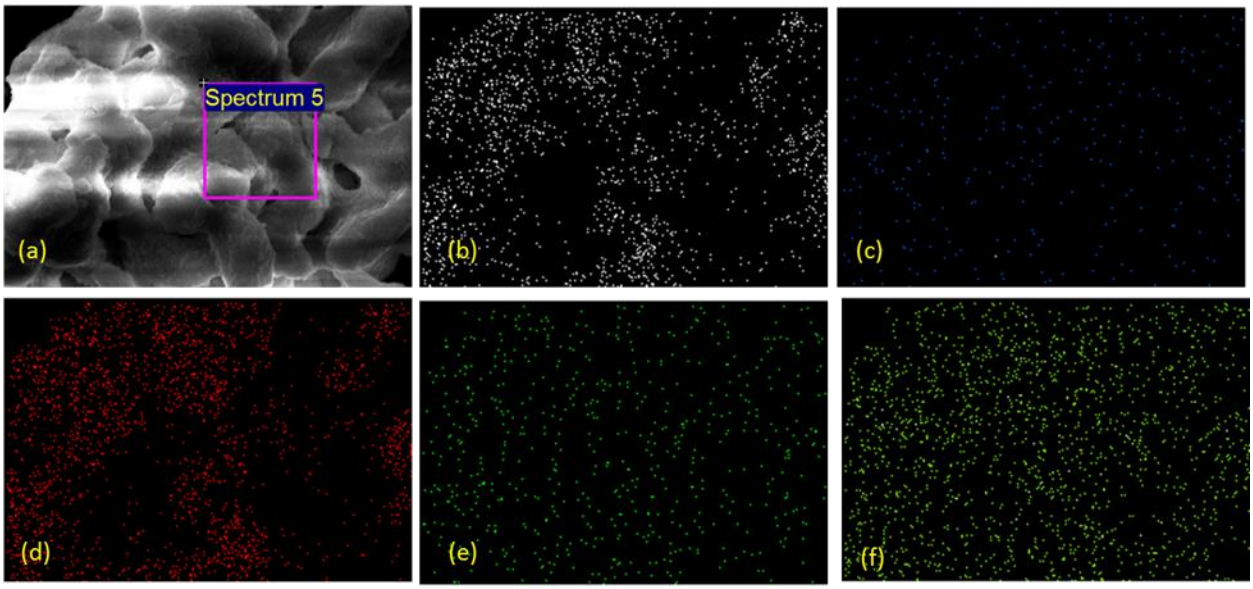


**Fig. 2B.4**: Elemental mapping for $SrGd_{(0.425}Nb_{0.5}O_3$:*0.075*$Eu^{3+}$corresponding to (b) O, (c) Sr, (d) Nb, (e) Eu and (f) Gd.

Elemental mapping analysis of the samples can be seen in Figure 2B.4. Figure shows the uniform distribution of elements in the sample.

### 2B 3.4 Optical Studies

Figure 2B.5 shows the UV visible absorption spectra of $SrGd_{(0.5-x)}Nb_{0.5}O_3:xEu^{3+}$. All the samples exhibit strong absorption in the 200-400 nm range.

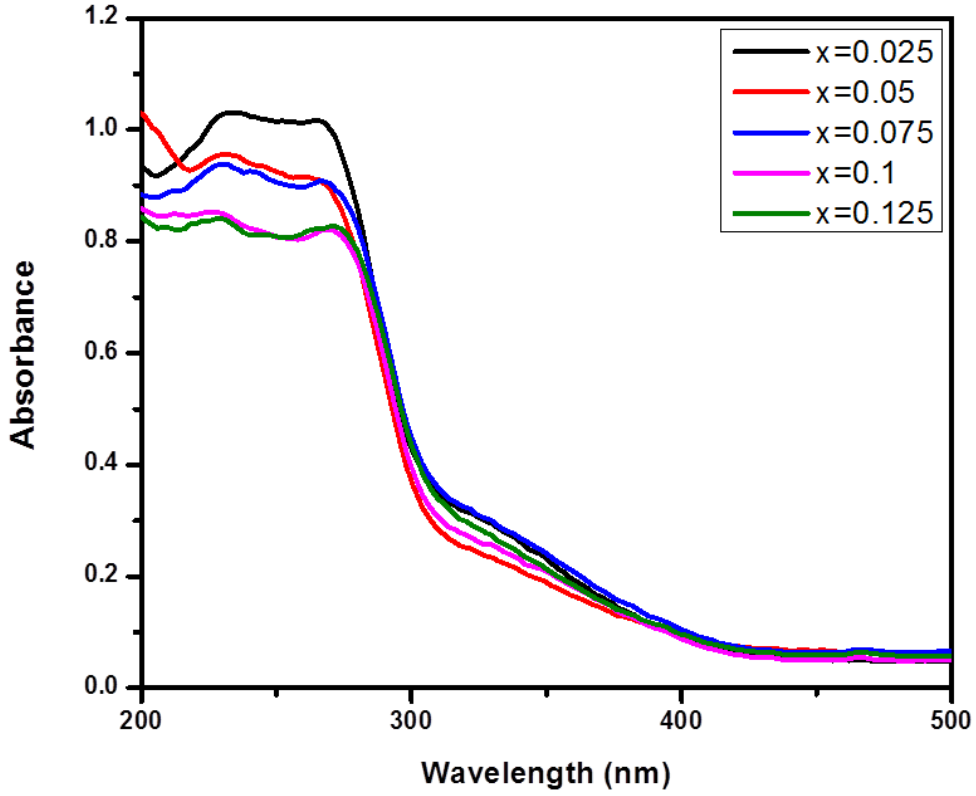


**Fig. 2B.5**: UV visible absorption spectra of $SrGd_{(0.5-x)}Nb_{0.5}O_3:xEu^{3+}$.

Figure 2B.6 shows the photoluminescent excitation spectra of $SrGd_{(0.5-x)}Nb_{0.5}O_3:xEu^{3+}$ for an emission at 593nm. All the samples exhibit broad and intense charge transfer band and the sharp peaks corresponding to $O^{2-}$-$Eu^{3+}$charge transfer and intraconfigurational 4f-4f transitions of $Eu^{3+}$ ions in the host. A slight red shift in the CT band emission peak with increase in $Eu^{3+}$ is observed. This shift can be attributed to an increase in covalency of Eu - O bonds and the co- ordination environment of $Eu^{3+}$ which

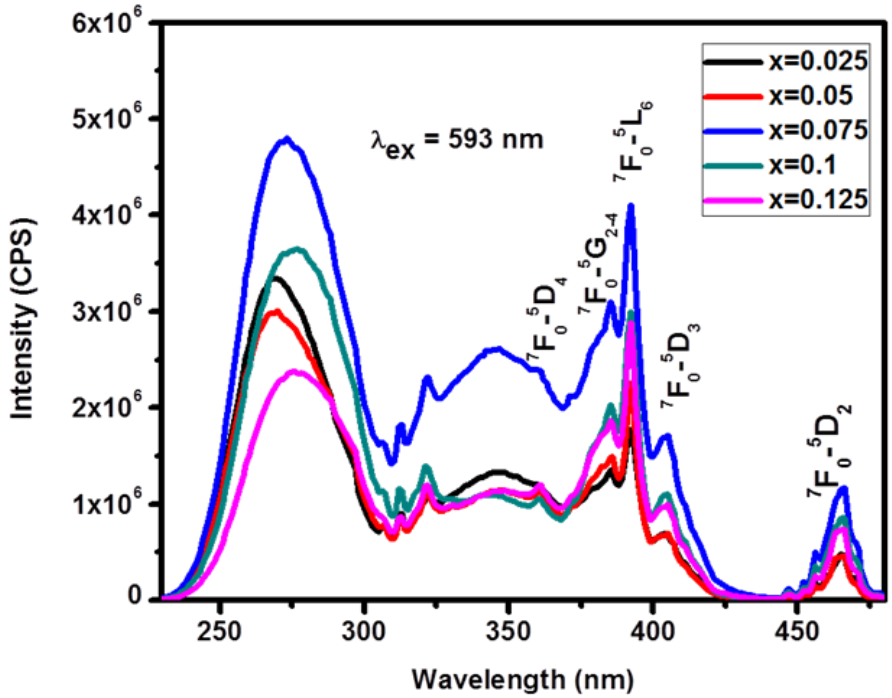


**Fig. 2B.6**: Photoluminescent excitation spectra of $SrGd_{(0.5-x)}Nb_{0.5}O_3:xEu^{3+}$ for emission at 593nm.

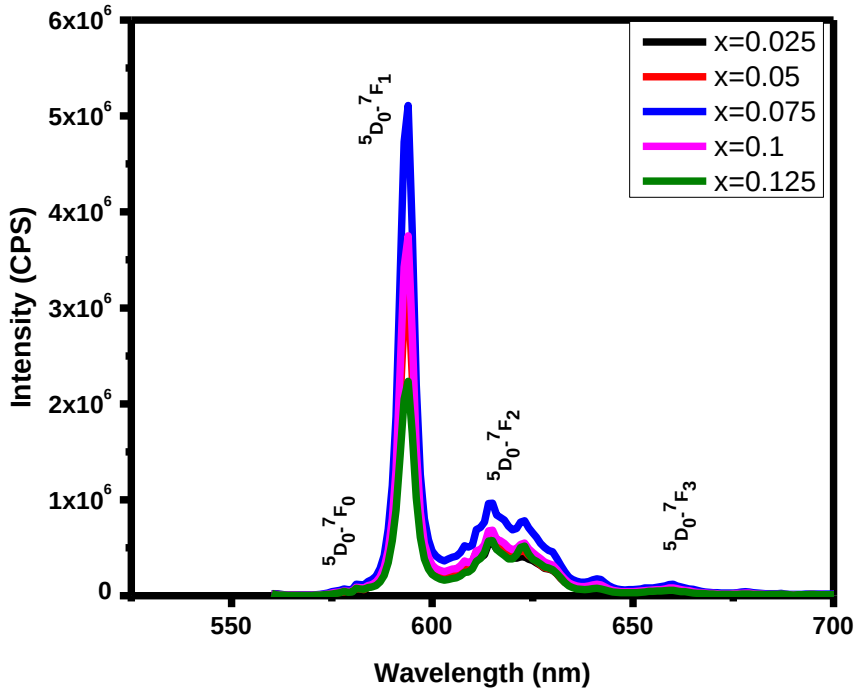


**Fig. 2B.7**: Photoluminescent emission of $SrGd_{(0.5-x)}Nb_{0.5}O_3$: $xEu^{3+}$ samples under CT band excitation

reduces the CT energy ( Sreena *et al.* 2015 ). The sharp excitation peaks at 360nm, 384 nm, 392 nm, 404 nm and 465 nm can be attributed to $^7F_0$-$^5D_4$, $^7F_0$-$^5G_{2\text{-}4}$,$^7F_0$-$^5L_6$, $^7F_0$-$^5D_3$, $^7F_0$-$^5D_2$ transitions of $Eu^{3+}$ ions in the host (Binnemans *et al.* 2016, Li *et al.* 2016). Excitation intensity of the doped samples increases with increase in $Eu^{3+}$ concentration and saturation occurs for 7.5 mol% doping. Excitation peaks at 392 nm and 465 nm matches well with the emission of UV and blue LEDs. This implies that the prepared phosphor materials could be possible candidates for phosphor converted WLEDs in conjunction with UV or blue LEDs.

Photoluminescent emission of $SrGd_{(0.5\text{-}x)}Nb_{0.5}O_3$: $xEu^{3+}$ samples under CT band excitation is given in Figure 2B.7. Samples exhibit orange emission peaking at 593 nm, due to $^5D_0 \rightarrow ^7F_1$ magnetic dipole transition. The narrow emission is suitable for WLED applications. Photoluminescent emission of $SrGd_{(0.5\text{-}x)}Nb_{0.5}O_3$: $xEu^{3+}$ samples under an excitation of 392 nm is given in Figure 2B.8. The phosphor samples exhibit two peaks at

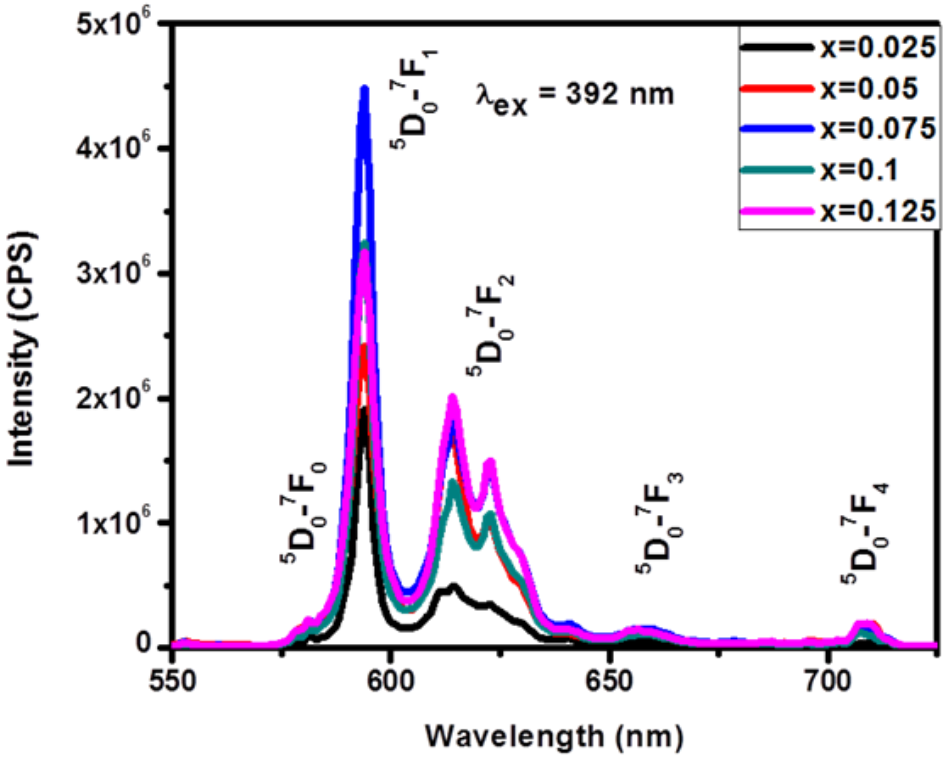


**Fig. 2B.8**: Photoluminescent emission of $SrGd_{(0.5\text{-}x)}Nb_{0.5}O_3$: $xEu^{3+}$ samples under an excitation of 392 nm

593 nm and 614 nm. The orange emission at 593 nm due to $^5D_0 \rightarrow ^7F_1$ magnetic dipole transition is dominating than the red emission at 614 nm due to $^5D_0 \rightarrow ^7F_2$ forced electric dipole transition. This indicates that $Eu^{3+}$ is mainly situating in a centro symmetric site in the Lattice(Fu *et al.* 2017). The emission intensity of the phosphor samples increases considerably with increase in $Eu^{3+}$ concentration upto 7.5 mol% and then decreases due to concentration quenching effect. As the $Eu^{3+}$ concentration increases $Eu^{3+}$ - $Eu^{3+}$ distance reduces and non radiative energy transfer occurs due to cross relaxation leading to concentration quenching (Uitert *et al.* 1967). The asymmetric ratio is a good measure of degree of distortion of $Eu^{3+}$

Table 2B.1: Lifetime, asymmetric ratio and efficiency of $SrGd_{(0.5-x)}Nb_{0.5}O_3:xEu^{3+}$ phosphors

| X | Life time (ms) | Asymmetric ratio | FWHM(nm) | Efficiency (%) |
|---|---|---|---|---|
| **0.025** | 3.27 | 0.26 | 4.4 | 33.3 |
| **0.05** | 2.48 | 0.73 | 6.3 | 32.9 |
| **0.075** | 2.61 | 0.42 | 5.1 | 30.8 |
| **0.1** | 1.84 | 0.41 | 5.0 | 21.2 |
| **0.125** | 1.43 | 0.64 | 5.9 | 18.9 |

site. Table 2B.1 gives the lifetime, asymmetric ratio and efficiency of the prepared samples. The low values of asymmetric ratio confirms the occupancy of $Eu^{3+}$ in a centrosymmetric site. Low values of fwhm is also favourable for WLED applications.

**2B 3.5 Lifetime Analysis**

Lifetime analysis of the samples was done. The decay curves of the samples were recorded under UV excitation and is shown in Figure 2B.7. The decay curves exhibit a single exponential behavior and the decay curves can be fitted to a single exponential function, $I = A \exp(-x/\tau)$ .where I, A and $\tau$ are intensity, fitting parameter, and decay time respectively. This confirms the single site occupancy of $Eu^{3+}$ in the lattice. Lifetime values of the samples are given in Table 2B.1. The lifetime decreases with increase of

$Eu^{3+}$ concentration which can be mainly attributed to the variation of distortion environment of $Eu^{3+}$. Further, the obtained quantum efficiency values are much higher than that of the reported ones in $CaMoO_4$ (12.78%) and perovskites $Ca_2MgWO_6$ (14.05%), $Y_6WO_{12}$ (20.6%) and $SrLa_2Mg_2W_2O_{12}$ (27.1%) (Lei *et al.* 2008, Chien *et al.* 2016, Long *et al.* 2013).

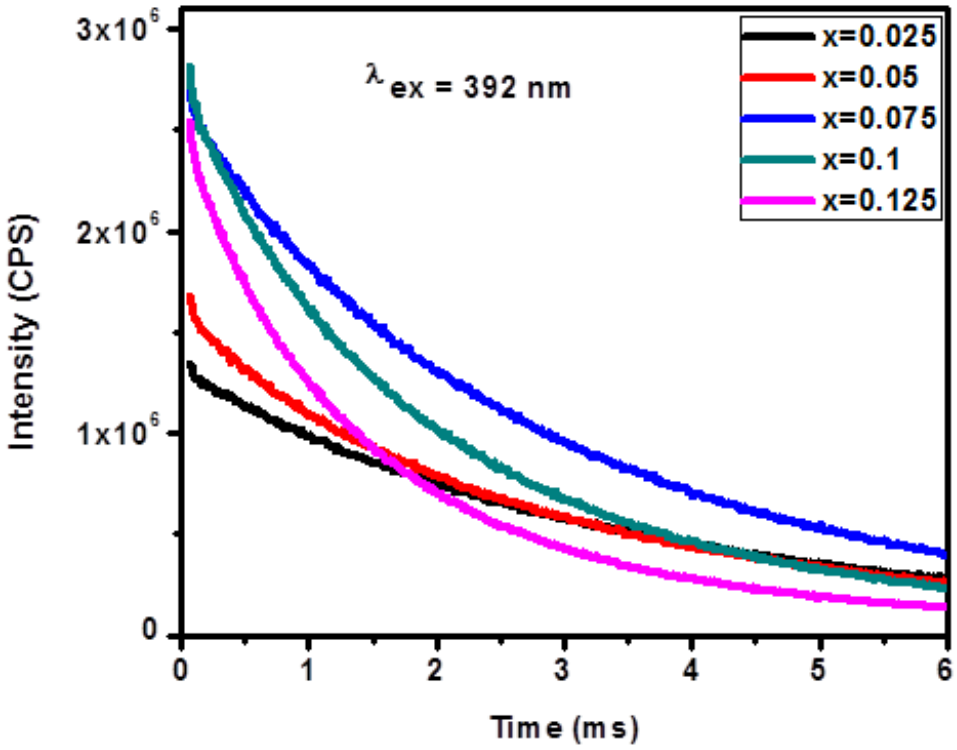


**Fig. 2B.9**: Decay curves of $SrGd_{(0.5-x)}Nb_{0.5}O_3$: $xEu^{3+}$ samples under UV excitation

## 2B 4. Conclusions

New perovskite type orange red emitting phosphors $SrGd_{(0.5-x)}Nb_{0.5}O_3:xEu^{3+}$ ($x$ = 0.025, 0.05, 0.075, 0.1, 0.125) were prepared via conventional solid state reaction route. All the samples crystallises to orthorhombic perovskite with space group pbam. UV Visible absorption analysis shows strong absorption in the 200-400 nm region. The $Eu^{3+}$ doped samples exhibit intense orange red emission under near UV (392nm) and blue (465nm) excitations. $Eu^{3+}$ doping is found to be optimum at 7.5 mol% with good quantum efficiency values that are much higher than that of the reported ones. Thus $SrGd_{0.425}Nb_{0.5}O_3:0.075Eu^{3+}$ can be used as a promising orange red phosphor with UV LEDs.

# Chapter 3

## Influence of B site cation on the photoluminescence properties of perovskite type $SrM_{0.425}Nb_{0.5}O_3$ : $0.075Eu^{3+}$ (M= Y, In, Gd) red phosphors.

*In this chapter, we have studied the role of B site cation on the structural morphological and optical properties of perovskite type $SrM_{(0.425)}Nb_{0.5}O_3$ : 0.075 $Eu^{3+}$ (M = Y, In, Gd) phosphors. As the B site cation varies from Gd to Y to In, there was a lot of variations in their structural, morphological and optical properties. Unlike the other samples $SrY_{0.425}Nb_{0.5}O_3$: 0.075 $Eu^{3+}$ possess dominant red emission with improved efficiency. Thus we have selected the Y based system to study further their structural and luminescence properties with different $Eu^{3+}$concentrations.*

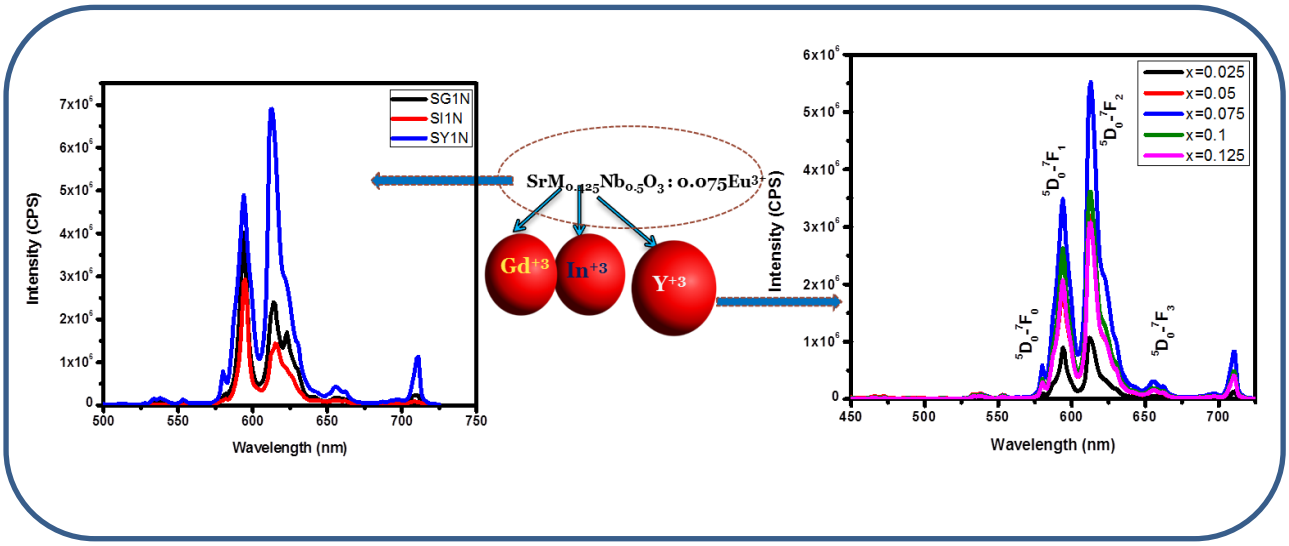

## 3.1 Introduction

Due to their promising properties such as environmental friendliness, high luminous efficiency and long life time etc , White light emitting diodes are considered as the ultimate form of lamp. There is a great demand for inorganic phosphors that can be excited by near UV and blue LEDs (Hoppe, *et al.* 2009). Rare earth ions ($RE^{3+}$) are particularly suitable for applications as activators due to their well-defined transitions within the 4f shell. $Eu^{3+}$ ions are considered to be preferable choice of activators for red luminescence as they exhibit a high lumen equivalent, quantum efficiency, and photostability. Luminescence originating from electronic transitions between 4f levels is predominantly due to magnetic dipole or electric dipole interactions that offer the possibility of efficient emissions (Luo *et al.* 2009, Zhang *et al.* 2014). In most of the inorganic luminescent materials, both the electric and magnetic dipole transitions occur simultaneously with different intensities. Asymmetric ratio, ratio of intensity of red emission to orange emission gives information about the local environment of $Eu^{3+}$ ions. The splitting of $^5D_0$-$^7F_J$ (J = 0, 1, 2, 3, 4) transitions gives information about the crystal field effect at the $Eu^{3+}$ site (Binnemans, *et al.* 2015).

The flexibility of A and B sites of Perovskites allows rich substitutions. Among the double perovskites, $A_2BB'O_6$, obtained by the partial substitution of half of B site cation with another cation B', shows great interest as the host material of photoluminecent applications. Multiple ion substitution in the structure can be used to alter their physical properties and results in complex perovskites. These perovskites had already proven their application potential in various fields such as super conductors, ferro-electrics, magneto dielectrics etc (Grabowska *et al.* 2015, Howard *et al.* 2006 ). In recent years Perovskite type phosphors are developed and they are found to be excellent host for photoluminescent materials. They possess good chemical stability, high levels of absorption in near UV region etc. $Eu^{3+}$ ion possess strong emission in red spectral region. Doping with suitable host materials, we can develop potential red phosphors for white light emitting diode (WLED) applications (Bhargavi, *et al.* 2015, Jiang *et al.* 2016).

We had already developed a series of highly efficient orange red emitting perovskite type phosphors, $SrGd_{0.5}Nb_{0.5}O_3 : xEu^{3+}$ ($x$ = 0.025, 0.05, 0.075, 0.1, 0.125) that can be used for WLED applications**.** Samples exhibit intense orange red emission under near UV (392nm) and blue (465nm) excitations. $Eu^{3+}$ doping is found to be optimum at 7.5 mol% with good quantum efficiency values. In this work, we studied the role of B site cation in the perovskite system of $SrM_{(0.425)}Nb_{0.5}O_3 : \mathit{0.075}\ Eu^{3+}$ (M = Y, In, Gd), on their structure, morphology and optical properties. Luminescence characterisics of Y based system is found to be much better compared to In and Gd based systems. So we have selected the Y based system and varied the $Eu^{3+}$ concentration from $x$ = 0.025 to 0.125 and their strutural morphological and optical properties were studied.

### 3.2 Experimental Procedure

A series of perovskite phosphor systems, $SrM_{(0.425)}Nb_{0.5}O_3 : \mathit{0.075}\ Eu^{3+}$ (M = Y, In, Gd) were prepared via conventional solid state reaction method by using $SrCO_3$, $Gd_2O_3$, $Nb_2O_5$, $In_2O_3$, $Y_2O_3$ and $Eu_2O_3$ as reagents. The required stoichiometric amount of these materials were weighed and mixed thoroughly in an agate mortar with acetone as the mixing medium. The homogeneous mixture was then calcined at 1400˚C for 6 h. The crystalline structure of the samples was examined using an X-ray powder diffractometer (X'Pert Pro PANalytical, operated at 40 kV and 30 mA, Cu-Kα = 0.15406nm, 2θ range = 10–90°). The morphological studies of the samples were done by a scanning electron microscope (JEOL, JSM-5600LV) operated at 15kV. Absorbance study of the samples were carried out using a Shimadzu, UV-2450 UV–Vis spectrophotometer in the 200–800 nm wavelength range using barium sulfate as a reference. The excitation and emission spectra were recorded on a Fluorolog HORIBA fluorescence spectrophotometer with a Xe lamp (450 W) as the excitation source. Luminescence lifetime of the phosphors was recorded by the phosphorimeter attached to Fluorolog 3 spectrofluorimeter. Also the series of phosphors, $SrY_{0.5}Nb_{0.5}O_3 : xEu^{3+}$ ($x$ = 0.025, 0.05, 0.075, 0.1, 0.125) were synthesized by the conventional solid state reaction route and their XRD, SEM, Photoluminescene, UV-Visible analysis, Lfetime analysis were done.

### 3.3. Results and Discussion

#### 3.3.1 Powder XRD analysis

X-ray diffraction patterns of the samples are shown in figures (Fig 3.1 and Fig 3.2). All the peaks of SGN and SIN (Fig 3.1) are in good agreement with the reported diffraction pattern of $PbZrO_3$ (JCPDS file no 01-087-0568; orthorhombic perovskite with a space group pbam (55). XRD pattern of SYN (Fig 3.2) shows some minor impurity peaks of $Y_2O_3$, all the other peaks can be indexed to monoclinic phase of SYN, space group P21/n (ICSD 163664). Incorporation of smaller Indium (0.8 Å) in the Gd (0.938 Å) site leads to the shifting of peaks towards right side. The degree of distortion from

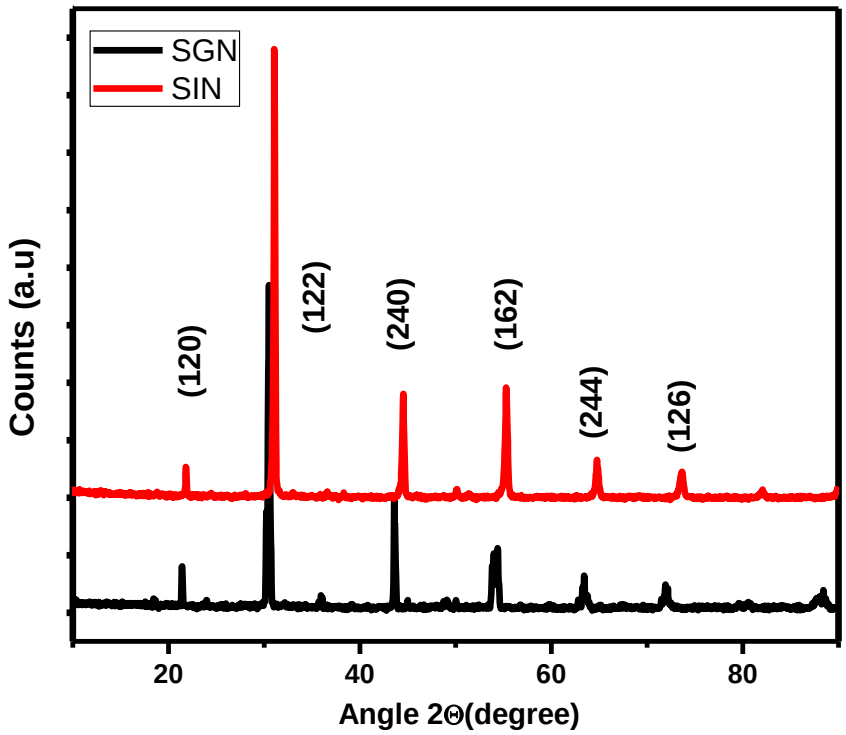


**Fig. 3.1**: Powder XRD patterns of $SrM_{(0.425)}Nb_{0.5}O_3$ : 0.075 $Eu^{3+}$ (M=Y, In, Gd)

Ideal perovskite structure is termed as tolerance factor and can be calculated as $\tau = (R_X+R_A) /\sqrt{2}\ (R_X+R_B)$. Values of $\tau$ are close to unity ($\tau$ (SGN) =0.92, $\tau$ (SYN) =0.93, $\tau$ (SIN) =0.95). As the ionic radii of B site decrease from 0.938Å (Gd) to 0.8 Å (In), value of $\tau$ increases from 0.92 to 0.95.

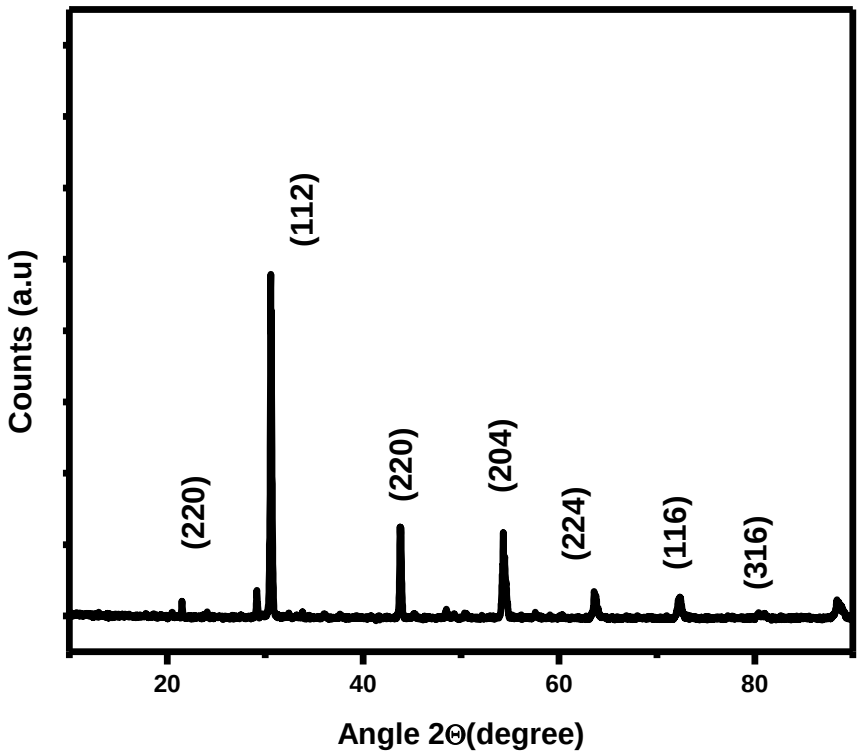


**Fig. 3.2**: Powder XRD patterns of $SrY_{(0.425)}Nb_{0.5}O_3$ : 0.075 $Eu^{3+}$

### 3.3.2 Morphological analysis

Fig 3.3 shows the scanning electron micrographs (SEM) of the samples. Substitution of smaller ions Y and In in Gd site results in decrease of grain growth. Grains and grain boundaries are highly visible from the SEM image of the samples. Spherical type of morphology reduces scattering losses and improves photoluminescent characteristics.

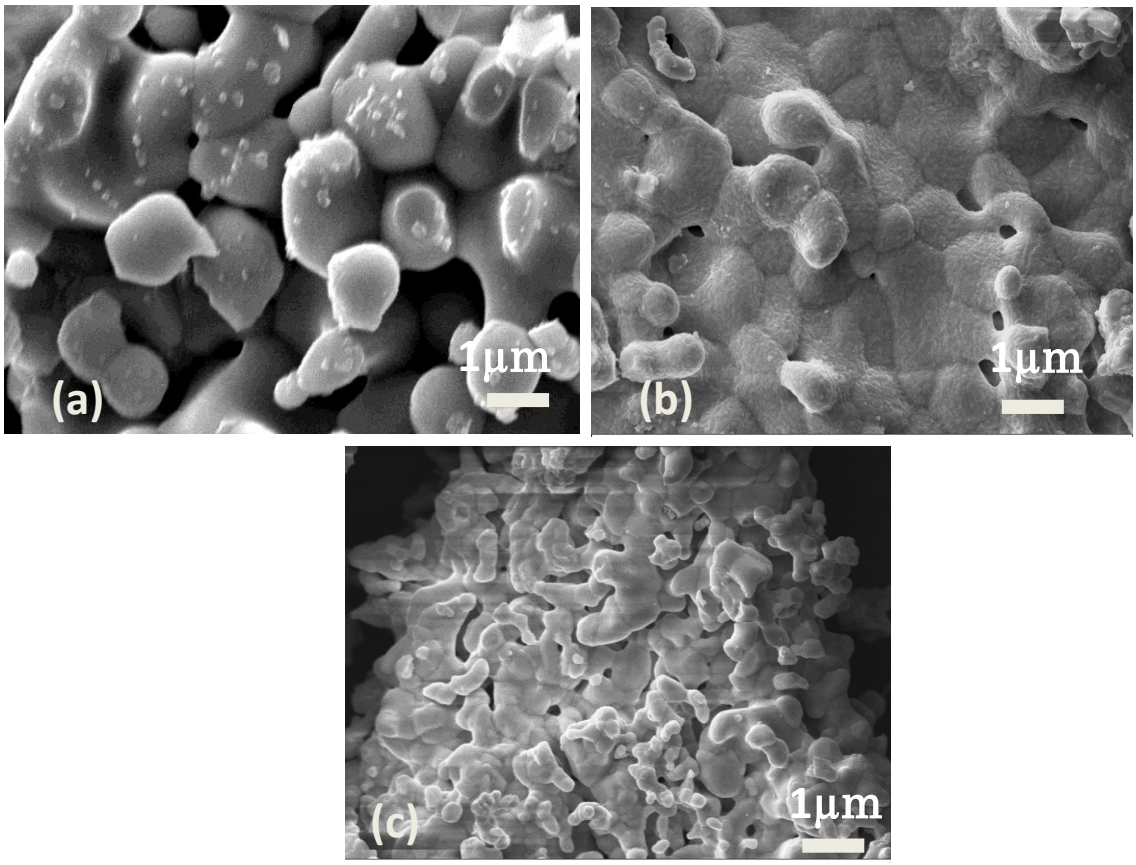


**Fig. 3.3** : SEM images of $SrM_{(0.425)}Nb_{0.5}O_3$ : *0.075* $Eu^{3+}$ [ (a) M = Gd, (b) M = Y, (c) M = In]

### 3.3.3 EDAX analysis

EDAX analysis of the samples were done. Inset table contains the elemental atomic percentage distribution in various samples. All the elements are present in stoichiometric amount.

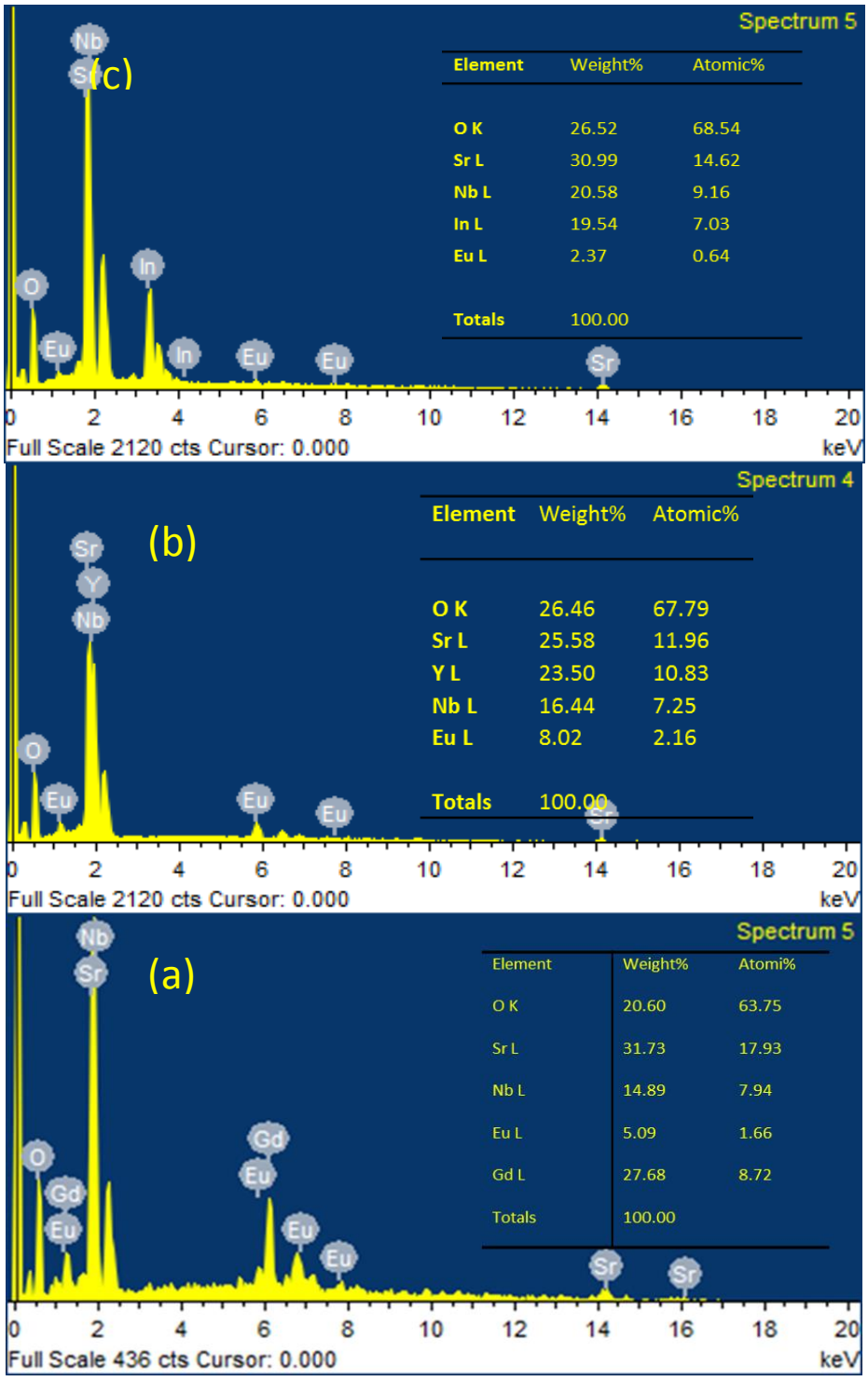


**Fig.3.4**: EDAX analysis of $SrM_{(0.425)}Nb_{0.5}O_3$ : *0.075* $Eu^{3+}$ [(a) M = Gd, (b) M=Y, (c) M = In]. [Inset shows elemental weight and atom % distribution]

### 3.3.4 Optical Studies

UV visible absorption spectra of the samples were recorded in the 200 to 800 nm range. Band gap of samples was determined by Shapiro's method, in which the absorbance edge is extrapolated to wavelength axis. Band gap shows decreasing trend with the replacement of Gd by Y and In ions. Band gap values are listed in Table 3.1. Strong absorption below 400 nm suggests the potentiality of the phosphor samples to incorporate with UV LEDs.

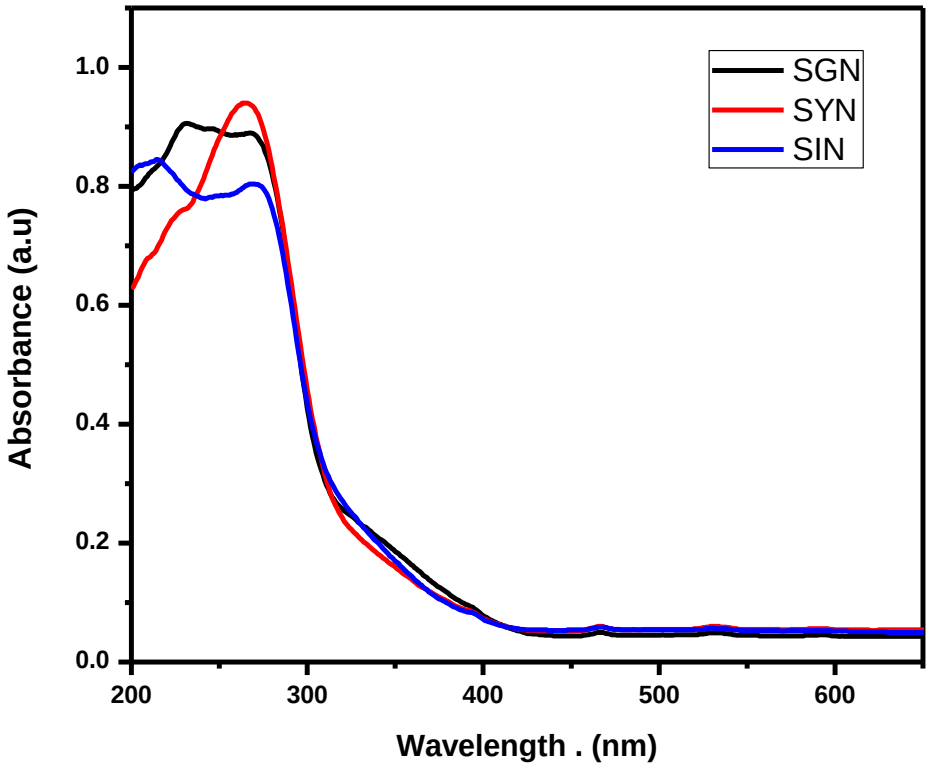


**Fig. 3.5** : UV visible absorption spectra of $SrM_{(0.425)}Nb_{0.5}O_3$ : *0.075* $Eu^{3+}$ (M = Y, In, Gd).

Photoluminescent excitation spectra of the samples are shown in Figure 3.6. Excitation spectra were recorded for an emission at 593 nm. The local environment of $Eu^{3+}$ ions affect its photoluminescent characteristics. Samples exhibit broad and intense charge transfer band and the sharp peaks corresponding to $O^{2-} - Eu^{3+}$charge transfer and intraconfigurational 4f-4f transitions of $Eu^{3+}$ ions in the host. SIN sample shows a red shift in CT energy compared to that of SGN. This shift can be attributed to an

increase in covalency of Eu-O bonds , because of the increased electronegativity of In (1.78) and lower ionization potential (5.78 eV), compared to that of Gd (electronegativity = 1.2, ionization potential =6.15 eV), which changes the co-ordination environment of $Eu^{3+}$ and reduces the CT energy (Linda *et al.* 2014). Characteristic f-f transition peaks of $Eu^{3+}$ is found to be less intense compared to CT band. This indicates that these phosphors have efficient excitation under near UV light. The sharp excitation peaks at 360 nm, 384 nm, 392 nm, 404 nm and 465 nm can be attributed to $^7F_0$-$^5D_4$, $^7F_0$-$^5G_{2\text{-}4}$,$^7F_0$-$^5L_6$, $^7F_0$-$^5D_3$, $^7F_0$-$^5D_2$ transitions of $Eu^{3+}$ ions in the host (Chien *et al.* 2016, Xin *et al.* 2011). The f-f transition peak at 392 nm ($^7F_0$-$^5L_6$) is very intense in the SGN and SYN phosphors compared to SIN, which indicates that efficient energy transfer to $Eu^{3+}$ ions takes place in these samples.

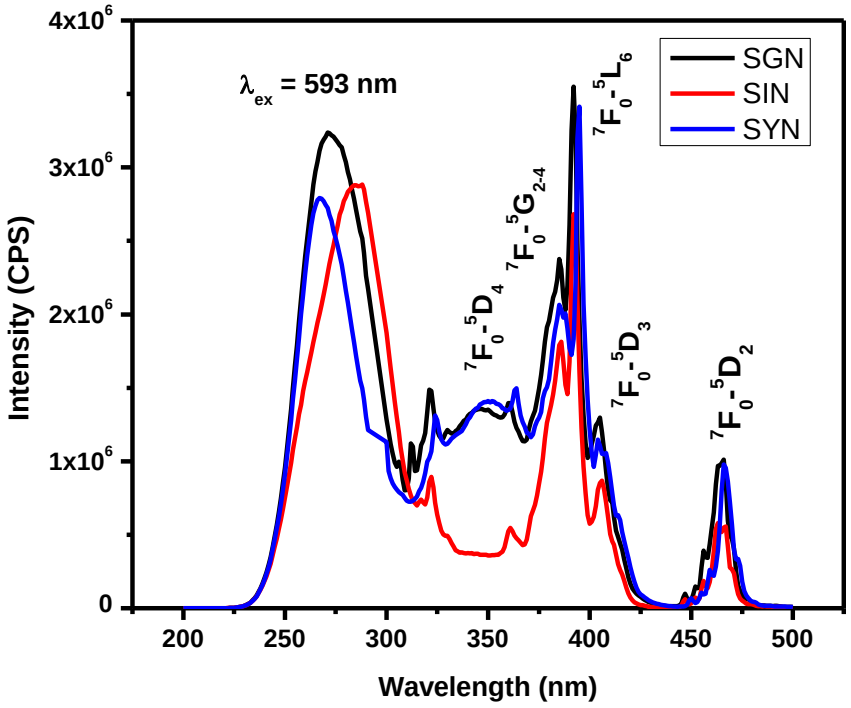


**Fig 3.6** : Photoluminescent excitation spectra of $SrM_{(0.425)}Nb_{0.5}O_3$ : *0.075* $Eu^{3+}$ (M= Y, In, Gd).

Photoluminescent emission spectra of $SrM_{(0.075)}Nb_{0.5}O_3$ : *0.075* $Eu^{3+}$ (M = Y, In, Gd) corresponding to an excitation wavelength of 392 nm is shown in Figure 3.7. The

two samples SGN and SIN possess intense orange red emission (593 nm) corresponding to the $^5D_0$-$^7F_1$ magnetic dipole transition of $Eu^{3+}$ in the lattice. It is due to the centro symmetric site occupancy of $Eu^{3+}$ ions in the lattice. But the SYN sample exhibit dominant red emission (613nm) corresponding to the $^5D_0$-$^7F_2$ forced electric dipole transition of $Eu^{3+}$ ions in the lattice, this indicates that $Eu^{3+}$is occupying in a site with low symmetry in the double perovskite lattice. This non inversion centre environment is favourable to acquire red phosphor with high color purity (Fu *et al.* 2017). Figure 3.8 depicts the Photoluminescent excitation spectra of SYN sample for emission at 613 nm. Here the CT band is found to be shallow compared to f-f transition intensities. The

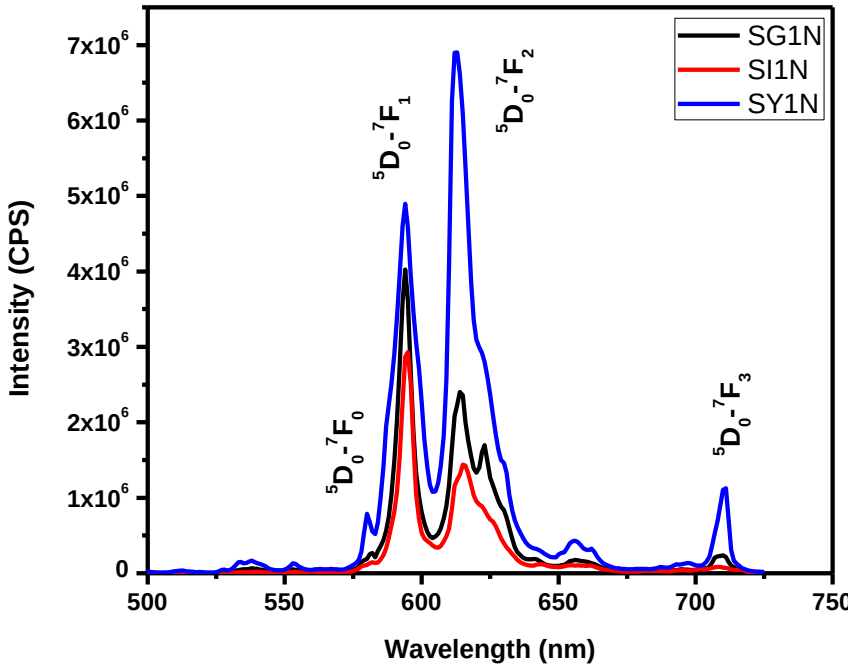


**Fig 3.7** : Photoluminescent emission spectra of $SrM_{(0.425)}Nb_{0.5}O_3$ : *0.075* $Eu^{3+}$ (M = Y, In, Gd).

sharp excitation peaks at 392 nm and 465 nm corresponds to $^7F_0$-$^5L_6$ and $^7F_0$-$^5D_2$ transitions of $Eu^{3+}$ ions in the host, which matches well with emission of UV and blue pumping LEDs (Jing *et al.* 2015). As the B site varies from Gd to In to Y there are lot of variations in their luminescence properties. The degree of asymmetry of $Eu^{3+}$ site affects the luminescence characteristics. Asymmetry ratio, the ratio of intensity of

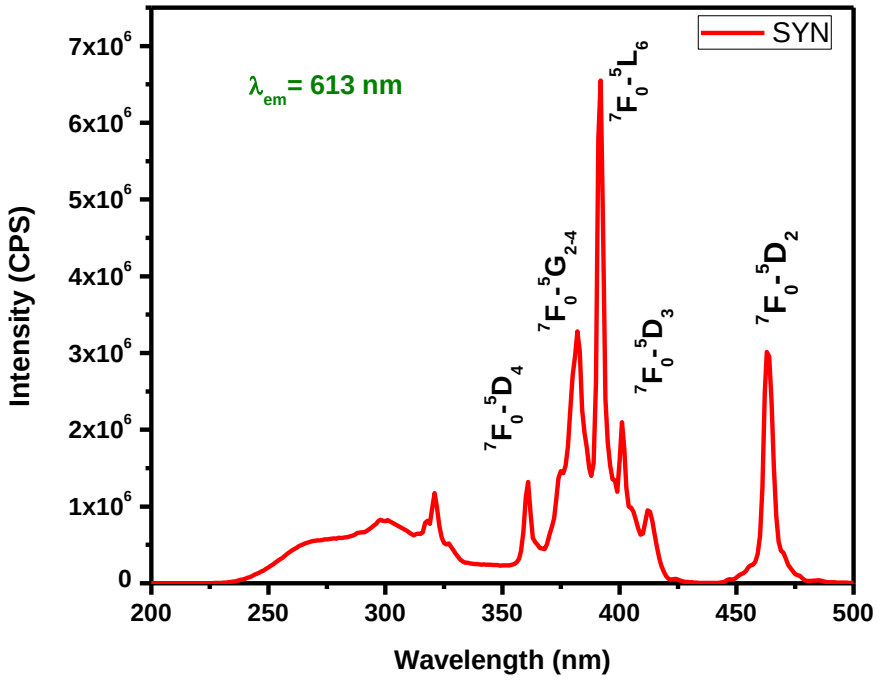


**Fig 3.8** : Photoluminescent excitation spectra of $SrY_{0.425}Nb_{0.5}O_3$ : *0.075* $Eu^{3+}$ for an emission at 613nm

$^5D_0$-$^7F_2$ transition to that of $^5D_0$-$^7F_1$ transition can tell us about the local site symmetry of $Eu^{3+}$ ion (Francis *et al.* 2015). Asymmetry ratio of the samples was calculated and listed in Table 3.1.

### 3.3.5 Lifetime analysis

Life time analysis of the samples was done. The decay curves of the samples under UV excitation is shown in Figure 3.9. The decay curves exhibit a single exponential behavior and the decay curves can be fitted to a single exponential function, $I = A \exp(-x/\tau)$, where I, A and τ are intensity, fitting parameter, and decay time respectively. This confirms the single site occupancy of $Eu^{3+}$ ions in the host. Assuming that only radiative and non radiative processes are essentially involved in the depopulation of $^5D_0$ states of $Eu^{3+}$ ion, the quantum efficiency ( η) can be expressed as;

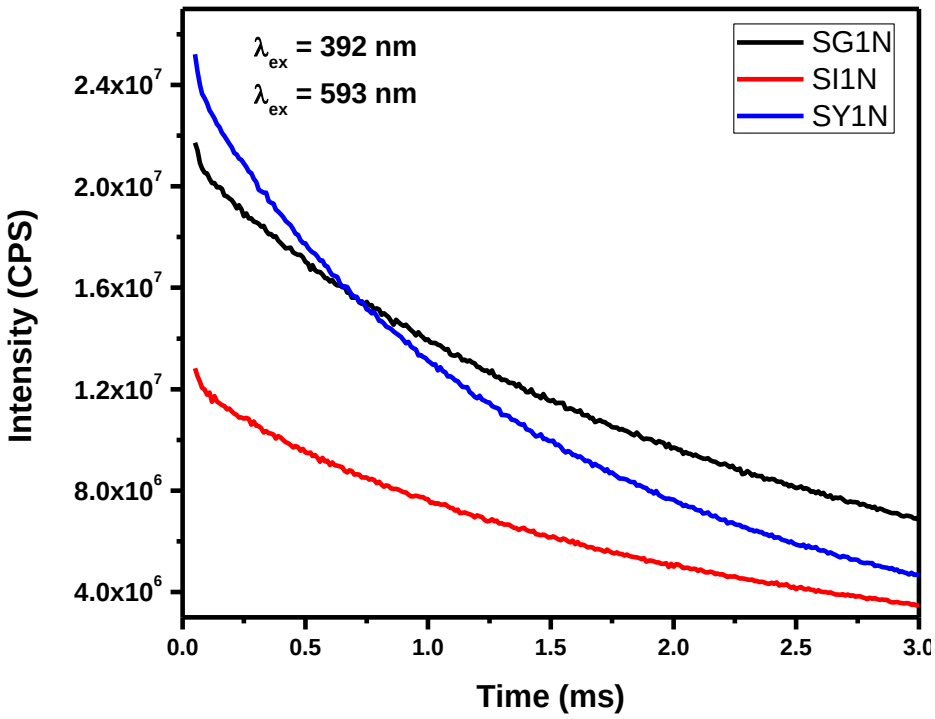


**Fig 3.9** : Decay curves of $SrM_{(0.425)}Nb_{0.5}O_3$ : *0.075* $Eu^{3+}$ (M = Y, In, Gd,) for an excitation at 392nm of $Eu^{3+}$ in the lattice.

$\eta = A_{rad}/( A_{rad} + A_{nrad})$

where $A_{rad}$ and $A_{nrad}$ are radiative and non radiative transition probabilities respectively. (Su *et al.* 2008, Antic *et al.* 2009). SYN possess higher quantum efficiency compared to the other two. Further, the obtained quantum efficiency values of SGN and SYN are much higher than that of the reported ones in $CaMoO_4$ (12.78%) and perovskites $Ca_2MgWO_6$ (14.05%), $Y_6WO_{12}$ (20.6%) (Lei *et al.* 2008, Chien *et al.* 2016, Long *et al.* 2013). The degree of distortions in the $Eu^{3+}$ site is more in SYN system than the other two. That may be the reason of enhancement of photoluminescent properties of SYN system compared to the other two. Thus we have selected the SYN system and series of phosphors with different $Eu^{3+}$ concentration were developed and their structural and photoluminescent properties were studied.

Table 3.1 : Bandgap Lifetime, asymmetric ratio, CIE color co-ordinates and efficiency of $SrM_{(0.425)}Nb_{0.5}O_3$ : *0.075* $Eu^{3+}$(M = Y, In, Gd)

| Samples | Bandgap (ev) | Lifetime (ms) | Asymmetry Ratio | CIE color Co-ordinates | Efficiency (%) |
|---|---|---|---|---|---|
| **SGN** | 3.86 | 2.61 | 0.599 | (0.61,0.36) | 30.83 |
| **SIN** | 3.77 | 1.68 | 0.493 | (0.60,0.35) | 13.32 |
| **SYN** | 3.78 | 2.1 | 1.42 | (0.64,0.33) | 34.45 |

### 3.3.6 Structural and Photoluminescent properties of $SrY_{(0.5-x)}Nb_{0.5}O_3 : xEu^{3+}$

We have studied the role of B site cation on the structural and photoluminescent properties of $SrM_{(0.425)}Nb_{0.5}O_3$ : *0.075* $Eu^{3+}$ ( M = Y, In, Gd) phosphors. By suitably chosing B site cations we can tailor the structural as well as luminescent properties of double perovskites. Comparing the performance of the three samples $SrM_{(0.425)}Nb_{0.5}O_3$ : *0.075* $Eu^{3+}$ ( M = Y, In, Gd,), we have selected $SrY_{(0.425)}Nb_{0.5}O_3$ : *0.075* $Eu^{3+}$ system because of its intense red luminescence, strong absorption in UV and blue regions, good quantum efficiency values and good chromaticity color co-ordinates. We have synthesized the series of phosphors $SrY_{(0.5-x)}Nb_{0.5}O_3$ : *x*$Eu^{3+}$ (x = 0.025, 0.05, 0.075, 0.1, 0.125) by conventional solid state reaction route. Their structural, morphological and photoluminescent properties were studied.

#### 3.3.6.1 XRD analysis

X-ray diffraction patterns of the samples are shown in Figure 3.10. XRD pattern of SYN shows some minor impurity peaks of $Y_2O_3$, all the other peaks can be indexed to monoclinic perovskite phase of SYN, space group P21/n (ICSD 163664). $Eu^{3+}$ ions are successfully incorporated into the lattice without any further impurity phase formation.

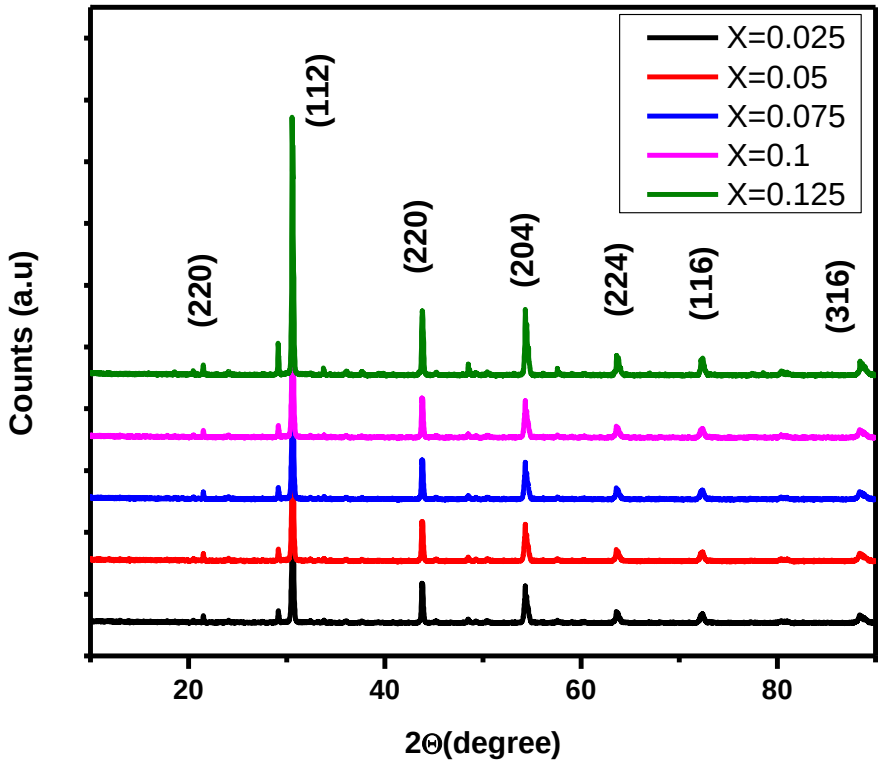


**Fig 3.10** : Powder XRD patterns of $SrY_{(0.5-x)}Nb_{0.5}O_3 : xEu^{3+}$ ($x$ = 0.025, 0.05, 0.075, 0.1, 0.125)

### 3.3.6.2 SEM analysis

SEM images of the samples were taken. We have got uniform distribution of particles having grain size distribution of 1-3μm. Spherical type of morphology can assist the enhancement of luminescent emission.

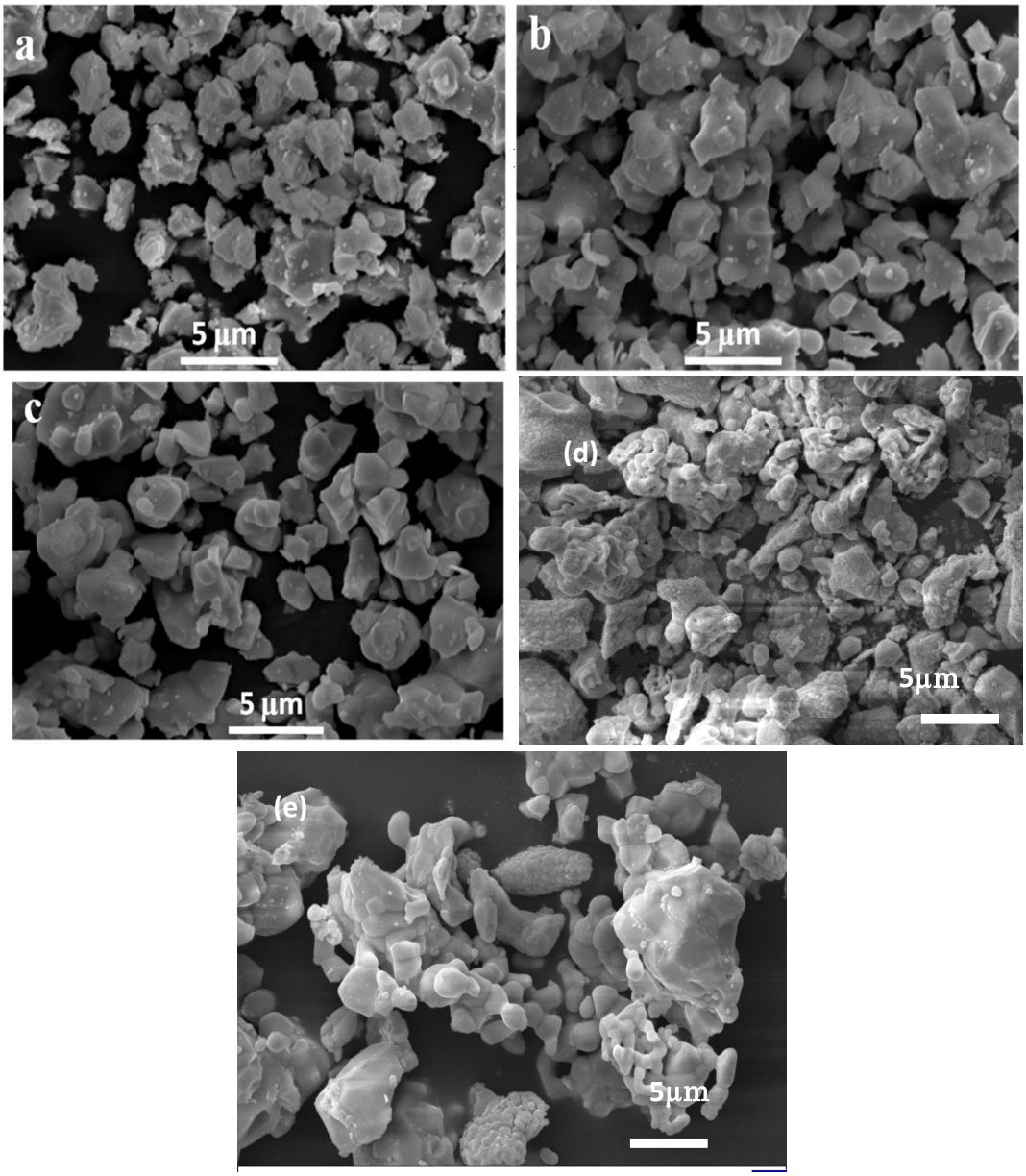


**Fig. 3.11**: SEM images of $SrY_{(0.5-x)}Nb_{0.5}O_3 : xEu^{3+}$ ($x$ = 0.025, 0.05, 0.075, 0.1, 0.125)

### 3.3.6.3 Optical studies

Photoluminescence properties of the prepared phosphors were recorded at room temperature. Photoluminescence excitation spectra of the samples for an emission at 613 nm are shown in Figure 3.12. All the samples exhibit shallow charge transfer band and sharp and intense intraconfigurational f-f transitions. The charge

transfer band extends from 235 nm to 309 nm. The sharp excitation peaks at 360 nm, 384 nm, 392 nm, 404 nm and 465 nm can be attributed to $^7F_0$-$^5D_4$, $^7F_0$-$^5G_{2-4}$,$^7F_0$-$^5L_6$, $^7F_0$-$^5D_3$, $^7F_0$-$^5D_2$ transitions of $Eu^{3+}$ ions in the host. As the concentration of $Eu^{3+}$ ions increases, excitation intensity also increases upto 10 mol% and then decreases. ie, Concentration quenching occurs at 10 mol%. The sharp excitation peaks at 392 nm and 465 nm matches well with the emission of UV and blue emitting pumping LEDs (Yahiaoui, *et al.* 2013). Therefore the prepared phosphors can be a potential candidate for WLED applications.

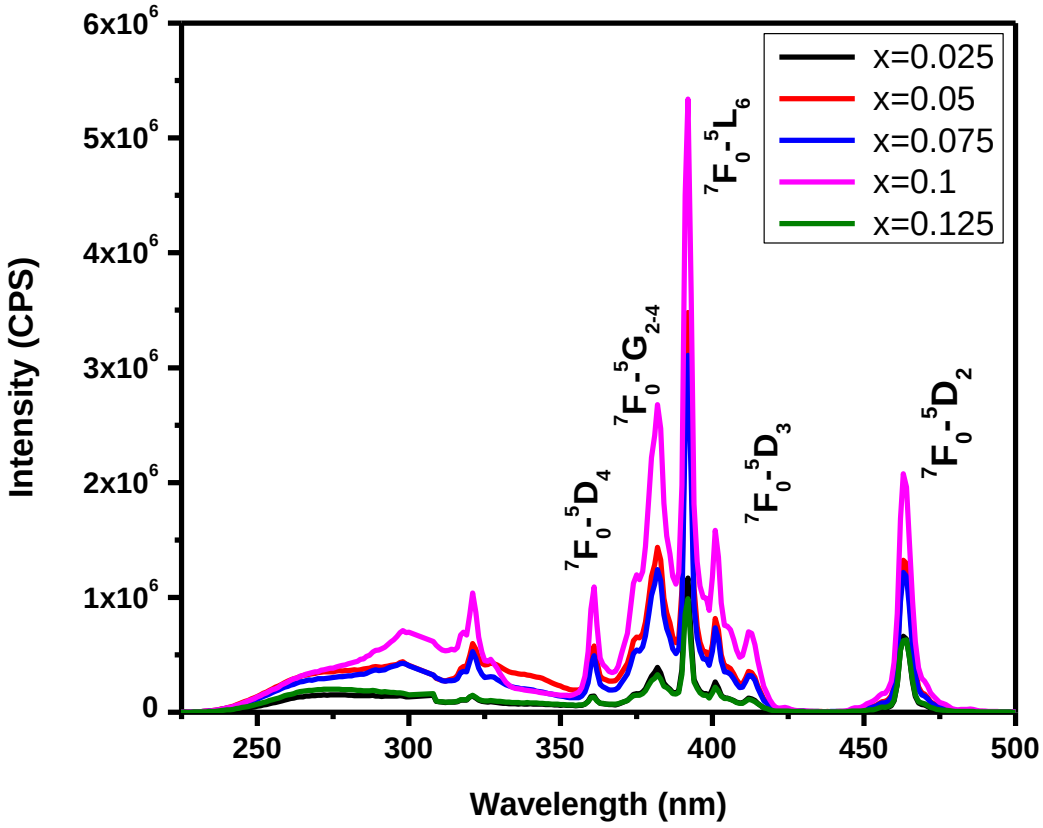


**Fig 3.12** : Photoluminescent excitation spectra of $SrY_{(0.5-x)}Nb_{0.5}O_3 : xEu^{3+}$ ($x$ = 0.025, 0.05, 0.075, 0.1, 0.125)

The photoluminescent emission spectra of the phosphors $SrY_{(0.5-x)}Nb_{0.5}O_3 : xEu^{3+}$ ($x$ = 0.025 -0.125) for excitations 392 nm and 465 nm are shown in Figures (Fig 3.13 and 3.14). Luminescent intensity is higher for UV light excitation. In all the samples, $^5D_0$-$^7F_2$ electric dipole transition is dominating than the $^5D_0$-$^7F_1$ magnetic dipole transition.

It is an indication of occupation of $Eu^{3+}$ in the noncentro symmetric site. In accordance with the photoluminescent excitation spectra photoluminescent emission intensity also increases with increase in $Eu^{3+}$ concentration upto 10 mol% and then decreases. There is no splitting in the $^5D_0$-$^7F_0$ transition, which confirms the single site occupancy of $Eu^{3+}$ in the lattice.

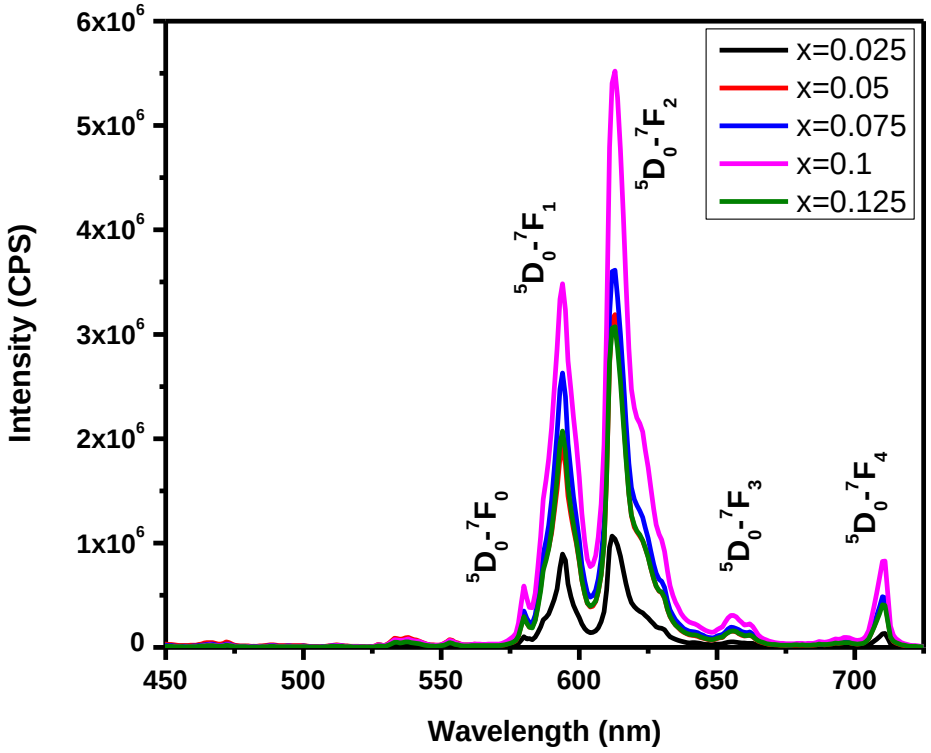


**Fig 3.13** : Photoluminescent emission spectra of $SrY_{(0.5-x)}Nb_{0.5}O_3 : xEu^{3+}$ ($x$ = 0.025, 0.05, 0.075, 0.1, 0.125) for 392 nm excitation.

Asymmetry ratio gives a measure of degree of distortion of the $Eu^{3+}$ in the lattice. (Xin *et al.* 2011, Jing *et al.* 2015). Asymmetry ratio of the samples are calculated and tabulated (Table 3.2). Figure 3.15 shows the variation of maximum emission intensity with different $Eu^{3+}$ concentrations. Concentration quenching occurs at 10 mol%. Variation of asymmetry ratio with different $Eu^{3+}$ concentrations is demonstrated in Figure 3.16.

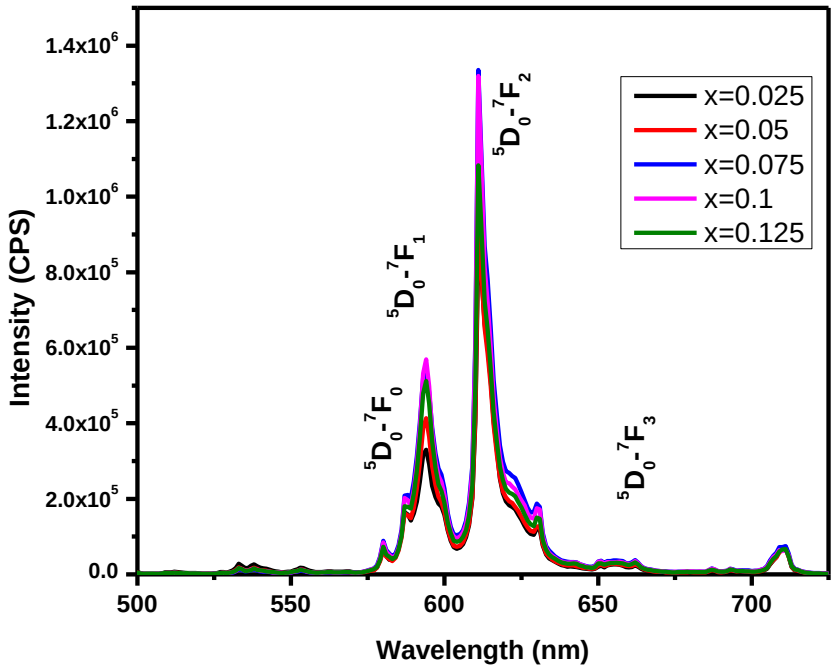


**Fg 3.14**: Photoluminescent emission spectra of $SrY_{(0.5-x)}Nb_{0.5}O_3 : xEu^{3+}$ ($x$ = 0.025, 0.05, 0.075, 0.1, 0.125) for 465 nm excitation

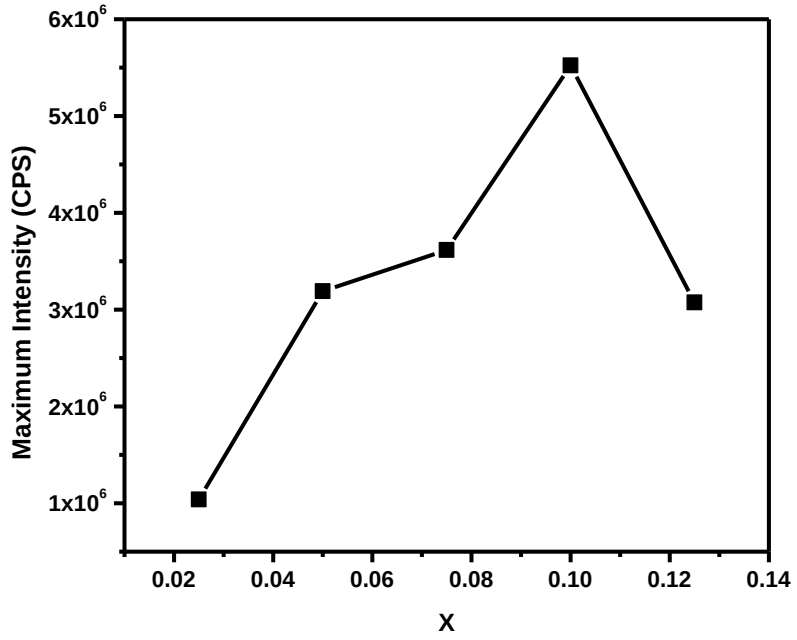


**Fig 3.15** : Variation of maximum emission intensity of $SrY_{(0.5-x)}Nb_{0.5}O_3 : xEu^{3+}$ ($x$ = 0.025, 0.05, 0.075, 0.1, 0.125) for 392 nm excitation

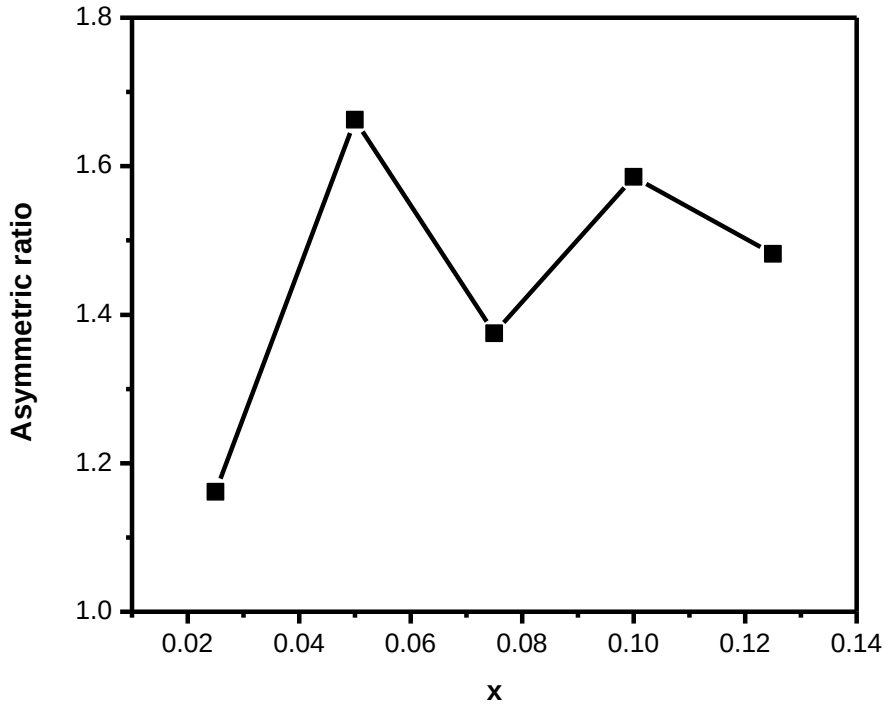


**Fig 3.16** : Variation of asymmetry ratio with different $Eu^{3+}$ ($x$ = 0.025, 0.05, 0.075, 0.1, 0.125) concentrations

### 3.3.6.4 Lifetime analysis

Photoluminescence decay curves of the samples for an excitation at 392 nm and emission at 613 nm are given in Figure 3.17. All the decay curves can be fitted well with a single exponential decay function, I = A exp (-x/τ), where I, A and τ are intensity, fitting parameter, and decay time respectively. This confirms the single site occupancy of $Eu^{3+}$ in the lattice. The quantum efficiency values of the samples are also calculated. Lifetime values as well as efficiency values are found to be decreased with $Eu^{3+}$ concentration. Quantum efficiency value of $SrY_{(0.49)}Nb_{0.5}O_3$:0.1$Eu^{3+}$ is 32.12%, which is higher than many of the reported systems in $CaMoO_4$ (12.78%) and perovskites $Ca_2MgWO_6$ (14.05%), $Y_6WO_{12}$ (20.6%) (Lei *et al.* 2008, Chien *et al.* 2016, Long *et al.* 2013). For the better understanding of emission color appearance, CIE color co-ordinates of the samples were calculated and tabulated. Color co-ordinates of $SrY_{(0.49)}Nb_{0.5}O_3$:0.1$Eu^{3+}$ is found to be (0.64,0.32), which are close to NTSC standard

values (0.67,0.33) for a potential red phosphor. Fig 3.18 shows the color co-ordinate diagram of the sample. Color purity of the sample was checked using

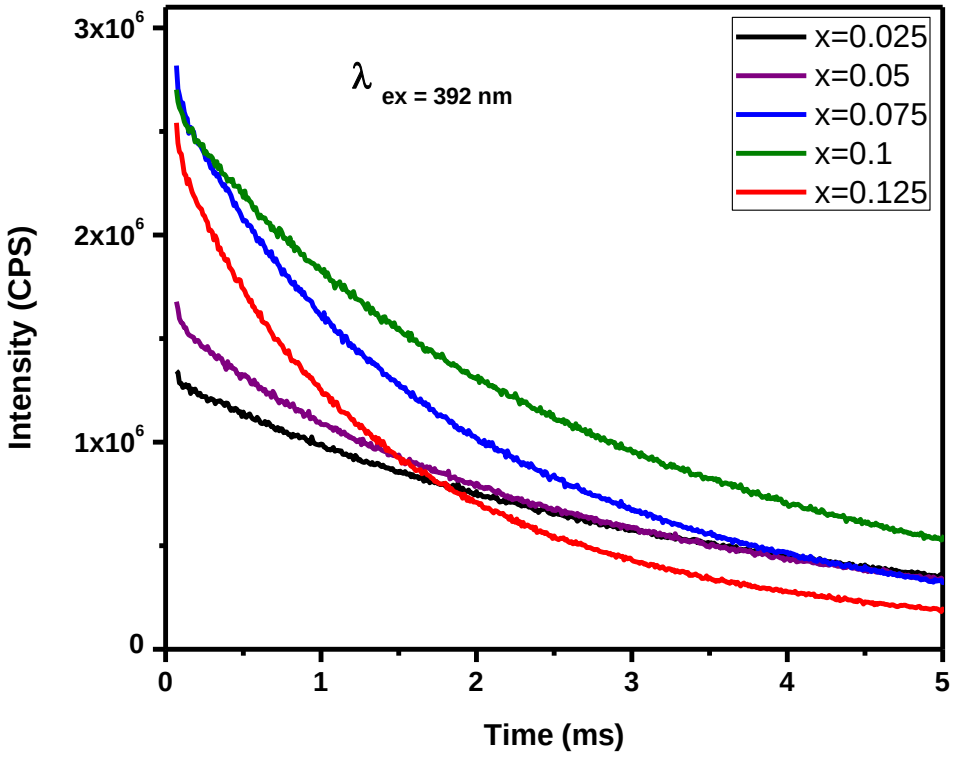


**Fig 3.17** : Decay curves of $SrY_{(0.5-x)}Nb_{0.5}O_3:xEu^{3+}$ (x = 0.025, 0.05, 0.075, 0.1, 0.125)

the equation, $color\ purity = \frac{\sqrt{\{(x-xi)2 + (y-yi)2\}}}{\sqrt{\{(xd-xi)2 + (yd-yi)2\}}} \times 100$, where (x,y) are the color co-ordinates of the sample, $(x_i,y_i)$ are color co-ordinates of white illuminant, and $(x_d,y_d)$ are chromaticity co-ordinates of the dominant wavelength. Here (x,y) = (0.64,0.32), $(x_i,y_i)$ = (0.33,0.33) and $(x_d,y_d)$= (0.67,0.33) (Jing *et al.* 2015, Wu *et al.* 2011). Substituting these, we got excellent value for color purity as 90%.

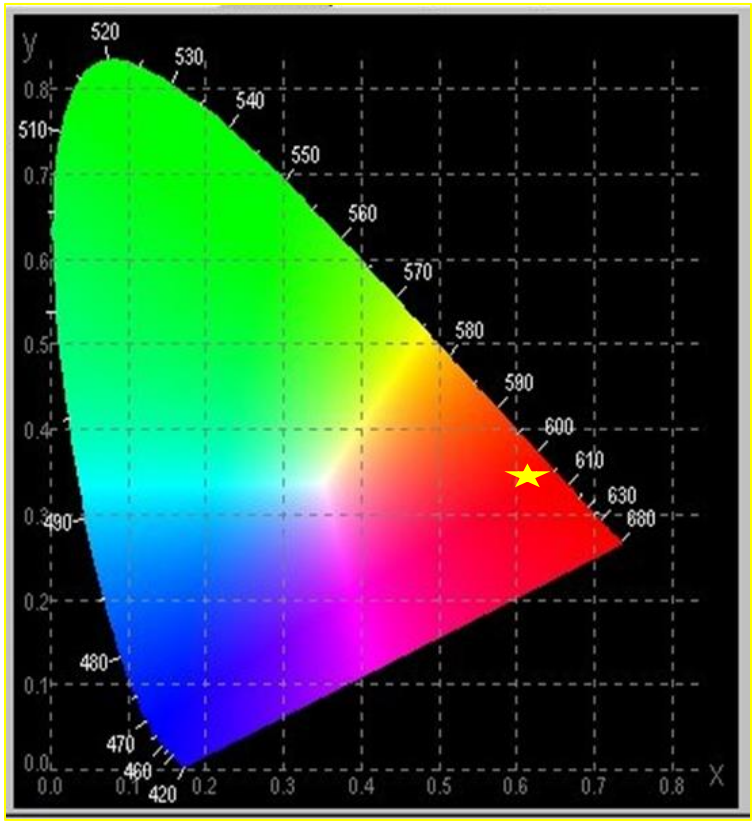


**Fig. 3.18**: CIE color co-ordinate diagram for $SrY_{(0.49)}Nb_{0.5}O_3:0.1Eu^{3+}$

Table 3.2 : Lifetime, Asymmetry ratio, Efficiency, CIE Color co-ordinates of $SrY_{(0.5-x)}Nb_{0.5}O_3:xEu^{3+}$($x$ = 0.025, 0.05, 0.075, 0.1, 0.125)

| X | Lifetime (ms) | Asymmetry ratio | Efficiency (%) | CIE Color co-ordinates |
|---|---|---|---|---|
| **0.025** | 3.2 | 1.16 | 36.83 | (0.62,0.32) |
| **0.05** | 2.8 | 1.66 | 35.32 | (0.63,0.33) |
| **0.075** | 2.6 | 1.37 | 34.45 | (0.60,0.33) |
| **0.1** | 2.5 | 1.59 | 32.12 | (0.64,0.32) |
| **0.125** | 1.9 | 1.48 | 27.34 | (0.65,0.31) |

## 3.4 Conclusions

In summary we have studied the role of B site cation on the structural morphological and optical properties of the $SrM_{(0.425)}Nb_{0.5}O_3$ : 0.075 $Eu^{3+}$ (M = Y, In, Gd) phosphors. As we varied the B site cation from Gd to Y and In, there was a lot of variations in their properties. SGN and SIN samples crystaliises to orthorhombic perovskite type phase but SYN crystallises to monoclinic perovskite type phase. Powder XRD pattern of SYN possess some impurity peaks of $Y_2O_3$. Morphological variations also shows a decrease in grain growth with the substitution of smaller ions such as In and Yitrium. EDAX analysis confirms the elements present in the sample. Band gap shows decreasing trend with the replacement of Gd by Y and In ions. Strong absorption below 400 nm suggests the potentiality of the phosphor samples to incorporate with UV LEDs. In PL excitation spectra, SIN sample shows a red shift in CT energy compared to that of SGN, this may be due to an increase in covalency of Eu-O bonds , because of the increased electronegativity of In (1.78), compared to that of Gd (1.2). Irrespective of the other samples, PL excitation spectra of SYN possess shallow CT band and intense characteristic f-f transition peaks $^7F_0$-$^5L_6$ and$^7F_0$-$^5D_2$ of $Eu^{3+}$ ion. PL emission of SGN and SIN possess intense orange red emission (593 nm) corresponding to the $^5D_0$-$^7F_1$ magnetic dipole transition of $Eu^{3+}$ in the lattice. It is due to the centro symmetric site occupancy of $Eu^{3+}$ions in the lattice. But the SYN sample exhibit dominant red emission (613nm) corresponding to the $^5D_0$-$^7F_2$ forced electric dipole transition of $Eu^{3+}$ions in the lattice, this may be due to the impurity phases which decreases the centro symmetric nature of $Eu^{3+}$ site. Quantum efficiency of the phosphors are calculated. SYN possess higher quantum efficiency compared to the other two. The quantum efficiency values of SGN and SYN are much higher than that of the reported ones in $CaMoO_4$ (12.78%) and perovskites $Ca_2MgWO_6$ (14.05%), $Y_6WO_{12}$ (20.6%). The degree of distortions in the $Eu^{3+}$ site is more in SYN system than the other two. That may be the reason of enhancement of photoluminescent properties of SYN system compared to the other two. Thus by varying the B site cation we can tailor the photoluminescent properties of perovskite $AB_{0.5}B'_{0.5}O_3$, perovskite system. Comparing the performance of the three samples $SrM_{(0.425)}Nb_{0.5}O_3$ : *0.075* $Eu^{3+}$ ( M = Y, In, Gd), we have selected $SrY_{(0.425)}Nb_{0.5}O_3$ : *0.075*

$Eu^{3+}$ . We have synthesized the series of phosphors $SrY_{(0.5-x)}Nb_{0.5}O_3 : xEu^{3+}$ ($x$ = 0.025 - 0.125) by conventional solid state reaction route. Their structural, morphological and photoluminescent properties were studied. Having high luminous excitation and emission intensity, good efficiency value of 32.12%, color co-ordinate value of (0.64, 0.32), and color purity value of 90%, $SrY_{(0.49)}Nb_{0.5}O_3$ : 0.1 $Eu^{3+}$ phosphor can be a potential red phosphor candidate for WLED applications.

# Chapter 4A

## New narrow orange emitting phosphors in 1:2 B-site cation ordered $Eu^{3+}$ doped triple Perovskite $Ba_3CaNb_2O_9$

*In this chapter. Structural, morphological and optical properties of triple perovskite type phosphors, $Eu^{3+}$ activated $Ba_3CaNb_2O_9$ is being discussed. They have efficient excitation under near UV light. They possess dominant and narrow orange emission at 593 nm. The higher quenching concentration of 20 mol% can be attributed to the 1: 2 ordering of Ca and Nb ions in the lattice.*

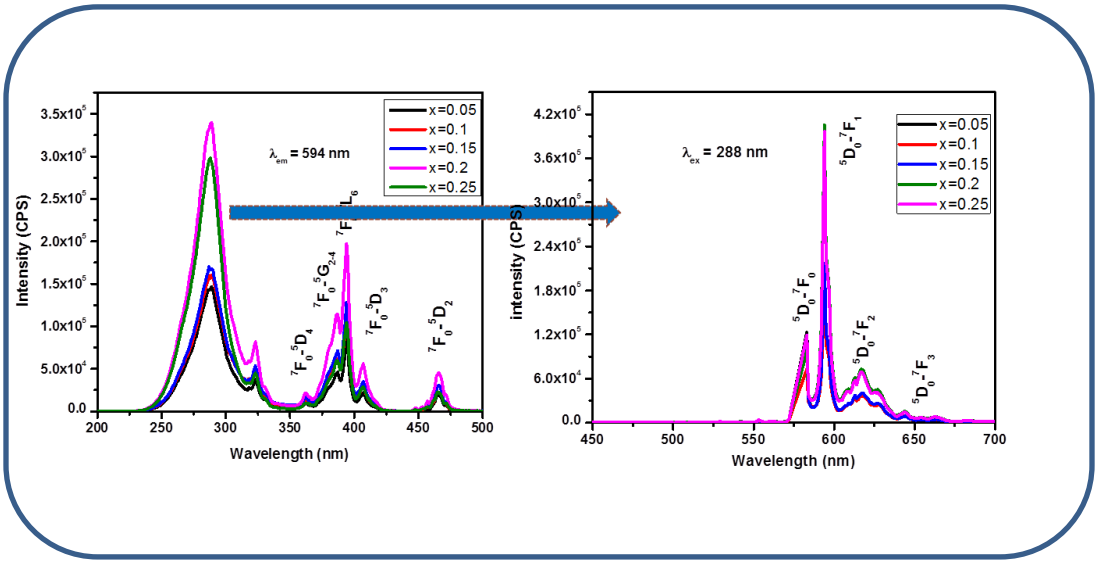

## 4A.1 Introduction

The past two decades has witnessed phenomenal advances in the area of solid state lighting, displays, solar cells etc with the discovery of exotic luminescence materials. These luminescent materials play a great role in determining the efficiency of the above said devices (Zhang *et al.* 2015, Zhao *et al.* 2013, Vijayakumar *et al.* 2019). These materials mostly act like a light converters either as a down converters in solid state lighting from near UV/blue light into visible or up converters in solar cells from NIR radiation into visible region for harvesting the solar radiations (Shalava *et al.*2005, Moraa *et al.*2017). Over the years, these materials have been developed in various systems such as sulfides, nitrides, halides, oxides, silicates etc with different crystal structures. Recent times, orange-red emitting materials are in great demand to improve the color rendering index and to develop warm white lighting systems. Currently these materials are reliant on $Eu^{2+}$ and $Ce^{3+}$ doped nitrides and sulfides based systems for applications in illumination grade lighting systems. However, they exhibit broad emission bands which limit the required luminous efficacy value for high power warm white LED based lighting systems. Because, a significant amount of emission spills out beyond the sensitivity range of human eye above 700 nm. Further, the preparation condition for nitride based phosphors is very tedious and time consuming which is not viable on a commercial scale. In addition, the sulfide based phosphors are not chemically stable degrading over a period of time which is harmful to the environment (Zhang *et al.* 2013, Li *et al.* 2018, Li *et al.* 2015, Zhang *et al.* 2016). Orange-red phosphors such as rare earth activated particularly europium doped molybdates, tungstates, silicates and other oxide systems have been investigated extensively for developing warm white LEDs with high CRI values of 80 and low CCT values of 2000-4700 K (Cao *et al.* 2020, Wei *et al.* 2019). However, these phosphors suffer from some drawbacks such as high $Eu^{3+}$ concentrations, for equivalent emission intensities (24 mol % of $Eu^{3+}$ doped $CaMO_4$), strong emission quenching with `temperature, broad emissions leading to low efficacy (Wang *et al.* 2020). Recently, $Mn^{4+}$ doped systems have also been studied for the development of narrow band red emitting phosphors. But they exhibit narrow band red emission at higher wavelength in the region 630-650 nm

which is less sensitive to human eye (Fu *et al.* 2017). Hence there are many challenges to discover narrow orange-red emitting phosphors to enhance the efficacy and quality of pc-WLEDs by way of improving the CRI and lower CCT values (Mbarek *et al.* 2017).

The $Eu^{3+}$ doped systems have gained a lot of interest for the development of narrow band red emission phosphors, since the excitation transitions 394 ($^7F_0$ - $^5L_6$) and 464 nm ($^7F_0$ - $^5D_2$) match very well with the emission bands of near UV and blue LED chips. However, the $Eu^{3+}$ transitions are highly hypersensitive which they depend strongly on the local site symmetry. According to the electronic transitions from the $Eu^{3+}$ $^5D_0$ state to low lying levels are both electric dipole and magnetic dipole. In a crystal site with inversion symmetry the electric dipole transitions are strictly forbidden and magnetic dipole transitions are allowed while for a site without inversion symmetry the forced electric dipole transitions are partially allowed due to the crystal field induced J mixing effect. The $Eu^{3+}$ transitions strongly depends on the local environment (the interaction between the $Eu^{3+}$ ion and the host), and the doping concentration, the distribution of activator ions in the host lattice and the energy transfer from the host lattice to the activator ions. Therefore, $Eu^{3+}$ ions act like a structural probe to gain knowledge on the co-ordination and environment around the cation substitutions in a crystalline lattice (Mahesh *et al.* 2012, Hou *et al.* 2012, Zhang *et al.* 2013). So our aim is to identify a suitable host lattice in which both electric and magnetic dipole transition of $Eu^{3+}$ ions are able to manifest. Among the existing materials perovskites system offers more scope due to their inherent properties such as their high thermal and chemical stability, ability to form a wide range of compositions with different elements and cation ordering on both A and B sites of the perovskite systems (Aswathy *et al.* 2018, Zhang *et al.* 2009).

Perovskite systems can exhibit in three forms: i) simple perovskites: $ABO_3$, ii) double perovskites: $A_2BB'O_6$; $AA'BB'O_6$ etc and iii) triple perovskites: $A_3B'B_2''O_9$ etc enabling different amounts of cation ordering on both A and B sites. The A site are occupied by larger cations whereas the B sites by smaller cations and forming a three dimensional frame work of corner sharing $BO_6$ octahedra in the larger A site cations occupying the 12 coordinate cubaoctahedral within this frame work. The substitutions

of various cations on A and B sites provides the compositional diversity that alter the symmetry and the properties. Some of these oxides exhibit rock salt type B site ordering with cubic symmetry with 1:1 and 1:2 ordering on the B site (Zhang *et al.* 2013, Souza *et al.* 2012, Wang *et al.* 2017, Rodrigues *et al.* 2016). In the case of the complex triple perovskite $Ba_3CaNb_2O_9$ have attracted much interest in the field of dielectric resonators. In these structures the Ca and Nb are alternatively distributed in the form of Ca/Nb/Nb/Ca/Nb/Nb... with this type of ordering arrangement on the B site that will facilitate partition of the $Eu^{3+}$ ions in the lattice which increases the concentration quenching (Rodrigues *et al.* 2016). So far $Eu^{3+}$ luminescence have been widely investigated in simple perovskites $CaTiO_3$, $LaTiO_3$ etc (Yang *et al.* 2017, Zhong *et al.* 2016) and double pervoskites $Sr_2CaMoO_6$, $NaGdMg(W, Mo)O_6$, $NaCaTiTaO_6$ etc (Zhang *et al.* 2013, Wang *et al.* 2015, Sun *et al.* 2013). However, these systems generally exhibit 1:1 ordering which allows easily $Eu^{3+}$ - $Eu^{3+}$ interaction on higher substitution leading to low concentration quenching by which the required emission intensities cannot be achieved. In this regard, so far no attempt has been made to study the $Eu^{3+}$ luminescence in this complex triple perovskite $Ba_3CaNb_2O_9$. We study the $Eu^{3+}$ doped $Ba_3CaNb_2O_9$ for their structure, morphology, absorbance and photoluminescence properties and investigated the concentration quenching, quantum efficiency and life time curves.

## 4A.2 Experimental

A series of perovskite type orange phosphors having the general formula $Ba_3Ca_{(1-x)}Nb_2O_9$: $xEu^{3+}$ ($x$ = 0.05, 0.1, 0.15, 0.2, 0.25) was prepared via conventional solid state reaction method by using $BaCO_3$, $CaCO_3$, $Nb_2O_5$ and $Eu_2O_3$ from Sigma–Aldrich, Steinhheim, Germany with 99.99% as reagents. The stoichiometric amount of the reagents were mixed and grinded well in an agate mortar with acetone as the wetting medium. Mixing is followed by drying in a hot air oven at 100˚C. Mixing and drying processes was carried out thrice to obtain a homogeneous mixture. The obtained mixture was calcined at 1300 ˚C for 6h. The temperature of the furnace is programmed with an initial heating rate of 10°C/min up to 900°C followed by a heating rate of 5°C/min to attain the 1300 ˚C.

The crystalline structure of the samples was examined using an X-ray powder diffractometer (X'Pert Pro PANalytical, operated at 40 kV and 30 mA, Cu-Kα = 0.15406 nm, 2θ range = 10–90°). The morphological studies of the samples were done by a scanning electron microscope (Carl Zeiss EVO SEM) operated at 15kV. The X-ray micro chemical analysis of the samples were carried out using Silicon Drift Detector–X-Max$^N$ attached with the SEM. Absorbance study of the samples were carried out using a Shimadzu, UV-2450 UV–Vis spectrophotometer in the 200–800 nm wavelength range using barium sulfate as a reference. The excitation and emission spectra were recorded on a Fluorolog HORIBA fluorescence spectrophotometer with a Xe lamp (450 W) as the excitation source. Luminescence lifetime of the phosphors was recorded by the phosphorimeter attached to Fluorolog3 spectrofluorimeter. All measurements were taken at room temperature.

### 4A.3 Results and Discussion

#### 4A.3.1 Powder XRD analysis

Fig. 4A.1 depicts the powder XRD patterns of the $Ba_3Ca_{(1-x)}Nb_2O_9$: $x$Eu$^{3+}$ ($x$ = 0.05, 0.1, 0.15, 0.2, 0.25) samples. All the peaks can be indexed to 1:2 ordered perovskite type structure with a space group P-3m1 (ICSD number 162758) with Z = 3. There is no additional impurity peaks were observed. This 1:2 cation ordering on the B-site can be ascertained by the presence of small intensity superlattice reflections at low 2θ values. That means on the B-site $Ca^{2+}$ and $Nb^{5+}$ ions are alternately arranged in the form Ca/Nb/Nb/Ca/Nb/Nb/…along $[001]_h$ hexagonal direction. As a consequence, super lattice reflections are visible in the XRD pattern (marked as +). With the increase in $Eu^{3+}$concentration, the peaks are found to be shifting towards right side, it indicates the successful incorporation of $Eu^{3+}$ in the lattice. Shifting of XRD peaks is due to the incorporation of smaller $Eu^{3+}$ (1.066 Å) in place of $Ca^{2+}$ (1.12 Å). This kind of ordering on the B-site is helpful for reducing the exchange interaction between the $Eu^{3+}$ ions achieving in higher intensity values at a lower concentration. It has been discussed in the later part of the text.

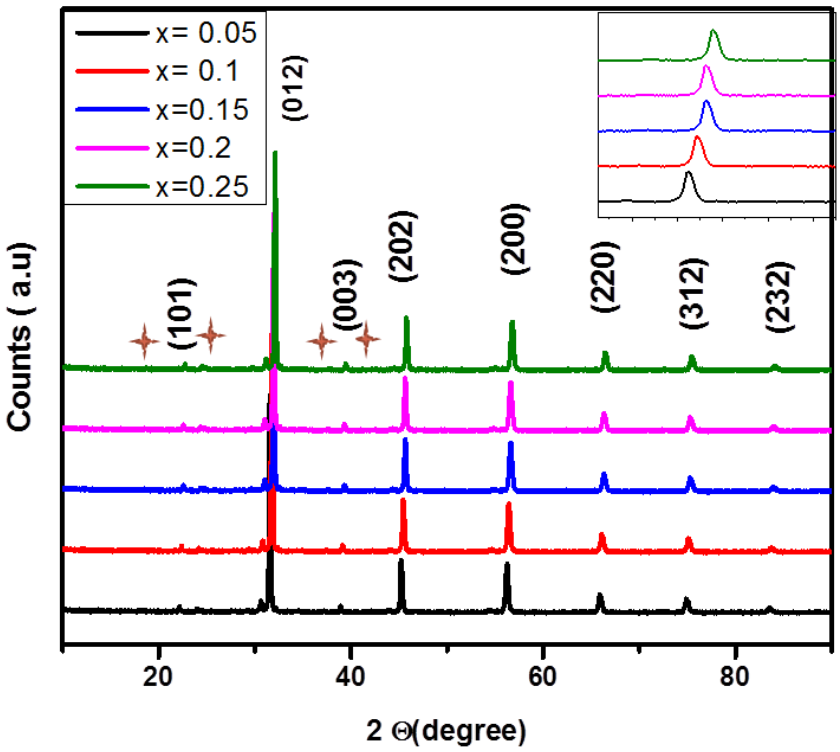


**Fig. 4A.1**: Powder XRD patterns of $Ba_3Ca_{(1-x)}Nb_2O_9$: $xEu^{3+}$ ($x$ = 0.05, 0.1, 0.15, 0.2, 0.25).

### 4A.3.2 Morphological analysis

Fig. 4A.2 shows the scanning electron micrographs (SEM) of $Ba_3Ca_{(1-x)}Nb_2O_9$:$xEu^{3+}$ samples. Particles are found to be uniformly distributed throughout the sample. Particle size varies from 0.5-1 μm with a slight increasing trend with $Eu^{3+}$ concentration. The phosphor particle of this size can be easily dispersible in any polymer matrix for encapsulation on the LED chip. Fig. 4A.3 shows the EDAX analysis of the typical sample $Ba_3Ca_{0.8}Nb_2O_9$: *0.20*$Eu^{3+}$ for identify the presence of the expected elements. Inset table contains the elemental atom percentage distribution in various samples. All the elements are present in the required stoichiometric amount as per the formula.

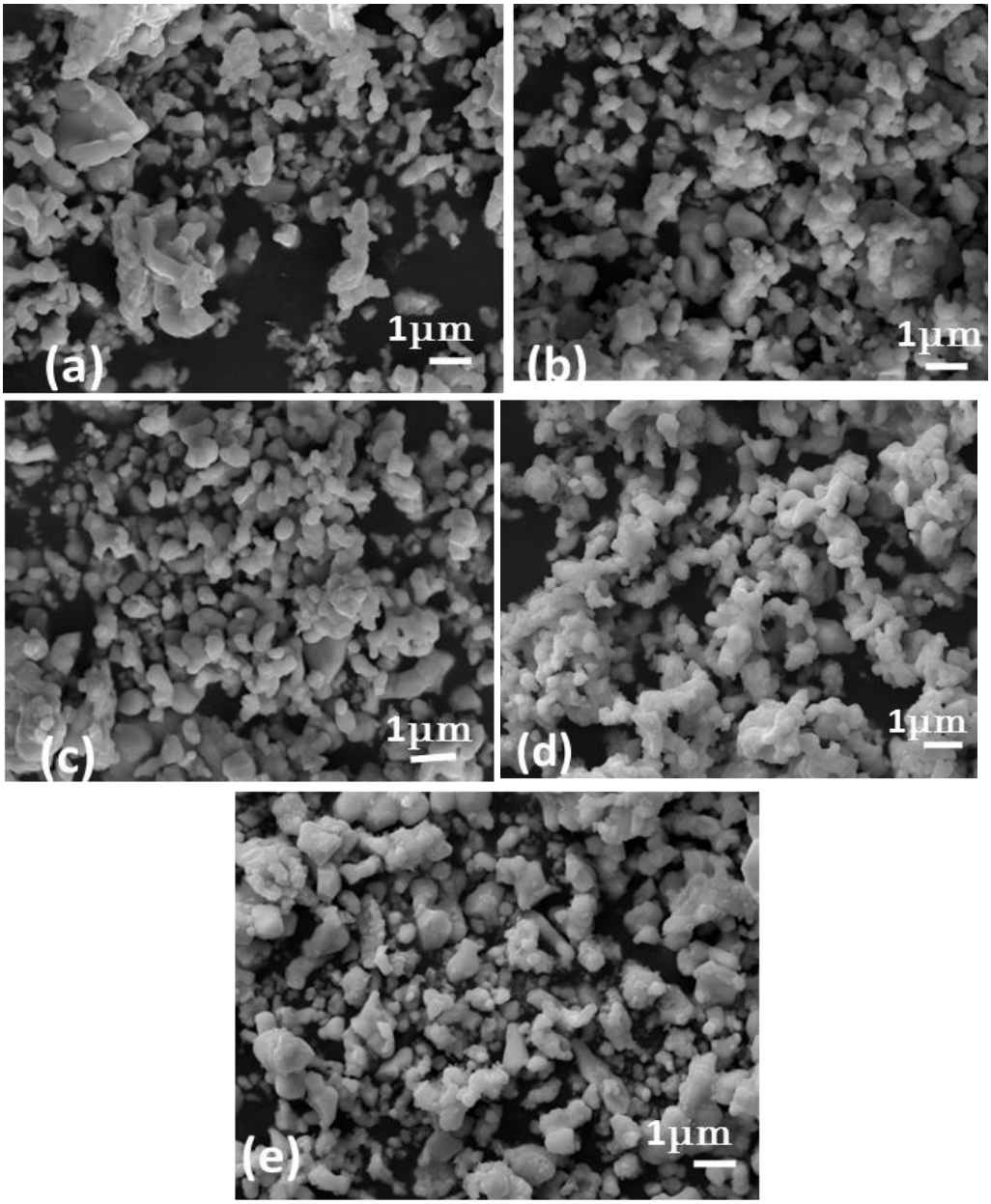


**Fig.4A. 2**: SEM images of $Ba_3Ca_{(1-x)}Nb_2O_9$: $xEu^{3+}$ samples ($x$ = 0.05, 0.1, 0.15, 0.2, 0.25).

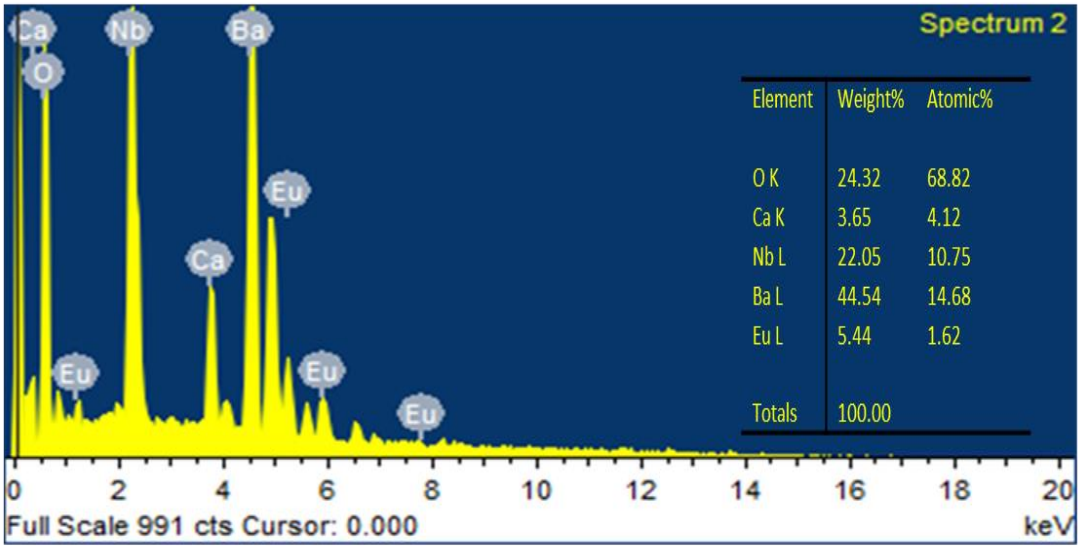


**Fig. 4A.3**: EDAX analysis of $Ba_3Ca_{0.8}Nb_2O_9$: 0.20$Eu^{3+}$ samples

### 4A.3.3 Optical Studies

UV visible absorption spectra of the samples are shown in Fig. 4A.4. All the samples exhibit broad absorption in the UV region. Band gap of samples was determined by Shapiro's method, extrapolating the absorbance edge to wavelength axis. Band gap values are listed in Table 4A.1. Strong absorption below 325 nm suggests the potentiality of the phosphor samples to incorporate with UV LEDs. The band gap values suggests a slight blue shift with the increase of $Eu^{3+}$ concentration ($x$ = 0.20) and then decreases. It can be further noticed that there is a decrease in the absorbance in the UV region with $Eu^{3+}$ concentration. This could be due to the effective energy transfer from the host to the $Eu^{3+}$ excitations.

Photoluminescent excitation spectra of the samples are shown in Figure 4A.5. Excitation spectra were recorded for an emission at 594 nm. Samples exhibit broad intense charge transfer band with *fwhm* ~31 nm and the sharp peaks corresponding to $O^{2-}$- $Eu^{3+}$ charge transfer and 4f-4f intraconfigurational transitions of $Eu^{3+}$ ions in the host respectively. The charge transfer band is mainly contributed from the transfer of O2p electrons to the partially filled f-f orbitals of $Eu^{3+}$ ions. Characteristic f-f transition

peaks of $Eu^{3+}$ is found to be less intense compared to CT band. This indicates that these phosphors have efficient energy transfer from the host to the $Eu^{3+}$ excitation levels. The

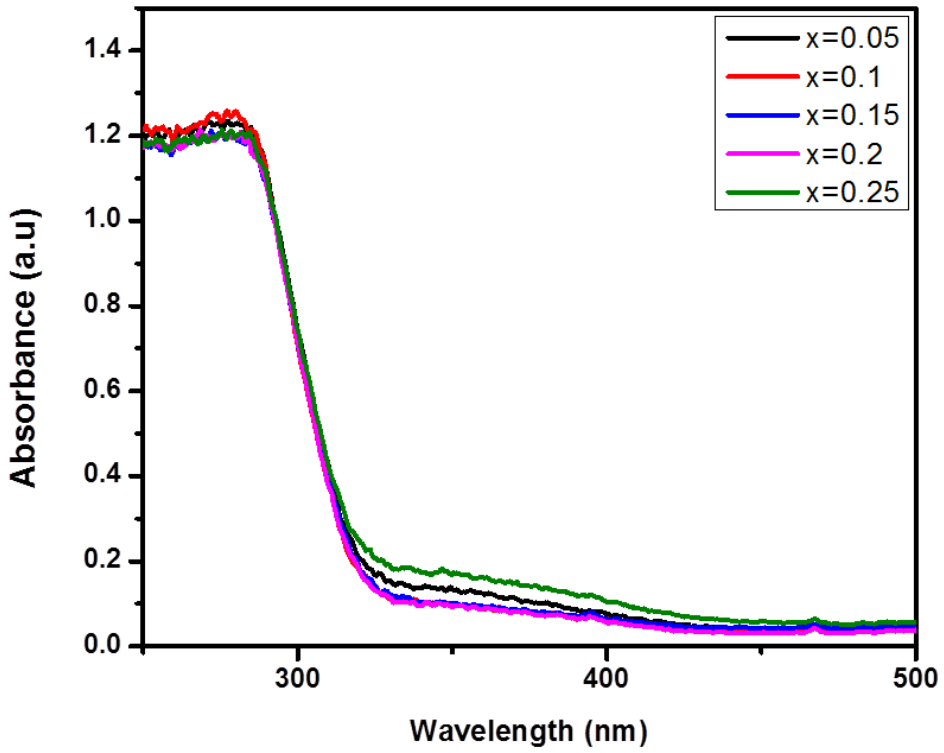


**Fig. 4A.4**: UV visible spectra of $Ba_3Ca_{(1-x)}Nb_2O_9$: $xEu^{3+}$($x$ = 0.05, 0.1, 0.15, 0.2, 0.25).

sharp excitation peaks at 360 nm, 384 nm, 394 nm, 404 nm and 465 nm can be attributed to $^7F_0$-$^5D_4$, $^7F_0$-$^5G_{2-4}$,$^7F_0$-$^5L_6$, $^7F_0$-$^5D_3$, $^7F_0$-$^5D_2$ transitions of $Eu^{3+}$ ions in the host (Blasse *et al.*1979). Luminescent excitation intensity increases with increase in $Eu^{3+}$ concentration upto 20 mol% and then decreases. The strong CT band at 288 nm and intense f-f transition (394 nm) due to $^7F_0$-$^5L_6$ indicates that these phosphors can be easily excited in the near UV region which makes them potential for the phosphor converted WLEDs.

The photoluminescent emission spectra of the phosphors $Ba_3Ca_{(1-x)}Nb_2O_9$: $xEu^{3+}$ for excitations at 394 nm and 288 nm are shown in figures (Fig 4A.6 and 4A.7). The emission spectra shows significantly three emission groups due to the $^5D_0$-$^7F_J$ (J = 0, 1 and 2) of the $Eu^{3+}$ ion (Blasse *et al.*1979). The presence of sharp single $^5D_0$-$^7F_0$ emission

line indicates only one crystallographic site for the $Eu^{3+}$ ions in the host. In addition, all the samples exhibit dominant orange emission at 593 nm and followed by red emission at 613 nm. In all the samples, the allowed magnetic dipole transition $^5D_0$-$^7F_1$ is

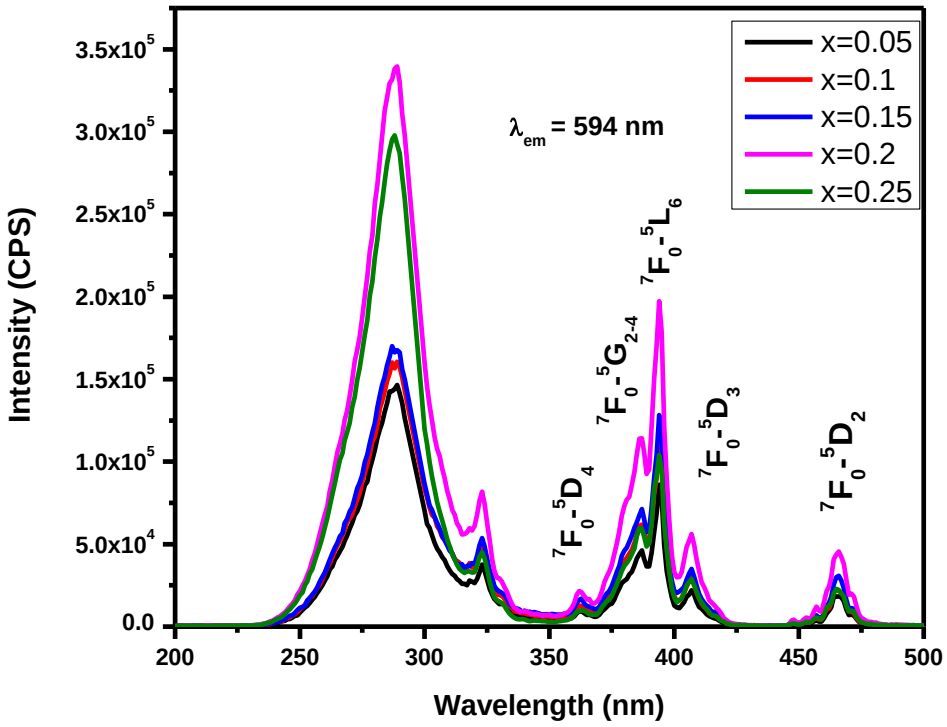


**Fig. 4A.5**: Photoluminescent Excitation spectra of $Ba_3Ca_{(1-x)}Nb_2O_9$: $xEu^{3+}$ ($x$ = 0.05, 0.1, 0.15, 0.2, 0.25) for emission at 594 nm

dominating than the forbidden electric dipole transition $^5D_0$-$^7F_2$. It is an indication of occupation of $Eu^{3+}$ in the centro-symmetric site in the lattice. In accordance with the photoluminescent excitation spectra the emission intensity also increases with increase in $Eu^{3+}$ concentration upto 20 mol% and then decreases. It can be further observed that the emission profile and peak positions remains the same except the change in intensity with increase of $Eu^{3+}$ concentration. This also reveals that the $Eu^{3+}$ ions are structurally stabilized in the host with a uniform environment. The higher quenching concentration can be attributed to the 1:2 ordered arrangement of Ca and Nb, which reduces the distance between $Eu^{3+}$ ions and the probability of non radiative energy transfer between the activators. CT band excited PL emission is found to be narrower with an *fwhm* ~ 4 nm. The degree of asymmetry of $Eu^{3+}$ site affects the luminescence

characteristics. Asymmetry ratio, the ratio of intensity of $^5D_0$-$^7F_2$ transition to that of $^5D_0$-$^7F_1$ transition can tell us about the local site symmetry of $Eu^{3+}$ ion. Asymmetry ratio of the samples was calculated and listed in Table 4A.1. In perovskite structure of $ABO_3$, $A_2BB'O_6$ or $A_3BB'_2O_9$, it has been shown that the dopant $Eu^{3+}$ ions can substitute either A site or B site depending on the relative sizes of the cations at A and B sites (Rodrigues *et al.* 2016). As reported earlier cation ions on the B site are occupied by smaller ions and the sites are regular and centro symmetric. In the present case, the B sites are occupied by Ca and Nb in a 1:2 order arrangement as proven in the XRD studies. It can be seen that the asymmetric values are below unity which also suggests the substitution of $Eu^{3+}$ ions at the B-site of Ca having centro symmetric site. The observed low asymmetric values indicate that the $Eu^{3+}$ ions prefer to occupy the centro symmetric B sites.

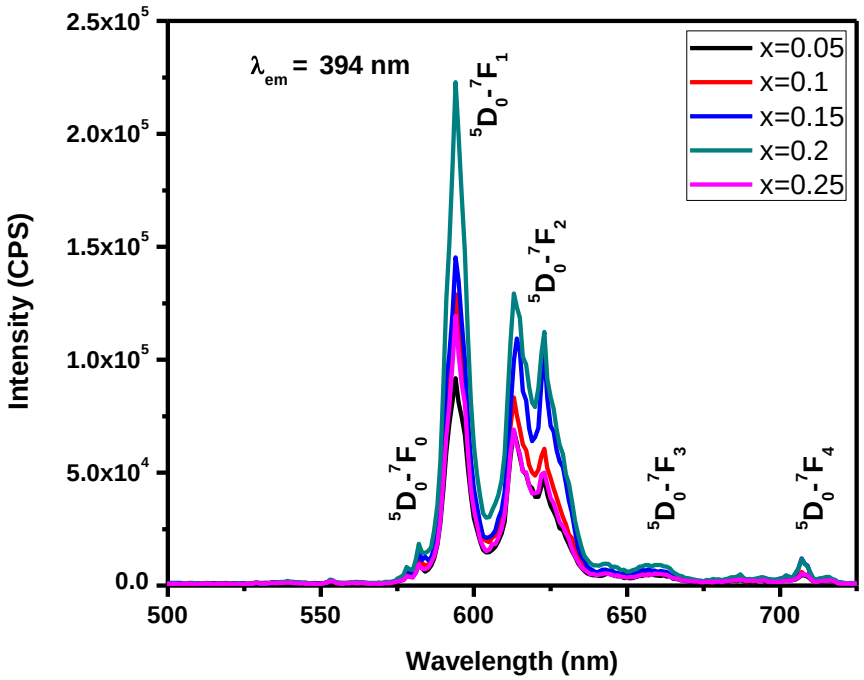


**Fig. 4A.6**: Photoluminescent emission spectra of $Ba_3Ca_{(1-x)}Nb_2O_9$: $xEu^{3+}$ ($x$ = 0.05, 0.1, 0.15, 0.2, 0.25) for excitation at 394 nm.

To assess the influence of the host on the luminescence properties, the emission intensities due to $^5D_0$-$^7F_1$ transition at 594 nm are compared for both CT band and

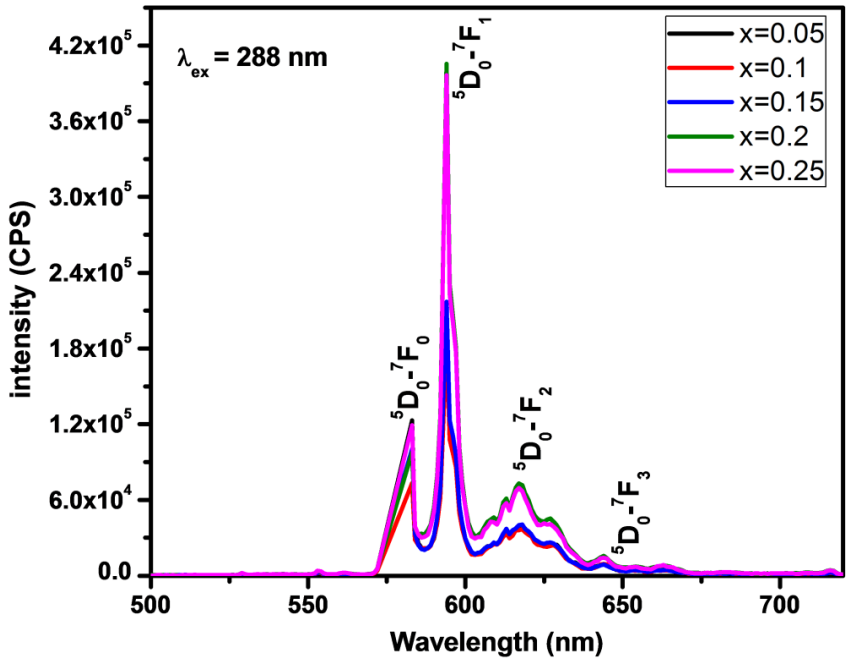


**Fig.4A. 7:** Photoluminescent emission spectra of $Ba_3Ca_{(1-x)}Nb_2O_9$: $xEu^{3+}$ ($x$ = 0.05, 0.1, 0.15, 0.2, 0.25) for excitation at 288 nm.

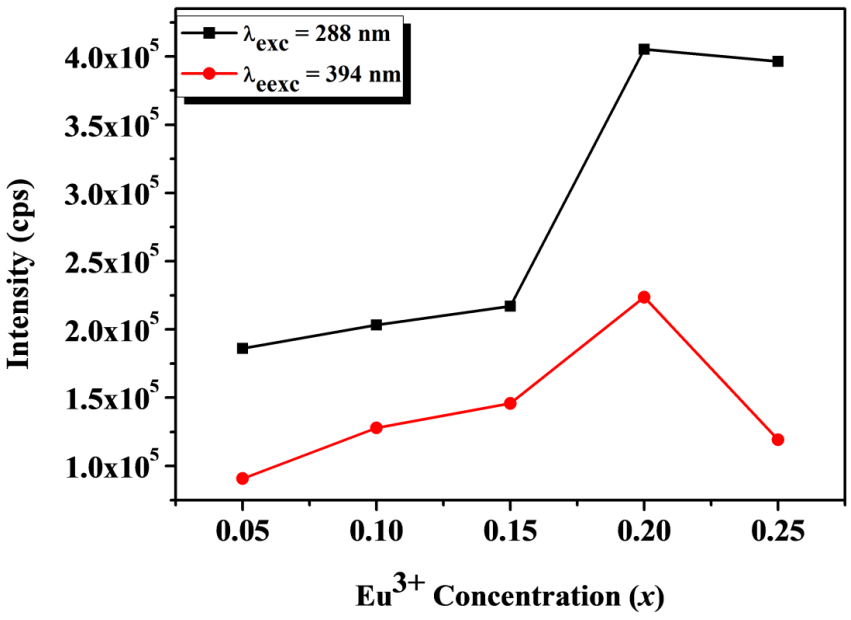


**Fig. 4A.8**:Variation of $Eu^{3+}$ intensity under 288 nm and 394 nm excitations of $Ba_3Ca_{(1-x)}Nb_2O_9$: $xEu^{3+}$ ($x$ = 0.05, 0.1, 0.15, 0.2, 0.25).

direct $Eu^{3+}$ excitations and shown in Fig. 4A.8. It can be observed that the emission intensities for the excitation at 288 nm are higher than the 394 nm excitations for all the concentrations. The intensity for the CT band excitation of $x$ = 0.2 is nearly double that of the direct $Eu^{3+}$ excitation at 394 nm. This can be inferred that the host sensitization is effectively taking place by way of energy transfer from the host to the $Eu^{3+}$ ions.

Table. 4A.1 The band gap values, average lifetime, asymmetric ratio and CIE color co-ordinates of $Ba_3Ca_{(1-x)}Nb_2O_9$: $xEu^{3+}$ ($x$ = 0.05, 0.1, 0.15, 0.2, 0.25)

| x | $A_1$ ($10^6$) | $\tau_1$ (ms) | $A_2$ ($10^6$) | $\tau_2$ (ms) | Average lifetime (ms) | Bandgap (eV) | Efficiency (%) | Asymmety ratio | (x,y) |
|---|---|---|---|---|---|---|---|---|---|
| 0.05 | 3.33 | 2.73 | 2.43 | 0.06 | 2.66 | 3.82 | 17.25 | 0.73 | (0.56,0.4) |
| 0.1 | 5.93 | 0.10 | 5.38 | 2.73 | 2.62 | 3.84 | 17.23 | 0.49 | (0.56,0.4) |
| 0.15 | 5.05 | 0.13 | 4.60 | 2.76 | 2.60 | 3.86 | 16.05 | 0.74 | (0.56,0.4) |
| 0.2 | 11.3 | 2.77 | 15.7 | 0.11 | 2.63 | 3.87 | 16.64 | 0.58 | (0.57,0.4) |
| 0.25 | 10.1 | 0.07 | 7.05 | 2.71 | 2.61 | 3.76 | 15.02 | 0.55 | (0.57,0.4) |

Lifetime analysis of the samples was done. The decay curves of the samples under UV excitation is shown in Figure 4A.9. The decay curves exhibit a double exponential behavior and the decay curves can be fitted to a double exponential function, $I = I_0+A_1\exp(-x/\tau_1)+A_2\exp(-x/\tau_2)$, where I, A , $\tau_1$ and $\tau_2$ are intensity, fitting parameter, the lifetime for fast and slow decay. The average lifetime can be evaluated using the relation $\boldsymbol{\tau} = \frac{\boldsymbol{A1\tau1^2+A2\tau2^2}}{\boldsymbol{A1\tau1+A2\tau2}}$ (Lia *et al*. 2019). The average lifetime values are in the range 2.62 to 2.70 ms which are significantly longer than the reported lifetime values in perovskite systems. Generally a long decay time for the activator ion is a characteristics of the most symmetrical surroundings while the short decay time is observed for the most distorted site. Hence, it is further clear from the longer life time values that $Eu^{3+}$ sites have more symmetrical surroundings at the B site substituting the Ca ions.

Assuming that only radiative and non radiative processes are essentially involved in the depopulation of $^5D_0$ states of $Eu^{3+}$ ion, the quantum efficiency ( η) can be expressed as; $\eta = A_{rad}/(A_{rad} + A_{nrad})$ where $A_{rad}$ and $A_{nrad}$ are radiative and non radiative transition probabilities respectively (Sun *et al*. 2008). Using the above equation and lifetime values the quantum efficiency (η) was calculated and presented in Table 4A.1. The η values is found to be in the range 15.02 to 17.25 % that are much higher than that of the reported ones $CaMO_4$: $Eu^{3+}$ (12.78%) and perovskite $Ca_2MgWO_6$:$Eu^{3+}$ (14.05%) (Aswathy *et al*. 2018).

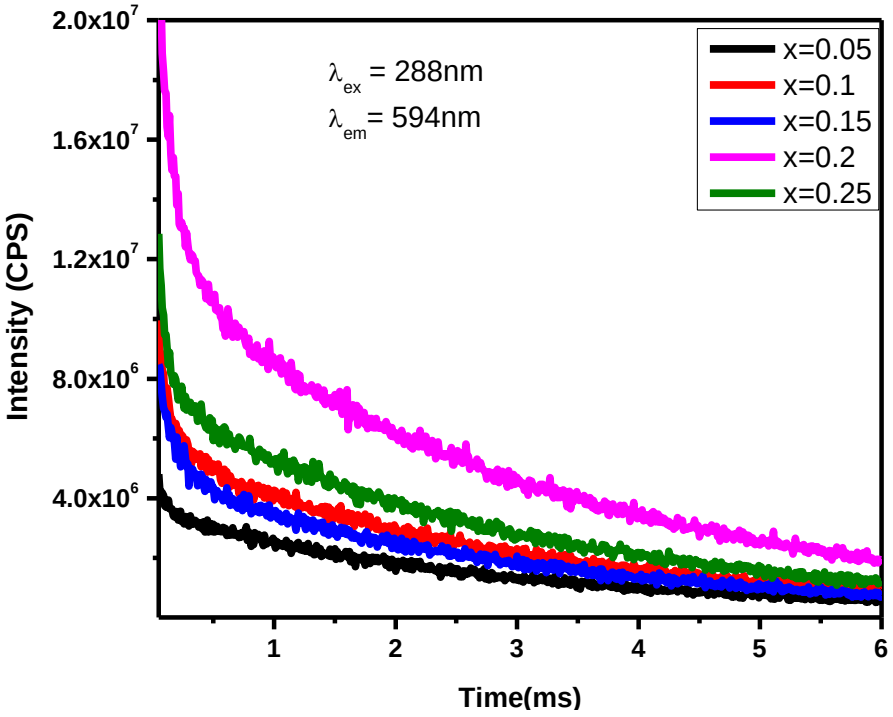


**Fig. 4A.9:** Decay curves of $Ba_3Ca_{(1-x)}Nb_2O_9$: $xEu^{3+}$ ($x$ = 0.05, 0.1, 0.15, 0.2, 0.25).

CIE Color co-ordinates of the samples were also calculated using CIE chromaticity calculator. The values obtained are provided in Table 4A.1. It can be noticed that the color co-ordinates lies in orange region of the chromacity diagram (Fig. 4A.10). The CIE color coordinates of $Ba_3Ca_{0.8}Nb_2O_9$:$0.2Eu^{3+}$ phosphor are (0.57, 0.41) that are close to the Nichia Corporation developed Amber LED NSPAR70BS (Wei *et al*. 2019).

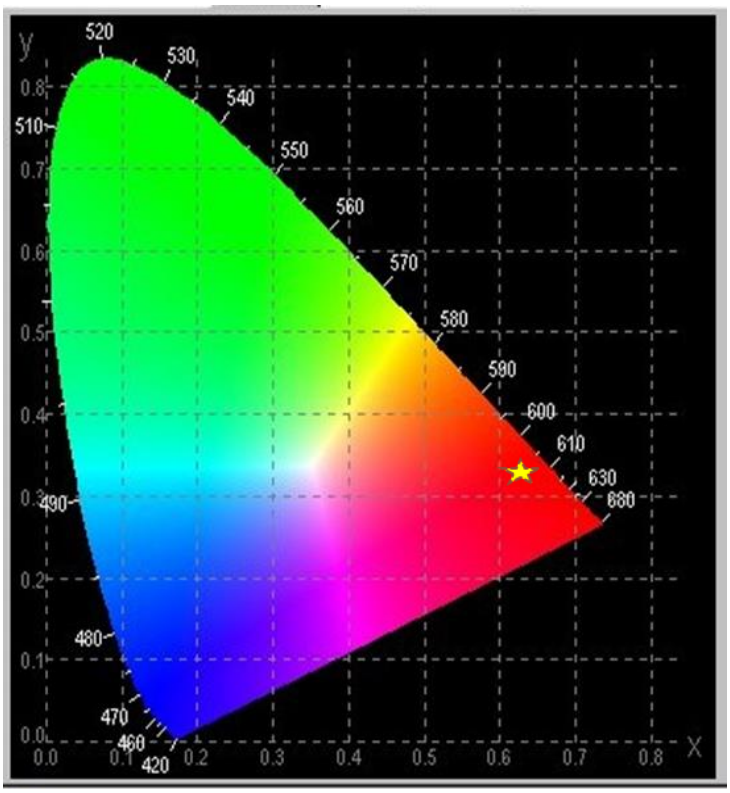


**Fig. 4A.10** : CIE color co-ordinates of $Ba_3Ca_{(1-x)}Nb_2O_9$: $xEu^{3+}$($x$ = 0.05, 0.1, 0.15, 0.2, 0.25)

## 4A.4 Conclusions

A new series of narrow orange red emitting phosphors $Ba_3Ca_{(1-x)}Nb_2O_9$: $xEu^{3+}$ were prepared via solid state reaction route successfully. Samples exhibit phase purity of trigonal perovskite type structure with 1:2 ordering of Ca and Nb on the B site. They possess strong absorption in UV region due to metal to ligand charge transfer transitions. Photoluminescence excitation spectra shows broad and intense charge transfer band around 288 nm and intense $Eu^{3+}$ excitations at 394 nm due to $^7F_0$-$^5L_6$. High concentration quenching of $Eu^{3+}$ occurs at 20 mol% due to more ordering of the activator ions in the lattice. These phosphors emit strong narrow orange light (*fwhm* ~ 4 nm) under charge transfer band (288 nm) with emission intensities double that of the $Eu^{3+}$ direct (394 nm) excitation which supports the host sensitization to the $Eu^{3+}$ luminescence. The low asymmetric values and high lifetimes confirm the occupation of $Eu^{3+}$ ions in the centro-symmetric sites of the host. Photoluminescence characteristics such as intense orange-red emission and good chromaticity co-ordinates (0.57, 0.41) indicates the potentiality of the phosphor sample for phosphor converted white LED applications.

# Chapter 4B

## Narrow red emitting phosphors, $Ba_2Y_{(1-x)}NbO_6$ :$xEu^{3+}$having high color purity for WLED applications

*This chapter is discussing about narrow red emitting double perovskite type phosphors, $Ba_2Y_{(1-x)}NbO_6$ :$xEu^{3+}$. Samples exhibit phase purity, high levels of absorption in UV and blue region, broad and intense charge transfer band and narrow emission lines. They possess different emission profiles for different excitations. As the value of exciting wavelength increases the emission color changes from orange to red.*

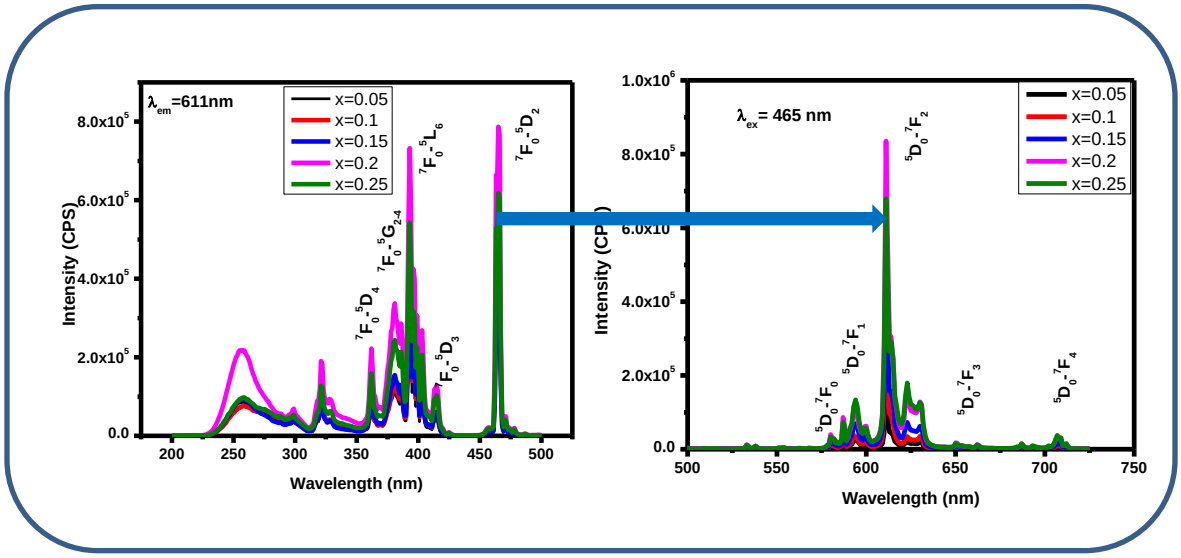

## 4B.1 Introduction

Narrow red emitting phosphors are highly demanding for WLED applications that will meet the requirements such as high color rendering index and luminous efficacy. Nitrides, silicates and oxides based $Eu^{2+}$ activated phosphors exhibit broad emission (Xie *et al.* 2011, Chuanyan *et al.* 2012). The emission into the deep red region in which eye is insensitive which is highly undesirable (Junhao *et al.* 2016). $Eu^{3+}$ activated red phosphors exhibit narrow red emissions due to the intraconfigurational f-f transition $^5D_0 \rightarrow {}^7F_2$ and have sharp excitation peaks at near UV ($^7F_0$-$^5L_6$) and blue region ($^7F_0$-$^5D_2$), matching with output of pumping LEDs. Photoluminescent characteristics of $Eu^{3+}$ activated phosphors strongly depend on their co-ordination environment. When $Eu^{3+}$ is occupying in a non-centrosymmetric site, $^5D_0 \rightarrow {}^7F_2$ electric dipole transition is dominating and if $Eu^{3+}$ is occupying in a site with centrosymmetry, $^5D_0 \rightarrow {}^7F_1$ magnetic dipole transition is dominating (Zhu, *et al.* 2015, Zhao *et al.* 2011). By suitably choosing the host lattice, narrow red emitting phosphors can be synthesized.

Double perovskites are found to be suitable host material for $Eu^{3+}$ activated red phosphors. They offer a lot of scope for wide variety of aliovalent cation substitutions at the A and B sites Because of this, lot of compositional modifications can be achieved in this system to tune the properties induced by the structural distortions(Li *et al.* 2012, Liu *et al.* 2016). Our aim is to develop $Eu^{3+}$ activated perovskite red phosphors with narrow red emission suitable for WLED applications.

## 4B.2 Experimental Procedure

A series of perovskite phosphor systems, $Ba_2Y_{(1-x)}NbO_6 : xEu^{3+}$ ($x$ = 0.05, 0.1, 0.15, 0.2, 0.25) were prepared via conventional solid state reaction method by using $BaCO_3$, $Y_2O_3$, $Nb_2O_5$ and $Eu_2O_3$ as reagents. The required stoichiometric amount of these materials were weighed and mixed thoroughly in an agate mortar with acetone as the mixing medium. The homogeneous mixture was then calcined at 1400˚C for 6 h. The crystalline structure of the samples was examined using an X-ray powder diffractometer (X'Pert Pro PANalytical, operated at 40 kV and 30 mA, Cu-Kα = 0.15406 nm, 2θ range = 10–90°). The morphological studies of the samples were done by a

scanning electron microscope (JEOL, JSM-5600LV) operated at 15kV. Absorbance study of the samples were carried out using a Shimadzu, UV-2450 UV–Vis spectrophotometer in the 200–800 nm wavelength range using barium sulfate as a reference. The excitation and emission spectra were recorded on a Fluorolog HORIBA fluorescence spectrophotometer with a Xe lamp (450 W) as the excitation source.

### 4B.3. Results and Discussion

#### 4B.3.1 Powder XRD analysis

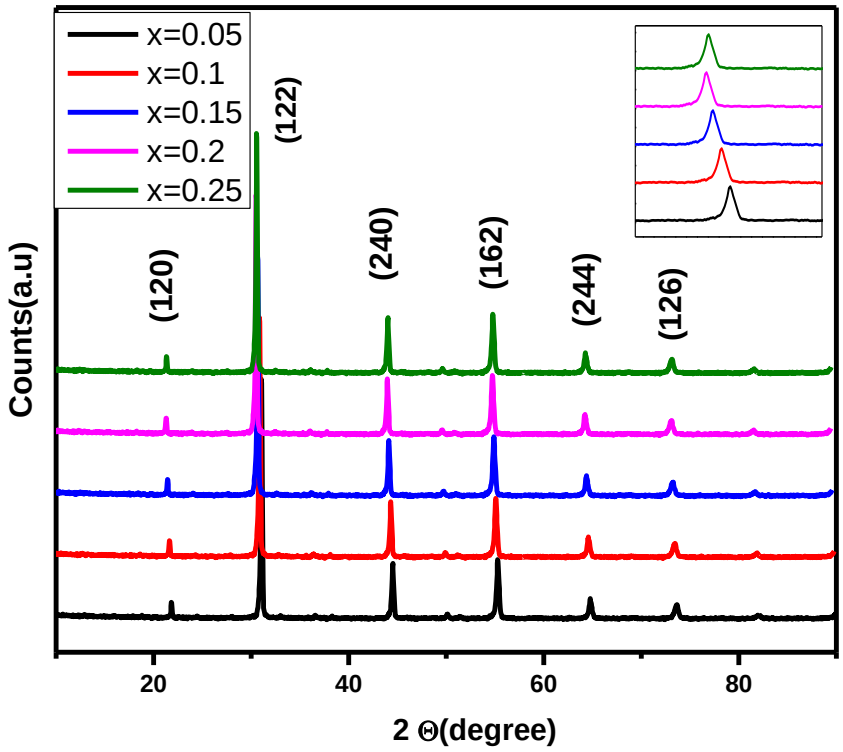


**Fig. 4B.1**: Powder XRD patterns of $Ba_2Y_{(1-x)}NbO_6 : xEu^{3+}$($x$ = 0.05, 0.1, 0.15, 0.2, 0.25)

Fig 4B.1 depicts the powder XRD patterns of the $Ba_2Y_{(1-x)}NbO_6 :xEu^{3+}$ samples. All the peaks can be indexed to Orthorhombic perovskite with space group Pbam (55), in accordance with the JCPDS file no 01-087-0568). With the increase in $Eu^{3+}$concentration, the peaks are found to be shift towards left side, it indicates the successful incorporation of $Eu^{3+}$ in the lattice. Shifting of XRD peaks is due to the

incorporation of bigger $Eu^{3+}$ (1.066 Å) in place of $Y^{3+}$(0.9 Å). No additional impurity peaks were observed.

### 4B.3.2 Morphological analysis

Fig 4B.2 shows the scanning electron micrographs (SEM) of $Ba_2Y_{(1-x)}NbO_6$ :$xEu^{3+}$

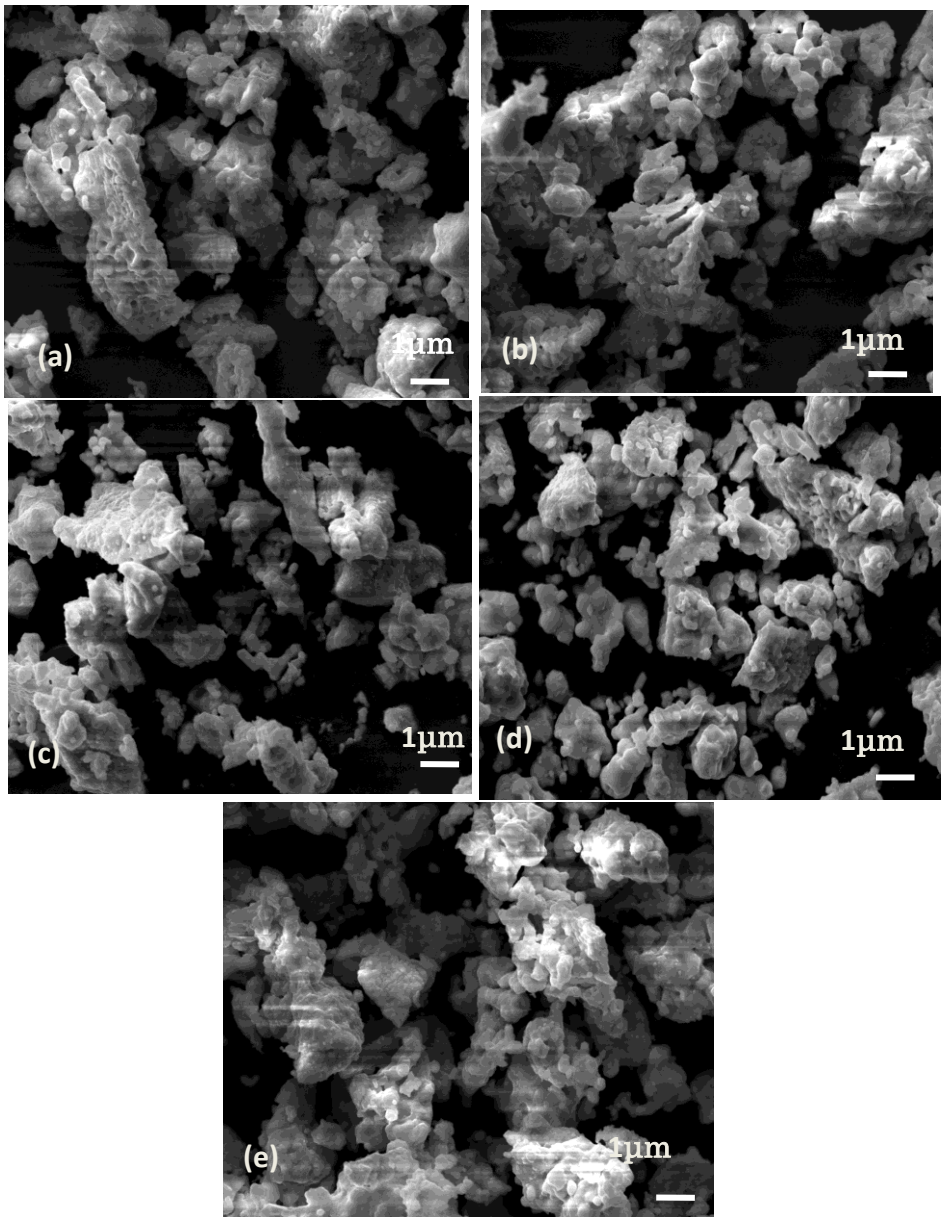


**Fig 4B.2**: SEM of $Ba_2Y_{(1-x)}NbO_6$ :$xEu^{3+}$($x$ = 0.05, 0.1, 0.15, 0.2, 0.25) samples.

samples. Particles are found to be agglomerated with a size distribution of 1-3 µm.

### 4B.3.3 EDAX analysis

Figure 4B.3 shows the EDAX analysis of the samples. Inset table contains the elemental and atom percentage distribution in various samples. All the elements are present in stoichiometric amount.

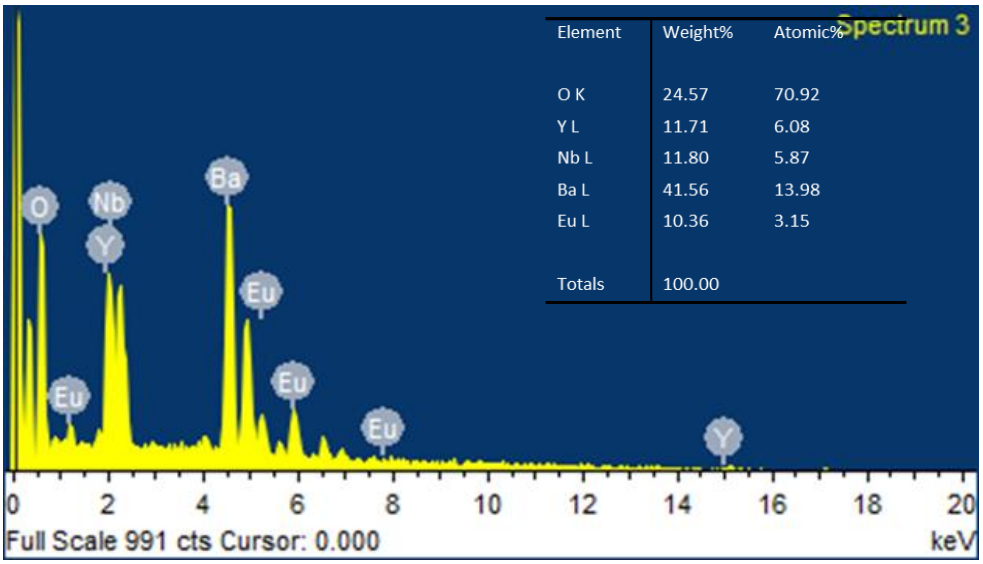


**Fig 4B.3**: EDAX analysis of $Ba_2Y_{(1-x)}NbO_6$ :$xEu^{3+}$($x$ = 0.05, 0.1, 0.15, 0.2, 0.25) samples.

### 4B.3.4 Optical studies

Fig. 4B.4 shows the UV Visible absorption spectra of $Ba_2Y_{(1-x)}NbO_6$ : $xEu^{3+}$. All the samples exhibit broad and strong absorption in 200 to 400 nm UV region. This indicates the potentiality of phosphors for the application in WLEDs.

Fig 4B.5 depicts the PL excitation spectra of $Ba_2Y_{(1-x)}NbO_6$ :$xEu^{3+}$ for an emission at 594 nm. Samples exhibit broad and intense charge transfer band. A slight red shift in the CT band emission peak with increase in $Eu^{3+}$ is observed. This shift can be attributed to an increase in covalency of Eu - O bonds and the co- ordination environment of $Eu^{3+}$ ,which reduces the CT energy (Linda *et al.* 2014, Sreena *et al.* 2015). The sharp excitation peaks at 360 nm, 384 nm, 392 nm, 404 nm and465 nm can be attributed to $^7F_0$-$^5D_4$, $^7F_0$-$^5G_{2-4}$,$^7F_0$-$^5L_6$, $^7F_0$-$^5D_3$, $^7F_0$-$^5D_2$ transitions of $Eu^{3+}$ ions in the host (Li *et al.*

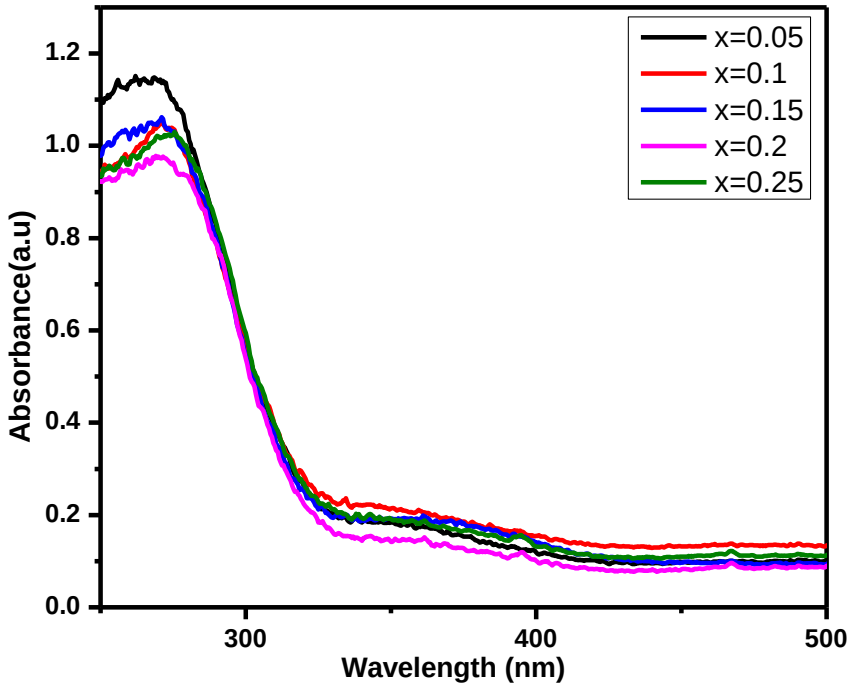


**Fig. 4B.4** : UV Visible absorption analysis of $Ba_2Y_{(1-x)}NbO_6$ :$xEu^{3+}$($x$ = 0.05, 0.1, 0.15, 0.2, 0.25)

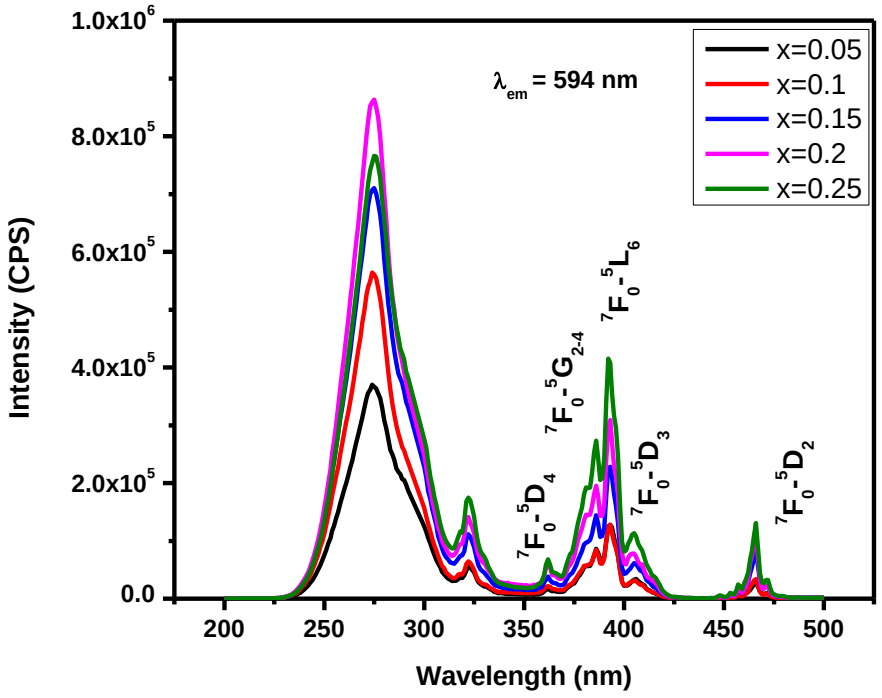


**Fig. 4B.5** : PL excitation spectra of $Ba_2Y_{(1-x)}NbO_6$ :$xEu^{3+}$ for an emission at 594 nm

2013, Lee *et al.* 2018). Excitation intensity of the doped samples increases with increase in $Eu^{3+}$ concentration and saturation occurs for 20 mol% doping. Fig. 4B.6 shows the PL excitation spectra of $Ba_2Y_{(1-x)}NbO_6$:$xEu^{3+}$ for an emission at 611 nm. Here the intensity of CT band is reduced and f-f transitions are found to be highly intense. That means efficient energy transfer takes place to $Eu^{3+}$ ions. Excitation peaks at 392 nm and 465 nm are highly intense and matches well with the emission of UV and blue LEDs.

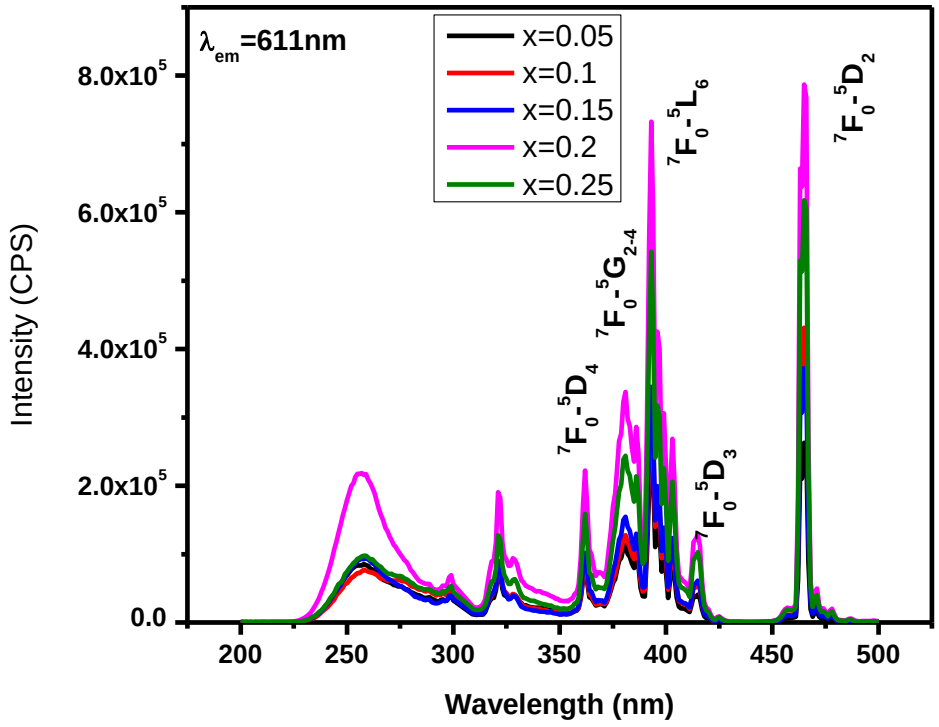


**Fig. 4B.6**: PL excitation spectra of $Ba_2Y_{(1-x)}NbO_6$ :$xEu^{3+}$ for an emission at 611 nm

PL emission of the samples for different excitations are shown in figures (Fig. 4B.7, Fig 4B.8 and Fig 4B.9). We got different emission profiles for different excitations. Emission lines are found to be very narrow of the order of 2 to 3 nm of fwhm. For CT band excitation, orange emission is dominating. But as the exciting wavelength increases the emission color changes from orange to red. Variation of asymmetric ratio for different excitation is also studied. For CT band excitation there is no much variation in the asymmetry ratio with different $Eu^{3+}$ concentration. But as the exciting wavelength increases asymmetry ratio also increases and is maximum for 465 nm blue

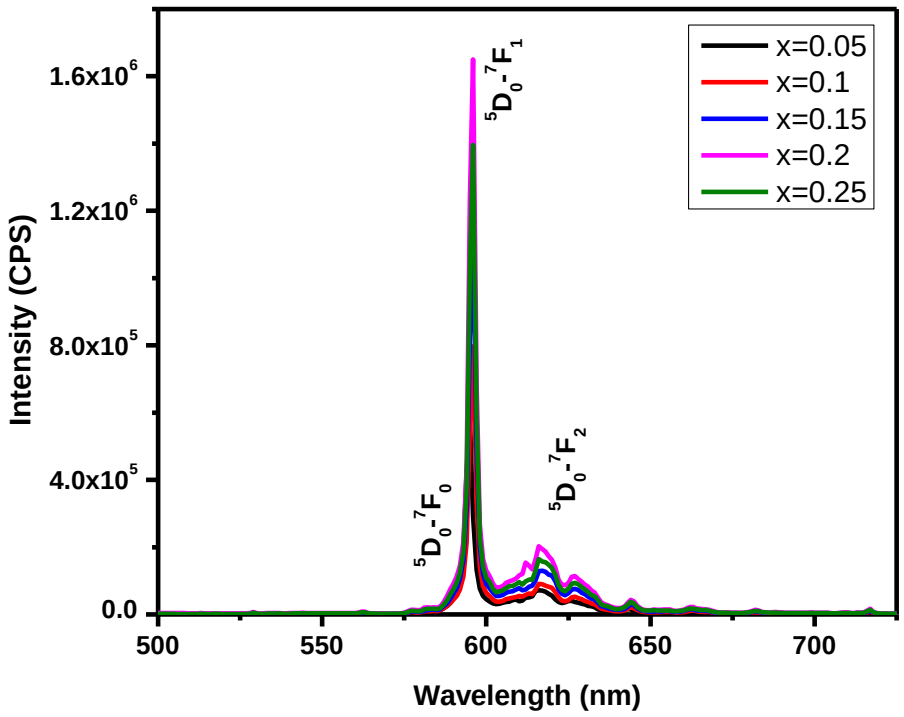


**Fig. 4B.7**: PL Emission spectra of $Ba_2Y_{(1-x)}NbO_6$ :$xEu^{3+}$ under CT band excitation

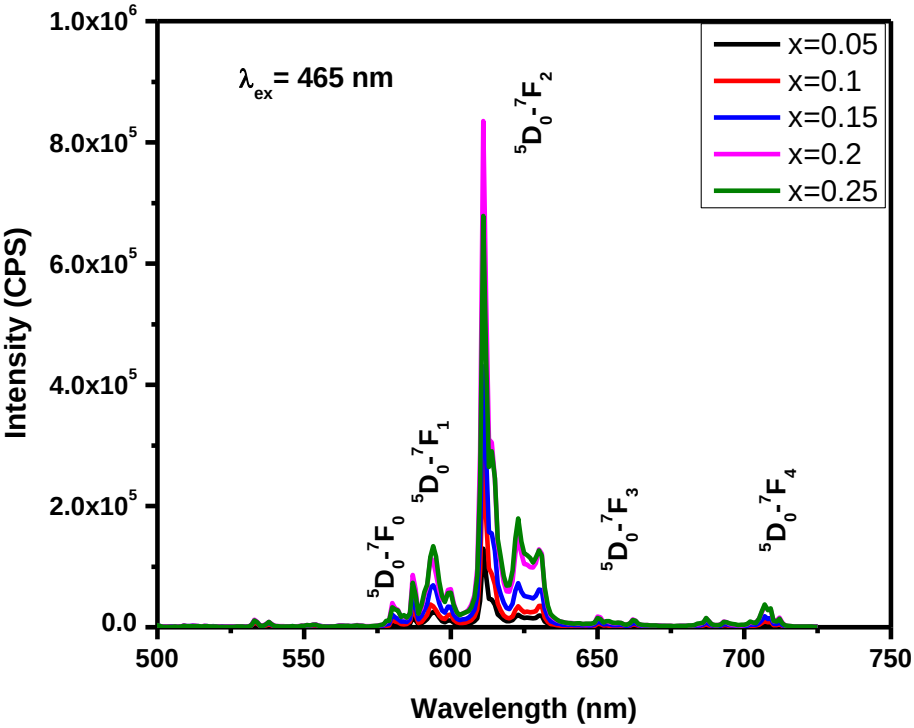


**Fig. 4B.8**: PL Emission spectra of $Ba_2Y_{(1-x)}NbO_6$ :$xEu^{3+}$ under 465nm excitation

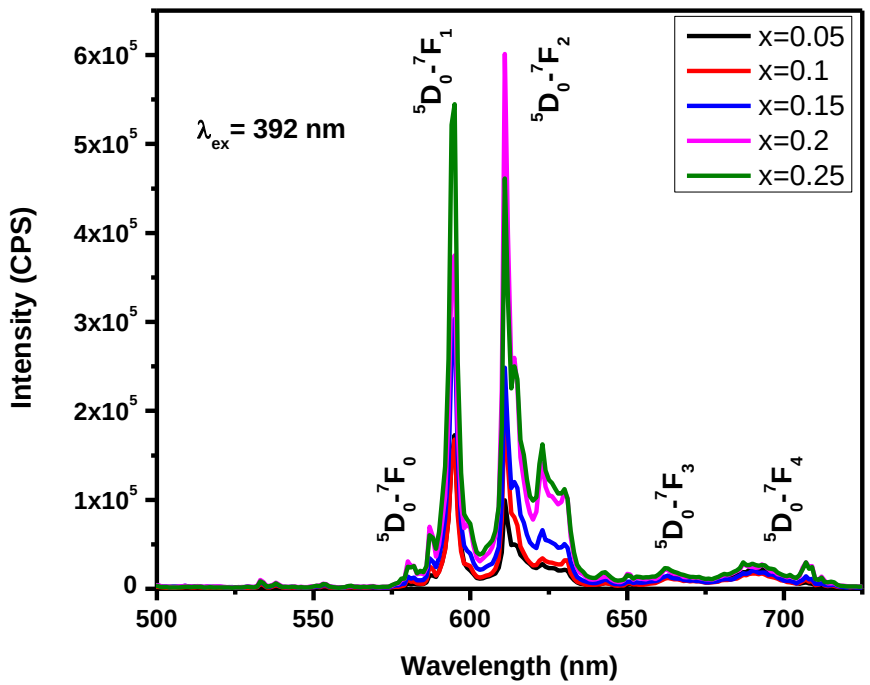


**Fig. 4B.9**: PL Emission spectra of $Ba_2Y_{(1-x)}NbO_6$ :$x$Eu$^{3+}$ under 392nm excitation

light excitation. Photoluminescent emission intensity also increases with increase in $Eu^{3+}$ concentration upto 20 mol% and then decreases. Color co-ordinates of the samples were determined using CIE chromaticity co-ordinate calculator and tabulated in table 4B.1. Color purity values of the samples for 465nm excitation also evaluated using the equation $color\ purity = \frac{\sqrt{\{(x-xi)2 + (y-yi)2\}}}{\sqrt{\{(xd-xi)2 + (yd-yi)2\}}} \times 100$, where (x,y) are the color co-ordinates of the sample, ($x_i$,$y_i$) are color co-ordinates of white illuminant, and ($x_d$,$y_d$) are chromaticity co-ordinates of the dominant wavelength. ($x_i$,$y_i$) = (0.33,0.33) and ($x_d$,$y_d$) = (0.67,0.33) (Lee *et al.* 2018) Color co-ordinates obtained are close to NTSC standard value for red phosphor (0.67,0.33). Having high color purity values, intense and narrow red emission with high asymmetric ratio, the prepared phosphors can be potential candidates for WLED applications.

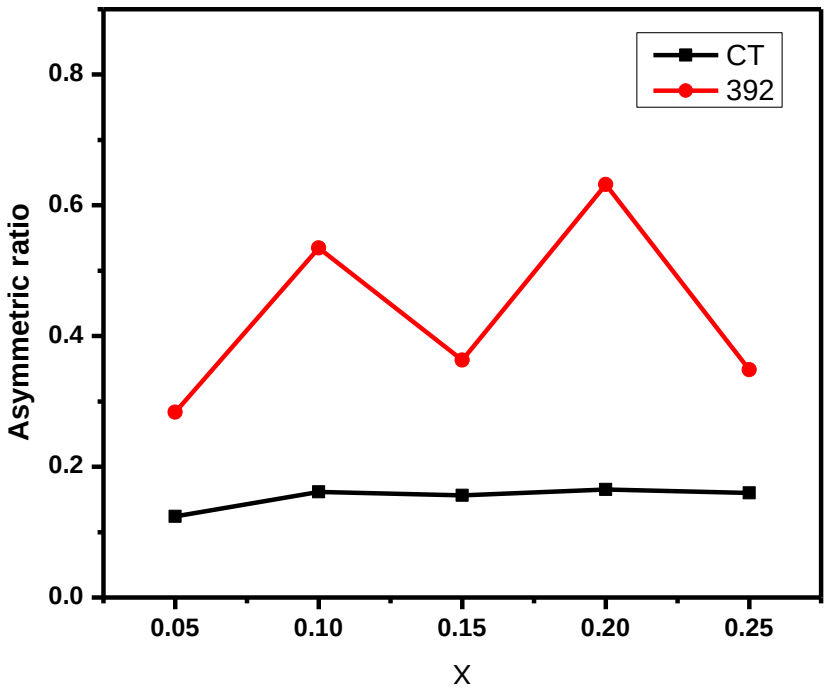


**Fig. 4B.10**: Variation of asymmetric ratio of $Ba_2Y_{(1-x)}NbO_6$ :$xEu^{3+}$ for CT band and 392 nm excitations

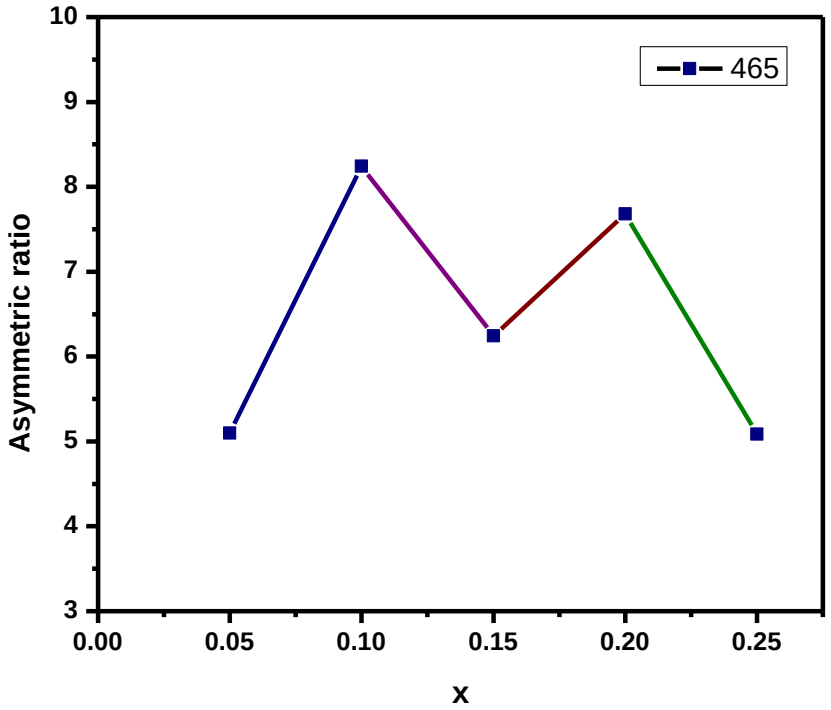


**Fig 4B.11**: Variation of asymmetric ratio of $Ba_2Y_{(1-x)}NbO_6$ :$xEu^{3+}$ for 465 nm excitation.

Table 4B.1 : Asymmetric ratio, Fwhm, CIE color co-ordinates and color purity of the $Ba_2Y_{(1-x)}NbO_6$ :$xEu^{3+}$ samples for 465 nm excitation.

| **x** | **Asymmetric ratio** | **Fwhm ( nm)** | **(*x*, *y*)** | **Color purity(%)** |
|---|---|---|---|---|
| **0.05** | 5.09 | 2.3 | (0.65,0.32) | 91 |
| **0.1** | 8.24 | 2.2 | (0.64,0.31) | 90 |
| **0.15** | 6.24 | 2.4 | (0.66,0.31) | 92 |
| **0.2** | 7.67 | 2.3 | (0.65,0.33) | 94 |
| **0.25** | 5.08 | 2.5 | (0.63,0.32) | 89 |

## 4B.4 Conclusions

Perovskite type red emitting phosphors $Ba_2Y_{(1-x)}NbO_6$: $xEu^{3+}$ were prepared via solid state reaction route. Samples exhibit phase purity, high levels of absorption in UV and blue region, broad and intense charge transfer band and narrow emission lines. They possess different emission profiles for different excitations. As the value of exciting wavelength increases the emission color changes from orange to red. Asymmetry ratio also increases with increase value of exciting wavelength and is maximum for 465 nm blue light excitation. Samples exhibit narrow red emission having high color purity, good chromaticity co-ordinates and high asymmetric ratio which makes them suitable for WLED applications.

# Chapter 5A

## New Self -Charge Compensating Perovskite Type Red Phosphors $Na_{(1+x)}Ca_{(1-2x)}SnNbO_6$: $xEu^{3+}$ Prepared via Ball Milling Process for pc-White Light Emitting Diode Applications

*In this chapter, structural, microstructural and luminescent studies on self-charge compensating red emitting perovskite type phosphors, $Na_{(1+x)}Ca_{(1-2x)}SnNbO_6:xEu^{3+}$ prepared by a high energy ball milling method is discussed. These phosphors exhibit intense red emission due to forced electric dipole transition, $^5D_0 \rightarrow {}^7F_2$ under near UV (395nm) and blue (463nm) excitations. High asymmetry ratio evidences the occupancy of $Eu^{3+}$ at the non-centrosymmetric A site of the perovskite.*

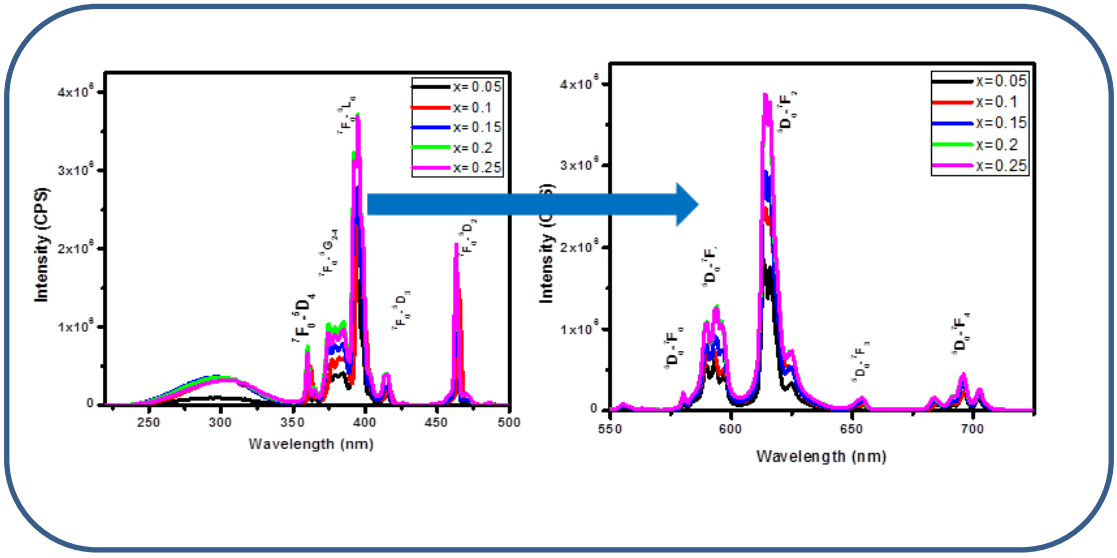

## 5A.1 Introduction

Lanthanide ions have been applied in various lighting devices because of its emission covering wide spectral region from near UV to IR (Nikol *et al.* 1998). $Eu^{3+}$ ions are well known for its red luminescence arising from the intra configurational f-f transitions (Binnemans *et al.* 2015). Also perovskites are found to be suitable host material for luminescence applications. Double perovskites offer a lot of scope for wide variety of aliovalent cation substitutions at the A and B sites Because of this, lot of compositional modifications can be achieved in this system to tune the properties induced by the structural distortions (Jiang *et al.* 2016, Dhananjay *et al.* 2016, Li *et al.* 2013). Photoluminescent properties of phosphors strongly depend on the synthesis method and synthesis conditions to a certain extent (Yang *et al.* 2010). Ball milling process can enhance the reactivity of the system, and hence reduce the reaction temperature. Also ball milling produces particles having uniform grain size distribution and better morphology, which improves the photoluminescent characteristics (Kong *et al.* 2002, Yang *et al.* 2010).

Charge compensation is very significant for betterment of photoluminescent properties. Most common charge compensation method is the suitable addition of alkali metals such as Li, Na, K, etc. However, such charge compensation methods are carried out intentionally by addition of some monovalent ions which may lead sometimes to some secondary phases. In the present study, the charge compensation is built in the system as Na ion is part of the composition (Rao *et al.* 2018, Zhang *et al.* 2016). Further, the aliovalent cations such as $Ca^{2+}$, $Eu^{3+}$, $Na^{+}$ are occupying the A site with the ionic radii for (VIII) co-ordination as 112 pm, 106 pm and 118 pm respectively. The incorporation of cations with different ionic radii can result in distortions in the lattice. Thus in our case stoichiometry is selected in such a way that charge compensation takes place automatically without the addition of alkaline ions.

## 5A.2. Experimental Procedure

$Na_{(1+x)}Ca_{(1-2x)}SnNbO_6$:$x$$Eu^{3+}$($x$ = 0.05, 0.1, 0.15, 0.2, 0.25) phosphors were prepared via high energy ball milling method by using $Na_2CO_3$, $CaCO_3$, $SnO_2$, $Nb_2O_5$, $Eu_2O_3$ as reagents. The stoichiometric amount of the powder mixture of the reagents was ball milled in a planetary mono mill pulveriser with a rotation speed of 250 rpm for 8h with acetone as the mixing medium. The ball milled powder was calcined at 1000˚C for 6 h. The crystalline structure of the samples was examined with an X-ray powder diffractometer (X'Pert Pro PANalytical, operated at 40kV and 30mA, Cu-Kα = 0.15406 nm, 2θ range = 10 - 90˚). The morphological study of the samples was done by a JEOL scanning electron microscope (model JSM - 5600LV), with an accelerating voltage of 15kV. Absorbance study of the samples were carried out using a Shimadzu, UV-2450 UV–Vis spectrophotometer in the 400–700 nm wavelength range using barium sulfate as a reference. The excitation and emission spectra were recorded on a Fluorolog HORIBA fluorescence spectrophotometer with a Xe lamp (450 W) as the excitation source.

## 5A.3 Results and Discussion

### 5A.3.1 XRD Analysis

Powder X-ray diffraction patterns of the samples $Na_{(1+x)}Ca_{(1-2x)}SnNbO_6$: $x$$Eu^{3+}$ ($x$ = 0.05, 0.1, 0.15, 0.2, 0.25) are given in Figure 5A.1. As the $Eu^{3+}$concentration increases $SnO_2$ peaks can be visible. All the other peaks can be indexed with the reported diffraction pattern of $NaCaTiNbO_6$ (JCPDS file no 25-0853; orthorhombic perovskite with a space group Pnma.

In $AA'BB'O_6$ double perovskites, the large differences of ionic radii and oxidation states of B site result in the ordering of $Nb^{5+}$ and $Sn^{4+}$ . The ions $Nb^{5+}$ and $Sn^{4+}$ alternate in positions to form $NbO_6$ and $SnO_6$ octahedra. Rock salt type arrangement of the B cations is expected to maximize the distance between similar cations. A site cations $Na^+$ and $Ca^{2+}$ are expected to offer a layered arrangement in the lattice (Jing *et al*. 2015, Davies *et al.* 2008).

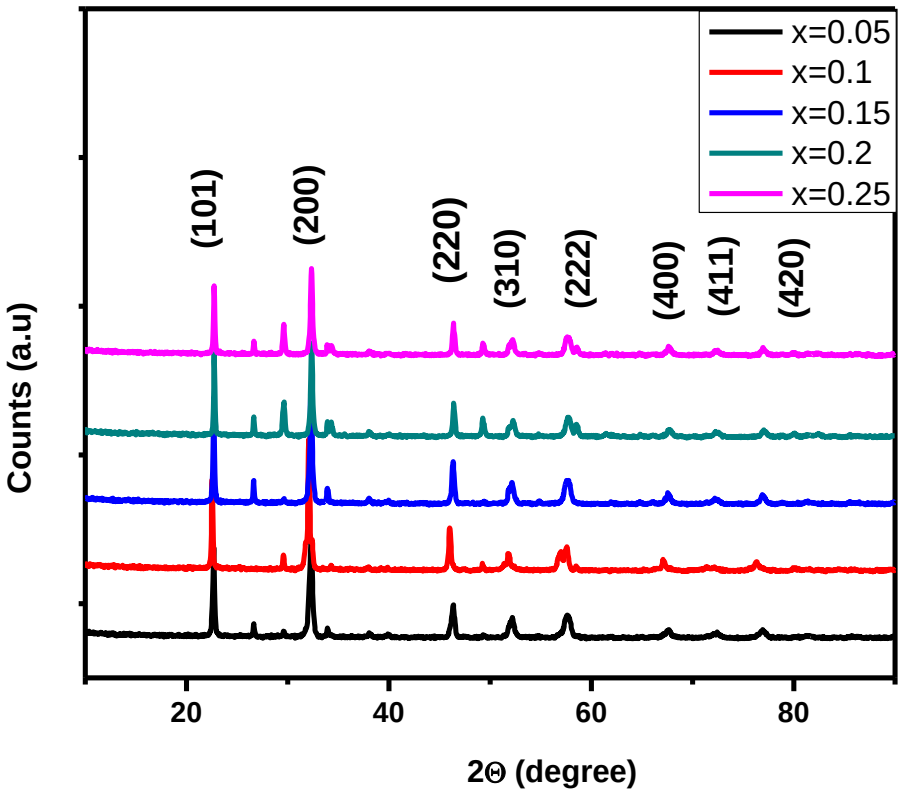


**Fig. 5A.1** : Powder X-ray diffraction patterns of the samples $Na_{(1+x)}Ca_{(1-2x)}SnNbO_6$: $xEu^{3+}$ ($x$ = 0.05, 0.1, 0.15, 0.2, 0.25)

### 5A.3.2 Morphological Analysis

Figure 5A.2 shows the scanning electron micrographs of the samples. The particles are finely grinded and have a size distribution of 0.1-1μm. The ball milled samples exhibit a uniform distribution of particles and better morphology. The spherical morphology is expected to assist photoluminescent properties of the system by the way of reducing the scattering of light (Yang *et al.* 2010)

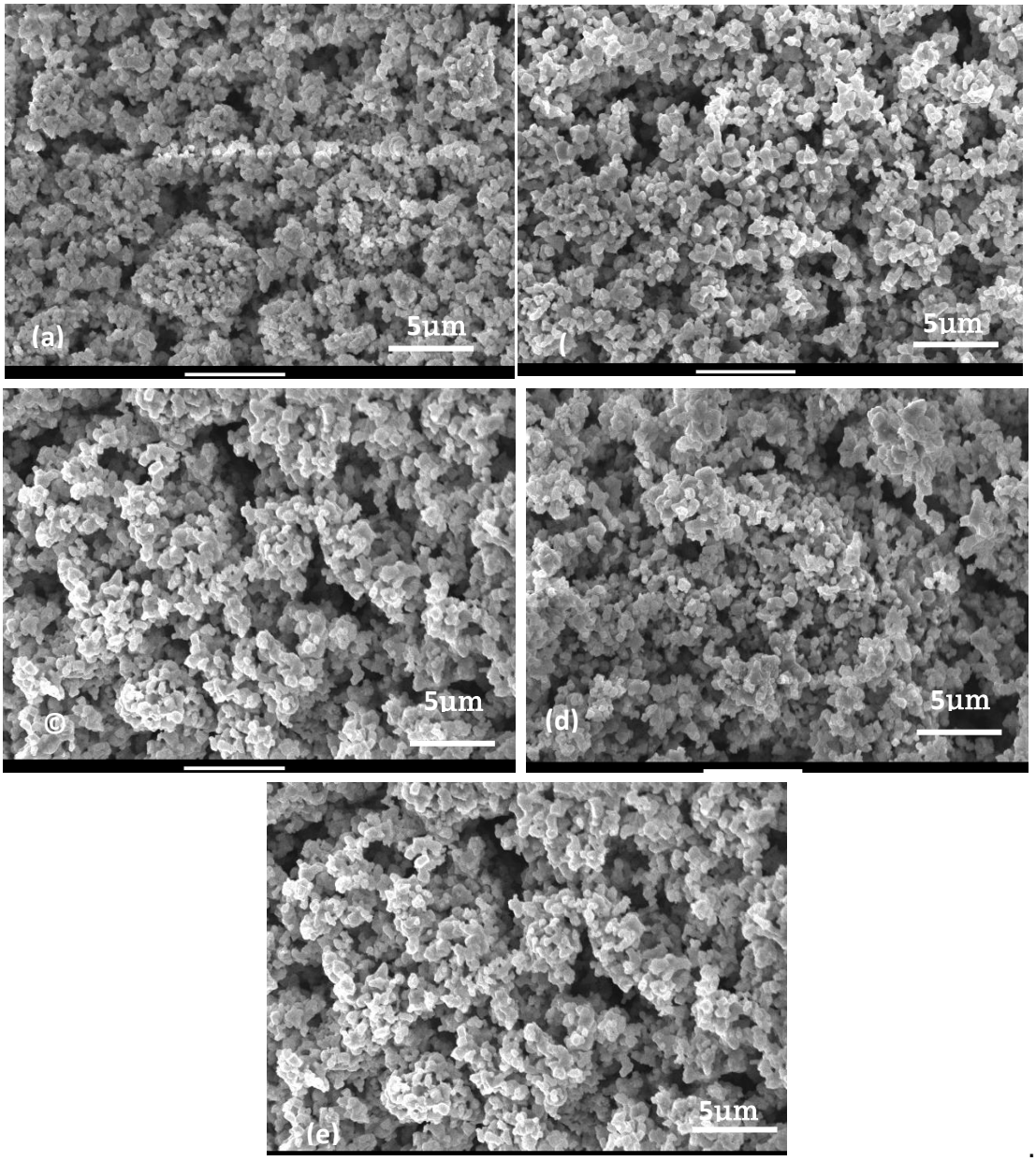


**Fig. 5A.2**: SEM images of $Na_{(1+x)}Ca_{(1-2x)}SnNbO_6$: $xEu^{3+}$ ($x$ = 0.05, 0.1, 0.15, 0.2, 0.25)

### 5A.3.3 Optical Studies

Fig 5A.3 shows the UV Visible absorption spectra of $Na_{(1+x)}Ca_{(1-2x)}SnNbO_6$: $xEu^{3+}$. All the samples exhibit broad and strong absorption in 200 to 400 nm UV region. This indicates the potentiality of phosphors for the application in WLEDs.

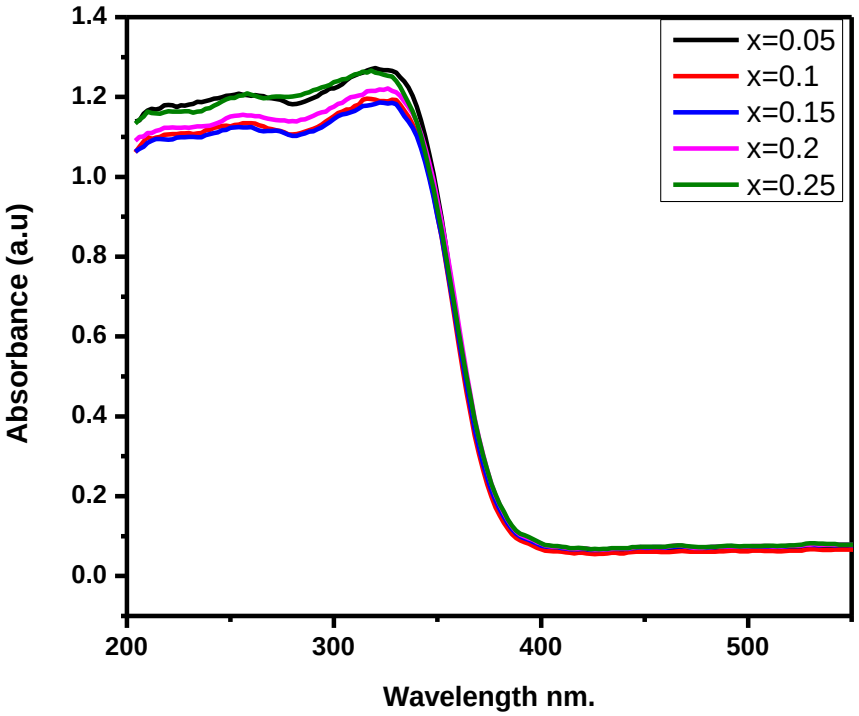


**Fig. 5A.3**: UV Visible analysis of $Na_{(1+x)}Ca_{(1-2x)}SnNbO_6$: $xEu^{3+}$ ($x$ = 0.05, 0.1, 0.15, 0.2,0.25)

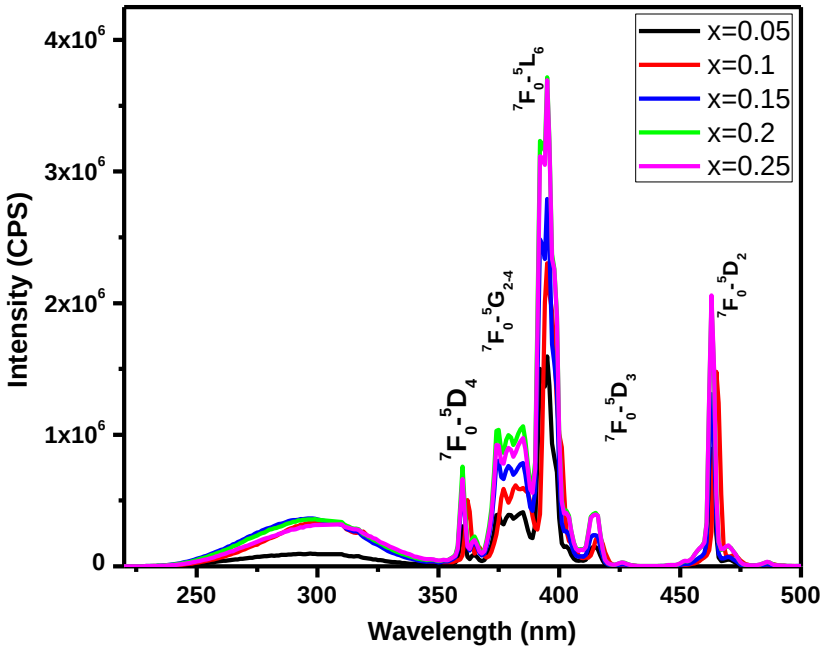


**Fig. 5A.4**: Photoluminecence excitation spectra of $Na_{(1+x)}Ca_{(1-2x)}SnNbO_6$: $xEu^{3+}$ ($x$ = 0.05, 0.1, 0.15, 0.2, 0.25)

Figure 5A.4 shows Photoluminescence excitation spectra of $Na_{(1+x)}Ca_{(1-2x)}SnNbO_6$:$xEu^{3+}$ samples for an emission at 613 nm. Charge transfer band is found to be less intense compared to intra configurational f-f transitions of $Eu^{3+}$ ions in the host. The sharp excitation peaks at 360 nm, 384 nm, 395 nm, 414 nm and 463 nm can be attributed to $^7F_0$-$^5D_4$, $^7F_0$-$^5G_{2\text{-}4}$,$^7F_0$-$^5L_6$, $^7F_0$-$^5D_3$, $^7F_0$-$^5D_2$ transitions of $Eu^{3+}$ ions in the host (Liu *et al.* 2017, Long *et al.* 2013). Excitation intensity of the doped samples increases with increase in $Eu^{3+}$ concentration and saturation occurs for 20 mol% doping. Excitation peaks at 392 nm and 465 nm matches well with the emission of UV and blue LEDs. This implies that the prepared phosphor materials could be possible candidates for phosphor converted WLEDs in conjunction with UV or blue LEDs.

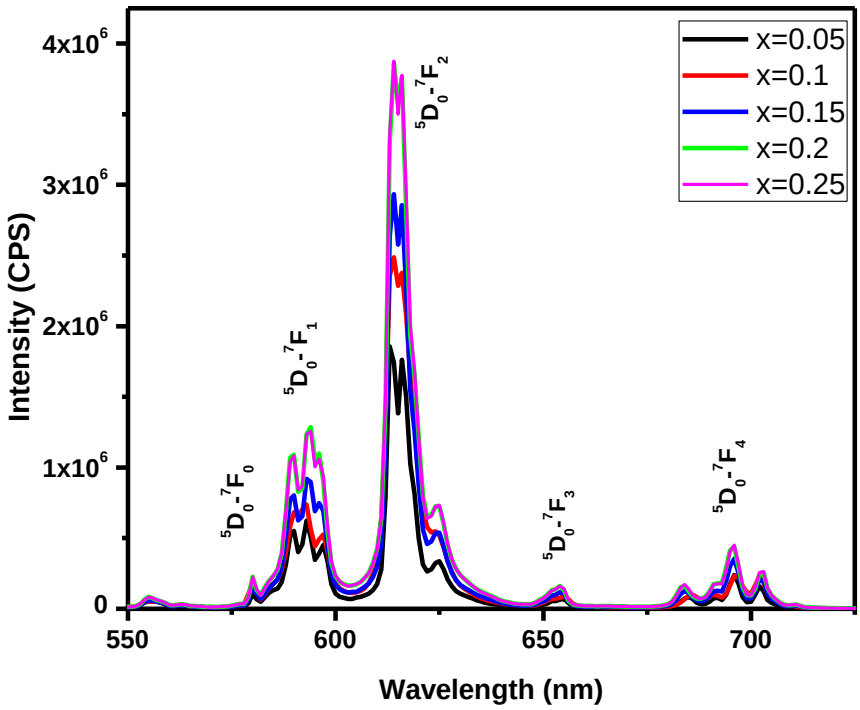


**Fig. 5A.5**: Photoluminescence emission spectra of $Na_{(1+x)}Ca_{(1-2x)}SnNbO_6$: $xEu^{3+}$ ($x$ = 0.05, 0.1, 0.15, 0.2, 0.25) for an excitation at 395 nm

The photoluminescent emission spectra of the phosphors, $Na_{(1+x)}Ca_{(1-2x)}SnNbO_6$: $xEu^{3+}$ for excitations 395 nm and 463 nm are shown in figure (Fig 5A.5 and 5A.6). Luminescent intensity is higher for UV light excitation. All the samples exhibit two

dominant emissions at 593 nm and 613 nm. In all the samples, $^5D_0$-$^7F_2$ electric dipole transition is dominating than the $^5D_0$-$^7F_1$ magnetic dipole transition. It is an indication of occupation of $Eu^{3+}$ in the noncentro symmetric A site (Ca site)(Nguyen *et al.* 2012, Li *et al.* 2011). In accordance with the photoluminescent excitation spectra photoluminescent emission intensity also increases with increase in $Eu^{3+}$ concentration upto 20 mol% and then decreases. Higher quenching concentration may be due to the layered ordering of A site ions the $Eu^{3+}$ in the lattice. Asymmetry ratio of the samples are calculated and tabulated. Asymmetry ratio gives a measure of degree of distortion of $Eu^{3+}$ site (Lee *et al.* 2018). Fig 5A.7 gives the variation of asymmetric ratio with different $Eu^{3+}$ concentrations. High value of asymmetric ratio is an indication of higher value of color purity of red emission from the samples. The highest value for asymmetric ratio obtained is 3.42 for the $Na_{(1.1)}Ca_{(0.8)}SnNbO_6$:$0.1Eu^{3+}$ sample. After 10 mol% of $Eu^{3+}$ doping, there is a slight decrease in the value of asymmetric ratio. There is no splitting in the $^5D_0$-$^7F_0$ transition, which confirms the single site occupancy of $Eu^{3+}$ in the lattice

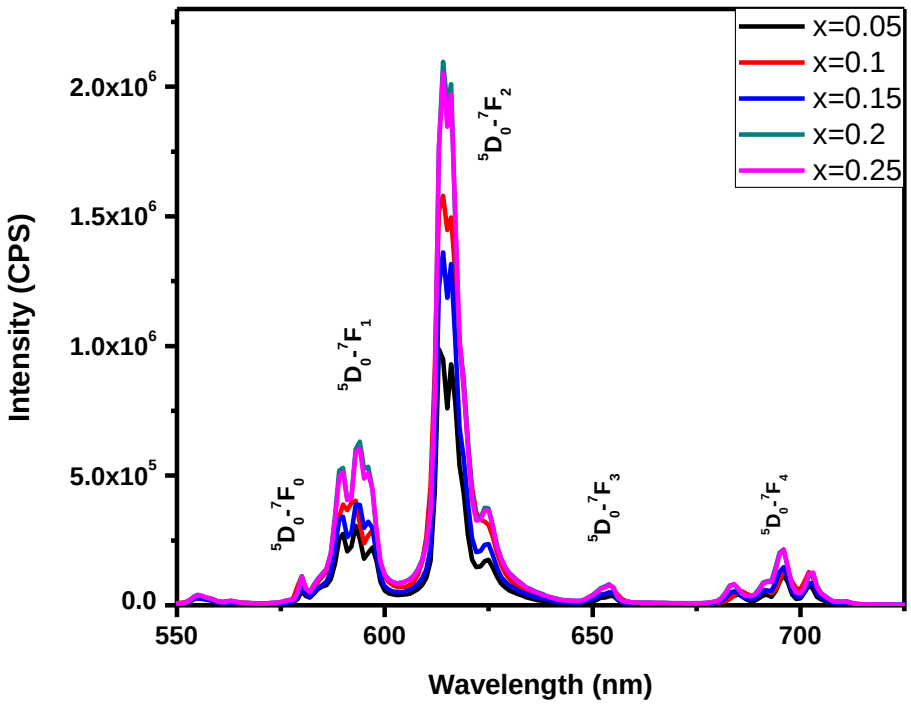


**Fig. 5A.6**: Photoluminescence emission spectra of $Na_{(1+x)}Ca_{(1-2x)}SnNbO_6$: $xEu^{3+}$ ($x$ = 0.05, 0.1, 0.15, 0.2, 0.25) for an excitation at 463 nm

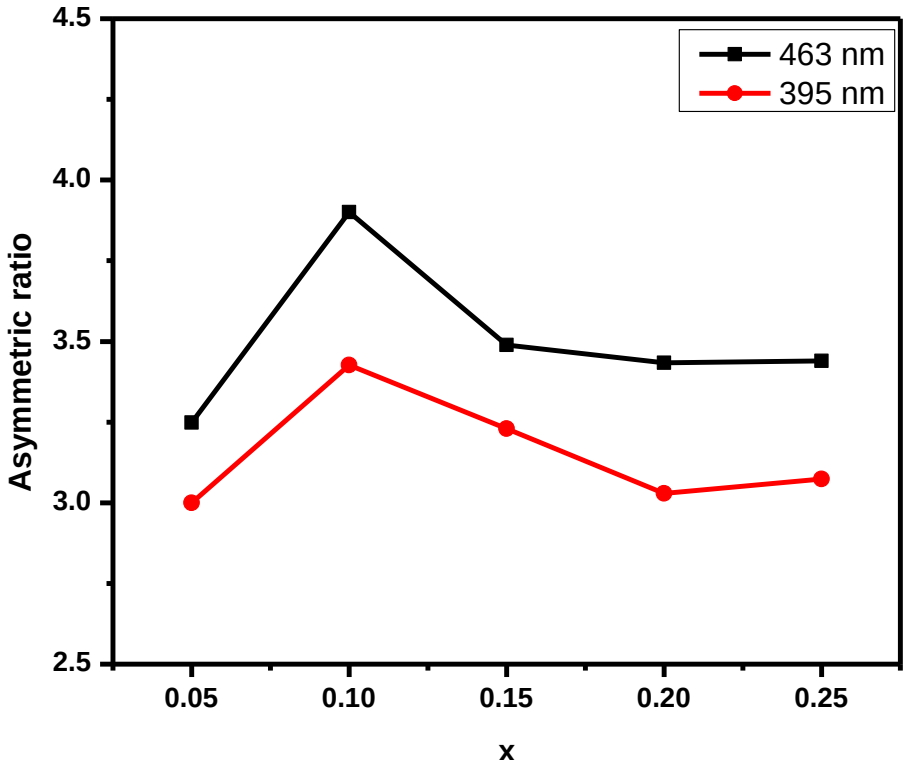


**Fig. 5A.7** : Variation of asymmetric ratio with $Eu^{3+}$ ($x$ = 0.05, 0.1, 0.15, 0.2, 0.25) concentrations

Table 5A.1 : Chromaticity color co-ordinate, Asymmetric ratio and color purity of $Na_{(1+x)}Ca_{(1-2x)}SnNbO_6$: $xEu^{3+}$

| Concentration | (x, y) | Asymmetry ratio | Color purity(%) |
|---|---|---|---|
| **0.05** | (0.60, 0.32) | 2.99 | 87 |
| **0.1** | (0.64, 0.31) | 3.42 | 92 |
| **0.15** | (0.61, 0.32) | 3.23 | 90 |
| **0.2** | (0.61, 0.33) | 3.02 | 89 |
| **0.25** | (0.60, 0.31) | 3.07 | 88 |

(Binnemans *et al.* 2015). CIE color co-ordinates of the samples were calculated using chromaticity calculator. Fig 5A.8 shows the CIE diagram of $Na_{(1.1)}Ca_{(0.8)}SnNbO_6$:$0.1Eu^{3+}$ sample. Color purity of the samples were checked using the equation, $color\ purity\ =$

$\frac{\sqrt{\{(x-xi)2+(y-yi)2\}}}{\sqrt{\{(xd-xi)2+(yd-yi)2\}}} \times 100$, where (x,y) are the color co-ordinates of the sample, ($x_i$,$y_i$) are color co-ordinates of white illuminant, and ($x_d$,$y_d$) are chromaticity co-ordinates of the dominant wavelength. ($x_i$,$y_i$) = (0.33,0.33) and ($x_d$,$y_d$)= (0.67,0.33).

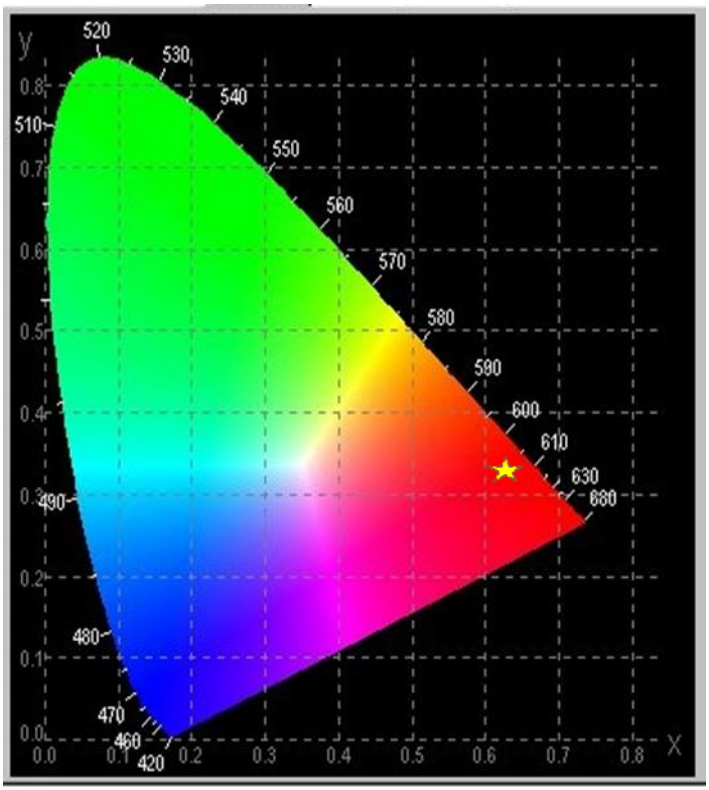


**Fig. 5A.8** : CIE color co-ordinate diagram of $Na_{(1.1)}Ca_{(0.8)}SnNbO_6$:0.1$Eu^{3+}$ sample

## 5A.4: Conclusions

A Series of self-charge compensating perovskite type red emitting phosphors $Na_{(1+x)}Ca_{(1-2x)}SnNbO_6:xEu^{3+}$ was prepared via high energy ball milling method. Ball milling method can enhance the reactivity of the system and reduce the reaction temperature. Also ball killing method is suitable for developing finely grinded particles with uniform size distribution and better morphology. Samples exhibit high levels of absorption the UV and blue region as well as intense red emission peaking at 613 nm. The Concentration quenching occurs at 20 mol% of $Eu^{3+}$ doping. The higher quenching concentration can be attributed to the layered ordering of A site ions in the lattice. Dominant red emission indicates $Eu^{3+}$ is situating in a non centrosymmetric site Samples exhibit intense red emission having high asymmetric ratio, good chromaticity co-ordinates and color purity. Among the samples, $Na_{(1.1)}Ca_{(0.8)}SnNbO_6:0.1Eu^{3+}$ phosphor exhibit better phase purity, high asymmetry ratio and better color purity values.

# Chapter 5B

## Effect of Ti substitution on the structural, morphological and optical properties of $Na_{(1.1)}Ca_{(0.8)}Eu_{0.1}Sn_{(1-x)}Ti_xNbO_6$ phosphors

*In this chapter we are discussing on the effect of Ti substitution on structural, microstructural and luminescent properties of phosphors* $Na_{(1.1)}Ca_{(0.8)}Eu_{0.1}Sn_{(1-x)}Ti_xNbO_6$ *( x= 0, 0.2, 0.4, 0.6, 0.8, 1) prepared via high energy ball milling method. Ti doping improves the phase purity of the system and the photoluminescent characteristics. Photoluminescent intensity is effectively increased with Ti substitution. Asymmetric ratio, band gap values and lifetime values are found to be decreasing with Ti incorporation.*

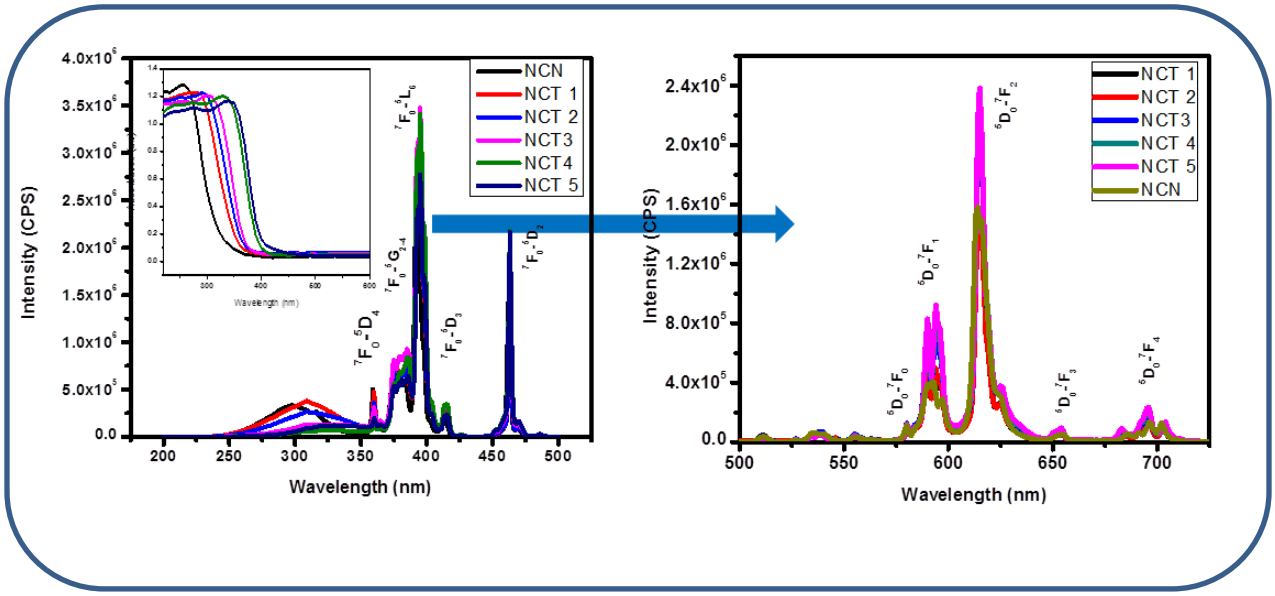

## 5B.1 Introduction

Development of potential red phosphors for WLED applications is still an active area of research in material science. Photoluminescence properties of LED phosphors can be controlled by the suitable choice of host material, modification of their chemical composition, suitable choice of activators etc. $Eu^{3+}$ activated red phosphors are well accepted due to their strong red luminescence arising from their intra configurational f-f transitions. Photoluminescent characteristics of $Eu^{3+}$ activated phosphors strongly depend on their co-ordination environment, crystal structure, chemical composition etc. So their luminescence can be tailored by the modification of co-ordination environment of $Eu^{3+}$ ions by substitution of suitable cations. . Double perovskites offer a lot of scope for wide variety of aliovalent cation substitutions at the A and B sites Because of this, lot of compositional modifications can be achieved in this system to tune the properties induced by the structural distortions. So $Eu^{3+}$ doped perovskites seek attention as promising red phosphors for WLED applications.

In chapter 5A, we have developed a series of self-charge compensating perovskite type red emitting phosphors $Na_{(1+x)}Ca_{(1-2x)}SnNbO_6{:}xEu^{3+}$ via high energy ball milling method and their structural and optical properties were discussed. We got finely grinded particles having uniform size distribution with better morphology that can assist the photoluminescence characteristics. Since $Eu^{3+}$ is doped in the non-centro symmetric A site, we got dominant red emission with high asymmetry value. Among the samples, $Na_{(1.1)}Ca_{(0.8)}SnNbO_6{:}0.1Eu^{3+}$ phosphor exhibit better phase purity, high asymmetry ratio and better color purity values. So we have selected the system and studied the effect of $Ti^{4+}$ substitution in their structural, morphological and optical properties.

## 5B.2. Experimental Procedure

$Na_{(1.1)}Ca_{(0.8)}Eu_{0.1}Sn_{(1-x)}Ti_xNbO_6$ ( x = 0, 0.2, 0.4, 0.6, 0. 8, 1) phosphors were prepared via high energy ball milling method by using $Na_2CO_3$, $CaCO_3$, $SnO_2$, $TiO_2$, $Nb_2O_5$, $Eu_2O_3$ as reagents. The stoichiometric amount of the powder mixture of the reagents was ball milled in a planetary mono mill pulveriser with a rotation speed of

250 rpm for 8h with acetone as the mixing medium. The ball milled powder was calcined at 1000˚C for 6 h. The crystalline structure of the samples was examined with an X-ray powder diffractometer (X'Pert Pro PANalytical, operated at 40kV and 30mA, Cu-Kα = 0.15406 nm, 2θ range = 10 - 90˚). The morphological study of the samples was done by a JEOL scanning electron microscope (model JSM - 5600LV), with an accelerating voltage of 15kV. Absorbance study of the samples were carried out using a Shimadzu, UV-2450 UV–Vis spectrophotometer in the 400–700 nm wavelength range using barium sulfate as a reference. The excitation and emission spectra were recorded on a Fluorolog HORIBA fluorescence spectrophotometer with a Xe lamp (450 W) as the excitation source. Luminescence lifetime of the phosphors was recorded by the phosphorimeter attached to Fluorolog3 spectrofluorimeter.

### 5B.3 Results and Discussion

#### 5B.3.1 XRD Analysis

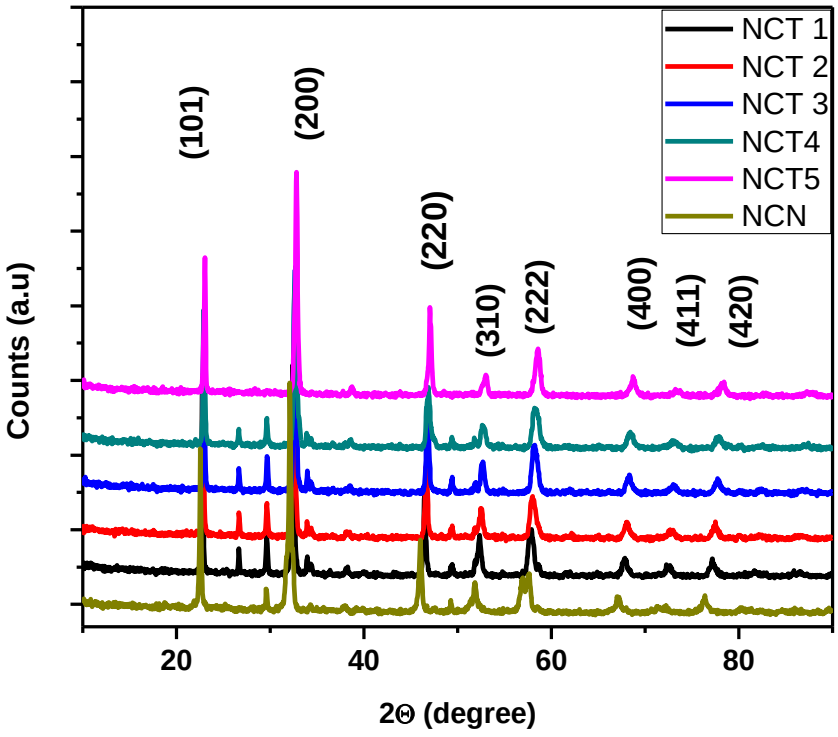


**Fig. 5B.1**: Powder XRD analysis of $Na_{(1.1)}Ca_{(0.8)}Eu_{0.1}Sn_{(1-x)}Ti_xNbO_6$ ( $x$ = 0, 0.2, 0.4, 0.6, 0.8, 1)

Powder X-ray diffraction patterns of the samples $Na_{(1.1)}Ca_{(0.8)}Eu_{0.1}Sn_{(1-x)}Ti_xNbO_6$ ( $x$ = 0, 0.2, 0.4, 0.6, 0.8, 1) are given in Figure 5B.1. As the $Ti^{4+}$concentration increases $SnO_2$ peaks becomes diminished. All the other peaks can be indexed with the reported diffraction pattern of $NaCaTiNbO_6$ (JCPDS file no 25-0853; orthorhombic perovskite with a space group Pnma

### 5B.3.2 Morphological Analysis

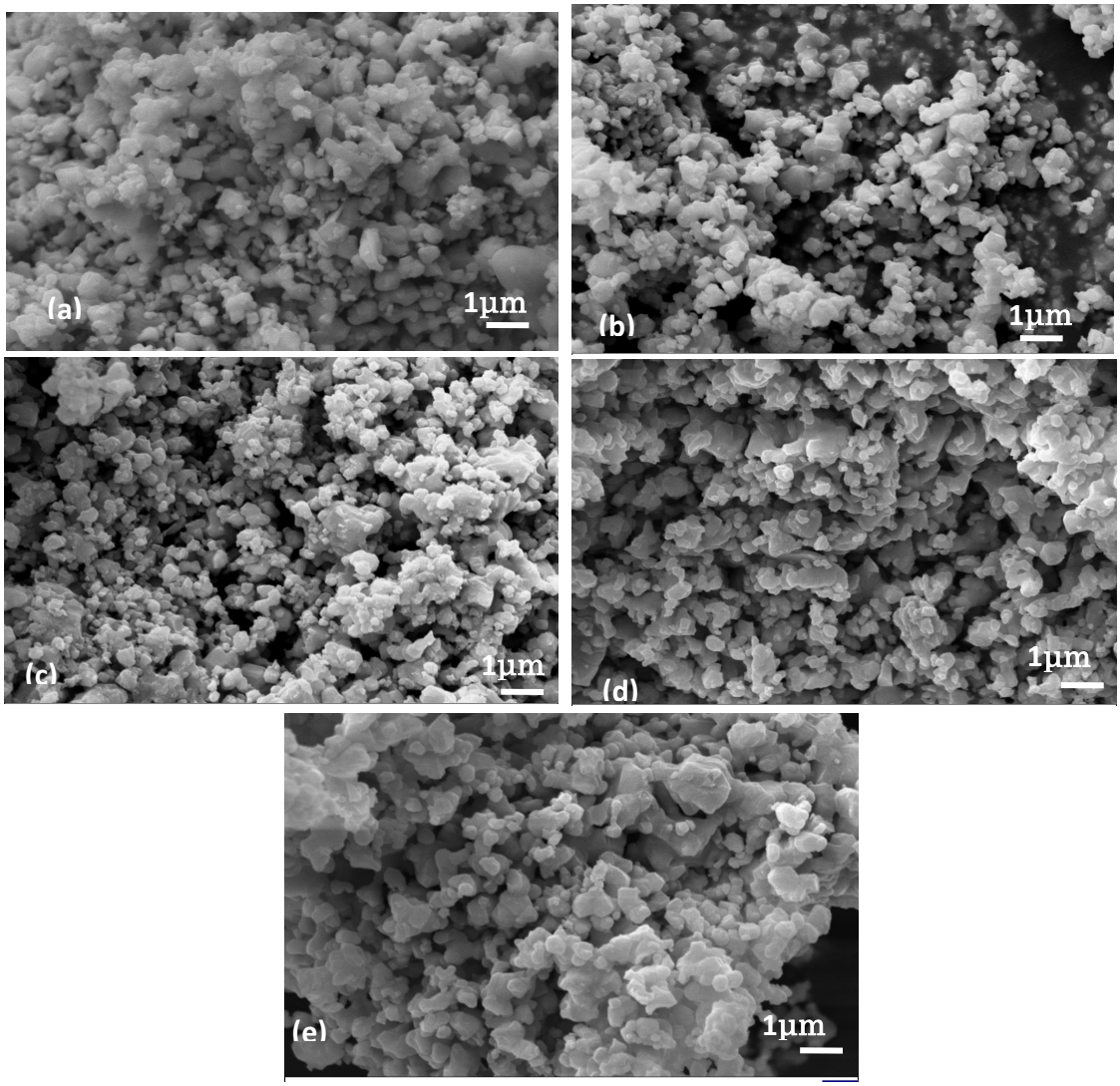


**Fig. 5B.2**: SEM analysis of $Na_{(1.1)}Ca_{(0.8)}Eu_{0.1}Sn_{(1-x)}Ti_xNbO_6$ (x=0, 0.2, 0.4, 0.6, 0.8, 1)

Figure 5B.2 shows the scanning electron micrographs of the samples. The particles are finely grinded and have a size distribution of 0.1-1µm. The ball milled samples exhibit a uniform distribution of particles and better morphology. $Ti^{4+}$substitution improves the morphology of the samples. The spherical morphology is expected to assist photoluminescent properties of the system by the way of reducing the scattering of light.

### 5B.3.3 Optical Studies

Fig 5B.3 shows the UV Visible absorption spectra of $Na_{(1.1)}Ca_{(0.8)}Eu_{0.1}Sn_{(1-x)}Ti_xNbO_6$ .All the samples exhibit broad and strong absorption in 200 to 400 nm UV region. Bandgap values of the samples are determined by extrapolating the absorption edge to wavelength axis. Bandgap values are tabulated in Table 5B.1. As the $Ti^{4+}$ concentration increases from 0 to 1, absorption edge shift towards higher wavelength

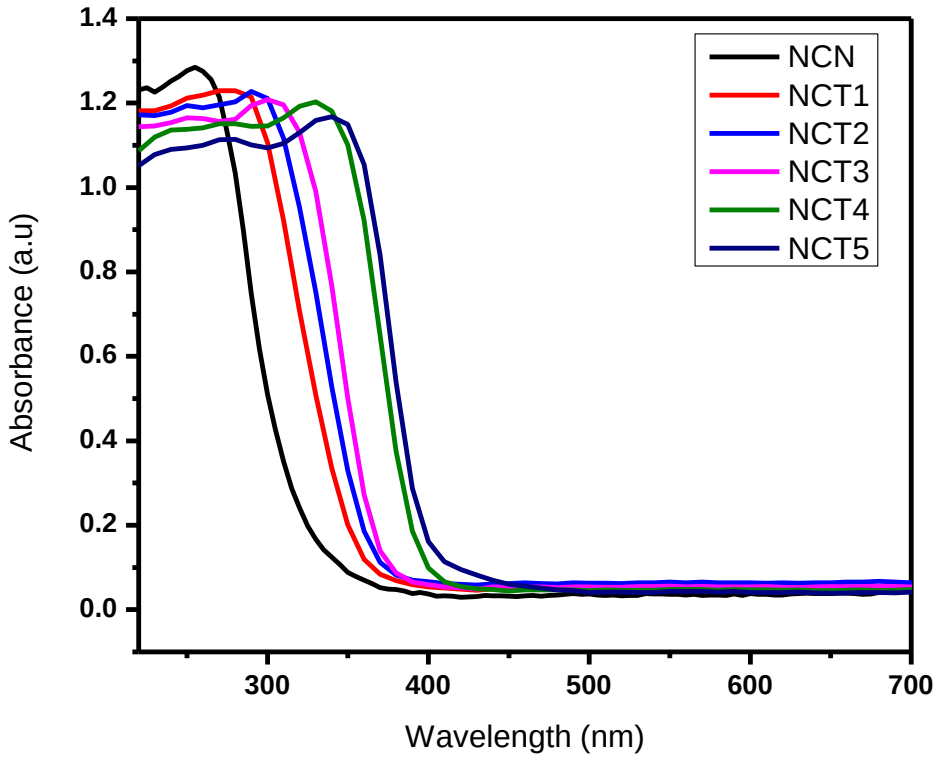


**Fig. 5B.3**: UV-Visible absorption spectra of $Na_{(1.1)}Ca_{(0.8)}Eu_{0.1}Sn_{(1-x)}Ti_xNbO_6$ (x = 0, 0.2, 0.4, 0.6, 0.8, 1)

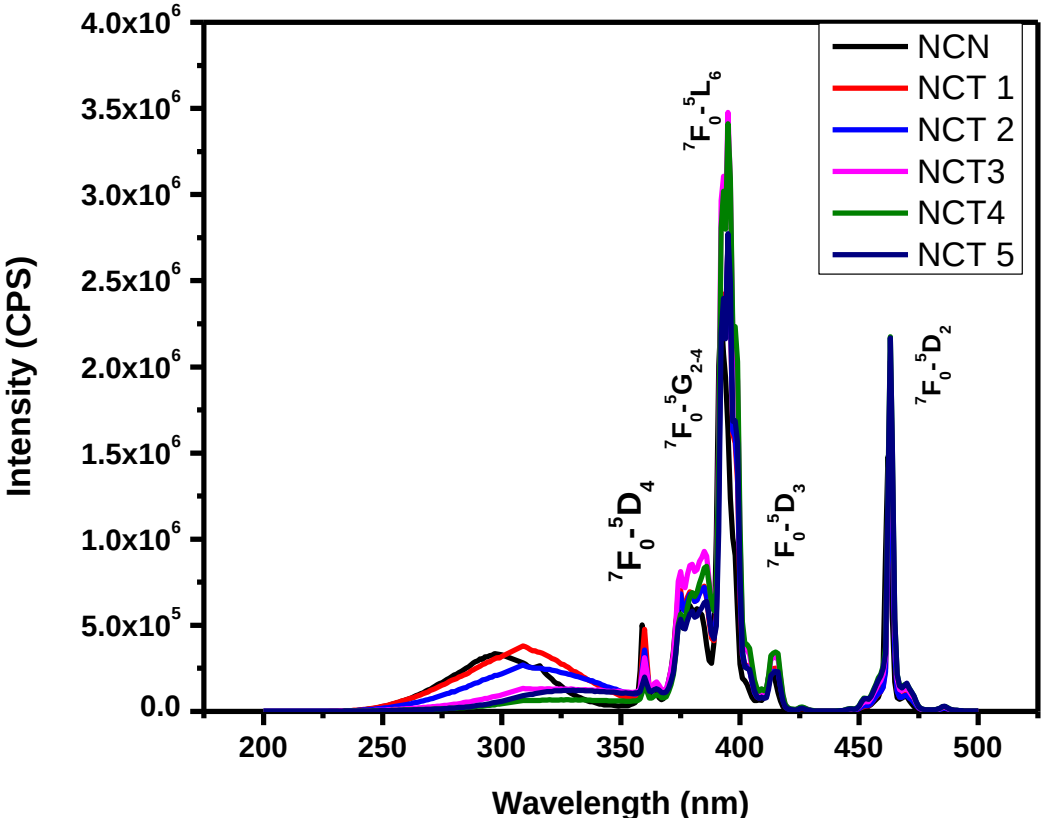


**Fig. 5B.4**: Photoluminescence excitation Spectra of $Na_{(1.1)}Ca_{(0.8)}Eu_{0.1}Sn_{(1-x)}Ti_xNbO_6$ (x=0, 0.2, 0.4, 0.6, 0.8, 1) for an emission at 613 nm

and bandgap values get reduced from 3.7 to 3 eV. The shift of absorption edge can be linked to the red shift of CT band in the photoluminescent excitation spectra, which arises due to the difference in electronegativity of $Sn^{4+}$ and $Ti^{4+}$. Strong absorption in the near UV and blue region indicates the potentiality of phosphors for the application in WLEDs.

Figure 5B.4 shows the photoluminescent excitation spectra of $Na_{(1.1)}Ca_{(0.8)}Eu_{0.1}Sn_{(1-x)}Ti_xNbO_6$ for an emission at 613 nm. Charge transfer band is found to be shallow compared to intra-configurational f-f transitions of $Eu^{3+}$ ions in the host. The sharp excitation peaks at 360 nm, 384 nm, 395 nm, 414 nm and 463 nm can be attributed to $^7F_0$-$^5D_4$, $^7F_0$-$^5G_{2-4}$,$^7F_0$-$^5L_6$, $^7F_0$-$^5D_3$, $^7F_0$-$^5D_2$ transitions of $Eu^{3+}$ ions in the host. CT band is found to be red shifted with increase in Ti concentration. This shift arises due to the substitution of Ti with lower electronegativity (1.54) in place of Sn (1.96),

which changes the co-ordination environment of $Eu^{3+}$ and reduces the CT energy (Linda *et al.* 2014). Excitation intensity of the doped samples increases with increase in Ti concentration. Excitation peaks at 395 nm and 463 nm are more dominant, which matches well with the emission of UV and blue LEDs. Thus the prepared phosphor materials could be possible candidates for phosphor converted WLEDs in conjunction with UV or blue LEDs (Chen *et al.* 2010) .

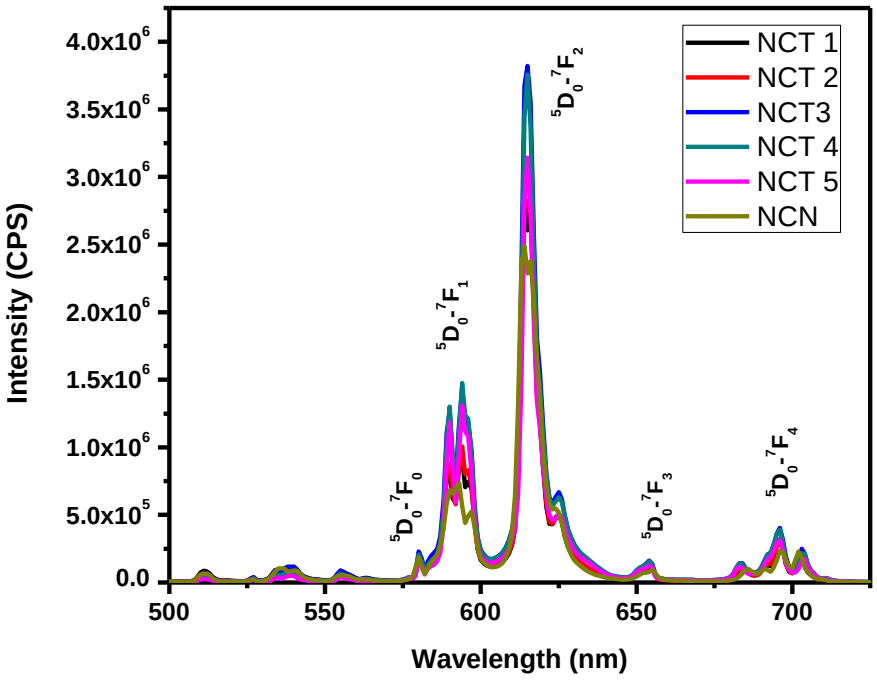


**Fig 5B.5**: Photoluminescence emission spectra of $Na_{(1.1)}Ca_{(0.8)}Eu_{0.1}Sn_{(1-x)}Ti_xNbO_6$ ($x$=0, 0.2, 0.4, 0.6, 0.8, 1) for an excitaion at 395 nm

The photoluminescent emission spectra of the phosphors $Na_{(1.1)}Ca_{(0.8)}Eu_{0.1}Sn_{(1-x)}Ti_xNbO_6$ for excitations 395 nm and 463 nm are shown in figure (Fig 5B.5 and 5B.6). Luminescent intensity is higher for UV light excitation. All the samples exhibit two dominant emissions at 593 nm and 613 nm. In all the samples, $^5D_0$-$^7F_2$ electric dipole transition is dominating than the $^5D_0$-$^7F_1$ magnetic dipole transition. It is an indication of occupation of $Eu^{3+}$ in the noncentro symmetric A site (Ca site). In accordance with the photoluminescent excitation spectra photoluminescent emission intensity also increases with increase in $Ti^{4+}$ concentration. Ti incorporation changes the

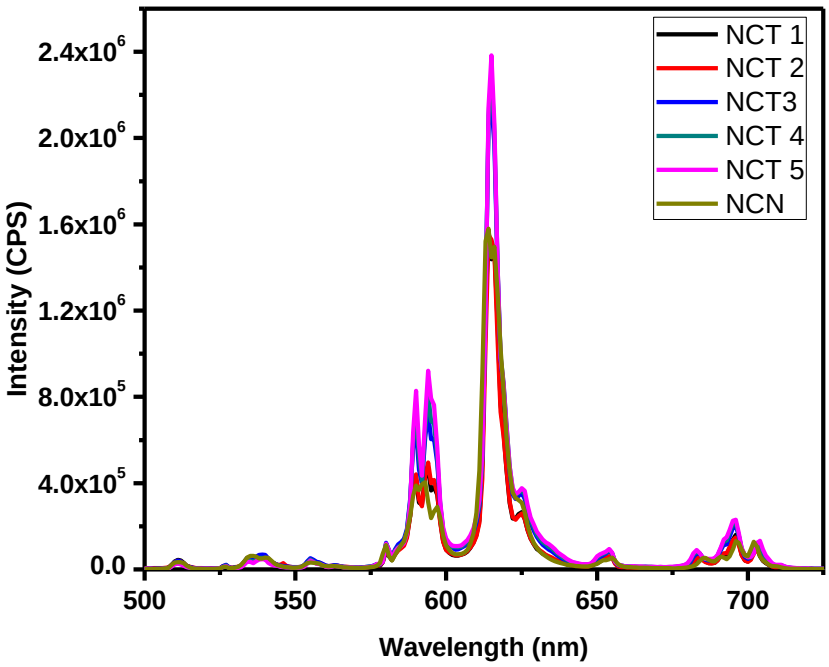


**Fig 5B.6**: Photoluminescence emission spectra of $Na_{(1.1)}Ca_{(0.8)}Eu_{0.1}Sn_{(1-x)}Ti_xNbO_6$ ($x$ = 0, 0.2, 0.4, 0.6, 0.8, 1) for an excitaion at 395 nm

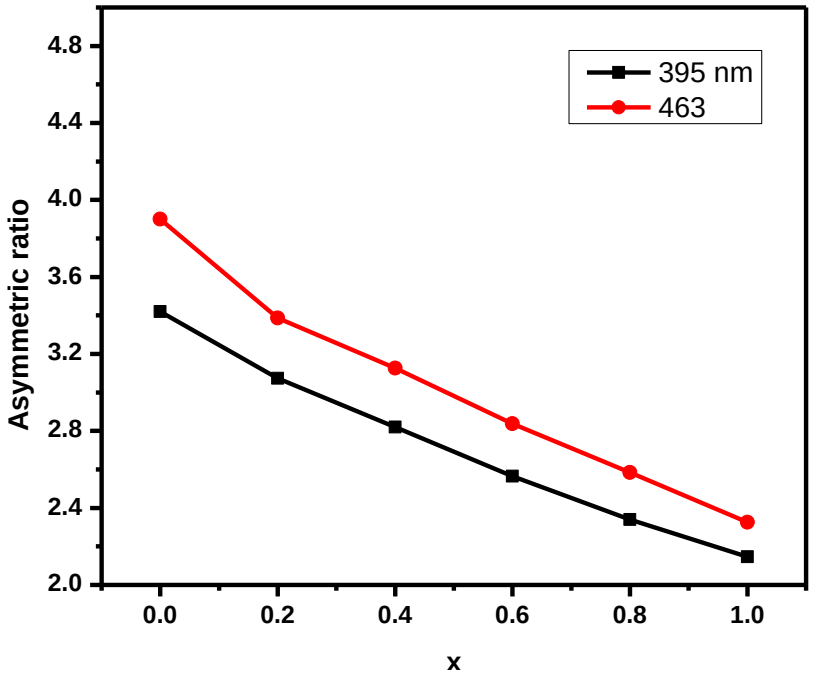


**Fig. 5B.7**: Variation of asymmetric ratio with different Ti ($x$ = 0, 0.2, 0.4, 0.6, 0.8, 1) substitution

co-ordination environment of $Eu^{3+}$ ion in the lattice and efficient energy transfer takes place to the activator ions. Higher quenching concentration may be due to the layered ordering of A site ions the $Eu^{3+}$ in the lattice. Asymmetry ratio of the samples are calculated and tabulated. Asymmetry ratio gives a measure of degree of distortion of $Eu^{3+}$ site. Fig 5B.7 gives the variation of asymmetric ratio with different $Eu^{3+}$ concentrations. High value of asymmetric ratio is an indication of higher value of color purity of red emission from the samples (Gyu *et al.* 2011). Asymmetric ratio is found to be decreasing with the increase in Ti concentration. There is no splitting in the $^5D_O$-$^7F_0$ transition, which confirms the single site occupancy of $Eu^{3+}$ in the lattice (Hou *et al.* 2012). CIE color co-ordinates of the samples were calculated using chromaticity calculator. Color co-ordinates are found to be close to the NTSC standard value for red phosphor (0.67, 0.33).

### 5B.3.4 Lifetime Analysis

The decay curves of the samples under UV excitation is shown in Figure 5B.8. The decay curves exhibit a single exponential behavior and the decay curves can be fitted to a single exponential function, $I = A \exp(-x/\tau)$, where I, A and $\tau$ are intensity, fitting parameter, and decay time respectively. This confirms the single site occupancy of $Eu^{3+}$ in the lattice of the phosphor sample (Yu *et al.* 2011). Table 5B.1 shows Lifetime and asymmetric ratio of $Na_{(1.1)}Ca_{(0.8)}Eu_{0.1}Sn_{(1-x)}Ti_xNbO_{6.}$ Lifetime values are found to be decreasing with increase in Ti concentration.

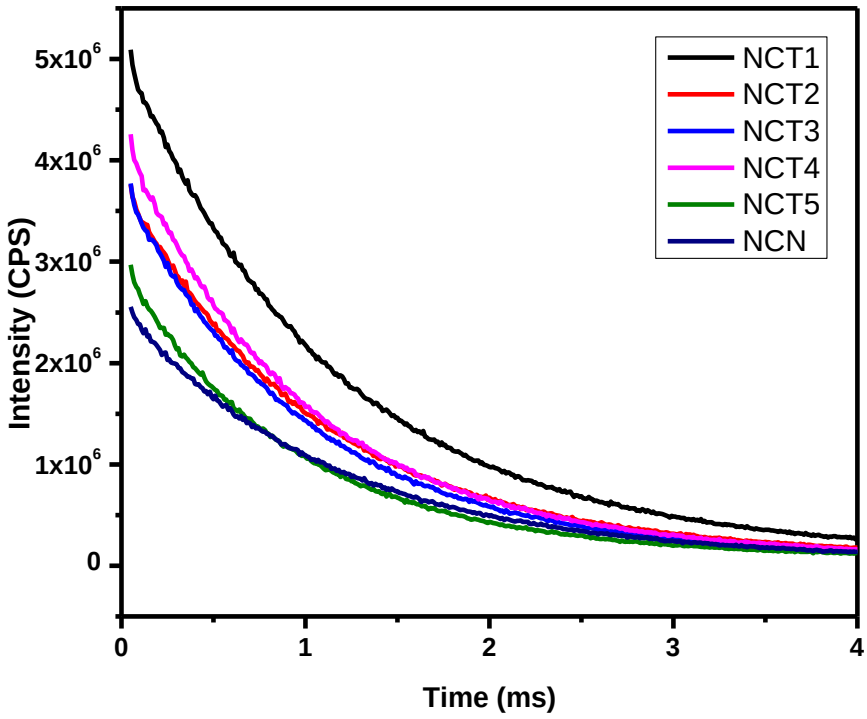


**Fig 5B.8** : Decay curves of samples $Na_{(1.1)}Ca_{(0.8)}Eu_{0.1}Sn_{(1-x)}Ti_xNbO_6$( $x$ =0, 0.2, 0.4, 0.6, 0.8, 1)

Table 5B.1 : Lifetime and asymmetric ratio, Bandgap and color co-ordinates of $Na_{(1.1)}Ca_{(0.8)}Eu_{0.1}Sn_{(1-x)}Ti_xNbO_6$($x$ = 0, 0.2, 0.4, 0.6, 0.8, 1).

| ***x*** | **Bandgap(eV)** | **Lifetime(ms)** | **Asymmetry ratio** | **(x,y)** |
|---|---|---|---|---|
| **0** | 3.7 | 1.11 | 3.42 | (0.64, 0.31) |
| **0.2** | 3.4 | 1.12 | 3.07 | (0.6, 0.32) |
| **0.4** | 3.3 | 1.04 | 2.81 | (0.61, 0.31) |
| **0.6** | 3.2 | 0.98 | 2.56 | (0.65, 0.30) |
| **0.8** | 3 | 0.96 | 2.33 | (0.60, 0.32) |
| **1** | 3 | 0.92 | 2.14 | (0.61, 0.33) |

## 5B.4 : Conclusions

A series of self-charge compensating $Ti^{4+}$ incorporated perovskite type red emitting phosphors $Na_{(1.1)}Ca_{(0.8)}Eu_{0.1}Sn_{(1-x)}Ti_xNbO_{6.}$ was prepared via high energy ball milling method. Ball milling method can enhance the reactivity of the system and reduce the reaction temperature. Also ball milling method is suitable for developing finely grinded particles with uniform size distribution and better morphology. $Ti^{4+}$ addition improves the morphology of the samples. Samples exhibit high levels of absorption the UV and blue region as well as intense red emission peaking at 613 nm. $Ti^{4+}$ substitution has positive effects on the structural, morphological and optical properties. Phase puriy was enhanced with Ti incorporation. Band gap values are found to be reduced with increase in $Ti^{4+}$ concentration. Band gap tuning is possible by varying $Ti^{4+}$ concentration. Dominant red emission indicates $Eu^{3+}$ is situating in a non centrosymmetric site. Samples exhibit intense red emission having high asymmetric ratio and good chromaticity co-ordinates. Luminescence intensity is found to be enhanced with Ti substitution.

# Chapter 6

## New Self- Charge Compensating Perovskite Type Red Phosphors $Na_{(1+x)}Ca_{(1-2x)}TiNbO_6$:$xEu^{3+}$ Prepared via Ball Milling Process for pc-White Light Emitting Diode Applications

*New self charge compensating red emitting perovskite type phosphors, $Na_{(1+x)}Ca_{(1-2x)}TiNbO_6$:x $Eu^{3+}$ were prepared by a high energy ball milling method and their photoluminescent properties were optimized for the calcination temperature. These phosphors exhibit intense red emission due to forced electric dipole transition, $^5D_0 \rightarrow {}^7F_2$ under near UV (395nm) and blue (463nm) excitations We got very good emission intensity in comparison with the commercial $Y_2O_3 : Eu^{3+}$.*

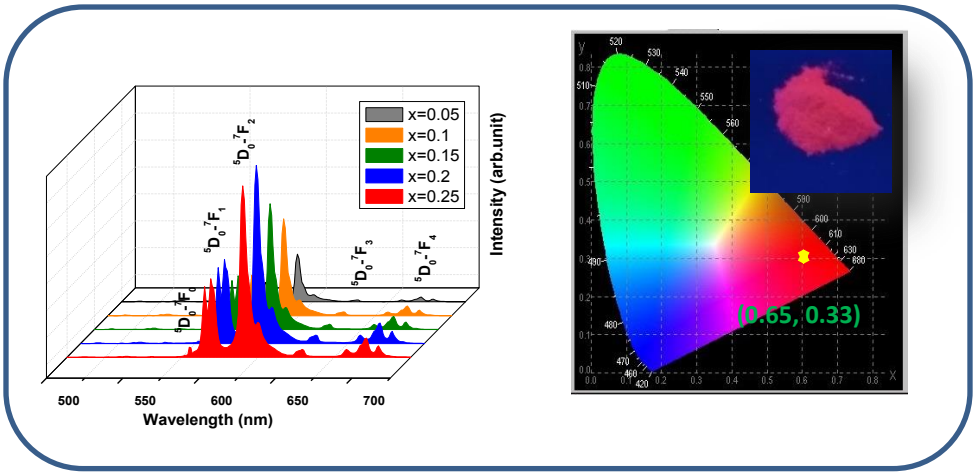


**Aswathy B A *et al.* Opt. Laser. Technol. 128 (2020)106217**

## 6.1 Introduction

Lighting plays a key role in the quality and productivity of human life. White Light emitting diodes have brought a lighting revolution over the existing lighting technologies with its spectacular properties such as high brightness, long operation time and environment friendliness. They are supposed to be the light source for future. Most of the WLED approaches are based on wavelength conversion by one or more phosphor materials. Common approach for white light generation is the combination of blue InGaN LED and $Y_3Al_5O_{12}$: $Ce^{3+}$ yellow phosphor. However, the white light obtained from this configuration possess low Color Rendering Index (CRI <80) due to lack of red component. Addition of suitable red phosphors easily pumped by NUV or blue LED combination can improve CRI (Huang *et al.* 2014, Zhou *et al.* 2016, Liu *et al.* 2019). Yet another technique is to incorporate blue, green and red emitting phosphors with near UV (380-420 nm) LED chip. Currently used red phosphors are sulphide or nitride based ones such as $Y_2O_2S$: $Eu^{3+}$, CaZnS:$Eu^{2+}$, $Sr_2Si_5N_8$:$Eu^{2+}$ and Sr[$LiAl_3N_4$]:$Eu^{2+}$. But for practical applications, they are chemically unstable and also the nitride and oxynitride phosphors are difficult to synthesize because of its tedious synthesis conditions such as nitrogen pressure and high temperature calcinations. So there is a great demand for energy efficient and stable oxide red phosphors that can be excited by near UV/ blue LEDs (Protesescu *et al.* 2015, Du *et al.* 2017).

Recent times double perovskites with general formula $AA'BB'O_6$, $A_2BB'O_6$ and $AB_{1/3}B'_{2/3}O_3$ have been studied extensively due to their interesting properties in various fields such as ferroelectrics, super conductors, photonics, photocatalysts and host of phosphor materials (Du *et al.* 2017, Zhang *et al.* 2016, Saparov *et al.* 2016). They offer a lot of scope for wide variety of aliovalent cation substitutions at the A and B sites Because of this, lot of compositional modifications can be achieved in this system to tune the properties induced by the structural distortions. The simple $ABO_3$ perovskite structure with three dimensional network of corner sharing $BO_6$ octahedra with A site cations located centrally in a cube of eight $BO_6$ octahedra, can be altered by substituting cations at either the A or the B sites (Noel *et al.* 2014, Li *et al.* 2013, Lee *et al.* 2018, Fu *et al.* 2017). In double perovskites, when the B' cation is a $d^0$ transition metal ion in a high

oxidation state ($W^{6+}$, $Mo^{6+}$, $Nb^{5+}$, $Ta^{5+}$, $Ti^{4+}$, etc.), dual ordering of cations such as layered ordering of A site cations and rocksalt ordering of B site cations occurs (Zhang *et al.* 2013, Hou *et al.* 2012, Taylor *et al.* 1994). The double perovskite system $NaCaTiNbO_6$ was already reported for their excellent electrical properties (Davies *et al.* 2008). We have selected the system and doped with $Eu^{3+}$ prepared a series of potential red phosphors by ball milling method. Also, their variation of structural, morphological and photoluminescence properties with an increase in calcination temperature was studied.

Charge compensation is very significant for betterment of photoluminescent properties. Most common charge compensation method is the suitable addition of alkali metals such as Li, Na, K, etc. However, such charge compensation methods are carried out intentionally by addition of some monovalent ions which may lead sometimes to some secondary phases. In the present study, the charge compensation is built in the system as Na ion that is part of the composition. Further, the aliovalent cations such as $Ca^{2+}$, $Eu^{3+}$, $Na^{+}$ are occupying the A site with the ionic radii for (VIII) co-ordination as 112 pm, 106 pm and 118 pm respectively. The incorporation of cations with different ionic radii can result in distortions in the lattice. Thus in our case stoichiometry is selected in such a way that charge compensation takes place automatically without the addition of alkaline ions (King *et al.* 2010,Rajendran *et al.* 2008, Shi *et al.* 2008). Some of the photoluminescent properties of this new series of perovskites and their optimization studies are presented in this paper.

## 6.2 Experimental Procedure

$Na_{(1+x)}Ca_{(1-2x)}TiNbO_6$:$x$$Eu^{3+}$ phosphors were prepared via high energy ball milling method by using $Na_2CO_3$, $CaCO_3$, $TiO_2$, $Nb_2O_5$, $Eu_2O_3$ as reagents. The high energy ball milling process can enhance the reactivity of the system and reduce the reaction temperature. The stoichiometric amount of the powder mixture of the reagents was ball milled in a planetary mono mill pulveriser with a rotation speed of 250 rpm for 8h with acetone as the mixing medium. The ball milled powder was calcined at 1000˚C for 6 h. The crystalline structure of the samples was examined with an X-ray powder diffractometer (X'Pert Pro PANalytical, operated at 40kV and 30mA, Cu-Kα = 0.15406

nm, 2θ range = 10 - 90˚). The morphological study of the samples was done by a JEOL scanning electron microscope (model JSM - 5600LV), with an accelerating voltage of 15kV. Absorbance study of the samples were carried out using a Shimadzu, UV-2450 UV–Vis spectrophotometer in the 400–700 nm wavelength range using barium sulfate as a reference. The excitation and emission spectra were recorded on a Fluorolog HORIBA fluorescence spectrophotometer with a Xe lamp (450 W) as the excitation source. Luminescence lifetime of the phosphors was recorded by the phosphorimeter attached to Fluorolog3 spectrofluorimeter. In order to investigate the variation of phosphor characteristics with an increase in calcination temperature, the samples were further calcined from 1000˚C to 1200˚C. Structural changes were studied using XRD analysis. Morphological differences and elemental composition and mapping were carried out using SEM and EDAX. Variation of photoluminescence with an increase in calcination temperature and comparison of photoluminescence with commercial red phosphor $Y_2O_3$:$Eu^{3+}$ was done using Fluorolog HORIBA fluorescence spectrophotometer.

## 6.3. Results and Discussion

### 6.3.1 Powder XRD analysis

Powder X-ray diffraction patterns of the samples $Na_{(1+x)}Ca_{(1-2x)}TiNbO_6$: $xEu^{3+}$ ($x$=0.05, 0.1, 0.15, 0.2, 0.25) are given in Figure 6.1. All the peaks are in good agreement with the reported diffraction pattern of $NaCaTiNbO_6$ (JCPDS file no 25-0853; orthorhombic perovskite with a space group Pnma having lattice parameters $a$ (Å) = 5.4830, $b$ (Å) = 7.7280, $c$ (Å) = 5.4440. In AA'BB'$O_6$ double perovskites, the large differences of ionic radii and oxidation states of B site result in the ordering of $Nb^{5+}$ and $Ti^{4+}$ (Hou *et al.* 2012). The ions $Nb^{5+}$ and $Ti^{4+}$ alternate in positions to form $NbO_6$ and $TiO_6$ octahedra. Rock salt type arrangement of the B cations is expected to maximize the distance between similar cations. A site cations $Na^+$ and $Ca^{2+}$ are expected to offer a layered arrangement in the lattice (Taylor *et al.* 1994). In the present system, charge compensation is done by the addition of $Na^+$ equivalent to the doping of $Eu^{3+}$ ions for the $Ca^{2+}$. Since all the ions are going to occupy the A site, we have assessed the ionic

radii of A site with $Eu^{3+}$ doping. For this, average ionic radius of A site with and without $Eu^{3+}$ doping was calculated. Without $Eu^{3+}$, average ionic radius is given by the equation $(rNa + rCa)/2$ and with $Eu^{3+}$ doping, it is given by [(1+$x$) rNa + (1-2$x$) rCa + $x$r$Eu^{3+}$] / 2. rNa+ =1.18 Å, $rCa^{2+}$ =1.12 Å and $rEu^{3+}$ = 1.066 Å for (VIII) co-ordination. Substituting the values, average ionic radius of A site without $Eu^{3+}$ is found to be 1.15 Å. With charge compensation and $Eu^{3+}$ doping the average ionic radius increases from

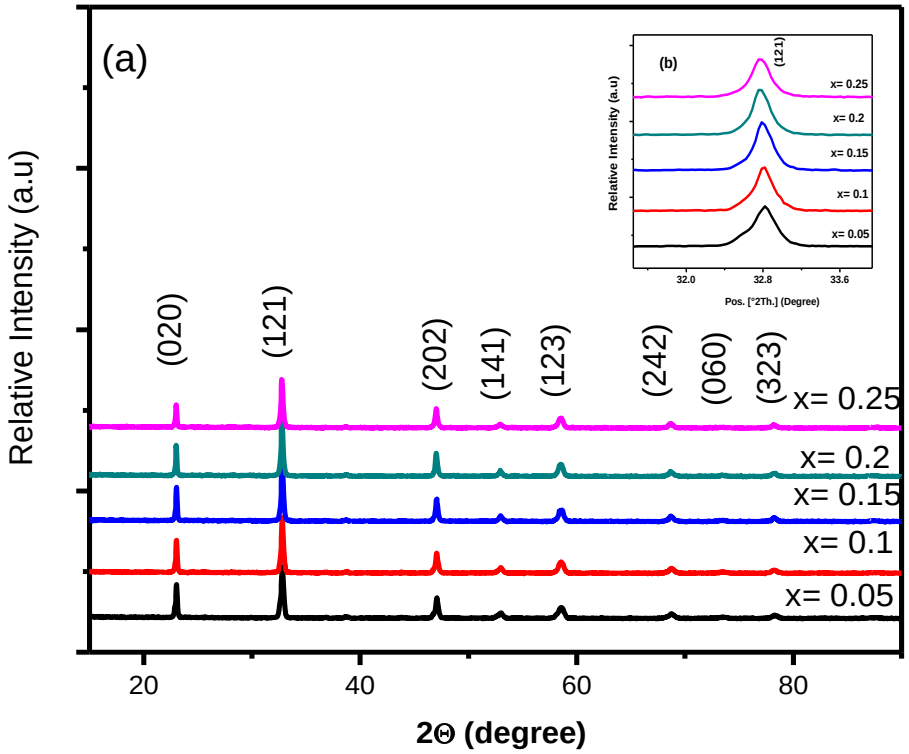


**Fig 6. 1** (a) Powder XRD patterns of $Na_{(1+x)}Ca_{(1-2x)}TiNbO_6$: $xEu^{3+}$ ($x$ = 0.05, 0.1, 0.15, 0.2, 0.25), (b) peak shift of (121) plane with $Eu^{3+}$ concentration.

1.1501 Å to 1.1507 Å. As expected, the peak shift of (121) reflection towards left side indicates expansion of the lattice because of the slight increase in the average ionic radius of A site. XRD analysis confirms the successful incorporation of $Eu^{3+}$ into the lattice with no additional impurity peaks.

### 6.3.2 Morphological Analysis

Figure 6.2 shows the scanning electron micrographs of the samples. The particles are slightly agglomerated and have a size distribution of 0.1-1μm. The ball milled samples exhibit a uniform distribution of particles and better morphology. The

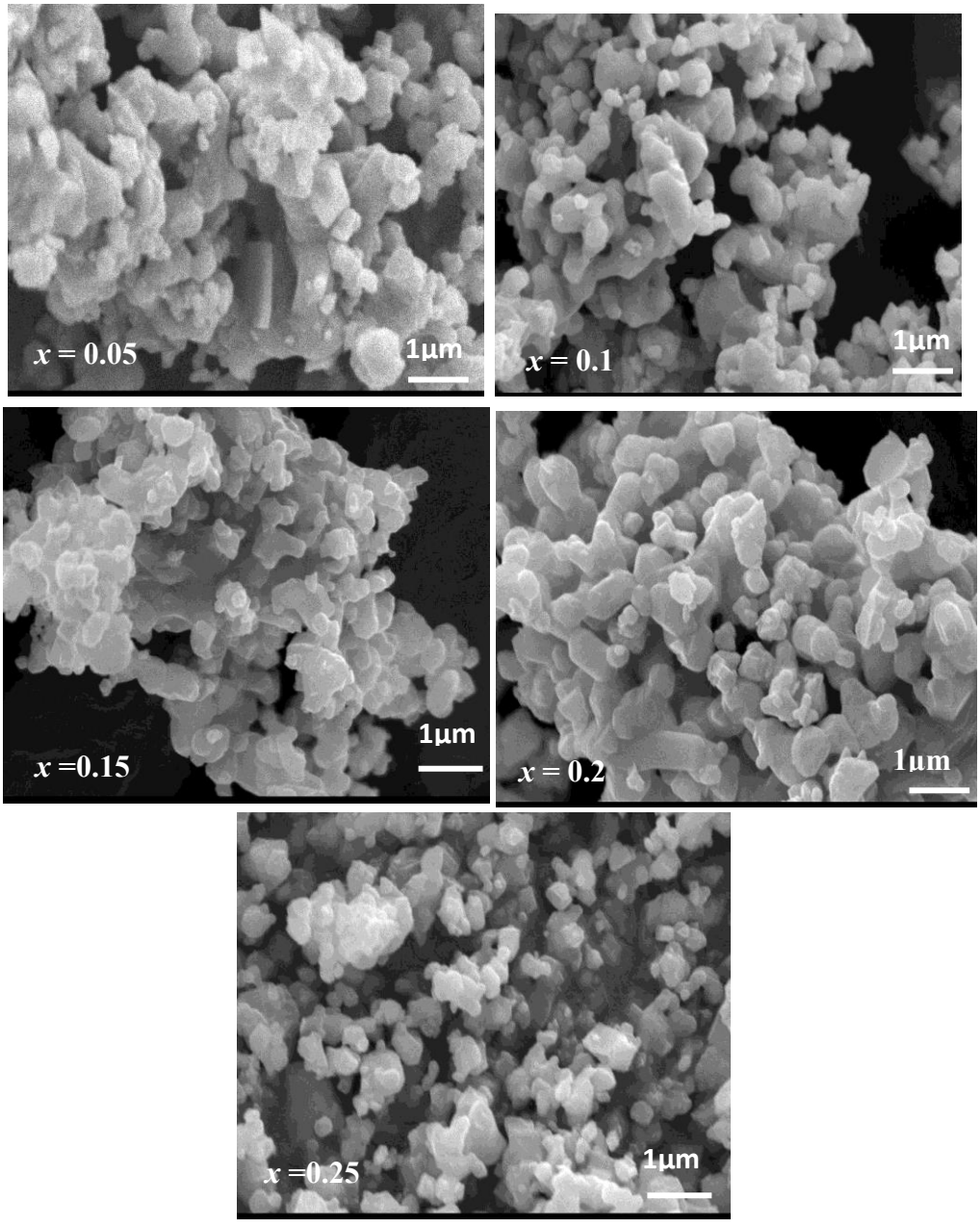


**Fig. 6.2**: SEM images of $Na_{(1+x)}Ca_{(1-2x)}TiNbO_6$: $xEu^{3+}$ ($x$=0.05, 0.1, 0.15, 0.2, 0.25)

spherical morphology is expected to assist photoluminescent properties of the system by the way of reducing the scattering of light.

### 6.3.3 Optical Studies

Figure 6.3 shows UV visible absorption spectra of $Na_{(1+x)}Ca_{(1-2x)}TiNbO_6$:$xEu^{3+}$ ($x$=0.05-0.25). Band gap is determined by extrapolating the onset of absorption edge to the energy axis. The variation of band gap with an increase in $Eu^{3+}$ concentration is given in Table 6.1. Band gap value of the material suggests that they have a strong absorption in the UV region that can be applied for WLED applications in combination with UV LEDs.

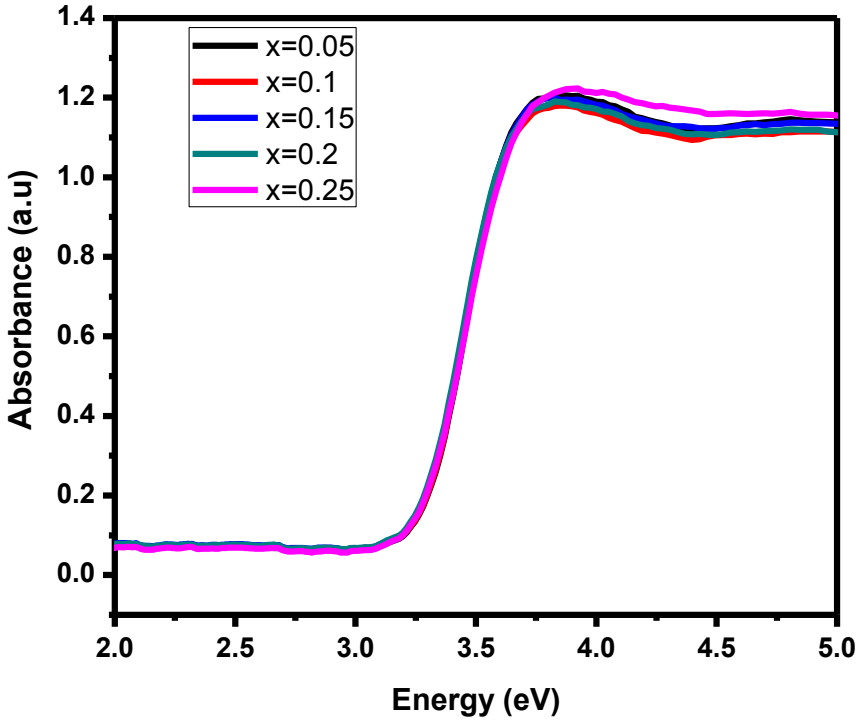


**Fig. 6.3** : UV visible absorption spectra of $Na_{(1+x)}Ca_{(1-2x)}TiNbO_6$: $xEu^{3+}$ ($x$=0.05, 0.1, 0.15, 0.2, 0.25)

Figure 6.4 shows the photoluminescent excitation spectra of $Na_{(1+x)}Ca_{(1-2x)}TiNbO_6$:$xEu^{3+}$ for an emission at 615 nm. Charge transfer band is found to be less intense compared to intra-configurational f-f transitions of $Eu^{3+}$ ions in the host. The sharp excitation peaks at 360 nm, 384 nm, 395 nm, 414 nm and 463 nm can be

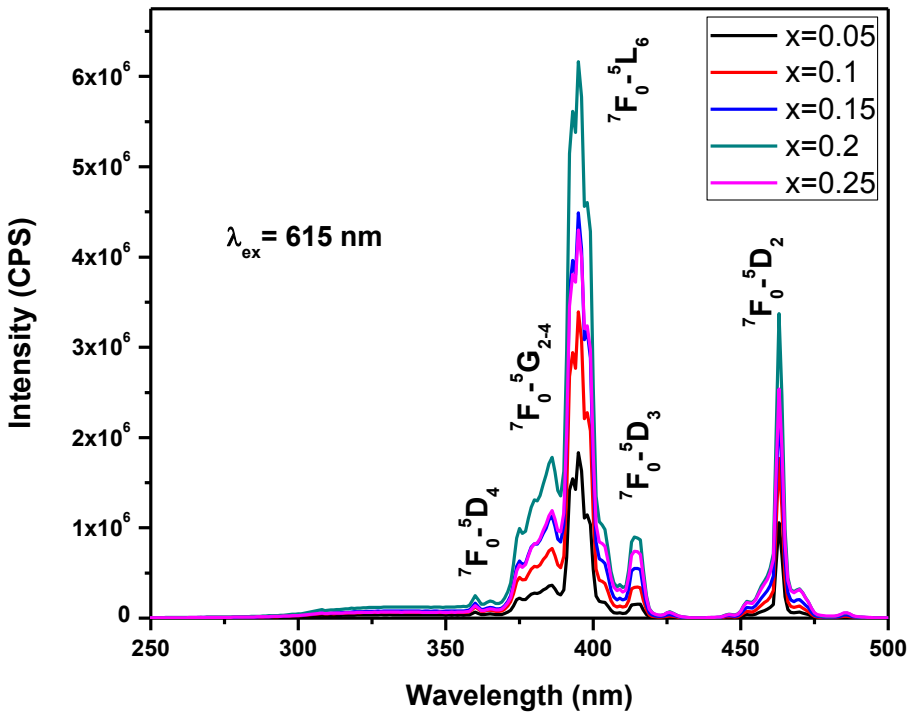


**Fig. 6.4** :Photoluminescent excitation spectra of $Na_{(1+x)}Ca_{(1-2x)}TiNbO_6$: $xEu^{3+}$ for an emission at 615 nm.

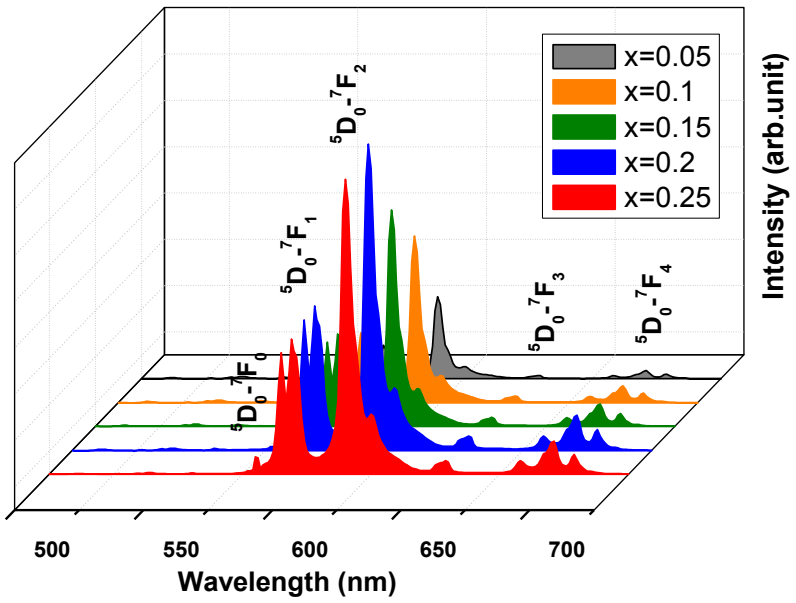


**Fig.6. 5** : Photoluminescent emission spectra of $Na_{(1+x)}Ca_{(1-2x)}TiNbO_6$: $xEu^{3+}$ for an excitation at 395 nm.

attributed to $^7F_0$-$^5D_4$, $^7F_0$-$^5G_{2\text{-}4}$,$^7F_0$-$^5L_6$, $^7F_0$-$^5D_3$, $^7F_0$-$^5D_2$ transitions of $Eu^{3+}$ ions in the host (Vance *et al.* 1996, Shomrat *et al.* 2014, Binnemans *et al.* 2015). Excitation intensity of the doped samples increases with increase in $Eu^{3+}$ concentration and saturation occurs for 20 mol% doping. Excitation peaks at 395 nm and 463 nm are more dominant, which matches well with the emission of UV and blue LEDs. Thus the prepared phosphor materials could be possible candidates for phosphor converted WLEDs in conjunction with UV or blue LEDs. The photoluminescent emission spectrum of the phosphor samples exhibit two intense peaks at 593 and 615 nm, which can be attributed to intraconfigurational f-f transitions of $Eu^{3+}$ in the host. The red emission at 615 nm due to $^5D_0 \rightarrow {}^7F_2$ forced electric dipole transition is dominating than the orange emission due to $^5D_0 \rightarrow {}^7F_1$ magnetic dipole transition (Vance *et al.* 1996, Shomrat *et al.* 2014, Binnemans *et al.* 2015). The intensity of emission increases with increase in $Eu^{3+}$ concentration up to 20 mol% and then decreases. Increased concentration quenching may be attributed to the layered ordering of $Eu^{3+}$ ions in the lattice (Yu *et al.* 2014).

In order to get an idea about the mechanism of concentration quenching, the critical distance, $R_c$ was calculated. It is generally believed that concentration quenching is mainly due to non radiative transition among $Eu^{3+}$ ions. Non radiative transitions can occur by means of exchange interaction, radiation re-absorption or multipole-multipole interaction. For exchange interaction to occur, $R_c$ should approximately equal to 5 Å (Zhang *et al.* 2014). According to Blasse, for oxide phosphors, if the activator ion is solely introduced into Z ion sites, if Xc is the critical concentration, N is the number of Z ions in the unitcell, V is the volume of the unit cell then there is on the average, one activator ion per ($V/X_cN$). The critical energy transfer distance is approximately equal to twice the radius of a sphere with this volume. So $R_c$ is given by the equation $R_c \sim 2 [3V/4\pi X_cN]^{1/3}$, we have $V = 230.68(Å)^3$, $X_c = 0.2$, $Z=2$ (Zhang *et al.* 2014, Liu *et al.* 2016). On substituting these values, we get $R_c \sim 10.32$ Å. Since the value of $R_c$ is greater than 5 Å, the probability of exchange interaction is very low. Since luminescence in $Eu^{3+}$ is the result of 4f-4f forced electric dipole transition, the energy migration may occur due to multipolar interaction.

According to the report of Van Uitert, if energy transfer taking place between the same sort of activators, emission intensity per activator follows the equation, $I/x = k[1+\beta (x)^{\theta/3}]^{-1}$. Where x is the activator concentration, I is the luminescence intensity, k and β are constants for same excitation condition for same host crystal, θ represents which type of multipolar interaction taking place between the activators. θ = 3, 6, 8 or 10 corresponding to energy transfer among nearest neighbours, dipole - dipole interaction, dipole - quadrupole interaction or quadrupole - quadrupole interaction. Assuming β (x) >> 1, the equation can be simplified as $\ln\left(\frac{I}{x}\right) = k' - \frac{\theta}{3} lnx$, where k' = ln k – ln β. From the slope of this equation, the type of multipolar interaction can be determined. The value of θ we got is approximately 6. θ≈ 6, corresponds to dipole-dipole interaction (Liu *et al.* 2016, Xin *et al.* 2015). Thus luminescence quenching of the system is due to dipole-dipole interaction among the $Eu^{3+}$ ions in the lattice

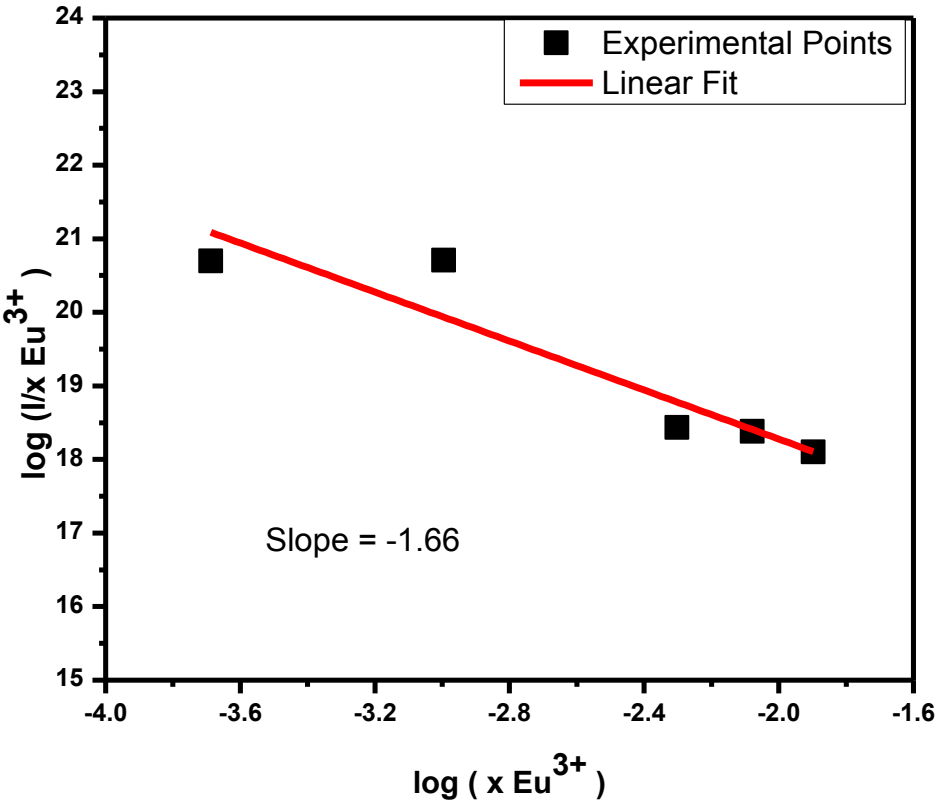


**Fig. 6.6** : Plot of ln ($I/x\ Eu^{3+}$) versus ln ($x\ Eu^{3+}$) in $Na_{(1+x)}Ca_{(1-2x)}TiNbO_6$: $xEu^{3+}$ ($x$=0.05, 0.1, 0.15, 0.2, 0.25).

### 6.3.4 Life time Analysis

The decay curves of the samples under UV excitation is shown in Figure 6.7. The decay curves exhibit a single exponential behavior and the decay curves can be fitted to a single exponential function, I = A exp (-x/τ), where I, A and τ are intensity, fitting

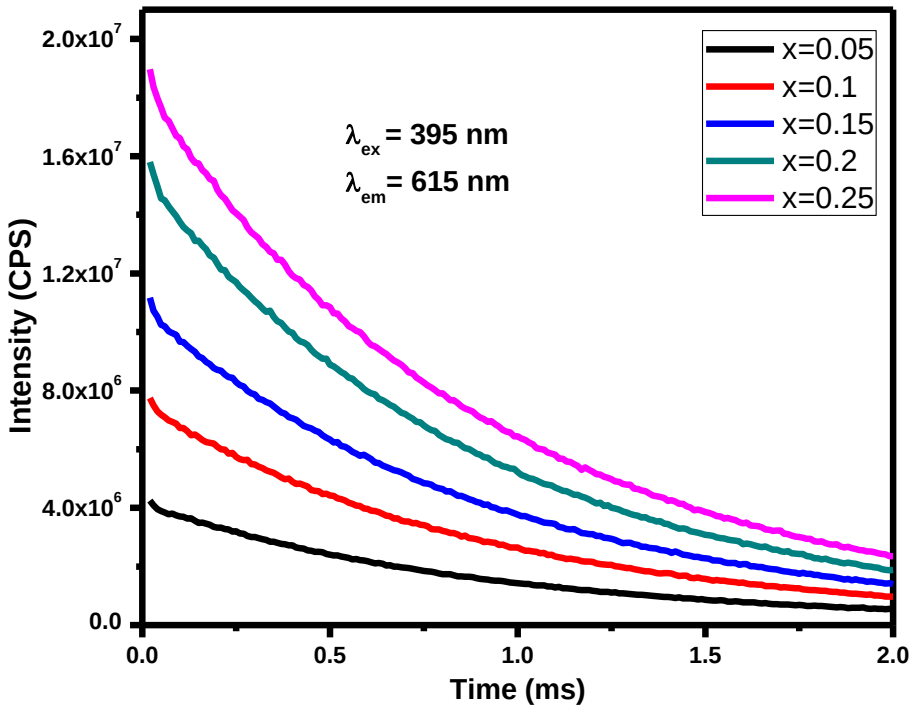


**Fig. 6.7** : Lifetime analysis of $Na_{(1+x)}Ca_{(1-2x)}TiNbO_6$: $xEu^{3+}$ ($x$=0.05, 0.1, 0.15, 0.2, 0.25) for an excitation at 395nm and emission at 615 nm

parameter, and decay time respectively. This confirms the single site occupancy of $Eu^{3+}$ in the lattice of the phosphor sample (Shomrat et al. 2014). The asymmetric ratio of the samples is found to be decreasing with $Eu^{3+}$ concentration up to 0.2 and then increasing. Table 6.1 shows Lifetime and asymmetric ratio of $Na_{(1+x)}Ca_{(1-2x)}TiNbO_6$: $xEu^{3+}$.

Table 6.1: Lifetime, asymmetric ratio and band gap of $Na_{(1+x)}Ca_{(1-2x)}TiNbO_6$: $xEu^{3+}$ phosphor

| *x* | Lifetime (ms) | Band gap (eV) | Asymmetric ratio |
|---|---|---|---|
| **0.05** | 0.87 | 3.18 | 2.44 |
| **0.1** | 0.89 | 3.21 | 2.39 |
| **0.15** | 0.89 | 3.22 | 2.33 |
| **0.2** | 0.88 | 3.18 | 2.12 |
| **0.25** | 0.88 | 3.20 | 2.18 |

### 6.3.5 Effect of calcination temperature on phosphor characteristics

We had chosen $Na_{(1.2)}Ca_{(0.6)}TiNbO_6$: $0.2Eu^{3+}$ phosphor sample from the series with highest emission intensity and the variation of its structural, luminescent and morphological properties with an increase in calcination temperature from 1000˚C to 1200˚C was studied

#### 6.3.5.1 XRD analysis

Powder XRD patterns for different calcination temperature (1000˚ C-1200˚ C) of $Na_{(1.2)}Ca_{(0.6)}TiNbO_6$: $0.2Eu^{3+}$ is shown in Figure 6.8. With an increase in calcination temperature intensity as well as crystallinity increases up to 1100˚ C and then decreases. Table 6. 2 shows FWHM and crystallite size of $Na_{(1.2)}Ca_{(0.6)}TiNbO_6$: $0.2Eu^{3+}$ phosphor sample at different calcination temperatures. FWHM values are found to be decreasing with an increase in calcination temperature. Crystallite size was calculated using the Scherrer equation, $\text{crystallite size} = \frac{k\lambda}{\beta\cos\theta}$, where k is the shape factor k~1, β is FWHM and λ is the wavelength of X-ray used (Zhang *et al*. 2017). The crystallite size was found to be increased with an increase in calcination temperature it is due to the fact that the high energy supply from higher synthesis temperature

improves crystallite growth. FWHM and crystallite size of $Na_{(1.2)}Ca_{(0.6)}TiNbO_6$: $0.2Eu^{3+}$ phosphor sample at different calcination temperatures are listed in Table 6.2.

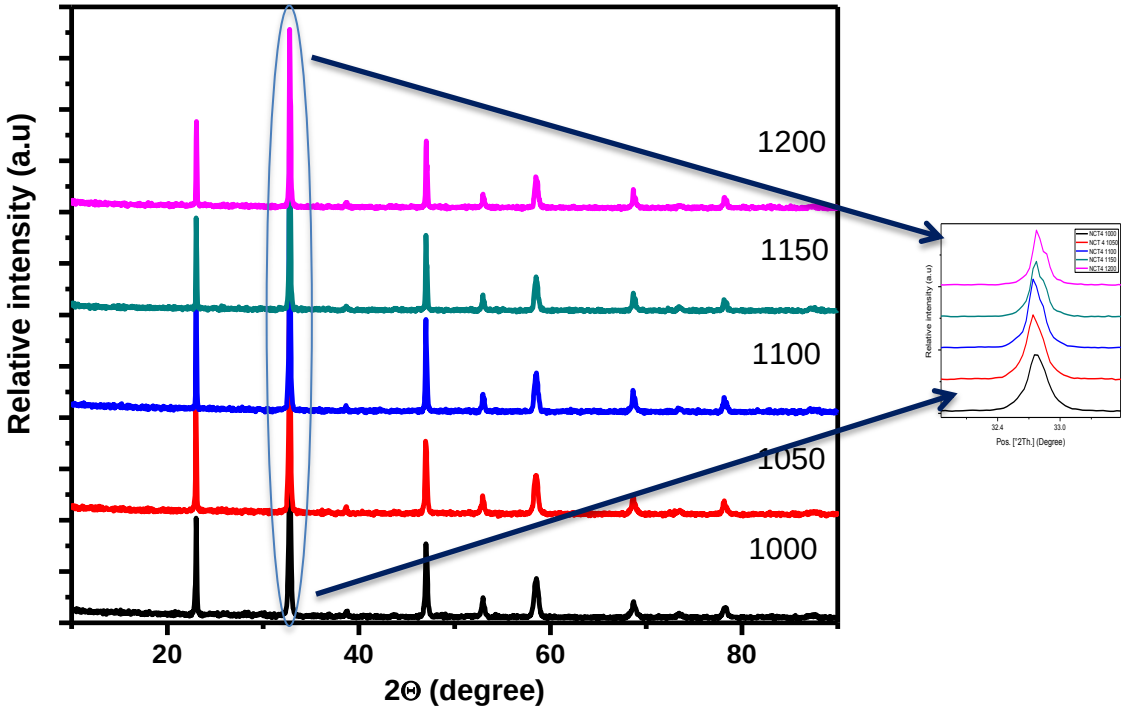


**Fig.6. 8** : Powder XRD patterns for different calcination temperature (1000˚ C-1200˚ C) of the $Na_{(1.2)}Ca_{(0.6)}TiNbO_6$: $0.2Eu^{3+}$.

Table 6. 2 : FWHM and crystallite size of $Na_{(1.2)}Ca_{(0.6)}TiNbO_6$: $0.2Eu^{3+}$ phosphor sample at different calcination temperatures

| Calcination Temperature (˚C) | FWHM (rad) | Crystallite size (nm) |
|---|---|---|
| **1000** | 0.2403 | 38 |
| **1050** | 0.2206 | 42 |
| **1100** | 0.1876 | 49 |
| **1150** | 0.1814 | 51 |
| **1200** | 0.1691 | 54 |

### 6.3.5.2 Morphological Variations

Figure 6.9 shows the variation of morphology with an increase in calcination temperature. Morphology was found to be improved with an increase in calcination temperature. After 1100˚C, some secondary structures can be found and sintering effects are visible at 1200˚C. Secondary phases may be due to the defects occurred during increased calcination.

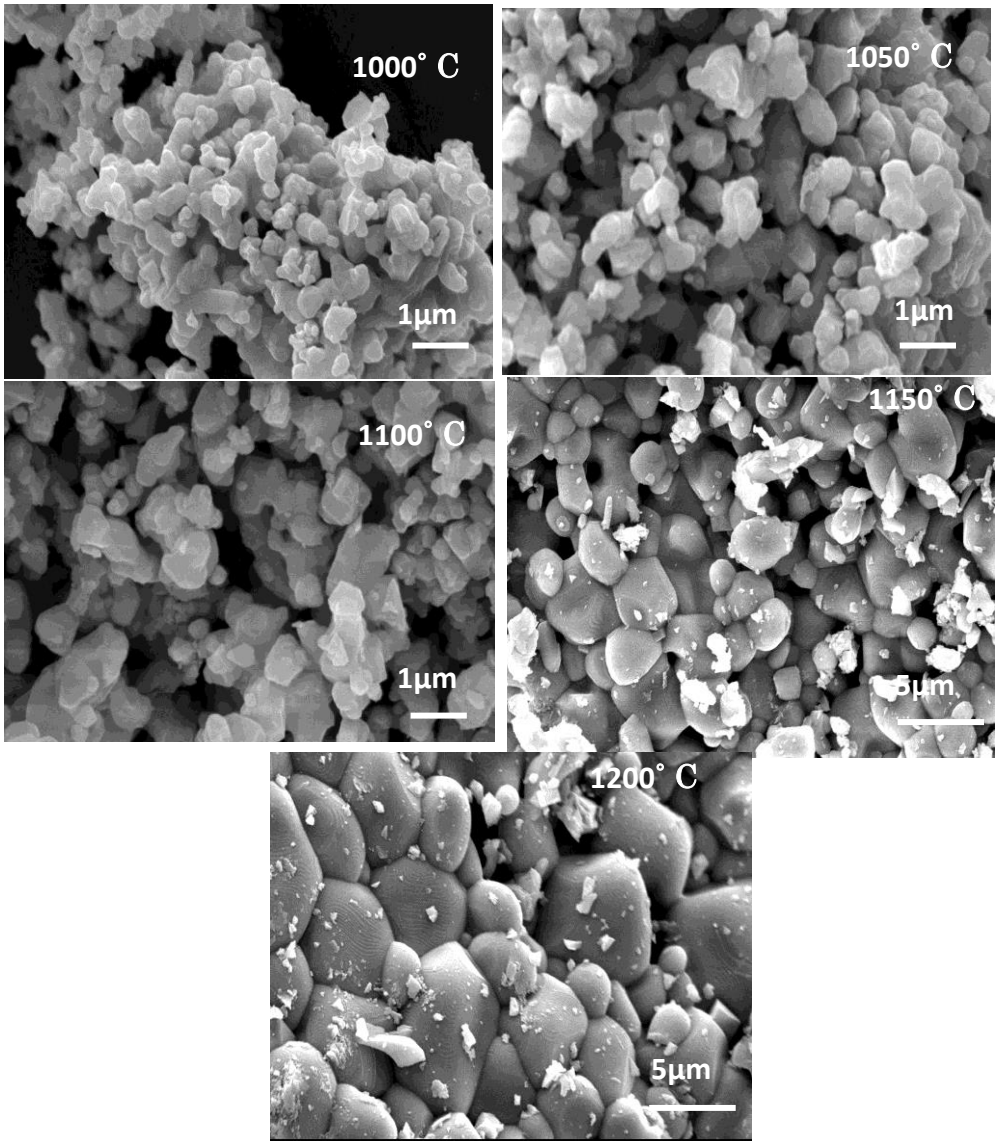


**Fig. 6.9** : Variation of morphology with an increase in calcination temperature of $Na_{(1.2)}Ca_{(0.6)}TiNbO_6:0.2Eu^{3+}$

### 6.3.5.3 EDAX analysis

EDAX analysis of $Na_{(1.2)}Ca_{(0.6)}TiNbO_6$:0.2$Eu^{3+}$ calcined at 1100˚C is shown in Figure 6.10. Inset table shows the elemental weight and atomic weight distribution of the elements present in the sample. All the elements are present in the expected stoichiometric amount.

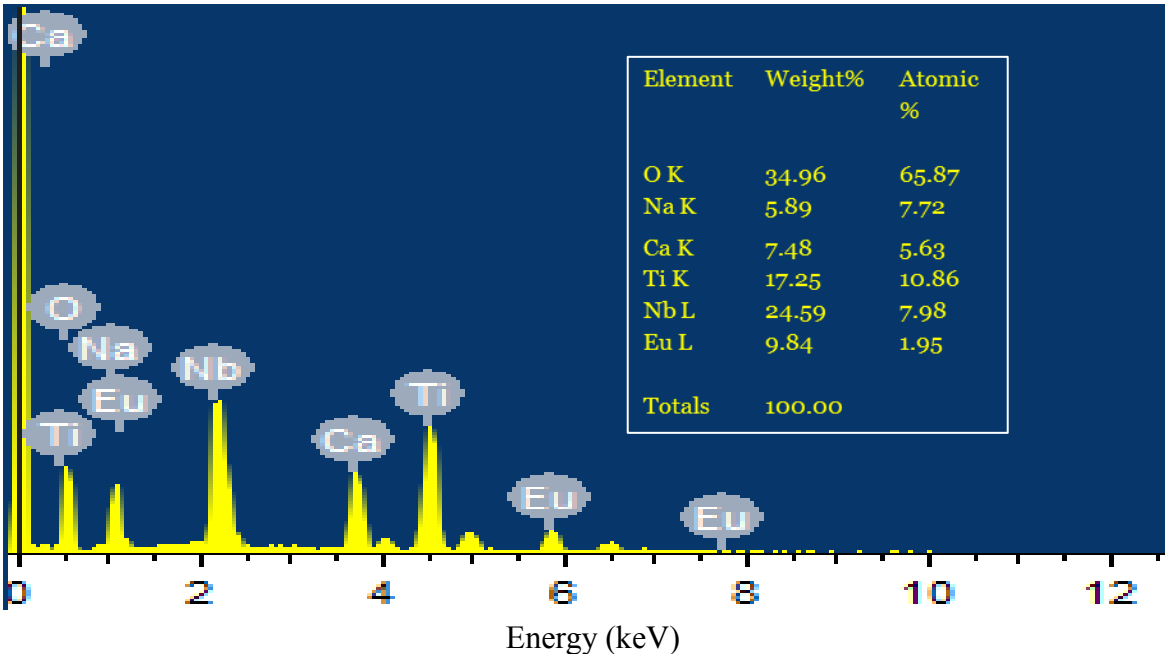


**Fig. 6.10** : EDAX pattern of $Na_{(1.2)}Ca_{(0.8)}TiNbO_6$: *0.2*$Eu^{3+}$calcined at 1100˚ C

### 6.3.5.4 Elemental Mapping Analysis

Elemental mapping analysis is shown in Figure 6.11. From the elemental mapping analysis, it is clear that all the elements are uniformly distributed in the sample

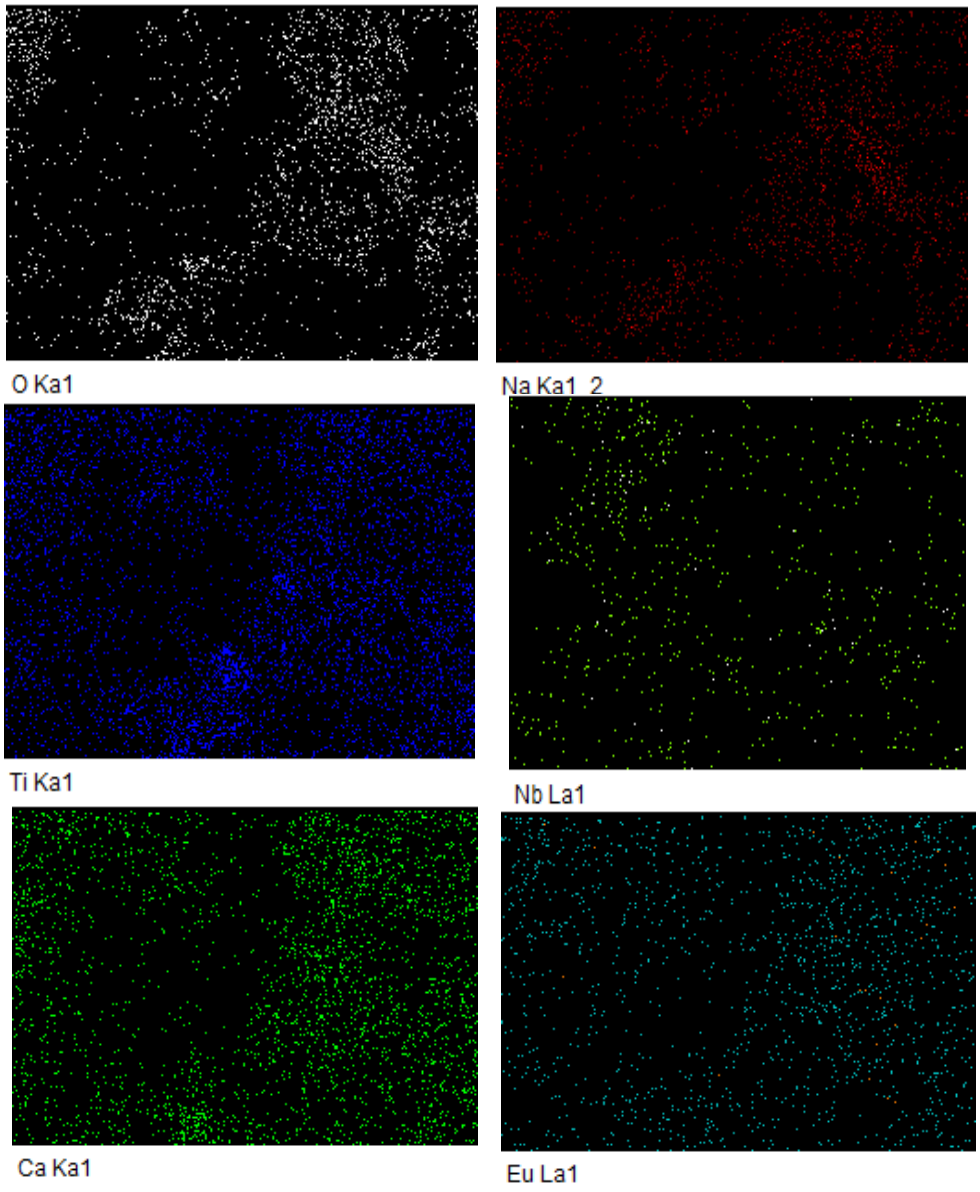


**Fig. 6.11** : Elemental mapping of $Na_{(1.2)}Ca_{(0.8)}TiNbO_6$: *0.2*$Eu^{3+}$calcined at 1100˚ C.

### 6.3.5.5 Variation of photoluminescent properties

Variation of photoluminescence with an increase in calcination temperature is shown in Figure 6.12. The intensity of luminescence emission is found to be increased with increase in calcination temperature upto 1100˚ C and then decreases. This may be due to the reduction of non radiative recombinations and increased crystallinity,

decreased defects and improved morphology in the sample. Beyond 1100˚C, the photoluminescent intensity is found to be decreasing. This may be due to the sintering effects and presence of secondary phases in the system. The energy transfer to neighbouring grains may be quenched by the grain boundaries and defects introduced by calcination(Van Uitert *et al*. 1967).

The emission spectrum of $Na_{(1.2)}Ca_{(0.8)}TiNbO_6$:*0.2*$Eu^{3+}$ calcined at 1100˚C along with commercial red phosphor $Y_2O_3$: $Eu^{3+}$ excited at 395 nm is shown in Figure 6.13. The prepared phosphor exhibit intense red emission as well as that of commercial one, which indicate the potentiality of the phosphor for WLED applications.We calculated CIE color co-ordinates and Correlated Color Temperature (CCT) and color purity of the samples.

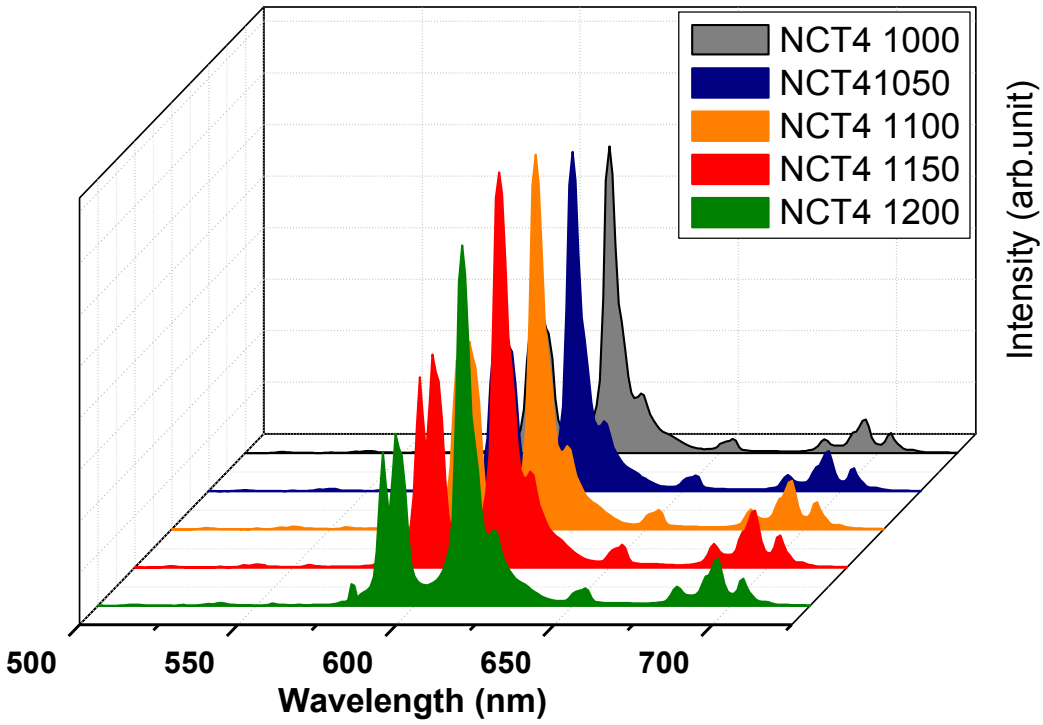


**Fig. 6.12** : Variation of Photoluminescence with an increase in calcination temperature

Color co-ordinates was calculated using CIE color co-ordinate calculator. CCT was calculated using McCamy method, $CCT = -449n^3 + 3525n^2 - 6823.3n + 5520.33$, where n = $(x-x_e)/(y-y_e)$, (x,y) are the chromaticity co-ordinates and $(x_e,y_e)$ are

(0.3320,0.1858), the co-ordinates corresponding to epicenter of convergence of iso temperature lines of the CIE 1931 chromaticity diagram (Yin *et al.* 2012 ,McCamy *et al.* 1931 ). Color purity of the sample was checked using the equation,

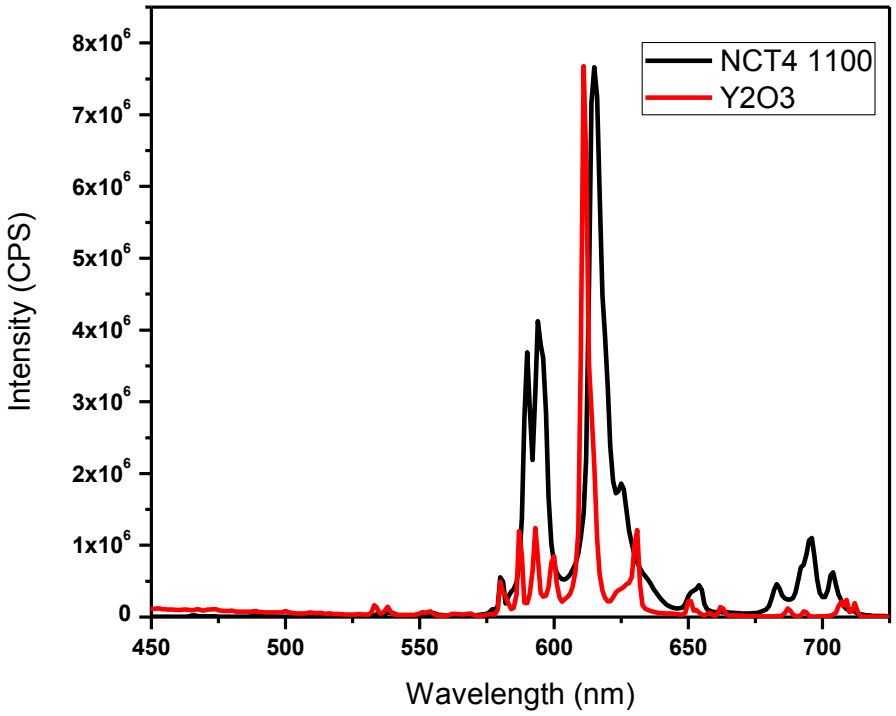


**Fig. 6.13** : Comparison of emission spectra of $Na_{(1.2)}Ca_{(0.8)}TiNbO_6$:*0.2*$Eu^{3+}$ (1100 ˚C ) with commercial $Y_2O_3$ : $Eu^{3+}$ phosphor for an excitation at 395 nm

$color\ purity\ = \frac{\sqrt{\{(x-xi)2+(y-yi)2\}}}{\sqrt{\{(xd-xi)2+(yd-yi)2\}}} \times 100$, where (x,y) are the color co-ordinates of the sample, $(x_i,y_i)$ are color co-ordinates of white illuminant, and $(x_d,y_d)$ are chromaticity co-ordinates of the dominant wavelength. Here (x,y) = (0.65,0.33), $(x_i,y_i)$ = (0.33,0.33) and $(x_d,y_d)$= (0.67,0.33) (Qazi *et al.* 2009, Wu *et al.* 2012). Substituting these, we got excellent value for color purity as 94%. Figure 6.13 shows CIE chromaticity diagram of $Na_{(1.2)}Ca_{(0.6)}TiNbO_6$:0.2$Eu^{3+}$ phosphor sample at 1100 ˚C. Chromaticity color co-ordinate, CCT and color purity of $Na_{(1.2)}Ca_{(0.6)}TiNbO_6$: 0.2$Eu^{3+}$ phosphor sample at different temperatures are tabulated in Table 6.3. Our phosphor sample exhibit intense red emission

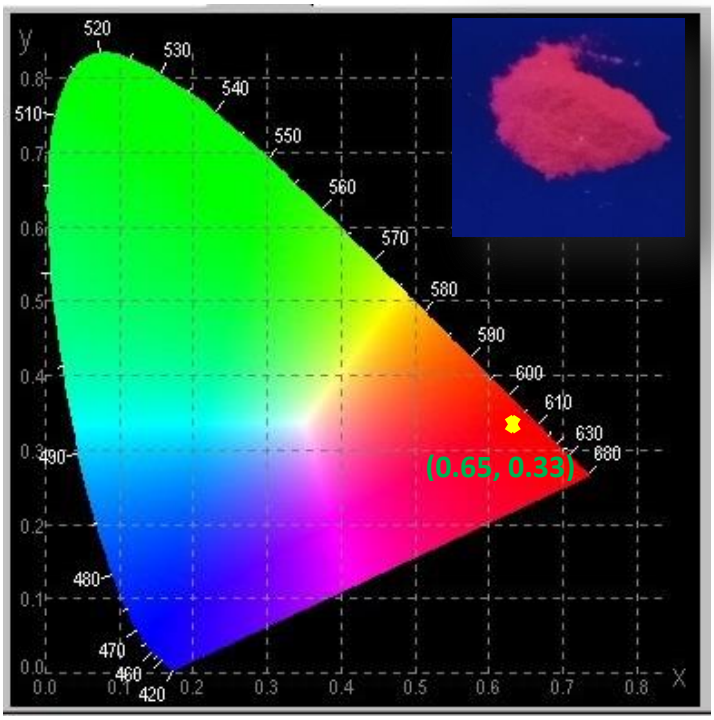


**Fig.6.14**: The CIE chromaticity diagram of $Na_{(1.2)}Ca_{(0.8)}TiNbO_6$:*0.2*$Eu^{3+}$.

Table 6.3 : Chromaticity color co-ordinate, CCT and color purity of $Na_{(1.2)}Ca_{(0.6)}TiNbO_6$: 0.2$Eu^{3+}$ phosphor sample at different temperatures.

| **Temperature(°C)** | **(*x*, *y*)** | **CCT (K)** | **Color Purity(%)** |
|---|---|---|---|
| **1000** | (0.63, 0.36) | 1914 | 88 |
| **1050** | (0.63, 0.35) | 2118 | 88 |
| **1100** | (0.65, 0.33) | 2799 | 94 |
| **1150** | (0.63, 0.36) | 1914 | 88 |
| **1200** | (0.62, 0.36) | 1829 | 85 |

with color co-ordinates (0.65,0.33) which is close to the commercial red phosphor $Sr_2Si_5N_8$ : $Eu^{2+}$ (0.62,0.37). The CCT obtained was 2799K. This low value of CCT is suitable for the phosphor for WLED application for the generation of warm white light

## 6.4. Conclusions

In summary, perovskite type $Eu^{3+}$ doped self-charge compensating red emitting phosphors were prepared via high energy ball milling method. Their structural, morphological and optical characterizations were done. Samples exhibit intense red emissions under near UV (395nm) and blue (463 nm) excitations. $Eu^{3+}$ doping was found to be optimum at 20 mol%. Luminescence quenching occurs due to the dipole-dipole interaction of $Eu^{3+}$ ions in the lattice. We selected $Na_{(1.2)}Ca_{(0.8)}TiNbO_6$:*0.2*$Eu^{3+}$ from the series and studied the effect of the increase of calcination temperature from 1000˚C to 1200˚C by steps of 50˚C in phosphor characteristics. Structural, morphological and optical variations were studied and results suggest that optimization of phosphor characteristics occurs at 1100˚C. $Na_{(1.2)}Ca_{(0.8)}TiNbO_6$:*0.2*$Eu^{3+}$ calcined to 1100 ˚C exhibited intense red emission with CIE color co-ordinates (0.65,0.33), CCT value of 2799K and excellent color purity value of 94%. Also, we compared the photoluminescent emission of our prepared phosphor sample with the commercial $Y_2O_3$: $Eu^{3+}$ phosphor. $Na_{(1.2)}Ca_{(0.8)}TiNbO_6$:*0.2*$Eu^{3+}$ exhibit intense red emission as well as that of the commercial one. Thus the obtained results suggest that the prepared self - charge compensating phosphor sample is suitable for WLED applications.

# Chapter 7

## Conclusions and future scope

This chapter summarizes the major conclusions derived from this work based on the development of novel $Eu^{3+}$ activated perovskite type red phosphors for phosphor converted WLED applications. The conclusions drawn from the study can serve as a guide line for designing of new phosphor materials with improved properties. Future scope of present work is also mentioned.

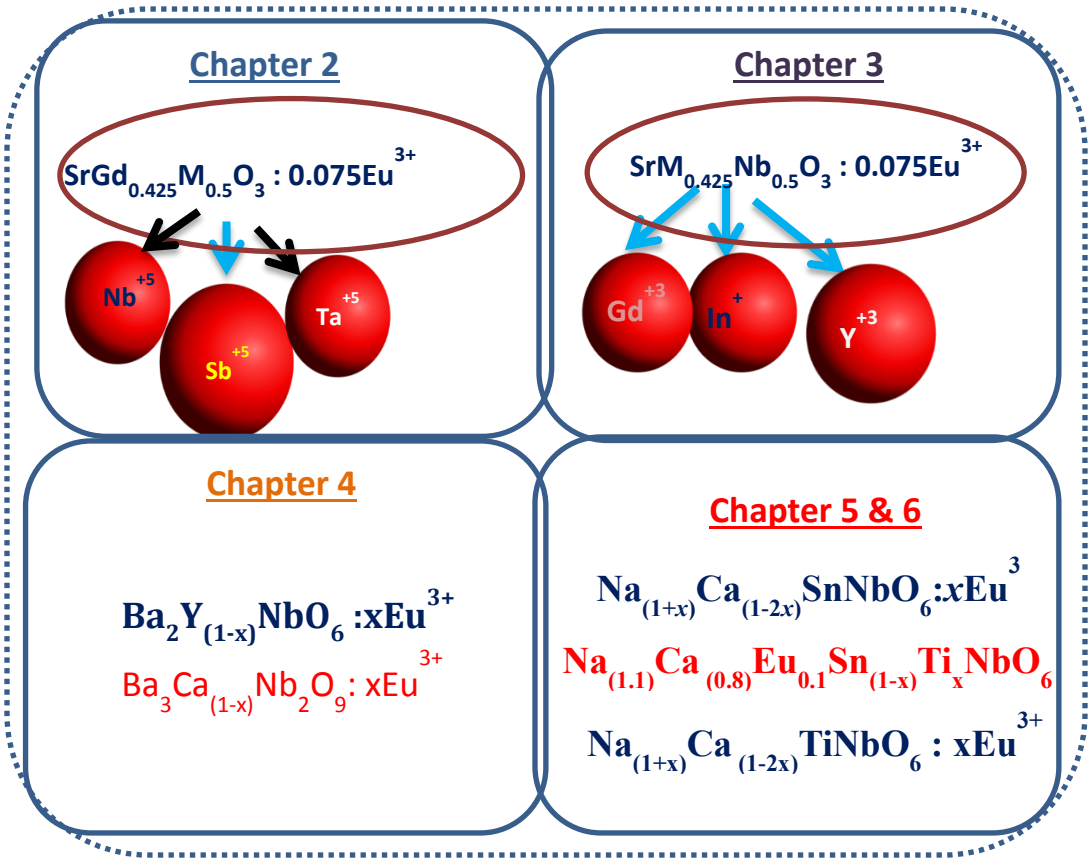

## 7.1 Conclusions

Development of stable and efficient red phophors are an active area of research in the field of materials science. Perovskite type red phosphors are found to be potential candidates for WLED applications. In this scenario, we have developed some series of $Eu^{3+}$ activated perovskite type red phosphors via solid state reaction route and ball milling method. Their structural, microstructural and optical properties were studied. The major conclusions drawn are

- Perovskite type red phosphors are found to be potential candidates for WLED applications.
- By choosing suitable cations at A and B sites, structural, microstructural and optical properties of perovskite red phosphors can be varied.
- Studies on the structural and optical properties of the systems $SrGd_{(0.425)}M_{0.5}O_3$:*0.075*$Eu^{3+}$ (M = Nb, Sb, Ta,) revealed that niobate sample exhibit better luminescent characteristics compared to other two.
- Niobate based series of perovskite phosphors $SrGd_{(0.5-x)}Nb_{0.5}O_3$:*x*$Eu^{3+}$ with different $Eu^{3+}$ concentrations were developed and they possess intense orange-red emission good quantum efficiency values greater than many of the reported systems.
- Among the systems $SrM_{(0.425)}Nb_{0.5}O_3$ : *0.075* $Eu^{3+}$ (M = Y, In, Gd), samples $SrY_{0.425}Nb_{0.5}O_3$: *0.075* $Eu^{3+}$ possess dominant red emission with improved efficiency
- The series of phosphors $SrY_{(0.5-x)}Nb_{0.5}O_3$ : *x*$Eu^{3+}$ were synthesized and their structural, micro-structural and luminescent characteristics were studied. They possess high levels of absorption in the region of emission of pumping LEDs and intense red emission with good quantum efficiency and color purity.
- Orange red emitting 1:2 ordered triple Perovskite type phosphors $Ba_3Ca_{(1-x)}Nb_2O_9$: *x*$Eu^{3+}$ were prepared. They exhibit intense and narrow orange red emission with a double exponential decay.

- Narrow red emitting Perovskite type phosphors $Ba_2Y_{(1-x)}NbO_6$ :$xEu^{3+}$ were prepared. Their emission profile varies for different excitations. narrow red emission having high color purity, good chromaticity co-ordinates and high asymmetric ratio which makes them suitable for WLED applications
- Self-charge compensating red emitting perovskite type phosphors, $Na_{(1+x)}Ca_{(1-2x)}SnNbO_6$:$x$ $Eu^{3+}$ with better morphology were prepared by a high energy ball milling method. Among the samples, $Na_{(1.1)}Ca_{(0.8)}SnNbO_6$:$0.1Eu^{3+}$ phosphor exhibit better phase purity, high asymmetry ratio and better color purity values
- $Ti^{4+}$ incorporated perovskite type red emitting phosphors $Na_{(1.1)}Ca_{(0.8)}Eu_{0.1}Sn_{(1-x)}Ti_xNbO_6$. is found to possess better structural, morphological and optical characteristics.
- Choosing the Ti based system, the series of red phosphors $Na_{(1+x)}Ca_{(1-2x)}TiNbO_6$: $x$$Eu^{3+}$ were prepared by a high energy ball milling method and their photoluminescent properties were optimized calcination temperature.
- Photoluminescence characteristics of perovskite type phosphors strongly depend on choice of host system, structural variations in the host lattice, concentration variation of activators, co-doping, morphology, synthesis routes and preparation temperature.
- Ball milling method is suitable in preparing phosphors with better morphology and uniform distribution of particles at reduced calcination temperature.
- Photoluminescence characteristics of perovskite type phosphors strongly depend on choice of host system, structural variations in the host lattice, concentration variation of activators, co-doping, morphology, synthesis routes and preparation temperature.
- By suitably choosing the host system and with proper modification of host lattices, we can tune the photoluminescence characteristics of $Eu^{3+}$ activated perovskite red phosphors.

## 7.2 Future scope

- Further characterizations of prepared phosphors.
- Incorporation of prepared phosphors with suitable UV/blue LEDs.
- Development of further derived red phosphors from the prepared ones.
- Optimization and comparison of photoluminescent characteristics of phosphors prepared via different synthesis routes.

## REFERENCES


Anderson, M. T.; Greenwood, K. B.; Taylor, G. A.; Poeppelmeier,K. R., B cation arrangements in Double perovskites. *Prog. Solid State Chem.* 22 **(1993)** 197–233.

Antic, Z., R. Krsmanovic, V. Dordevic, T. Dramicanin, and M. D. Dramicanin,"Optical Properties of $Y_2$ $O_3$ : $Eu^{3+}$ Red Emitting Phosphor Obtained via Spray Pyrolysis."*ACTA Phys. Pol. A* 116 **(2009)** 622–24.

Bandi, Vengala Rao, Yung-tang Nien, Tzung-heng Lu, and In-gann Chen. "Effect of Calcination Temperature and Concentration on Luminescence Properties of Novel $Ca_3$ $Y_2$ $Si_3$ $O_{12}$ :$Eu^{3+}$ Phosphors." *J. Am.Ceramic Soc* , 2956 **(2009)** 2953–2956.

Belsky, A. N. and J. C. Krupa. "Luminescence Excitation Mechanisms of Rare Earth Doped Phosphors in the VUV Range." *Displays 19* **(1999)**185–196.

Bhargavi, G. Nag and Ayush Khare. "Luminescence Studies of Perovskite Structured Titanates :", *Opt Spectrosc* 118 (2015) 902–917.

Binnemans, Koen. "Interpretation of Europium(III) Spectra." *Coord. Chem. Rev* 295 **(2015)**1–45.

Blasse.G, Grabmaier B.C, Luminescent Materials, Berlin **(1994)**.

Chang, Yee-shin. "The Effects of Heat Treatment on the Crystallinity and Luminescence Properties of $YInGe_2$ $O_7$ Doped with Eu $^{3+}$ Ions."*J. Electron. Mater* 37 **(2008)** 1024–1028.

Chen, Lei, Chun-che Lin, Chiao-wen Yeh, and Ru-shi Liu.. "Light Converting Inorganic Phosphors for White Light-Emitting Diodes."*Materials* 3**(2010)**2172–2195.

Chien, Tzu Chin, Ji Chun Yang, Chii Shyang Hwang, and Masahiro Yoshimura. "Synthesis and Photoluminescence Properties of Red-Emitting Y6WO12:$Eu^{3+}$phosphors." *J. Alloys Compd.* 676 **(2016)** 286–91.

Crawford, Mary H. “LEDs for Solid-State Lighting : Performance Challenges and Recent Advances.”,*J. Sel. Top. Quantum. Electron.* 15 **(2009)**1028–40.

Davies, P. K., H. Wu, A. Y. Borisevich, I. E. Molodetsky, and L. Farber. 2008. “Crystal Chemistry of Complex Perovskites: New Cation-Ordered Dielectric Oxides.” *Annu Rev Mater Res* 38 **(2008)**369–401.

Dias, Anderson, L. Abdul Khalam, Mailadil T. Sebastian, Carlos William A. Paschoal, and Roberto L. Moreira.. “Chemical Substitution in Ba ( RE $_{1/2}$ Nb $_{1/2}$ ) $O_3$ ( RE ) La , Nd , Sm , Gd , Tb , and Y ) Microwave Ceramics and Its Influence on the Crystal Structure and Phonon Modes.” *Chem. Mater* 3 **(2006)**:214–20.

Divya, Saraswathy, P. Prabhakar Rao, S. Sameera, and Athira K. V Raj.. “Dyes and Pigments In Fl Uence of Aliovalent Cation Substitutions on the Optical Properties of $In_2$ $Cu_2O_5$ System.” *Dyes Pigm* 134 **(2016)** 506–15.

Du, Xiafang, Guan Wu, Jian Cheng, Hui Dang, Kangzhe Ma, Ya-wen Zhang, Peng-feng Tan, and Su Chen.. “High-Quality $CsPbBr_3$ Perovskite Nanocrystals for Quantum Dot Light-Emitting Diodes.” *RSC Adv*7 **(2017)**10391–96.

Feldmann C, Justel T, Ronda C. R, Schmidt P. J, “Inorganic Luminescent Materials - 100 Years of Research and Application” *Adv. Funct. Mater.*13 **(2003)** 511-516

Ferreira, Danilo, De Souza, Pedro Paulo, Luiz Fernando, Almeida Fontenele, Gunther Damaceno, and Marcelo De Oliveira.. “Efficiency , Quality , and Environmental Impacts : A Comparative Study of Residential Artificial Lighting.” *Energy Reports* 5 **(2019)** 409–424.

Francis, Linda T., P. Prabhakar Rao, S. K. Mahesh, T. S. Sreena, and Parvathi S. Babu.. “Novel Red Phosphors Gd2GaTaO7:Eu3+,Bi3+ for White LED Applications.” *J. Mater. Sci: Mater Electron* 26 **(2015)**5743–5747.

Francis, T. Linda, P. Prabhakar Rao, S. K. Mahesh, T. S. Sreena, and S. Parvathi Babu. "Effect of Host Structure on the Photoluminescence Properties of $Ln_3TaO_7$ : $Eu^{3+}$ Red Phosphors." *Optical Materials* 52 **(2016)**134–143.

Francis, T. Linda, P. Prabhakar Rao, Mariyam Thomas, S. K. Mahesh, and V. R. Reshmi. "Effect of $Zr^{4+}$ and $Si^{4+}$ Substitution on the Luminescence Properties of $CaMoO_4$:$Eu^{3+}$ Red Phosphors." *J. Mater. Sci: Mater Electron* 25 **(2014)**2387–2393.

Fu, Anjie, Anxiang Guan, Fangfang Gao, Xiaoshan Zhang, Liya Zhou, Yingbin Meng, and Haiman Pan.. "A Novel Double Perovskite $La_2ZnTiO_6$ : $Eu^{3+}$ Red Phosphor for Solid-State Lighting : Synthesis and Optimum Luminescence." *Opt. Laser Technol* 96 **(2017)**43–49.

Fu, Anjie, Qi Pang, Hong Yang, and Liya Zhou. "$Ba_2YNbO_6$ : $Mn^{4+}$ -Based Red Phosphor for Warm White Light-Emitting Diodes ( WLEDs ): Photoluminescent and Thermal Characteristics." *Opt. Mater* 70 **(2017)**144–52.

George, Nathan C., Kristin A. Denault, and Ram Seshadri.. "Phosphors for Solid-State White Lighting.", *Annu. Rev. Mater. Res*, 43 **(2013)** 2.1–2.21.

Gorodea, Ioana A.. "Influence of the B-Site Cation Nature on Crystal Structure and Magnetic Properties of $Ca_2BMoO_6$ ( B = Cr , La , Sm ) Double Perovskite." *ACTA Chemica* 154 **(2014)** 145–54.

Gyu, Myoung, Jin Hwa, Jong Seong, Jong Pil, K. S. Hong, and Ho-soon Yang. "Photophysical Properties of Highly Ef Fi Cient Red-Emitting $CaTiO_3$ : $Eu^{3+}$ Phosphors under near Ultra-Violet Excitation." *Curr. Appl Phys* 11**(2011)**1379–83.

Hou, Jingshan, Xin Yin, Yongzheng Fang, Fuqiang Huang, and Weizhong Jiang. "Novel Red-Emitting Perovskite-Type Phosphor $CaLa_{(1-x)}MgMO_6$ : $xEu^{3+}$ ( M = Nb , Ta ) for White LED Application." *Opt Mater* 34**(2012)**1394–97.

Howard, Christopher J., Brendan J. Kennedy, and Patrick M. Woodward. "Research Papers Ordered Double Perovskites, a Group-Theoretical Analysis Research Papers." ACTA Crystallogr. B B59**(2003)**463–471.

Huang X., "Solid-state lighting: Red phosphor converts white LEDs", *Nat Photon*., 8 (**2014)** 748-749

Jiang, Pengfei, Zhengyang Zhou, Wenliang Gao, Rihong Cong, and Tao Yang.. "B-Site Ordered Double Perovskite $LaBa_{1-x}Sr_xZnSbO_6$ ($0 \leq x \leq 1$): $Sr^{2+}$-Doping-Induced Symmetry Evolution and Structure–Luminescence Correlations." *Dalton. Trans* 6 **(2016)** 3949–57.

Jing, Lindan, Xiaohua Liu, and Yuntong Li.. "Synthesis and Optical Properties of Novel Red Phosphors Sr3MoO6:$Eu^{3+}$with Highly Enhanced Emission by $W^{6+}$doping." *J. Lumin* 158 **(2015)**351–55.

Kaufman J.E., Christensen J.F., Lighting Handbook, *Waverly Press*, **(1972)** Maryland

King, Graham and Patrick M. Woodward. "Cation Ordering in Perovskites." *J, Mater. Chem* 20 **(2010)** 5785–5796.

Kong, L. B., J. Ma, and H. Huang.. "Low Temperature Formation of Yttrium Aluminum Garnet from Oxides via a High-Energy Ball Milling Process." *Mater.Lett* 56 **(2002)**344–348.

Lal, Sariga C., A. M. Aiswarya, K. S. Sibi, and G. Subodh.. "Insights into the Structure , Photoluminescence and Judd-Ofelt Analysis of Red Emitting $SrLaLiTeO_6$ : $Eu^{3+}$ Phosphors." *J. Alloys Compd* 788 **(2019)**1300–1308.

Lal, Sariga C., Vidhya Lalan, and Subodh Ganesanpotti.. "Structural Characterization of B-Site Ordered Ba2Ln2/3TeO6 (Ln = La, Pr, Nd, Sm, and Eu) Double Perovskites and Probing Its Luminescence as Eu3+ Phosphor Hosts." *Inorg. Chem.* 57 **(2018)**6226–36.

Lee, Soo Hyun, Youngjin Cha, Hyosung Kim, Seungmoo Lee, and Jae Su Yu. "Luminescent Properties of Eu3+-Activated Gd2ZnTiO6 Double Perovskite Red-Emitting Phosphors for White Light-Emitting Diodes and Field Emission Displays." *RSC Adv* 8 **(2018)**11207–15.

Lei, F. and B. Yan. "Synthesis and Photoluminescence of Perovskite-Type Ca2 MgWO6:Eu3+ Micrometer Phosphor." .*J Optoelectron. Adv Mater* 10**(2008)**158–63.

Li, Huaiyong, Hyun Kyoung, Byung Kee, Byung Chun, Jung Hyun, Kiwan Jang, Ho Sueb, and Soung Soo. "Color-Conversion and Photoluminescence Properties of Ba2MgW(Mo)O6 : Eu Phosphor." *J. Alloys Compd* 509 **(2011)** 8788–8793.

Li, Jinkai, Ji-guang Li, Jing Li, Shaohong Liu, and Xiaodong Li.. "Journal of Solid State Chemistry Development of $Eu^{3+}$ Activated Monoclinic , Perovskite , and Garnet Compounds in the $Gd_2O_3$ – $Al_2O_3$ Phase Diagram as Efficient Red-Emitting Phosphors." *J. Solid State Chem* 206 **(2013)**104–112.

Li, Junhao, Jing Yan, Dawei Wen, Wasim Ullah Khan, Jianxin Shi, Mingmei Wu, Qiang Su, and Peter A. Tanner.. "Advanced Red Phosphors for White Light-Emitting Diodes." *J. Mater. Chem. C* 4 **(2016)**8611–8623.

Maths, Yuan-chih Lin and Karlsson Marco. "Inorganic Phosphor Materials for Lighting." *Top Curr Chem* 374 **(2016)**1–47.

Morgan, M. Granger, Fritz Morgan, and By Ine.. "The Transition to Solid-State Lighting.", *Proc. IEEE*, 97 **(2009)** 481-510.

McCamy C.S, Correlated Color Temperature as an Explicit Function of ChromaticityCoordinates, *Color Res. Appl.* 17 **(1931)** 142–144.

Nakamura S., Senoh M., Mukai T., "P-GaN/N-InGaN/N-GaN double-heterostructure bluelightemitting diodes", *J. App. Phys.,* 32 (**1993)** L8-L11

Nalwa H. S, Rohwer L. S, "Handbook of Luminescence, Display Materials, and Display Devices", *American Scientific Publishers,* California **(2003).**

Nbo, Na K. "Effect of Mechanical Activation on the Structure and Ferroelectric Property." *Mater Res Bull* 46 **(2011)**1467–72.

Nguyen, Hoang-duy, Seung-joo Kim, In-hyeong Yeo, and Sun-il Mho.. "Luminescent Properties of Eu 3 + -Doped $Ba_2$ $Bi_{2/3}TeO_6$ and $BaBiNaTeO_6$ Double Perovskite as New Orange-Red." *J. Electrochem. Soc* 159**(2012)**54–60.

Nikol, H. "Rare Earth Phosphors: Fundamentals and Applications ¨, *J. Alloy Compd* ,277**(1998)**669–676.

Noel, Nakita K., Samuel D. Stranks, Antonio Abate, Christian Wehrenfennig, Simone Guarnera, Amir Abbas Haghighirad, Aditya Sadhanala, Giles E. Eperon, Sandeep K. Pathak, Michael B. Johnston, Annamaria Petrozza, Laura M. Herz, and Henry J. Snaith. "Lead-Free Organic-Inorganic Tin Halide Perovskites for Photovoltaic Applications." *Energy and Environ Sci.* 7**(2014)**3061–3068.

Oliveira, Larissa H., Julia Savioli, Ana P. De Moura, Içamira C. Nogueira, Maximo S. Li, Elson Longo, José A. Varela, and Ieda L. V. Rosa. "Investigation of Structural and Optical Properties of CaTiO3 Powders Doped with $Mg^{2+}$ and $Eu^{3+}$ Ions." *J. Alloys Compd* 647**(2015)**265–75.

Phillips, Julia M., Michael E. Coltrin, Mary H. Crawford, Arthur J. Fischer, Michael R. Krames, Gerd O. Mueller, Yoshi Ohno, Lauren E. S. Rohwer, Jerry A. Simmons, and Jeffrey Y. Tsao,"Research Challenges to Ultra-Efficient Inorganic Solid-State Lighting.", *Laser and Photon Rev* 333**(2007)**307–33.

Qazi, S. Junaid S., Adrian R. Rennie, Jeremy K. Cockcroft, and Martin Vickers.. "Journal of Colloid and Interface Science Use of Wide-Angle X-Ray Diffraction to Measure Shape and Size of Dispersed Colloidal Particles." *J. Colloid Interface Sci* 338 **(2009)**105–110.

Rajendran, Deepthi N., K. Ravindran Nair, P. Prabhakar Rao, K. S. Sibi, Peter Koshy, and V. K. Vaidyan. "New Perovskite Type Oxides: $NaATiMO_6$ (A = Ca or Sr; M = Nb or Ta) and Their Electrical Properties." *Mater Lett* 62 **(2008)**623–628.

Renju, Ushakumari A., Padala Prabhakar Rao, and Divakaran S. Vaisakhan Thampi. "Influence of Phase Transition from Order to Disorder and Philip ' s Ionicity on the Thermal Expansion Coefficient of Pyrochlore Type Compositions with a Multivalent Environment †." *New J. Chem* 41 **(2016)**245–255.

Ronda, Cees R. *Luminescence: From Theory to Applications*. Wiley-VCH Verlag GmbH & Co. KGaA, (**2008**) Germany

Ropp .R. C, Luminescence and Solid state, **(2004)***USA*

Saparov, Bayrammurad and David B. Mitzi. "Organic – Inorganic Perovskites : Structural Versatility for Functional Materials Design."*Chem Rev* 116 **(2016)** 4558-4596

Shi, Shikao, Jing Gao, and Ji Zhou. "Effects of Charge Compensation on the Luminescence Behavior of $Eu^{3+}$ Activated $CaWO_4$ Phosphor." *Opt. Mater* 30 **(2008)**1616–1620.

Shionoya S., Yen W. M., Yamamoto H., (Eds.), "Phosphor Handbook", *CRC press* (**2006**)

Shur, Michael S. and A. R. T. Uras.. "Solid-State Lighting : Toward Superior.", *Proc. IEEE* 93 **(2005)** 1691–1703.

Sivakumar, V. Ã. and U. V. Ã. Varadaraju. "Synthesis , Phase Transition and Photoluminescence Studies on $Eu^{3+}$ -Substituted Double Perovskites — A Novel Orange-Red Phosphor for Solid-State Lighting." *J. Solid. Chem* 181**(2008)**3344–3351.

Smet, Philippe F., Anthony B. Parmentier, and Dirk Poelman.. "Selecting Conversion Phosphors for White Light-Emitting Diodes." *J. Electrochem. Soc,* 158 **(2011)** R37-R54.

Sreena, T. S., P. Prabhakar Rao, Athira K. V Raj, and T. R. Aju Thara. "Narrow-Band Red-Emitting Phosphor , $Gd_3Zn_2Nb_3O_{14}$ :$Eu^{3+}$ with High Color Purity for Phosphor-Converted White Light Emitting Diodes." *J. Alloys Compd* 751**(2018)**148–58.

Sreena, T. S., P. Prabhakar Rao, T. Linda Francis, Athira K. V. Raj, and Parvathi S. Babu. "Structural and Photoluminescence Properties of Stannate Based Displaced Pyrochlore-Type Red Phosphors: $Ca_{3-x}Sn_3Nb_2O_{14}$ :$xEu^{3+}$." *Dalton Trans.* 44 **(2015)** 8718–8728.

Steigerwald, Daniel A, Jerome C. Bhat, Dave Collins, Robert M. Fletcher, Mari Ochiai Holcomb, Michael J. Ludowise, Paul S. Martin, and Serge L. Rudaz. "Illumination With Solid State Lighting Technology", *IEEE J. Sel. Top. Quantum Electron* 8 **(2002)**310–320.

Stevens W. R., "Building Physics: Lighting", *Pergamon Press*, London, (**1969**)

Sun, Chun, Zhiyuan Gao, Yuchen Deng, Hanxin Liu, Le Wang, Sijing Su, Peng Li, Huanrong Li, Zihui Zhang, and Wengang Bi. "Orange to Red , Emission-Tunable Mn-Doped Two-Dimensional Perovskites with High Luminescence and Stability." *ACS Applied Mater & Interfaces* 11**(2019)**34109–34116.

Sun, Qi, Shaoying Wang, Balaji Devakumar, Liangling Sun, Jia Liang, Thangavel Sakthivel, Sanjay J. Dhoble, and Xiaoyong Huang.. "Double Perovskite $Ca_2LuTaO_6$ : $Eu^{3+}$Red-Emitting Phosphors : Synthesis , Structure and Photoluminescence Characteristics." *J. Alloys Compd.* 804 **(2019)**230–236.

Uitert, L. G. Van, J. Electrochem Soc, and I. G. Van Uitert.. "Characterization of Energy Transfer Interactions between Rare Earth Ions Characterization of Energy Transfer Interactions between Rare Earth Ions."*J. Chem. Phys* 114 **(1967)**1048–1053.

Vasala, Sami and Prof Maarit Karppinen, $A_2B'B''O_6$ Perovskites, A Review,*Prog.Solid State Chem* 43 **(2014)** 1-36

Vance, E. R., R. A. Day, Z. Zhang, B. D. Begg, C. J. Ball, and M. G. Blackford “Charge Compensation in Gd-Doped $CaTiO_3$.” *J. Solid state Chem*. 82. **(1996)**77–82.

Vinicius, Marcos, Mario Ernesto, Giroldo Valério, Rodolpho Mouta, Eduardo Moraes, Carlos William, and De Araujo Paschoal. “Mechanism of Luminescent Enhancement in $Ba_2GdNbO_6 : Eu^{3+}$ Perovskite by Li+Co-Doping.” *J. Lumin* 158 **(2015)**75–80.

Wu, Bin, Qinghong Zhang, and Yaogang Li. “CrystEngComm Low-Temperature Preparation of Monodispersed Eu-Doped $CaTiO_3$ LED.” **(2012)**2094–2099.

Wu, Yun-fang, Yung-tang Nien, Yi-jhang Wang, and In-gann Chen. “Enhancement of Photoluminescence and Color Purity of $CaTiO_3$ :Eu Phosphor by Li Doping.” *J. Am. Ceram. Soc.* 1366(2012)1360–66.

Xin, Shuangyu, Yuhua Wang, Zhaofeng Wang, Feng Zhang, Yan Wen, and Ge Zhu.. “An Intense Red-Emitting Phosphor $YBa_3(PO_4)_3 : Eu^{3+}$ for Near-Ultraviolet Light Emitting Diodes Application.” *ECS Solid State Lett* 14 **(2011)**438–441.

Yahiaoui, Z., M. A. Hassairi, and M. Dammak.. “Synthesis and Optical Spectroscopy of $YPO_4 : Eu^{3+}$ Orange – Red Phosphors.” *J. Electron. Mater* 46 **(2017)**4765–4773.

Yamamoto, Haijme, Shinji Okamoto, and Hiroshi Kobayashi.“Luminescence of Rare-Earth Ions in Perovskite-Type Oxides : From Basic Research to Applications.” *J. Lumin* 100 **(2002)**325–332.

Yang, Hyun Kyoung and Jung Hyun Jeong.. “Synthesis , Crystal Growth , and Photoluminescence Properties of YAG : $Eu^{3+}$ Phosphors by High-Energy Ball Milling and Solid-State Reaction.” *J. Phys. Chem. C* 12 **(2010)**226–230.

Ye, S., F. Xiao, Y. X. Pan, Y. Y. Ma, and Q. Y. Zhang.. “Phosphors in Phosphor-Converted White Light-Emitting Diodes : Recent Advances in Materials , Techniques and Properties.” *Mater. Sci. Eng* 71**(2010)**1–34.

Yin, Xin, Jiyong Yao, Yaoming Wang, Chengchun Zhao, and Fuqiang Huang.. "Novel Red Phosphor of Double Perovskite Compound $a_2MgTiO_6$:$x$Eu$^{3+}$."*J. Lumin*132 **(2012)**1701–1704.

Yu, Ruijin, Caifeng Wang, Jingtao Chen, Yongkun Wu, Hongjuan Li, and Hailong Ma. "Photoluminescence Characteristics of Eu$^{3+}$ -Doped Double-Perovskite Phosphors." *ECS. Solid. state Sci. Techol.* 3 **(2014)**33–37.

Zhang, Le, Pengde Han, Yong Han, Zhou Lu, Hao Yang, Lixi Wang, and Qitu Zhang. "Structure Evolution and Tunable Luminescence of for White LEDs." *J. Alloys Compd* 558 **(2013)**229–35.

Zhang, Le, Bingheng Sun, Quan Liu, Nan Ding, Hao Yang, Lixi Wang, and Qitu Zhang.. "Novel Layered Perovskite Sr3Ti2O7:Eu$^{3+}$ Phosphor with High-Efficiency Luminescence Enhanced by Charge Compensation." *J. Alloys Compds*657 **(2016)**27–31.

Zhang, Qiang, Xicheng Wang, Xin Ding, and Yuhua Wang.. "A Potential Red-Emitting Phosphor $BaZrGe_3O_9$ :Eu$^{3+}$ for WLED and FED Applications: Synthesis, Structure, and Luminescence Properties." *Inorg Chem* 56 **(2017)**6990–66998.

Zhang, Xinguo, Jilin Zhang, and Menglian Gong. "Synthesis and Luminescent Properties of UV-Excited Thermal Stable Red-Emitting Phosphor $Ba_3Lu(PO_4)_3$: Eu$^{3+}$ for NUV LED." *Opt. Mater* 36 **(2014)**850–853.

Zhao, Chengchun, Xin Yin, Fuqiang Huang, and Yin Hang. "Novel Red Perovskite Phosphor Ca 2 AlNbO 6 : Eu$^{3+}$ for White Light-Emitting Diode Application." *Physica B Condens. Matter* 406 **(2011)**4608–4611.

Zhou, Zhenzhen, Guanghui Liu, Jieqiong Wan, and Jia Ni. "A Novel Tunable White Light Emitting Multiphase Phosphor Obtained from $Ba_2TiP_2O_9$ by Introducing Eu$^{3+}$." *Appl Phys A* 122 **(2016)**1–6.

# LIST OF PUBLICATIONS

1. New perovskite type orange red emitting phosphors, $SrGd_{0.5}Nb_{0.5}O_3$:$xEu^{3+}$ for WLED applications, **B. A. Aswathy**, Padala Prabhakar Rao, and V.G. Suchithra, ***Mater Lett***, 2018, 229, 182–184.

2. New self charge compensating perovskite type red phosphors prepared via ball milling process for pc-white light emitting diode applications, **B. A. Aswathy,** Padala Prabhakar Rao, and V.G. Suchithra, ***Opt Laser technol***, 2020, 128, 106217.

3. Color - Tunable Phosphors in Weberite Type System, $La_3SbO_7$:$Bi^{3+}$, $Eu^{3+}$ for Near-UV-LED Applications, V.G. Suchithra, Padala Prabhakar Rao, and **B. A. Aswathy,** ***ChemistrySelect***, 2017, 2, 7602– 7611.

4. New full color emitting phosphor through energy transfer in $Bi^{3+}$ and $Eu^{3+}$ co-doped $La_3TaO_7$ weberite system, V.G. Suchithra, Padala Prabhakar Rao, and **B. A. Aswathy,** ***J. Mater. Sci. Mater. Electron.*** 2020, 31 (7), 5141-5151.

5. New narrow orange emitting phosphors in 1:2 B-site cation ordered $Eu^{3+}$ doped triple Perovskite $Ba_3CaNb_2O_9$ ***J. Mater. Sci. Mater. Electron*** (Communicated)

# List of Conference Papers

1. **B. A. Aswathy**, P. Prabhakar Rao, *Investigation on the effect of Ti doping on the Sn site of $Na_{(1.1)}Ca_{(0.8)}Eu_{0.1}SnNbO_6$ : novel perovskite red phosphor prepared by ball milling method for WLED application***,** National Conference on critical and strategic materials for advanced technologies (CSMAT), 9-11 March 2017. (**Best Poster Award**).

2. **B. A. Aswathy**, P. Prabhakar Rao, *Novel perovskite Orange red phosphors for WLED applications***,** National Conference on luminescence and its applications (NCLA), Feb 14-16, 2018 held at CSIR NIIST, Trivandrum

3. **B. A. Aswathy**, P. Prabhakar Rao, V.G. Suchithra, *Photoluminescence properties of $Na_{(1+x)}Ca_{(1-2x)}TiNbO_6:xEu^{3+}$ (x=0.05-0.3):perovskite red phosphor with spherical morphology prepared by ball milling method,* National Conference on emerging trends in science, technology and application of electron microscopy (STEAM), 19-21 December 2018, held at CSIR NIIST, Trivandrum

4. Suchithra V. G., P. Prabhakar Rao, **B. A. Aswathy**, *Morphological Assisted Luminescence Enhancement In Bismuth Doped Weberite Type Systems,* Poster presented in National Conference on Emerging Trends in Science, Technology & Application of Electron Microscope (STAEM-2018) and 5th Annual Meeting of the Academy of Microscope Science & Technology (AMST), India December 19 – 21, 2018, Trivandrum.

5. Suchithra V. G, P. Prabhakar Rao, **B. A. Aswathy,** *Photoluminescence and Color Tunability of $Bi^{3+}$Doped $Y_3Sb_5O_{12}$ Phosphor,* poster presented in International Conference on Science, Technology and Interdisciplinary Reasearch ICSTAR 2018 July 14, held at Tirupati.